Palacký University Olomouc

Faculty of Science

Department of Physical Chemistry

# Magnetic properties of heteroatomic transition-metal dimers supported on defective graphene

Master's Thesis

Author: Bc. Jan Navrátil

Supervisor: doc. Mgr. Piotr Błoński, Ph.D.

Study program: Chemistry

Field of study: Physical Chemistry

Form of study: Full-time

Year: 2021

## Declaration

I declare that I elaborated this Master's Thesis independently under the guidance of doc. Mgr. Piotr Błoński, Ph.D. and thoroughly cited all used sources.

In Olomouc: .....  .....

Handwritten signature

# Acknowledgement

At first, I would like to thank doc. Mgr. Piotr Błoński, Ph.D. for his enormous support, endless patience, his time, and the overall opportunity for me to work in this interesting field of research. Our collaboration already led to the publishing of our paper in *Nanotechnology*.

I would also like to credit doc. RNDr. Petr Jurečka, Ph.D. and other people taking care of our computational clusters, it would be impossible to complete the thesis without them.

I express my gratitude to my partner Jana Poštolková who supported me the most. She always patiently listened to my talks about the thesis and gave me many useful suggestions how to further improve the work.

I would also like to thank my friends and my family that always enthusiastically helped me to relax in the meantime, so I could get back to work with verve.

I also acknowledge the support by Palacký University Olomouc (project IGA_PrF_2021_031).

# Bibliografické údaje


| | |
|---|---|
| Autor: | Bc. Jan Navrátil |
| Název: | Magnetické vlastnosti dimerů heteroatomů přechodných kovů podporovaných na defektním grafenu |
| Typ závěrečné práce: | Diplomová |
| Vedoucí práce: | doc. Mgr. Piotr Błoński, Ph.D. |
| Rok prezentace: | 2021 |
| Katedra: | Katedra fyzikální chemie, Univerzita Palackého v Olomouci |
| Klíčová slova: | DFT, magnetismus, magnetická anizotropní energie, ukládání informací, defektní grafen, atomy a dimery přechodných kovů |
| Počet stran: | 81 |
| Počet příloh: | 2 |
| Jazyk: | Anglický |



Abstrakt: Vylepšování digitálních záznamových médií už nestačí splňovat požadavky na stále rostoucí kapacity. Zmenšování zrn v současných záznamových médiích sice může vést ke zvýšení kapacity, ale jejich rozměry pod $\sim$ 10 nm vedou k paramagnetickému efektu, kdy se energie vztažená na jedno zrno stává příliš malou na to, aby odolala tepelně aktivované spontánní změně magnetizace a tudíž ke ztrátě uložené informace. Alternativně je možné použít přesnou matrici izolovaných magnetů o velikosti jednoho nebo pár atomů, kde by každý tento magnet uchovával 1 bit informace. Abychom dosáhli těchto absolutních limitů, musíme najít magnetická centra (tedy samostatné atomy nebo klastry skládající se z pár atomů), která mají dostatečně vysoké hodnoty magnetické anizotropní energie (MAE), aby spolehlivě odolaly náhodným tepelným excitacím, které mohou vyústit ve ztrátu informace. Tato centra musí být pevně držena na jednom konkrétním místě. Tato teoretická diplomová práce využívá teorii funkcionálu hustoty (DFT) a rozšiřuje mou Bakalářskou práci s názvem "Insights into the interaction of transition metal atoms with defective graphene from DFT", kde jsme zkoumali vlastnosti samostatných atomů přechodných kovů (PK) adsorbovaných na defektním grafenu a našli jsme zajímavé hodnoty MAE, které jsou ale stále příliš nízké na praktické využití těchto systémů, tedy aby spolehlivě udržely informaci alespoň za teploty 77 K (teplota kapalného dusíku, který je snadno dostupný a poměrně levný). Tato Diplomová práce rozšiřuje tento výzkum přidáním druhého atomu PK na už předem adsorbovaný atom PK, protože kolmá geometrie dimeru PK je nezbytná pro dosažení velkých hodnot MAE. Stabilitu této geometrie jsme dále posuzovali a pouze stabilní dimery jsme zkoumali dále, vyhodnotili jsme jejich geometrické vlastnosti, adsorpční energii druhého atomu PK, magnetické momenty a náboje nacházející se na jednotlivých atomech. Také jsme vysvětlili mechanismus vzniku vazby a navrhli jsme rovnice, které jej popisují matematicky. Všechny magnetické systémy byly také zkoumány v nekolineárním módu, který předpověděl vysoké hodnoty ($\geq$ 15 meV) MAE ve 22 systémech s horním (vzdálenějším od grafenu) atomem Os nebo Ir. Podle našeho nejlepšího vědomí jsme spoustu systémů spočítali jako úplně první. Nejvyšší hodnota MAE ($\sim$170 meV) byla dosažena v sysému OsPd@NSV, který odpovídá blokovací teplotě $\sim$ 44 K při enormní teoretické hustotě informací $\sim$ 490 Tb$\cdot$inch$^{-2}$. Fyzikální původ MAE je diskutován na základě elektronové struktury. Vysoká hodnota MAE je následována významnou anizotropí magnetického momentu na atomu PK vzdálenějším od grafenu.

# Bibliographic identification


| | |
|---|---|
| Author: | Bc. Jan Navrátil |
| Title: | Magnetic properties of heteroatomic transition-metal dimers supported on defective graphene |
| Type of thesis: | Master's |
| Supervisor: | doc. Mgr. Piotr Błoński, Ph.D. |
| Year of presentation: | 2021 |
| Department: | Department of Physical Chemistry, Palacký University Olomouc |
| Keywords: | DFT, magnetism, magnetic anisotropy energy, information storage, defective graphene, transition metal atoms and dimers |
| Number of pages: | 81 |
| Number of appendices: | 2 |
| Language: | English |



Abstract: Improvements of data storage devices hardly fulfil the demand for even increasing capacities. A reduction of the grain size of the present storage medium can increase the storage capacity, however, the reduction of the grain size below $\sim$ 10 nm leads to superparamagnetic effect, where the magnetic energy per grain becomes too small to avoid a thermally activated magnetization reversal and the loss of information. Alternatively, a well-ordered array of isolated magnets the size of single-to-few atom can be used, each of which storing a single bit of information. To achieve the ultimate limits, we need to find magnetic centres (*i.e.*, single atoms or clusters consisting of few atoms), that have high values of magnetic anisotropy energy (MAE) to stably withstand random thermal excitations that can result in the information loss. The centres also need to be thoroughly hold at one specific place. Present theoretical thesis with the usage of density functional theory (DFT) expands my Bachelor Thesis "Insights into the interaction of transition metal atoms with defective graphene from DFT" where we examined the properties of single transition metal (TM) atoms adsorbed at defective graphene and found systems with interesting MAEs but still too low to allow a practical usage of the systems, *i.e.*, at least corresponding to 77 K (the temperature of liquid nitrogen, which is abundant and cheap). This thesis expands the research by adding second TM atom on top of the already adsorbed atom, as an upright geometry is essential to achieve a large MAE. We examined the stability of the perpendicular orientation of the dimer; the stable dimers were investigated further, we evaluated various geometry properties, an adsorption energy of the second atom, magnetic moments, and charges located on the atoms. We also elucidated the bonding mechanism and proposed equations describing it. All magnetic systems were also examined in the non-collinear mode that predicted high values ($\geq$ 15 meV) of MAE in 22 systems with Os or Ir as the atom farther from graphene and according to the best of our knowledge, many of the systems were calculated for the very first time. The highest value of MAE ($\sim$170 meV) was achieved in OsPd@NSV, which corresponds to the blocking temperature $\sim$ 44 K with an enormous theoretical information density $\sim$ 490 Tb$\cdot$inch$^{-2}$. The physical origin of the MAE was discussed based on the electronic structure. The large MAE is followed by a substantial magnetic moment anisotropy on the TM atom farther from graphene.

**CONTENTS**

## INTRODUCTION

A magnetic-storage technology is essential in data centres because it is more reliable and still cheaper than other techniques. One of the biggest problems of the current digital universe is in the widening gap between the storage capacity demand and the real storage capacity. That is due to the constantly slower improvements of the present hard-disk drives (HDDs) caused by the superparamagnetic effect that arises due to the small volume of magnetic grains that hold the information. In the very beginning, the information density in them followed the famous More's law: it doubled itself every second year. Unfortunately, now it is not true, as it's value approaches some limit, which was theoretically determined by Wood[1] to be 1 Tbit·inch$^{-2}$. This limit was broken in 2010s [2] but it is clear that we are reaching boundaries and new technologies need to come. Modern possibilities are summarized in paper by Shiroishi[3], some of them are intensively researched by HDD manufacturers, and they are considered to be very promising for future applications.[4]

A fundamental research in this field is focused on the classical limit of the data storage centre. Experiments[5–8] have shown that the storing and retrieval of the information saved in single atoms adsorbed at surfaces is possible, however, at extremely low temperatures and methods involved are neither user-friendly nor affordable. At higher temperatures, magnetic centres can change their magnetization due to random thermal excitations (RTEs) and the information is lost then. Actually, the MAE set a fundamental constrain for the minimal size of a bit for magnetic data storage. The MAE competes with RTEs, long information lifetimes in HDDs must correspond to high values of the MAE of its magnetic recording medium. According to the Néel relaxation theory, we would need to have the MAE $\sim$ 285 meV to achieve a 10 year thermal stability up to temperature of 77 K (the temperature of liquid nitrogen), which is impractical in personal devices, but could be achieved in the professional data centres.

One of the most important requirements to achieve such information densities is a suitable magnetic material. The use of atomistic first principles simulations to design materials with magnetic properties tailored on the level of single atoms at the core of the present thesis was proved to be very useful. Theoretical works[9–11] showed that dimers of $5d$-$3d$ transition-metal (TM) atoms have a high MAE which can be enhanced to $\sim$ 0.1 eV if the dimer is placed on pristine graphene. For real applications, the magnetic dimers need to be thoroughly anchored to prevent them from clustering. The clustering may

alter the desired magnetic properties of the individual dimers, but more importantly, the information held in the magnetic centres would gradually shuffle and so it would be completely lost.

Atomic vacancies in the graphene lattice can be created intentionally.[12] A highly ordered array of vacancy defects may be used for engineering the position of atom-sized magnets with an atomic precision and prevent their diffusion, at the same time conserving their size, symmetry, and MAE. Therefore, in my Bachelor Thesis we decided to explore the possibilities to use defective graphene as an anchoring site for the TM atoms from the VIII B group (Fe, Co, Ni, Ru, Rh, Pd, Os, Ir, Pt). The examined defects were following: single vacancy (SV) and divacancy (DV) in its pristine form as well as decorated by pyridinic nitrogen atoms (NSV and NDV). We showed that defective graphene is able to anchor TM atoms strongly in contrast to the other adsorption sites on an ideal part of the graphene layer and also that the adsorbed TM atoms in many cases remained magnetic. We also showed that single Ir atom adsorbed at defective graphene has a significant MAE of $\sim 7$ meV. This is a remarkable result (comparable to the MAE reported for Co atoms on Pt(111) in the seminal work by Gambardella *et al.*[5]) for a single TM atom, but the MAE needs to be significantly enhanced for real applications.

All these results are also included in our recent paper[13] with significantly developed explanations of the observed properties. Inspired by the possibility to achieve a large MAE in heteroatomic TM dimers (Refs. 9–11), the mentioned paper[13] also contains a section of TM dimers, where we examined defective graphene with Ir atoms pinned by defects as an initial geometry and added another TM atom on top of the Ir atom. We showed that these TM dimers are stable and the adsorption of the second TM atom is energetically favourable. The magnetic moment of the Ir atom closer to graphene is significantly quenched while the magnetic moment of the upper TM atom is usually high. We proposed a simple method to estimate the total magnetic moment of the supercell. We found three perpendicularly-stable systems with interesting MAE values: $Ir_2$@NSV ($\sim 36$ meV), $Ir_2$@NDV ($\sim 38$ meV), and OsIr@NSV ($\sim 50$ meV). The high MAE values are always accompanied by a significant magnetic anisotropy of the upper TM atom. We also deeply examined the properties obtained in the non-collinear mode.

Our paper[13], which is also attached to this Thesis, presents an essential part of this Master's Thesis. Here we further extend it by an investigation of all possible dimers that can be formed from TM atoms from the VIII B group to provide a thorough summary of

this field of interest together with the results already published in Ref. 13. We followed the same procedure to examine the scalar-relativistic (SR) and non-collinear (NCL) properties. We also added new procedures in the SR mode, namely a more thorough examination of the perpendicular stability. We also significantly generalized the proposed model describing the magnetic moments and the bonding mechanism within the TM dimer. This Thesis does not contain all already published[13] NCL properties due to its already extensive size, and we therefore recommend the reader to find the additional information in the paper. NCL properties of the systems with a high MAE discovered in this Thesis will be thoroughly examined further and it shall also result in another publication.

# I. THEORETICAL BACKGROUND

## A. Current Hard Disk Drives and Future Options

Data centres, desktop computers, and laptops use HDDs[14] or solid-state drives (SSDs)[15] to store the information. While the history of the former type is much longer, the latter experienced a great boom in the past decade and none of them is now unequivocally superior. In a personal sphere, SSDs overpower HDDs in their reading and writing speed of a random scattered information and therefore they are often used to store the operating system. SSDs are moreover very light, small, and resistant to the mechanical damage caused by the movement of the device during its operation. HDDs are nowadays still cheaper (currently $\sim$ 1 CZK/GB; SSDs cost $\sim$ 2.5 CZK/GB), they theoretically allow more rewriting cycles and the information should be in principles saved for longer time (SSDs may theoretically lose the information over time). The most importantly for data centres, in the event of a device failure, the information can be retrieved from the magnetic storage, while with SSDs it is virtually impossible. When it comes to the reading of long blocks of data, HDDs are slower than SSDs but both achieve such speeds that a normal user cannot spot the difference.

In the very beginning of the computational technologies, all the information was stored in the magnetic tapes that were packed in cassettes. With the invention of HDDs, this very slow kind of data storage (in terms of a random access) vanished from the personal computers and now it is usable only for large blocks of data that can be read progressively. They are currently used as a backup in large data centres. New materials renewed the interest in magnetic tapes as they provide a cheap alternative to HDDs. IBM with Fujifilm in December 2020 presented a cassette that should have an enormous capacity of 580 TB.[16]

The information is in SSDs saved in integrated circuits (that is the source of their unique properties) and therefore they do not benefit from the development in the research of the magnetic nanostructures, and they will not be considered further in the present work. Magnetic tapes and HDDs use magnetic materials to keep each single information bit, and they can be further improved by the usage of better materials, which is also the aim of our research.

Let us now focus on the principles of HDDs to completely understand the aim of the thesis. Present HDDs contain more than one disk, these disks are called platters, *cf.*, **Fig. 1**. The basic function of a single platter is similar to a gramophone disc. It rotates

and it is continually read by a reading head and the obtained information is passed to the rest of a computer. In contrast with a gramophone disc, the information is not saved continually but discretely in well-separated grains. Each grain can hold maximally one state (bit) that can have two possible values that are determined by an orientation of local magnetization; but now it is a common practice to have more grains (a domain) to hold one bit because of the reliability. Another difference is the ability of HDDs to read the information randomly by an easily adjustable position of the reading head in contrast with the spiral-like movement of the reading head of a gramophone. Platters are made of non-magnetic material that is covered by a layer of grains of ferromagnetic material (traditionally an alloy consisting of Co, Cr, and Pt with additional admixtures depending on the manufacturer). Grains are separated by a non-magnetic material that prevents the neighbouring grains from affecting each other. A concrete bit can be accessed by a proper combination of the position of the reading head and the rotation phase of the platter. The writing is performed similarly, the head needs to be above the intended spot and then it applies a strong magnetic field to change the magnetization of the given bit.

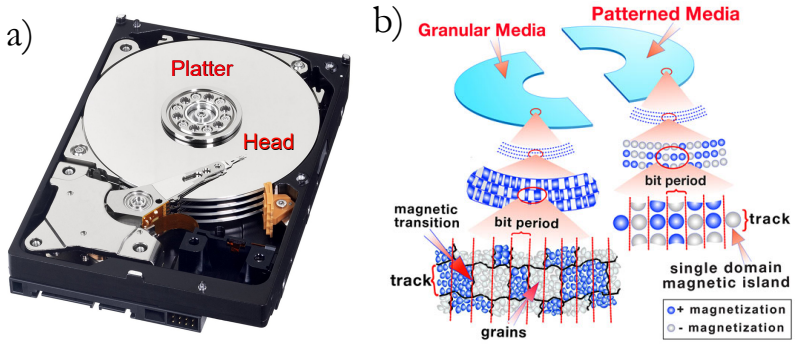


**FIG. 1:** HDD. a) Real image showing platters and the reading-writing head. b) Scheme highlighting the grain structure and a comparison with the bit-patterned media. Reprinted from https://www.printerland.co.uk/product/lexmark-320gb-hard-disk-drive/137373 and https://www.techrepublic.com/index.php/pictures/images-new-hard-drive-technologies/.

As we mentioned earlier, the information density stopped to rapidly increase and it approaches a limit. The initial rapid increment followed the More's law that stated that any computer component can double its performance every second year. The inceptive development was caused by the improvement of the used manufacturing technologies that allowed to place more of smaller building blocks to the same place as less bigger blocks that were used in the previous technological generation. Nowadays, each of the component reached (or is reaching) an absolute limit of the downsizing that is determined by the quantum mechanics. The smaller the object is, the more important role of quantum

effects we can expect. That effects are connected with a probability, *i.e.*, the downsizing of the basic building blocks inherently leads to a lower reliability or certainty of the information.

The limit of the currently used HDDs originates from the magnetic stability of the grains. Too small grains are in (or close to) a superparamagnetic regime, *i.e.*, they can spontaneously (due to RTEs) change their magnetization and the information in them would be easily lost. R. Wood in 1999 derived[1] that the highest achievable information density is in orders of 1 Tbit·inch$^{-2}$, so that the grains have such size to remain ferromagnetic at room or increased temperature and the platter is engineered to have $\sim 5$ grains holding one bit because due to the manufacturing reasons (the precision of the grain position) it would be risky to have smaller number of such grains. The reading and writing head was also considered to be a limiting part but that was due to the technology that was not fully developed yet.

An enormous demand of devices with higher information capacities led to an extensive research how to break the Wood's limit, which can be divided to two branches.[3] 1) Bit-patterned magnetic recording (BPMR) that emphasizes the role of a perfect alignment and a uniform size of the magnetic centres. In a perfect case, we could expect one centre to be holding one bit. That centres need to be perfectly aligned, so they could be precisely addressed by the reading/writing head without any significant noise from its neighbouring centres. The information density could reach 4 Tbit·inch$^{-2}$ if the magnetic islands were made of the same material as it is used in the conventional HDDs. Smaller centres of the same material would get into the superparamagnetic regime; they must be made of a magnetically harder material (than the presently used) to resist RTEs. The current head would not be able to write an information to a such hard material by a simple application of the magnetic field, which emphasizes the necessity of the second branch. 2) More advanced writing heads are necessary to be able to write to the magnetically harder materials as they require an additional locally applied energy to be able to change the magnetization of the magnetic centre. The most promising techniques are a Microwave assisted magnetic recording (MAMR) and a Heat assisted magnetic recording (HAMR), the latter should theoretically lead to the enormous densities of 100 Tbit·inch$^{-2}$ and now it is extensively tested by the HDD manufacturers[4]. These techniques are more or less connected with a more traditional BPM. In the small magnetic centres with the size of a single atom, we can focus on a direct manipulation with the MAE: a large MAE is needed

to stabilize a magnetic bit against a thermal agitation; a low MAE is desired during writing information. Since ferromagnetism critically depends on the exchange interaction between unpaired electrons, the change in the occupation number of TM-*d* orbitals and the MAE may be controlled by electric fields.[17–19] We will examine the dependece of MAE on the magnitude of the external field in our next research.

Despite the recent success in the research of the BPM[20–22], a serial manufacturing of the BPM in widespread areas (the area of a platter is extensive if compared with the area of one bit) presents the biggest obstacle to be overcome before the commercial production of a new generation of HDDs. Recent approaches rely on the usage of self-assembly of polymers or even of single Dy atoms[6] on graphene deposited on the Ir(111) surface, *vide infra*. We decided to examine defective graphene as a basis material that would hold TM dimers thoroughly in the defects that could be made in graphene by other sophisticated techniques, *e.g.*, by an irradiation[23] or by the gas bombardment.[24]

### B. Systems Containing Magnetic Centres Consisting of Few Atoms

Only the magnetic centres with hysteresis are able to store the information that is saved in the orientation of the magnetic moment; the stability increases with the increasing magnetic hardness of the material. While classical hysteresis originates in a collective phenomenon, it is more convenient to express the stability of the information in the single nanostructures in terms of the MAE. Naturally, atoms in a gas phase cannot have non-zero values of the MAE as there is no barrier to prevent them from the change of their magnetic moment. The smallest objects that can have non-zero values of the MAE are dimers (discussed in the end of the subchapter) or single atoms that are adsorbed at surfaces (they are discussed in the following paragraphs).

A highly-ordered lattice of Dy atoms can be prepared by a self-assembly of Dy atoms at graphene that was grown on the surface of Ir(111).[6] Graphene and Ir(111) have a small mismatch of their lattice constants which leads to the formation of a moiré-like pattern, *i.e.*, periodically repeated areas with a different potential to adsorb the Dy atoms; they tend to adsorb at C-rings that are placed directly above an Ir atom. There is one such place in one 10 x 10 graphene cell. Nevertheless, the binding is too weak and can be achieved at temperatures bellow 10 K. The Dy atoms start to move along the surface at higher temperatures and the Dy super-lattice is destroyed. The authors observed long magnetic relaxation times (in the order of 1000 s) at extremely low temperatures (2.5 K).

Theoretical calculations predicted the MAE of the system of 21.4 meV but there was another tunnelling path with an energy barrier of 5.6 meV. Further calculations revealed that the higher rotational symmetry of the Dy atom's surrounding results in fewer paths available for a quantum tunnelling. Graphene plays another important role: it separates well electronic states of the Dy atom from the phonon bath of the bulk Ir that would introduce an unwanted noise.

Another important milestone in the magnetic storage of the information in magnets the size of a single atom was a preservation of magnetization of a single Ho atom that was demonstrated[7] on an Ag(100) surface that was covered by a MgO(100) film. The relaxation of magnetization at 2.5 K and 10 K happened after more than 20 minutes. A rise of temperature to 20 K led to a decrement of relaxation time to $\sim$ 10 minutes. Magnetic hysteresis was observed until temperature reached $\sim$ 30 K. The authors also proved that more than 3 layers of MgO are necessary to separate phonons of bulk Ag from the states of the Ho atom to obtain the strongest hysteresis of the magnetization on the Ho atom.

The research of the same system was later extended[8] to examine the possibility to read the saved information remotely. The authors added a single Fe atom to the vicinity of an already adsorbed Ho atom. Then they wrote the information (one bit) to the Ho atom by using a scanning tunnelling microscope (STM) tip placed above the Ho atom (by applying voltage pulses). The change of magnetization was confirmed by the local change of magnetoresistance. A change in electron spin resonance (ESR) spectra of the neighbouring Fe atom happened in the same time (they are measured remotely). Fe aligns its magnetic moment with an external magnetic field (a common practice in ESR measurements) but the absorption frequency of an iron atom is slightly affected by an orientation of a local magnetic moment presented on the Ho atom; the effect is called Zeeman splitting. The adsorption frequency generally shifts to lower frequencies if the magnetic moment of the neighbouring Ho atom is parallel to the external magnetic field and to higher frequencies if the orientation is antiparallel. The shift in frequencies is inversely-proportional to the distance of atoms. Thanks to that the authors were able to distinguish 4 different states of 2 neighbouring Ho atoms (one closer to the Fe atom and the second one farther, *c.f.*, **Fig. 2**). The closer Ho atom had a bigger impact on the adsorption frequency, while the farther Ho atom slightly modified it.

The same authors further extended[25] their research of the same system under an ex-

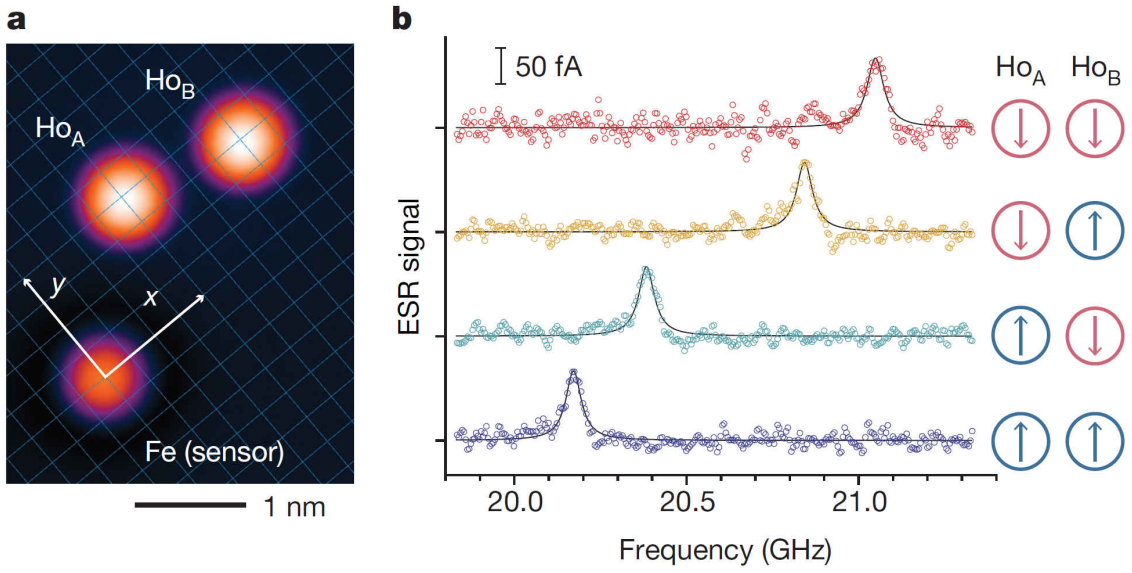


**FIG. 2:** A scheme illustrating the experiment performed by Natterer *et al.*[8], a) positions of the sensor Fe atom and of the Ho atoms, each holding one information bit, b) measured ESR spectra. Reprinted from Ref. 8 ("Reading and writing single-atom magnets", by Natterer *et al.*, 2017, *Nature, vol. 543, 226.* Copyright 2017 Nature).

treme magnetic field of 8 T. The stable magnetic state of a single adsorbed Ho atom (magnetic moment is parallel to the external magnetic field) is in energies by 9.4 meV lower than the metastable state with an antiparallel magnetic moment. The authors wrote the information to the antiparallel state and observed its stability at given temperatures. Despite the high energy difference, the authors did not spot spontaneous switching from the metastable to the stable state at 35 K which implies that the energy barrier is high. The magnetic moment started to spontaneously switch at 45 K which allows a reader to approximately estimate the height of the barrier. The Ho atom started to move along the surface at 50 K which points to the limitations in the real applications.

Above mentioned seminal works showed that the single atom data storage is indeed possible but at very low temperatures and there are two reasons for that. 1) The barrier of the magnetic moment switching of the examined single atoms is too low to retain RTEs at more than 40 K, and we need to search for atoms/clusters with a higher barrier. 2) The magnetic atoms at higher temperatures started to move along the surface which would lead to the loss of the information in the real HDDs. We therefore need to thoroughly anchor the magnetic centre to a concrete spot. We theoretically addressed both issues by a utilization of the TM dimers anchored to defective graphene.

The traditional costly and time-consuming, trial-and-error approaches to develop new magnetic materials with desired properties can be overtaken by detailed understanding

of the magnetic phenomena on the level of individual atoms and structure-property relationships, with the help of theoretical modelling. We assume that the height of the energy barrier is equal to the MAE. The advantage of that approach is that we are able to directly identify the determining properties responsible for high values of the MAE, and we can attempt to utilize the knowledge to engineer systems with desired properties. A systematic study[9] of homoatomic TM dimers from VIII B group revealed three systems with remarkable values of the MAE: $Rh_2$ ($\sim$ 47 meV), $Ir_2$ ($\sim$ 70 meV), and $Pt_2$ ($\sim$ 46 meV). The authors also pointed out that the origin of the high MAE is related to the presence of the two-fold degenerate state at the Fermi energy ($E_F$) that is occupied by a single electron.

Since a high MAE requires large spin and orbital magnetic moments and a strong spin-orbit coupling (SOC), heteroatomic dimers of $5d$-$3d$ atoms attracted a significant attention as candidates for systems with a large MAE.[10] $3d$ atoms (Fe, Co, and Ni in particular) have high magnetic moments even in their bulk state but a very low SOC constant as an element. Oppositely, $5d$ elements have high values of the SOC constant, but they are magnetic only in small clusters, not in the bulk state. A combination of proper $3d$ and $5d$ atoms may lead to an enhancement of the magnetic moment of the $5d$ atom which may result in a higher MAE caused by a strong SOC of the $5d$ atom. Indeed, the MAE of the IrCo dimer is similar to the MAE of $Ir_2$. The same work also proved that DFT is able to calculate properties of the dimers with a similar precision as methods resulting from the wave function theory. The authors also examined MAE after the adsorption of a TM dimer in a perpendicular position on pristine graphene. It led in general to a reduction of the MAE or to its complete quenching in most systems, but in IrCo@graphene (Co atom down, placed above the centre of a hexagon formed by 6 neighbouring C atoms) it even enhanced MAE to $\sim$ 90 meV. A closer inspection revealed that the adsorption decreased magnetic moment on Co and also weakened the bond within the TM dimer which gave the upper Ir atom more free-like properties and significantly enhanced its anisotropy of orbital magnetic moment. The placement of the IrCo@graphene on Cu(111) surface[11] led to a further enhanced interaction between the Co atom and the support which lifted the MAE to an enormous value of $\sim$ 200 meV. The main contribution to MAE comes again from the two-fold degenerate state at $E_F$ occupied by a single electron.

Our recent research[13] revealed that single TM atoms are in most cases hold thoroughly at defects in graphene and many retain high magnetic moments. Neverthe-

less, only Ir showed interesting values of the MAE: Ir@DV ($\sim$ 7 meV) and Ir@NSV ($\sim -10$ meV). TMIr dimers also showed a high MAE, mainly of $Ir_2$@NSV ($\sim$ 36 meV), $Ir_2$@NDV ($\sim$ 38 meV), and OsIr@NSV ($\sim$ 50 meV). Magnetic moments of Ir atoms closer to graphene were always significantly decreased in contrast with the systems with one adsorbed Ir atom, while magnetic moment of the upper TM atom remained high and experienced a substantial increment of orbital magnetic moment if the magnetization was perpendicular to the graphene plane (parallel to the TM dimer). The aim of the present thesis is to extend that research to all possible TMTM dimers (TM from VIII B group) and to completely and systematically describe mechanisms determining the predicted properties.

### C. Graphene

As we showed above, the magnetic centre needs to be placed on a non-metallic substrate to preserve its magnetic state. The presence of the phonon bath of metal would speed up the spontaneous relaxation of centre's magnetization. Pristine graphene acts as a good filter and, moreover, defective graphene can thoroughly anchor the magnetic centres and prevent them from clustering.

Pure carbon can exist in many structural forms, *i.e.*, allotropes. The most known allotropes of C are diamond and graphite, both have completely different properties. The former is formed by $sp^3$ hybridized carbon atoms and the whole structure is held together by covalent bonds (therefore diamond is one of the hardest materials), while the second mentioned contains $sp^2$ hybridized carbons that form sheets which are held together by a relatively weak van der Waals interactions (therefore we are able to write by pencils). Scientist were for a long time wondering whether it would be possible to split graphite to single layers. That was experimentally proved in 2004 by Konstantin Novoselov and Andre Geim[26] that were able to use an ordinary adhesive tape to prepare an one-atom-thick layer of graphite that they called graphene. The existence of 2D materials had been earlier considered to be unreal but this direct evidence renewed the interest in this field of research and hundreds of 2D structures have been already described. We are going to focus only on graphene as it is the most important material for the thesis.

As it was mentioned in the previous paragraph, C atoms in graphene are $sp^2$ hybridized, each C atom is surrounded by 3 other C atoms and many of such C atoms together form a planar sheet. If we visualize the bonds between neighbouring C atoms as sticks, the

whole structure is similar to the honeycomb. Carbon has 4 valence electrons, therefore it in graphene posses one electron that is not involved in the $sp^2$ hybridization. As it is in the $p_z$ orbital and each atom has the same configuration, it is energetically advantageous to delocalize these electrons in the whole structure. This provides graphene with its unique electronic properties. Graphene is widely considered to be one of the best conductors but it is actually a zero-band-gap semiconductor. It also has a very unusual shape of electronic bands, *i.e.*, Dirac cones. Thanks to that, electrons in graphene behave as they were massless which results in the new phenomena of quantum Hall effects and an ultra-high electron mobility.[27] Its other extraordinary properties (the extreme strength, thermal conductivity, and optical transmittance) are not important for the aims of the thesis and will not be discussed further.

Pristine graphene has only limited applications. It is also chemically nearly non-reactive and therefore it is not very suitable for direct modifications. Graphene derivatives are becoming more important because their properties can be well tuned to suit the desired needs, and they have therefore a much greater application potential. The expansion of the chemistry of graphene begin with the discovery of fluorographene[28,29] that allows to perform many reactions that are similar to that commonly carried out in the organic chemistry, *e.g.*, the synthesis of nitrogen doped graphene[30] or of cyanographene (CN-Gr) and graphene acid followingly[31]. CN-Gr has been shown to trap Pt as single atoms that then act as single-atom catalysts.[32] Another possibility how to induce a reactivity of graphene is by the creation of vacancies in it (*i.e.*, to create defective graphene);[33–35] the C atoms surrounding the defect are more reactive as they possess an unpaired electron, a dangling bond, or they form new bonds that are often longer than in the ideal case.

Pristine graphene is also unsuitable for our purposes. Experiments[36] showed that Pt atoms are mobile on pristine graphene; DFT calculations[37] predicted relatively small diffusion barriers for all $d$ elements. That would mean that the information saved in the magnetic cluster in these systems would be therefore easily lost. On the other hand, TM atoms are in vacancy defects bound much more strongly[13], so defects may anchor the individual atoms or dimers preventing them from clustering and preserve their desired magnetic properties. The defects can be created unintentionally during the growth of graphene or intentionally[12], *e.g.*, by an irradiation. While the former would cause complications in the fabrication of nano-HDDs as it would introduce additional (interstitial) position to the perfectly aligned lattice of magnetic centres, the latter would need to be

done additionally with a perfect precision and it will probably cause the hardest difficulties during the mass fabrication of the nano-HDDs.

A thorough discussion of defective graphene is presented in Ref. 27. A graphene defect can be formally most easily created from pristine graphene by a removal or a substitution of atom(s), *cf.*, **Fig. 3**. SV is created by a removal of a single C atom. That leaves 1 unpaired electron on two neighbouring C atoms and 2 electrons (a dangling bond) on the remaining atom. Unpaired electrons are energetically unfavourable and therefore they usually form a new bond that is slightly longer than the other bonds in graphene. Both configurations were identified by high-resolution transmission electron microscopy (HRTEM). The dangling bond remains unaffected but it is responsible for the reactivity of the whole defect. The formation energy of SV is $\sim$ 7.5 eV and it can migrate with a barrier of $\sim$ 1.5 eV. SV is spin-polarized and, thus, creates paramagnetic centres in graphene.

DV is created by a removal of two neighbouring C atoms from pristine graphene or by

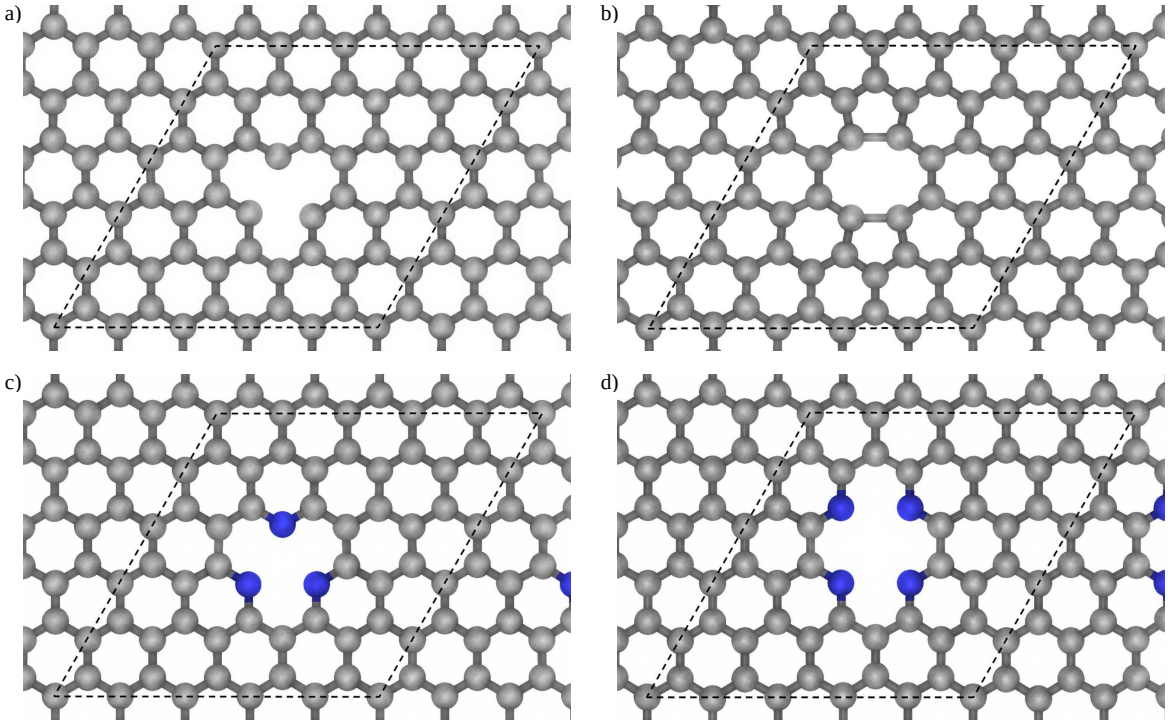


**FIG. 3:** Relaxed supercells of defective graphene: a) single vacancy (SV), b) divacancy (DV), c) single vacancy decorated by pyridinic nitrogen atoms (NSV) and d) divacancy decorated by pyridinic nitrogen atoms. Grey / blue spheres represent C / N atoms. Supercells are enclosed by broken lines. Reprinted from Ref. 13 ("Large magnetic anisotropy in an OsIr dimer anchored in defective graphene", by Navrátil *et al.*, 2021, *Nanotechnology, vol. 32, 230001.* Copyright 2021 Nanotechnology).

the conjunction of two single vacancies. Pristine DV would leave one unpaired electron on each of the 4 C atoms surrounding the defect. The structure often undergoes a reconstruction and two new bonds are formed; it leads to the formation of 2 fivefold rings and 1 eightfold ring, the defect is systematically labelled $V_2$(5-8-5). Energetically slightly favourable defect $V_2$(555-777) cannot be thoughtfully created as straightforwardly. The formation of both reconstructed defects and of the unreconstructed defect was experimentally proved by HRTEM. The formation energy of the reconstructed divacancy defects is $\sim$ 8 eV and thus comparable with the formation energy of SV. That illustrates how energetically disadvantageous the dangling bond in single vacancy is, *i.e.*, the removal of the C atom with the dangling bond nearly does not require any additional energy. The reconstructed $V_2$(5-8-5) contains neither unpaired electrons nor dangling bonds and it is therefore non-magnetic.[38]

We are also interested in vacancies decorated by pyridinic nitrogen atoms, *i.e.*, N atoms that are members of the sixfold rings and the N atom is not bound with any additional atom outside the ring. N atoms are in NSV placed farther from each other[39] which may be caused by the mutual repulsion of the electron pairs oriented to the vacancy. One N atom should posses an unpaired electron (that is confirmed by magnetic moment of $\sim$ 1 $\mu_B$) but the structure is symmetrical and the electrons in the vicinity of defect are therefore rather delocalized. The substitution of C atoms by N atoms at single vacancy should be energetically favourable.[40]

N atoms in NDV are also farther from the centre of the defect, and they preserve the initial shape of the vacancy[39,41], in contrast with the pristine divacancy. This type of defect does not contain any unpaired electrons and it is therefore non-magnetic. It is also energetically advantageous to substitute the C atoms by N atoms.[40]

We end this subchapter by a seminal work of Lin *et al.*[24] that experimentally showed that the intentional preparation of graphene defects decorated by pyridinic nitrogen atoms is indeed possible. They bombarded pristine graphene by a gas mixture consisting of $N_2$ and $O_3$ (1:1) and then they were able to observe the formation of single vacancies decorated by 1 – 3 N atoms and divacancies decorated by 4 N atoms. The authors report more than 60 defects in the 50 x 50 nm area which would correspond (if in each of such defect one magnetic center with a sufficiently large MAE would be stable) to the information density of $\sim$ 15.5 Tbit·inch$^{-2}$ which is much higher than in the currently available HDDs, but the achieved lattice is not highly ordered as it would be necessary. Most importantly for the

aims of our thesis, the research also experimentally showed that TM atoms are strongly attracted by the defects, and they spontaneously and thoroughly anchor to the vacancies.

### D. Theoretical Part

A brief introduction to the computational chemistry is well summarized in the book *Theoretical Surface Science* by Axel Groß.[42] There are two possible approaches how to *ab-initio* tackle the computational chemistry problems: the wave function theory (WFT) and density functional theory (DFT). The former is older and practically more accurate but it is generally much more demanding and therefore allows calculating of smaller systems than DFT. The latter, in contrast, manages to calculate bigger systems and it may be less accurate but it offers possibilities how to achieve a similar precision as WFT. We carried out the DFT calculations and therefore we focus on its description, but we start with the common background of WFT and DFT.

The origins of quantum chemistry are strictly connected with a time-independent Schrödinger equation:

$$H\Psi(r) = E\Psi(r), \tag{1}$$

$\Psi(r)$ represents the wave function, $E$ are energy eigenvalues, and $H$ is the Hamiltonian in the form:

$$H = T_{nucl} + T_{el} + V_{nucl-nucl} + V_{nucl-el} + V_{el-el}, \tag{2}$$

where $T_{nucl}$ and $T_{el}$ stand for kinetic energies of nuclei and electrons respectively, and $V_{nucl-nucl}$, $V_{nucl-el}$, and $V_{el-el}$ for electrostatic energies of each pair nucleus-nucleus, nucleus-electron, and electron-electron respectively. The system is fully described by its wave function but this form is analytically soluble only for few systems, *e.g.*, atoms (ions) with a single electron because the solution consist in solving the differential equations. The numerical solution is not easy either as each electron in the system adds three independent variables to the wave function.

Electrons have extremely low mass when compared with the nuclei they surround and therefore they can very easily follow the nuclei's motion. The Born-Oppenheimer (BO) approximation is based on that and states that nuclei and electrons can be treated independently, *i.e.*, that electrons find their groundstate in any configuration of the nuclei. The spatial configuration of electrons, on the other hand, creates the potential that acts on nuclei and forces them to shift. This allows us to separate full Hamiltonian (**Eq. 2**)

to two independent parts:

$$H_{el} = T_{el} + V_{nucl-el} + V_{el-el}, \tag{3}$$

$$H_{nucl} = T_{nucl} + V_{nucl-nucl} + V_{nucl-el}. \tag{4}$$

In normal conditions, the quantum nature of nuclei can be neglected, and they can be treated as classical objects following the Newtonian dynamics, *i.e.*, for the n$^{th}$ nucleus:

$$M_n \frac{\partial^2 R_n}{\partial t^2} = -\frac{\partial E_{el}}{\partial R_n}, \tag{5}$$

where $M_n$ is the mass and $R_n$ are coordinates of the n$^{th}$ nucleus, $t$ stands for time, and $E_{el}$ are eigenenergies of the electronic Hamiltonian. The BO approximation is one of the most important and successful scientific approximations and in most cases it causes only small deviations from the experimental values.

The BO approximation has also a practical impact on the codes performing the calculations. Most codes perform the relaxation in two nested loops. The inner loop relaxes electrons in a fixed set of the nuclei coordinates, the outer one relaxes the nuclei according to the electrostatic potential of the relaxed electrons. This division to two loops allows to separately assess the convergence success and also to define independent breaking condition for each loop, *e.g.*, many codes break the outer loop if the forces acting on each atom are smaller than a given parameter, and the inner loop if changes in the total energies of two successive steps are smaller than a given value.

We need to know in all calculations how close we are to the values of groundstate properties. If the implemented equations are correct and the used method is variational, we may take an advantage of the variational principle. It states that the lowest energy corresponds to the most preferred configuration, the other configurations therefore inherently need to have higher total energies. Each step during the relaxation leading to the lowering of the total energy therefore also leads to the more realistic electronic structure. Here we need to emphasize that it may not be true in some case, *e.g.*, the famous band-gap problem of conventnional DFT[43]. Moreover, not all the computational methods are necessarily variational, and they need another criterion how to assess the precision of their solution.

Now we skip the other aspects of WFT calculations as they are not crucial for the thesis, and we focus on the usage of pseudopotentials that are very advantageous for both WFT and DFT approaches. As it was previously noted, the complexity of calculations increases with an increasing number of electrons in the system. Concurrently, it has been

known for a long time that the properties of elements are determined mostly by their valence electrons, although their core electrons (*i.e.*, the electrons that are not valence; in many cases also the valence electrons that form a full shell, *e.g.*, $d^{10}$) cannot be easily omitted in the thought processes. Calculations showed that the core electrons are hardly affected by the atom's neighbourhood and therefore it is not necessary to include them explicitly to the calculations; instead it is advantageous to include them implicitly in the form of some potential. The usage of a simple electrostatic potential would be a very rough approximation, the potential must be energy dependent and therefore it is called a pseudopotential. Pseudopotentials of light atoms (from the second period) have only a small impact on the performance but it becomes crucial in the heavier atoms, *e.g.*, we can use 8 electrons instead of 76 electrons to reasonably describe an Os atom. Pseudopotentials must well represent the interactions of the core with objects outside the core radius and it should be as soft as possible inside the core radius to save computational time. There are different kinds of pseudopotentials but it is beyond the aims of the thesis to compare them. We close this subchapter by a statement that pseudopotentials are extremely useful but their creation is very time-consuming and there are some teams that focus mainly on the generation of pseudopotentials for different applications.

### *1. Density Functional Theory*

Theories based pristinely on the wave function and their derivatives, *e.g.*, Hartree-Fock (HF) and post-HF initially achieved a great success, but they very quickly reached their limits as they were unable to calculate with tens of atoms and even now with a much greater computational power they present a very tough task. This motivated Pierre Hohenberg and Walter Kohn to look for other ways how to tackle the quantum chemistry calculations, and they laid the groundwork for DFT.[44]

Chronologically, the first theory similar to DFT was proposed by Llewellyn Thomas and Enrico Fermi; now it is known as the Thomas-Fermi theory of the homogeneous electron gas. They proposed that a potential of the homogeneous electron gas is dependent on the electron density $n(r)$ at each point of the examined supercell. It is apparent that the theory is inapplicable in real systems because negatively charged electrons cannot be homogeneously distributed around positively charge nuclei. Its another significant disadvantage is that the connection between the Thomas-Fermi theory and WFT is far from being straightforward.

Hohenberg and Kohn proved that a system with a given external potential (the potential of the nuclei does not originate from the electron gas and therefore is labelled as external) can have in the groundstate only one specific corresponding electron density, *i.e.*, the system is fully described by its electron density and the role of the electron density is similar as of the wave function. If the electron density of a system is known, it is formally possible to determine its full Hamiltonian and all its properties accordingly.

The evaluation of the total energy is necessary for a proper relaxation (*cf.*, a variational principle), and therefore the functional of the total energy is of the highest importance. The total energy of a system can be expressed as the minimal value of the total energy functional (of various electron densities) that consists of more members:

$$E_{tot} = \min_{n(r)}(E[n]) = \min_{n(r)}(T[n] + V_{ext}[n] + V_H[n] + E_{xc}[n]), \tag{6}$$

where $T[n]$ is the kinetic energy functional of non-interacting electrons, $V_{ext}[n]$ is the energy functional of the interaction between electrons and nuclei, $V_H[n]$ is the energy functional of the electrostatic interaction between electrons (similar as in the HF theory), and $E_{xc}[n]$ is the exchange-correlation energy functional that evaluates all the remaining effects. $T[n]$ is problematic in conventional DFT but can be elegantly solved by the treatment of electrons as plane waves. Electrostatic functionals $V_{ext}[n]$ and $V_H[n]$ are even more natural in DFT than in WFT because DFT directly operates with the electron density that enters the formula of the electrostatic potential. $E_{xc}[n]$ is the most problematic term and it is not certain that its analytical form can be derived. Fortunately, it was shown that its value is nearly negligibly dependent on the system and can be therefore evaluated from the electron density by using mathematical expressions with empirical parameters.

Pristine DFT should have much better performance than the HF methods because the electron density within a 3D system is a function of 3 variables; in contrast with WFT where the wave function of system with N electrons is a function of 3 N variables. The problem lies in the relaxation algorithm because it is extremely hard or impossible to exactly construct it. This approach is used in the so-called orbital free DFT, which is very fast but less precise than other DFT methods and it is therefore used only in large systems that are insoluble by other methods.

All other DFT methods stand on the basis developed by Walter Kohn and Lu Jeu Sham. They decided to make a seeming step back and to again incorporate the wave function. The relation between the wave function and the electron density was described

(a long time before the invention of DFT) by Max Born:

$$n(r) = |\Psi(r)|^2. \tag{7}$$

Kohn and Sham decided to split the overall wave function to single-particle wave functions ($\psi_i$) and the Born's equality can be adapted to the new form:

$$n(r) = \sum_{i=1}^{N} |\psi_i(r)|^2. \tag{8}$$

This can be done because all many-body effects are already evaluated in the $E_{xc}[n]$ functional. This allowed the authors to derive equations similar to the HF equations:

$$\left\{ -\frac{\hbar}{2m}\nabla^2 + \nu_{ext}(r) + \nu_H(r) + \nu_{xc}(r) \right\} \psi_i(r) = \varepsilon_i \psi_i(r), \tag{9}$$

which are today known as Kohn-Sham equations.[45] The first term corresponds to the kinetic energy, the other represent potentials describing the same effects as functionals with the same subscripts in **Eq. 6** and together they form the potential acting on one electron. This procedure leads to the formation of so-called Kohn-Sham orbitals that do not have an exact physical representation. Total energy of a system can be expressed as the sum of Kohn-Sham orbital energies that is further modified by other terms:

$$E = \sum_{i=1}^{N} \varepsilon_i + E_{xc}[n] - \int \nu_{ext}(r) n(r) d^3r - V_H[n] + V_{nucl-nucl}. \tag{10}$$

If we knew the exact form of the exchange-correlation terms, the equation to this point would be strictly exact. As we stated earlier, their form has not been sufficiently determined yet and it has to be sophisticatedly substituted by other approximations which then directly affect the precision of the DFT calculations.

This brings us back to the roots of DFT, *i.e.*, to the homogeneous electron gas of which the exchange-correlation term is well known. Local density approximation (LDA) suggests assigning energy to each point in the supercell that would correspond to the exchange-correlation term in the homogeneous electron gas with the same electron density. The main advantage (speed) and simultaneously also drawback (low precision) is the aim to describe the non-local effects (exchange and correlation) by locally assigned values. Because of that, LDA significantly fails in the description of most systems as it tends to overestimate the binding energies and the length of bonds accordingly. LDA surprisingly predicts the properties of bulk systems very well, but it is probably caused by the mutual annulment of both erroneous terms (exchange and correlation) in these systems.

Generalized gradient approximation (GGA) presents a much more sophisticated approach than LDA which is reflected in its success. It uses not only the electron density but also its gradient to describe the exchange and correlation effects. The gradient contains an extremely important information to describe the non-locality of the effects. There are many existing GGA functionals (*e.g.*, very popular functionals of Perdew and Wang (PW91) or of Perdew, Burke, and Ernzerhof (PBE)) and their choice may significantly affect the results. It is therefore necessary to be aware of the strengths and weaknesses of the given functional and to well parametrize it if it accounts with external parameters.

GGA is not able to cover long-range and van der Waals interactions because they act in too large areas to be sufficiently described by local densities and density gradients that enter GGA functionals. The problems can be partly solved by using *meta*-GGA functionals that account with second derivatives of the electron density or by using orbital functionals that aim to assign electron density to orbitals and then to variously treat them. The mentioned procedures are very demanding, and they are used only if it is necessary.

### *2. Spin-polarized Density Functional Theory*

So far, we have completely neglected the spin of electrons, however, it is necessary to include it even in the simple molecule $O_2$. The spin is also crucial in calculations of magnetism. The electron density is in these spin-polarized calculations substituted by a 2 x 2 Hermitian density matrix. **Eq. 10** needs to be adapted to the form[46]:

$$E = \sum_{i=1}^{N_\uparrow} \varepsilon_{\uparrow,i} + \sum_{i=1}^{N_\downarrow} \varepsilon_{\downarrow,i} + E_{xc}[n_\uparrow, n_\downarrow] - \int \nu_{ext}(r) n(r) d^3r - V_H[n] + V_{nucl-nucl}, \qquad (11)$$

where the first two terms contain the Kohn-Sham orbitals for spin-up and spin-down channels, respectively, that may in principle differ. It is apparent that the electrostatic terms are not affected by a spin while the more complex terms are, *i.e.*, the Kohn-Sham orbitals may be different in both spin channels and therefore they may be summed separately. It is also necessary to construct the exchange-correlation functionals that are able to account with the additional effects if they are provided with the electron densities in both spin channels separately instead of a single electron density.

The first attempt to formulate such functional originated from LDA by a small expansion; it is called local spin density approximation (LSDA). This led in systems with unpaired electrons to much better results than with the usage of LDA. However, it may predict wrong spin densities, *e.g.*, in the stretched $H_2$ molecule it predicts localized spin

densities (spin-up density localized on one hydrogen atom and spin-down on the other) while the correct density is the same for both spins. Interestingly, the calculated total energy in the system is correct. Even better improvement was achieved with the implementation of GGA that is from the beginning mostly used in its spin-polarized form and most GGA exchange-correlation functionals are adapted for it.

A collinear mode of the external magnetic field is much less demanding than the non-collinear (discussed later) and it is therefore used more often, unless it is necessary to investigate specific magnetic properties connected with non-collinear magnetism. Collinear external magnetic field can be conveniently oriented to be parallel to the $z$-axis and then it is possible to calculate with spin-up and -down branches nearly independently. The total magnetic moment of the supercell (in Bohr magnetons) can be easily estimated as the difference of the population of spin-up and -down components.

### *3. Bloch Theorem and Plane Waves*

Real systems are very extensive (with respect to the size of atoms) and properties of the bulk are different from that of the surface. Without the periodic boundary conditions (**Fig. 4**), a scientist would need to calculate system with an enormous number of atoms to obtain the real characteristics of the bulk. The periodic boundary conditions lead to such effects that the left side of the supercell "feels" the right side and adapts to its potential. Alternatively it can be viewed as a supercell that is surrounded by the same supercells that strictly copy the original supercell, and that is similar to the real supercells in bulk. Thanks to the conditions, we are able to model the endless structure of, *e.g.*, graphene or diamond by using only two C atoms.

The periodic boundary conditions are also advantageous because they allow to use a theorem formulated by Felix Bloch. If we apply the conditions, the one-particle effective potential must fulfil the following equation:

$$\nu_{eff}(r) = \nu_{eff}(r + R), \tag{12}$$

where R stands for any Bravais lattice vector. Accordingly, we can expect that the single-particle wave function fulfils the equality:

$$\psi_i(r + R) = c_i(R)\psi_i(r), \tag{13}$$

where $c_i(R)$ is a complex number, its modulus must be 1, and therefore it meets the

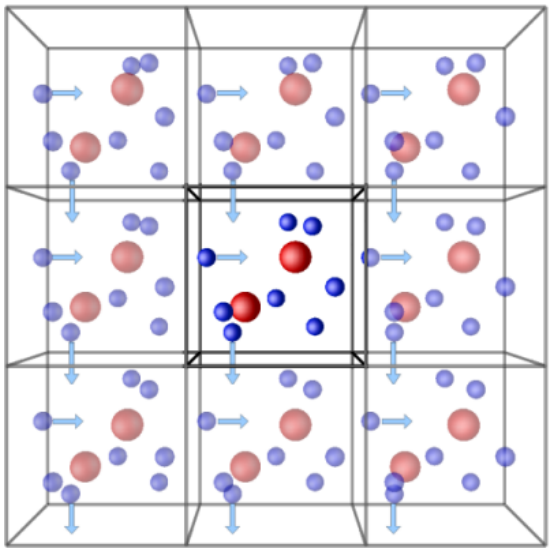

**FIG. 4:** A scheme of the periodic boundary conditions. The supercell in the centre is virtually surrounded by its identical copies and it therefore determines the properties of itself also from outside the examined supercell. Reprinted from http://lammpstube.com/2019/10/30/periodic-boundary-conditions/.

following equality:

$$c_i(R) = e^{ikR}. \tag{14}$$

$k$ stands for a crystal momentum and has a similar role as a quantum number. Now we need to define a general periodic function $u_k(r)$ that meets criterion $u_k(r) = u_k(r+R)$ for any Bravais lattice vector R. Finally, we are able to derive the form of the wave function in the periodic boundary conditions:

$$\psi_k(r) = e^{ikR} u_k(r). \tag{15}$$

Thanks to that we can omit the usage of classical basis sets that can be tricky to choose, and we can use the basis set consisting of plane waves which can be easily controlled by a single parameter. Plane waves can be easily converted to an electron density (and *vice versa*) via a Fast Fourier transformation (FFT). The electron density in the real space is beneficial for the electrostatic interaction terms, and the reciprocal (momentum) space including the plane waves enables to easily evaluate the kinetic energy of electrons. The kinetic energy serves as the criterion determining whether this plane wave is included in the basis set, *i.e.*, its energy must be smaller than a parameter that is often called the cutoff energy.

All plane waves entering the calculation must be in the form required by Bloch theorem. Any wave function entering the Kohn-Sham equations then includes plane waves that

differ only by the reciprocal lattice vector. The wave functions are therefore in the form:

$$\psi_k^G(r) = \frac{1}{\sqrt{V}} e^{i(k+G)r}, \tag{16}$$

where $G$ is a vector in the reciprocal lattice and $k$ must lie in the first Brillouin zone. In the ideal case, the total energy should be calculated by an integration of the whole first Brillouin zone and it should therefore include all occupied energy bands. This would be extremely demanding but, luckily, it is not necessary; the integration can be completely omitted by the usage of only few $k$-points. Moreover, more $k$-points necessarily lead to better results and therefore it is a well-controllable approximation because it can be easily inspected. The Kohn-Sham equations are solved for every $k$-point and the energies of the occupied states are then averaged, and then they are converted to the electron density via the FFT.

The usage of plane waves requires different kind of pseudopotentials and their efficiency is even more important than in the convectional DFT calculations because the plane waves are more influenced by core regions. Pseudopotentials are judged by their softness, *i.e.*, how many plane waves are necessary to describe the system with a suitable precision. Naturally, the fewer waves we need to describe the system, the better. One of the first kind of such pseudopotentials was the augmented plane waves (APW) method proposed by John C. Slater. The waves should be described by different basis inside and outside the core region. In the core region, he suggested to use spherical harmonics and radial functions and thus to augment the plane waves. Although it is in principle exact, this approach is very costly and also experiences problems if the system contains waves with an extensive range of energies. Linearized APW (LAPW) approach helped to significantly reduce the computational costs (waves are energy-independent; the radial parts inside the core radius must be determined only once) and led only to small errors. Resulting forces acting on cores require additional correcting term and they are called Pulay forces. Probably the most advantageous approach, projected augmented waves (PAW), allows to consider the effect of all core electrons with a very high precision while it remains only modestly computationally demanding. PAW method does not require the continuity at the boundary of the core region and instead it exploits the overlap with localized projector functions. If the PAW method is used, the local density of states (DOS) of each atom is projected from the plane waves into its surrounding sphere with a radius determined by a parameter often called a Wigner-Seitz radius. DOS thus can be affected by its choice and it needs to be chosen carefully. In a collinear mode, local magnetic moments on atoms

are calculated as the difference in integrated occupations in both spin channels.

### *4. Relativistic Effects in Density Functional Theory*

DFT in the collinear mode (as we discussed so far) is much less demanding than its non-collinear counterpart. The former is very often sufficient to describe most of the properties and therefore it is used more frequently. The latter approach is necessary to obtain properties that are connected with the magnetic anisotropy, *e.g.*, MAE. We also need to include relativistic effects to obtain reasonable results. Velocities of the core electrons may approach the speed of light and therefore their movement must be additionally described by Lorentzian transformations. This effect is normally included in the pseudopotentials and does not need to be considered further in the calculations. Another important relativistic effect is the spin-orbit coupling (SOC) which arises due to the interaction of the spin of an electron with the magnetic field that is induced by the electron's movement within its orbital. The SOC term is often small and can be reasonably approximated by a scalar in so-called scalar-relativistic (SR) calculations. Once again, the calculations of MAE require explicitly included SOC terms.

The spin-orbit coupling acts predominantly in the immediate vicinity of the nuclei and one assumes its effects to be negligible outside of the PAW spheres. The PAW potentials have been derived from fully relativistic calculations of the atomic or ionic reference calculations.[47] The wave function can be expressed as:

$$\left|\psi_n^\alpha\right\rangle = \left|\tilde{\psi}_n^\alpha\right\rangle + \sum_i \left(\left|\phi_i\right\rangle - \left|\tilde{\phi}_i\right\rangle\right)\left\langle\tilde{p}_i\middle|\tilde{\psi}_n^\alpha\right\rangle, \tag{17}$$

where $\left|\tilde{\psi}_n^\alpha\right\rangle$ represents a pseudo-wave function, $\left|\phi_i\right\rangle$ partial waves, $\left|\tilde{\phi}_i\right\rangle$ pseudo-partial waves, $\tilde{p}_i$ projector functions, and $i$ contained in the terms represents all possible variables, *i.e.*, principal quantum number, orbital angular momentum quantum number, and number $k$ corresponding to the reference energy $\varepsilon_{kl}$. For the total number of N eigenvalues, pseudo-wave functions consist of 2 N eigenspinors. $\left|\phi_i\right\rangle$ are calculated for a non-magnetic atom serving as reference, $\left|\tilde{\phi}_i\right\rangle$ are the same outside the core radius, but they may differ inside the radius because they are not restricted by the non-magnetic criteria; the wave in the vicinity of the core boundary must be continuous. This is in line with the expectations that the greatest influence of relativistic effects is in the vicinity of the nucleus while it is negligible in the space between atoms.

Thanks to the properties described in Ref. 48, following the reference, the Hamiltonian of SOC contributions ($\tilde{H}_{SO}$) can be simplified to the one-centre contributions:

$$\tilde{H}_{SO}^{\alpha\beta} = \sum_{ij} |p_i\rangle\langle\phi_i|H_{SO}^{\alpha\beta}|\phi_j\rangle\langle p_j|, \tag{18}$$

where $\alpha$ and $\beta$ are the spin-up and -down components of the spinor, and $H_{SO}^{\alpha\beta}$ can be approximated as

$$H_{SO}^{\alpha\beta} = \frac{\hbar^2}{(2m_e c)^2}\frac{K(r)}{r}\frac{dV(r)}{dr}\vec{\sigma}^{\alpha\beta}\cdot\vec{L}, \tag{19}$$

where $\vec{L}$ is an angular momentum operator that can be expressed as $\vec{L} = \vec{r}\times\vec{p}$, $\vec{\sigma}$ are the Pauli spin matrices, $V(r)$ is the spherical part of the effective all-electron potential inside the core region, and $K(r)$ is a substitution defined as

$$K(r) = \left(1 - \frac{V(r)}{2m_e c^2}\right)^{-2}. \tag{20}$$

After a few mathematical operations, it is possible to derive the form of $\tilde{H}_{SO}^{\alpha\beta}$ from $H_{SO}^{\alpha\beta}$. This form then acts on pseudo orbitals accordingly:

$$|\tilde{\psi}_n^{\alpha}\rangle = \sum_{\alpha\beta}\tilde{H}_{SO}^{\alpha\beta}|\tilde{\psi}_n^{\beta}\rangle. \tag{21}$$

The self-consistent NCL calculations including SOC may be very demanding. According to Ref. 49 we can treat MAE as a perturbation by using so-called Magnetic force theorem. Starting from the collinear calculations, we can determine the charge density of both spin channels and also the magnetic moments on all atoms within the supercell. Change of the total energy (originally denoted $\delta E$, we label it as MAE to be consistent with the rest of the thesis) can be then evaluated as

$$\mathrm{MAE} = 2\sum_j J_{0j}(1-\cos\theta) \approx J_0\theta^2, \tag{22}$$

where $\theta$ is an angle between the initial and final spin orientation, the exchange parameter ($J_0$) can be evaluated as

$$J_0 = \sum_j J_{0j}, \tag{23}$$

where $J_{ij}$ are pair interaction parameters that can be determined from the rotation energy of two spin moments presented on different sites $i$ and $j$ with opposite angles $\frac{\pm\theta}{2}$. Then the interaction energies of the given ions need to be subtracted. After many steps, it is possible to derive that the variation of the total energy becomes the same as the sum of

one-particle energy changes of the occupied states with a fixed potential. This approach allows to directly calculate MAE of each given site ($i$) and momentum state ($m_l$) as

$$\mathrm{MAE}^i_{m_l} = \int^{E_F} (E - E_F)\Delta n^i_{m_l}(E)dE, \tag{24}$$

where $\Delta n^i_{m_l}(E)$ is the difference in the orbital-decomposed partial DOS (PDOS) between two examined directions of magnetization. Total MAE can be calculated as a sum over both variables as

$$\mathrm{MAE} = \sum_i \sum_{m_l} \int^{E_F} (E - E_F)\Delta n^i_{m_l}(E)dE. \tag{25}$$

This approach is computationally beneficial, because it allows to calculate the charge density in a collinear mode and then the calculations including all relativistic effect are performed in the systems with a fixed charge distribution, therefore they converge rapidly. The main drawback is that it is still an approximation and, *e.g.*, we showed in our previous work[13] that the results are not always consistent with the non-collinear self-consistent calculations.

### *5. Beyond Conventional Density Functional Theory*

Conventional DFT in a GGA approach still has many weak spots, mainly in the description of the electron-electron interactions. It may underestimate the short-range correlation effects in $d$ and $f$ orbitals and also the long-range correlation effects connected with the van der Waals interactions. While their effect may be negligible in some systems, they may be crucial in the other. The exact inclusion of these effects in DFT is problematic because of its nature and it requires very demanding computational procedures. Fortunately, these effects can be approximated by a lightweight terms and therefore we decided to examine their impact on our calculations, namely the DFT+$U$ approach and the usage of the optB86b-vdW functional.

Pristine DFT is unable to describe some systems with strongly correlated $d$ or $f$ electrons,[50] *e.g.*, LSDA (before the widespread using of GGA) predicts FeO and CoO to be metals, while they are Mott insulators. That is due to the neglecting of quasi-atomic interactions. One of the most important terms can be described by the Hubbard parameter $U$ that is defined as

$$U = E(d^{n+1}) + E(d^{n-1}) - 2E(d^n), \tag{26}$$

where $U$ represents the Coulomb energy that must be supplied to place 2 electrons to the same site. That arises due to the relatively slow transitions of $d$-$d$ electrons (it needs more changes in all $d$ orbitals) in a comparison with $d$-$s$ and $p$-$s$ transitions. If we add the $U$ term to the calculations, $d$ electrons avoid each other more and the states are more separated. As a side effect, this also leads to the elimination of the double occupancy error.

The $U$ parameter is also advantageous in GGA calculations[51]. $U$ in some computational codes can be determined during the calculations self-consistently without the need to supply its empirical value. It is necessary to note that this approach adds only few additional terms to the GGA equations and does not add any complexity. $U$ may be implemented in various ways, *e.g.*, in a form proposed by Dudarev *et al.*[52,53]:

$$E_{\mathrm{DFT}+U} = E_{\mathrm{DFT}} + \frac{U-J}{2}\sum_{m,\sigma}(n_{m,\sigma} - n_{m,\sigma}^2), \tag{27}$$

where $E$ is the energy functional of DFT and DFT+$U$ calculations, $n_{m,\sigma}$ is the occupation number of $m^{th}$ $d$ state and $\sigma$ stands for the spin. $J$ is the approximation of the Stoner exchange parameter that is usually close to 1 eV. Dudarev's approach does not take into account $U$ and $J$ terms separately but calculates only with their difference. The usage of the $U$ parameter with suitable values can significantly improve the results to be more realistic, specifically the properties directly resulting from the DOS, *e.g.*, magnetic moments, the MAE, and a width of the band-gap.

As it was mentioned earlier, GGA functionals cannot sufficiently describe the long-range interactions, *e.g.*, the dispersion interaction, nevertheless, their proper description may be necessary to obtain real values of given properties in, for instance, biomolecules or molecules adsorbed at surfaces. The terms accounting with the dispersion interaction can be externally added[54–57] to the existing DFT codes, *e.g.*, in a form of the van der Waals density functional (vdW-DF) where the exchange-correlation energy ($E_{xc}$) consist of three parts:

$$E_{xc} = E_x^{\mathrm{GGA}} + E_c^{\mathrm{LDA}} + E_c^{nl} \tag{28}$$

where $E_x^{\mathrm{GGA}}$ stands for the exchange energy part that is calculated by using the revised PBE (revPBE) functional within GGA. The short-range correlation energy $E_c^{\mathrm{LDA}}$ is calculated by using LDA. The last term $E_c^{nl}$ is responsible for the long-range interactions by calculating a double space integration. Despite a significant improvement in many systems, this form of vdW-DF fails in the description of, *e.g.*, hydrogen bonds. Another

problem arises with the used functionals, for instance revPBE may have different lattice constants than PBE and it may cause problems in calculations of the adsorption of molecules on surfaces. These drawbacks can be overcome by a proper combination of other functionals or by their parametrization, *e.g.*, as in the functional optB86b-vdW.[57]

Functional optB86b-vdW is based on B86b exchange proposed by Becke in 1986.[58] optB86b-vdW is a successor to the optB88-vdW that was proposed by the same group[56], it has similar precision but an improved asymptotic behaviour. Both opt-vdW functionals predict lattice constants of the examined metals more precisely than revPBE-vdW and rPW86-vdW2 functionals, their errors lie within the range of errors of PBEsol and PBE, optB86b-vdW is slightly better than optB88-vdW.[57] Both opt-vdW functionals also predict atomization energies with less than half error magnitude in contrast with conventional PBE. opt-vdW algorithms are implemented to run partly independently of the conventional parts of the DFT calculation, *i.e.*, vdW routines only utilize the fine FFT grid, enter FFTs and the final energy summation, no other data flow is needed.

Exchange enhancement factor ($F_x$) is responsible the most for the lattice constant elongation. Its value has direct impact on the position of the repulsive Pauli wall. Properties of $F_x$ in areas with small density gradients significantly affect the lattice constants but may also act in longer distances that are mainly a domain of the vdW interactions. If the lattice constants are overestimated (typically by using functionals of the PBE type), we need to use functional that has a lower $F_x$ term. LDA is an extreme case where there is no effect of $F_x$ because it does not count with the charge gradient; that is also one of the sources of its overbinding problem. The form of $F_x$ in optB86b-vdW is

$$F_x^{\mathrm{optB86b}} = 1 + \frac{\mu s^2}{(1+\mu s^2)^{4/5}}, \mu = 0.1234, \tag{29}$$

where $s$ is a small reduced density gradient. This form is less repulsive than in optB88-vdW in distances longer than the optimum.

## II. COMPUTATIONAL DETAILS

We used the Vienna *ab-initio* simulation package (VASP)[59–62] in all calculations, which describes the electron-ion interaction by using the projected augmented wave (PAW) method[63,64]. We used the functional of Perdew, Burke, and Ernzerhof (PBE)[65] within the Generalized gradient approximation (GGA).[66] Electrons in VASP are treated as plane waves, we set their cutoff energy to 400 eV and 600 eV in the scalar-relativistic (SR) mode and the non-collinear (NCL) mode, respectively. All calculations were treated with the symmetry switched off and SR calculations were spin-polarized.

Defective graphene was represented by 5 x 5 hexagonal supercell (in pristine form containing 50 C atoms) with a graphene lattice constant 2.47 Å (experimental value: 2.46 Å)[67]. Two graphene layers were separated by a vacuum layer 14 Å wide to avoid spurious interactions between neighbouring supercells due to the periodic boundary conditions. Examined defects in graphene were SV, NSV, DV, and NDV (**Fig. 3**); we used relaxed supercells from the Bachelor Thesis.

Examined TM atoms were Fe, Co, Ni, Ru, Rh, Pd, Os, Ir, and Pt. Let us define abbreviations for the TM atom closer to graphene (TM↓) and for the TM atom farther from graphene (TM↑). Whole systems are labelled according to the pattern TM↑TM↓@DG. TM atoms are in some cases for clarity divided to horizontal groups: Fe- (Fe, Co, Ni), Ru- (Ru, Rh, Pd), and Os group (Os, Ir, Pt); and to vertical groups according to groups of the periodic table: TM8 (Fe, Ru, Os), TM9 (Co, Rh, Ir), and TM10 (Ni, Pd, Pt). Let us also define triads as the three systems with a given TM atom as TM↑, the same defect, and differing TM↓ from the same vertical group (*e.g.*, OsCo@NSV, OsRh@NSV, and OsIr@NSV form an OsTM9@NSV triad).

We performed calculations with a single Γ-centred $k$-point to get a quick insight into the stability of the perpendicular orientation of the TM dimer with respect to the graphene plane. That stability ($E_{perp}$) can be defined as

$$E_{perp} = \min(E_{tot,tilted}) - E_{tot,perpendicular}, \tag{30}$$

where $E_{tot,perpendicular}$ is the total energy of the given system with the TM dimer perpendicular (or nearly perpendicular) to the graphene plane; $E_{tot,tilted}$ is the total energy of any geometry of the same system where the lower TM atom is still in the vacancy and the second TM atom forms bonds with graphene (the TM dimer is thus tilted). Values of $E_{perp}$ may be, according to our methodology, in some cases overestimated. If no other

local geometry groundstate of the TM dimer is found in the vicinity of the defect (all such calculations lead to the perpendicular geometry), we need to calculate $E_{perp}$ from the closest system where TM↑ adsorbs farther from the defect. This could be overcome by running the calculations with a constrained relaxation of just selected degrees of freedom, nevertheless, the currently used procedure is satisfactory for an assessment whether the perpendicular geometry is stable or not.

As it is apparent, we discarded the calculations where the TM atoms within the dimer switched their position. $E_{perp}$ is positive in systems where the TM dimer prefers an upright position. We used 6, 6, 8, and 4 different initial positions for each combination of each possible TM dimer (81 in total) and SV, NSV, DV, and NDV defect, respectively, giving together nearly 2000 calculations. In rare cases, it was necessary to perform additional calculations, as none of the original calculations converged to the perpendicular, or to the tilted geometry. The usage of a just single Γ-centered $k$-point in calculations was shown to be qualitatively reliable for the prediction of the preferred dimer orientation: the discrepancy in $E_{perp}$ is smaller than 0.1 eV in PdCo@NSV, OsNi@NSV, and RuIr@NDV in comparison with the relaxations performed with 11 x 11 x 1 Γ-centered $k$-point mesh. Calculations required two successive steps within the self-consistent loop ($E_{diff}$) to be smaller than $10^{-5}$ eV and forces acting on each atom smaller than 10 meV $\cdot$ Å$^{-1}$. We treated partially-occupied orbitals by using Gaussian smearing with width 0.02 eV.

Only systems with positive $E_{perp}$ were considered in the next steps, as it significantly saved computational resources. Relaxations consisted of several steps with tightening criteria, the final step had Γ-centred $k$-point mesh consisting of 11 x 11 x 1 $k$-points, and $E_{diff} = 10^{-6}$ eV. Static calculations with the tetrahedron method[68–70] with Blöchel corrections[71] to describe the partial occupancies were performed then to obtain more accurate DOS and magnetic moments.

Systems are characterized by distance between TM atoms in a dimer ($d_d$), distance of TM↓ above the nearest neighbours in graphene ($d_{van}$) and above the average graphene $z$ coordinate ($d_{vag}$), and the graphene buckling amplitude ($d_{ba}$) defined as $d_{ba} = d_{vag} - d_{van}$. The strength of bonding of the second TM atom is quantified by its adsorption energy ($E_{ad2}$), calculated as

$$E_{ad2} = E_{\mathrm{VG+TM\downarrow+TM\uparrow}} - (E_{\mathrm{VG+TM\downarrow}} + E_{\mathrm{TM\uparrow}}), \tag{31}$$

where $E_{\mathrm{VG+TM\downarrow+TM\uparrow}}$ is the total energy of defective graphene with an adsorbed TM dimer. $E_{\mathrm{VG+TM\downarrow}}$ and $E_{\mathrm{TM\uparrow}}$ represent the total energy of defective graphene with an adsorbed TM↓

atom and the total energy of TM↑ atom in vacuum, both were taken from our previous calculations.[13] The more the adsorption energy is negative, the more the adsorption is energetically favourable.

We also performed the Bader charge analysis[72–74] that enabled us to calculate charge located on TM↓ ($q_{\mathrm{TM}\downarrow}$) and TM↑ ($q_{\mathrm{TM}\uparrow}$) as the difference of number of electrons in free atom and number of electrons attributed to the given atom by the Bader charge analysis.

Systems are also characterized by magnetic properties: the total magnetic moment of the supercell ($\mu_{tot}$) and the sum of all local magnetic moments in the supercell ($\mu_{sum}$). Other magnetic and related properties are, because of their complexity, separately fully described in **Sec. III B**.

NCL calculations with included SOC[47,75–77] were performed in systems that had non-zero magnetic moment in the static SR calculations. The $k$-point mesh was reduced to 6 x 6 x 1 $k$-points to save computational resources. It was then enhanced to 11 x 11 x 1 $k$-points in selected systems to prove the validity of this simplification. The MAE is calculated as

$$\mathrm{MAE} = \min(E_x, E_y) - E_z, \tag{32}$$

where $E$s denote the total energy of the system with the initial magnetization along the given axis, $z$-axis is perpendicular to graphene and parallel to the TM dimer. Positive value of MAE corresponds to an easy $z$-axis.

## III. RESULTS AND DISCUSSION

### A. Theoretical Predictions: Single TM Atoms at Defective Graphene

We derived in our previous work[13] a formula of the total number of unpaired electrons ($N_{ue}$) in systems with a single adsorbed TM atom at defective graphene. The formula takes the form

$$N_{ue} = \begin{cases} 2O - G - D & \text{if } (2O - G) \geq D, \\ |2O - G - D| \pmod 2 & \text{otherwise,} \end{cases} \tag{33}$$

where $O$ is number of energetically available valence orbitals of the TM atom (1 $s$ orbital and 5 $d$ orbitals; $O = 6$), $G$ stands for the group number of the TM atom in the Periodic Table of Elements (*e.g.*, 10 for Ni) and $D$ represents the number of unpaired electrons (or its equivalent; *cf.*, SV, DV, and NDV) in pristine defective graphene.

The C atoms surrounding the SV defect are not equal in the sense that 2 C atoms possess 1 unpaired electron each, and the third C atom has 2 electrons forming a dangling bond ($D = 4$). Similar situation is in the vicinity of the DV defect: 4 surrounding C atoms have 1 unpaired electron each ($D = 4$). It has been shown[33] in the experimentally examined systems that the unpaired electrons can pair up and form bonds that are then broken after the adsorption of the TM atom. We therefore do not need to consider this phenomenon in the $D$ term. N atoms in the vicinity of NSV are not equal too: just 1 of them has 1 unpaired electron ($D = 1$). The situation in NDV is completely different, as we need to consider different bonding mechanism (*c.f.*, Ref. 13); we expect that TM atoms form dications and $D = 2$ then.

**Equation 33** allowed us to successfully predict magnetic moments in 32 of 36 studied systems, *i.e.*, in accord with the VASP calculations. The 4 remaining systems violating the equation were examined and the reasons of the exceptions were found. Fe@DV (in contrast with Fe@SV) is farther from the neighbouring C atoms and the lower electron density supports its higher-spin state ($N_{ue} = 0$, $\mu_{tot} = 3.39\ \mu_{\mathrm{B}}$). The opposite case was found in Ru@NSV and Os@NSV: the high electron density quenched out the magnetic moments of TM atoms and the systems remained non-magnetic ($N_{ue} = 3$, $\mu_{tot} = 0.00$). Os@NDV was initially nearly non-magnetic, but after the employment of the additional $U$ term (*cf.*, **Sec. I D 5**) with $U - J = 2$ and $U - J = 4$ it achieved $\mu_{tot} = 2.00\ \mu_{\mathrm{B}}$, in agreement with **Eq. 33**.

## B. Theoretical Predictions: Transition from Single Adsorbed TM Atoms towards Dimers

If we want to get an insight into the mechanisms determining the properties of the TM dimers adsorbed at defective graphene, we need to propose a model and then to test its validity with the results obtained from the DFT calculations. If we prove that the model is well-suited, we can use it to engineer the systems that should have the desired properties and then to fully examine them by performing the DFT calculations. Motivated by the success of the model proposed for single TM atoms adsorbed at defective graphene, we decided to build-up the predictions on the same concept, *i.e.*, the pairing of the unpaired electrons.

### *1. Total Magnetic Moment*

The conclusions for a single adsorbed TM atom need to be adapted for the TM dimers. If we assume that the bond within a TM dimer is formed by the maximal pairing of the unpaired electrons on both TM atoms, we can consecutively derive a formula to predict the total magnetic moment of the supercell, $\mu_{tot,pred}$ (as a total number of unpaired electrons multiplied by $\mu_{\mathrm{B}}$):

$$\mu_{tot,pred} = |N_{ue,\mathrm{TM}\uparrow} - N_{ue,\mathrm{SA}}| \cdot 1 \ \mu_{\mathrm{B}}., \tag{34}$$

where $N_{ue,\mathrm{SA}}$ is the number of initially unpaired electrons of the system with a single adsorbed TM atom (*i.e.*, the TM atom together with the substrate, **Eq. 33**) and $N_{ue,\mathrm{TM}\uparrow}$ is the number of the initially unpaired electrons of TM↑ ($N_{ue,\mathrm{TM}\uparrow} = 2O - G$). **Eq. 34** can be interpreted in the following manner: the magnitude of the total magnetic moment (in $\mu_{\mathrm{B}}$) is the number of unpaired electrons on the TM atom with an initially higher number of unpaired electrons lowered by a number of initially unpaired electrons on the other TM atom (these electrons pair and do not contribute to magnetism), regardless whether more unpaired electrons are on TM↑ or TM↓. The local magnetic moment should be greater on a TM atom with larger $N_{ue}$ (it possesses the free electrons that remained after the creation of the bonds) and nearly equal to $\mu_{tot,pred}$ (there are no other unpaired electrons within the supercell). Clearly, we are more interested in the cases where $N_{ue,\mathrm{TM}\uparrow} > N_{ue,\mathrm{SA}}$ (because they have a greater potential to have high values of the MAE), but the opposite case needs also to be considered for the completeness. The predicted total magnetic moments are compared in **Table I** with the total magnetic moments resulting from DFT

**TABLE I:** Number of initially unpaired electrons on TM↑ ($N_{ue,\mathrm{TM}\uparrow}$), number of initially unpaired electrons predicted in the systems with a single adsorbed TM atom ($N_{ue,\mathrm{SA}}$), the resulting predicted total magnetic moment calculated by **Eq. 34** ($\mu_{tot,pred}$, in $\mu_\mathrm{B}$) compared with the total magnetic moments of the supercell resulting from the DFT calculations ($\mu_{tot,\mathrm{DFT}}$, in $\mu_\mathrm{B}$) in selected illustrative systems. The left column presents the ideal cases, the right presents systems that need additional parameter to be reliable.

| System | $N_{ue,\mathrm{TM}\uparrow}$ | $N_{ue,\mathrm{SA}}$ | $\mu_{tot,pred}$ | $\mu_{tot,\mathrm{DFT}}$ | System | $N_{ue,\mathrm{TM}\uparrow}$ | $N_{ue,\mathrm{SA}}$ | $\mu_{tot,pred}$ | $\mu_{tot,\mathrm{DFT}}$ |
|---|---|---|---|---|---|---|---|---|---|
| FeIr@SV | 4 | 1 | 3 | 3.00 | FePt@SV | 4 | 0 | 4 | 2.00 |
| CoIr@SV | 3 | 1 | 2 | 2.00 | FeFe@NSV | 4 | 3 | 1 | 2.90 |
| PtFe@NSV | 2 | 3 | 1 | 1.00 | PdFe@NSV | 2 | 3 | 1 | 0.00 |
| RuOs@NSV | 4 | 3 | 1 | 1.15 | NiCo@NSV | 2 | 2 | 0 | 4.00 |
| RhOs@NSV | 3 | 3 | 0 | 0.00 | FePd@NSV | 4 | 1 | 3 | 5.00 |
| OsCo@NSV | 4 | 2 | 2 | 2.04 | FeOs@NDV | 4 | 2 | 2 | 4.00 |
| OsRu@NDV | 4 | 2 | 2 | 1.85 | IrCo@NDV | 3 | 1 | 2 | 3.51 |

calculations ($\mu_{tot,\mathrm{DFT}}$). It is apparent that some systems were predicted well, but many systems also differ, and we therefore need to improve our model.

### *2. Bond Order as a Parameter*

We noticed that the total predicted magnetic moment is often smaller than the one calculated by using DFT calculations. The reason is a wrong initial assumption that the new bond within the dimer is created by combining all available unpaired electrons. We therefore need to introduce additional parameters. If we consider the creation of bonds only by pairing of unpaired electrons of both TM↓ and TM↑, *i.e.*, according to the classical covalent mechanism, we achieve the maximal number of newly formed covalent bonds ($N_{bom,coval}$, the maximal bond order by considering only covalent bonds) within the TM dimer:

$$N_{bom,coval} = \min(N_{ue,\mathrm{SA}}, N_{ue,\mathrm{TM}\uparrow}), \tag{35}$$

Now we can discuss cases with special values of $N_{bom,coval}$. If $N_{bom,coval} = 0$, the dimer cannot be formed as there is no available classical covalent bond that would hold it. As we do not consider any TM atoms with $N_{ue,\mathrm{TM}\uparrow} = 0$ among our examined TM atoms, $N_{bom,coval} = 0$ is only possible if $N_{ue,\mathrm{SA}} = 0$ (consider following combinations of the TM↓ and defective graphene: TM8@SV, TM10@SV, TM8@DV, TM10@DV, and

TM10@NDV). In the systems with $N_{bom,coval} = 0$, the creation of bonds between the TM atoms would require a significant electron relocation. Such charge transfer is possible only in TM atoms with a greater polarizability, *i.e.*, the higher the period of the TM atom, the better. The second option to form such dimers is a different binding mechanism, *e.g.*, donor-acceptor bonds, *vide infra*.

Other complex cases are the systems, where the initially unpaired electron is rather delocalized and cannot easily contribute to the bond with TM↑ (see TM9@SV and TM9@DV). Together with the relatively big size of the DV defect it implies that a perpendicular TM dimer with TM8 – TM10 as TM↓ at DV cannot be achieved: the upper TM atom is strongly attracted by the defect and the resulting TM dimer is significantly tilted and the interaction with the defect remarkably quenches its magnetism. The instability of the TM dimers proposed in the last two paragraphs is an essential contribution of the model to the explanations of the properties calculated by DFT.

As we mentioned earlier, the real bond order ($N_{bor}$) does not always achieve the value of $N_{bom,coval}$. If all bonds within the dimer are of covalent origin, it is within the range $\langle 0,\ N_{bom,coval} \rangle$. We need to emphasize that the donor-acceptor bond counts also as the bond and it is included in $N_{bor}$, which may then be outside the above defined range, as we discuss further in this subchapter. **Eq. 34** can be adapted to predict the total magnetic moment if we know the real bond order within the TM dimer:

$$\mu_{tot,pred} = [|N_{ue,\mathrm{TM}\uparrow} - N_{ue,\mathrm{SA}}| + 2 \cdot (N_{bom,coval} - N_{bor})] \cdot 1\ \mu_{\mathrm{B}}, \tag{36}$$

*i.e.*, we start with the total magnetic moment as the bond order would be maximal (as described above). The second term represents the "unformed" bonds within the TM dimer; each such bond leaves one unpaired electron on each TM atom (2 electrons in total) and their contribution to the total magnetic moment therefore needs to be multiplied by 2.

### *3. Calculations of Bond Order*

So far, we have expected that the value of $N_{bor}$ is known, and then we could use it as a parameter. Nevertheless, there is no sufficient information background for its determination and therefore we need to get an insight how its values are affected by both TM atoms and the defect. We decided to explore the trends of $N_{bor}$ to be able to roughly estimate its value in the future research of similar systems.

Bond order cannot be easily directly obtained from the VASP calculations, but we can

deduce it by an inspection of other properties of the given system, *e.g.*, the bond order is loosely related to the adsorption energy (a higher bond order corresponds to the more negative $E_{ad2}$) and, more importantly, to the magnetic properties: $N_{bor}$ can be calculated by the reverse procedure than proposed in **Eq. 36** (*i.e.*, the equation of $\mu_{tot,pred}$) with the usage of the calculated $\mu_{tot,\mathrm{DFT}}$. By simple mathematical operations, $N_{bor}$ can be estimated as

$$N_{bor} = N_{bom,coval} - \frac{\frac{\mu_{tot,\mathrm{DFT}}}{\mu_{\mathrm{B}}} - |N_{ue,\mathrm{TM}\uparrow} - N_{ue,\mathrm{SA}}|}{2}, \tag{37}$$

where all the quantities are known from the previous thought process or from the SR calculations. Obviously, it would be redundant to calculate $N_{bor}$ and then to insert it to the equation of the predicted total magnetic moment (**Eq. 36**). We emphasize that from now $N_{bor}$ is not a parameter but an additional physical quantity that needs to be calculated by using **Eq. 37** and that helps us to better describe the examined TM dimers. One of the aims of the Thesis is to elucidate the trends in $N_{bor}$ so it could be in the first approach treated as a parameter in the future. $N_{bor}$ also enters equations in the next subchapters and its value is required to obtain reasonable values.

High bond orders are unlikely achieved in those cases with TM atoms from Fe- and Ru groups because they have quite rigid orbitals when compared to the Os group, *e.g.*, it is energetically unfavourable for the former to adapt their orbitals to the formation of the higher-order bonds.

#### *4. Local Magnetic Moments and Number of Relocated Electrons*

If $N_{bor} = N_{bom,coval}$, one would expect that the only local magnetic moment is located on the TM atom that initially had more unpaired electrons and its value is similar to the total magnetic moment. If $N_{bor} < N_{bom,coval}$, each "unformed" bond (*cf.*, **Eq. 36**) would leave an unpaired electron on each of the bonding partners and it would contribute to TM atoms' local magnetic moments, *i.e.*, the local magnetic moments should increase on both TM atoms nearly equally by $\sim (N_{bom,coval} - N_{bor}) \cdot 1\ \mu_{\mathrm{B}}$ with respect to the state with a maximal bond order, *i.e.*, $N_{bor} = N_{bom,coval}$. Formulas for predicting the local magnetic moment at TM$\downarrow$ and defective graphene ($\mu_{\mathrm{VG+TM}\downarrow,pred}$), and TM$\uparrow$ ($\mu_{\mathrm{TM}\uparrow,pred}$) can be formulated as:

$$\begin{aligned} \mu_{\mathrm{VG+TM}\downarrow,pred} &= (N_{ue,\mathrm{SA}} - N_{bor}) \cdot 1\ \mu_{\mathrm{B}}, \\ \mu_{\mathrm{TM}\uparrow,pred} &= (N_{ue,\mathrm{TM}\uparrow} - N_{bor}) \cdot 1\ \mu_{\mathrm{B}}. \end{aligned} \tag{38}$$

The equations can be interpreted in the following manner: the magnitude of the local magnetic moment (in $\mu_B$) on each atom is equal to the initial number of its unpaired electrons lowered by a number of electrons that form the bond within the TM dimer.

By comparing SR local magnetic moments with the magnetic moments predicted by **Eq. 38** (*cf.*, **Table II**) it is clear that there is an additional parameter influencing the values. A close inspection revealed that one of the predicted moments is often underestimated while the second moment is overestimated. The prediction can be improved if we introduce another quantity: number of relocated electrons ($N_{rel}$). If we assume that the spin-up channel is more populated than the spin-down channel (the excess electrons in the spin-up channel are responsible for the magnetism), we can use the following derivation of $N_{rel}$. It represents the number of electrons from the spin-down channel that are presented on the TM↑ less and on the TM↓ more with respect to the state predicted by using only covalent bonds without any electron shift, *e.g.*, if $N_{rel} = 1$, the magnetic moment of the lower atom is decreased by 1 $\mu_B$ (the presence of one excess electron in the spin-down channel decreases the magnetic moment), whereas the magnetic moment of the upper atom is increased by 1 $\mu_B$. The negative value of $N_{rel}$ means that the spin-down electrons

**TABLE II:** Number of initially unpaired electrons on TM↑ ($N_{ue,\mathrm{TM}\uparrow}$), number of initially unpaired electrons predicted in the systems with a single adsorbed TM atom ($N_{ue,\mathrm{SA}}$), the resulting predicted total magnetic moment calculated by **Eq. 34** ($\mu_{tot,pred}$, in $\mu_B$) compared with the total magnetic moments of the supercell resulting from the DFT calculations ($\mu_{tot,\mathrm{DFT}}$, in $\mu_B$), maximal covalent bond order ($N_{bom,coval}$, **Eq. 35**), bond order ($N_{bor}$, **Eq. 37**). Predicted local magnetic moments (*pred*, **Eq. 38**, in $\mu_B$), and calculated magnetic moments (*calc*, adapted values from DFT calculations, **Eq. 42**, in $\mu_B$) on defective graphene + TM↓ or on TM↑. Selected illustrative systems, the upper rows present the ideal cases, the lower present systems that need additional parameter to be reliable.

| | | | | | $N_{bom}$, | | $\mu_{\mathrm{VG+TM}\downarrow}$ | | $\mu_{\mathrm{TM}\uparrow}$ | |
|---|---|---|---|---|---|---|---|---|---|---|
| System | $N_{ue,\mathrm{TM}\uparrow}$ | $N_{ue,\mathrm{SA}}$ | $\mu_{tot,pred}$ | $\mu_{tot,\mathrm{DFT}}$ | $coval$ | $N_{bor}$ | *pred* | *calc* | *pred* | *calc* |
| CoIr@SV | 3 | 1 | 2 | 2.00 | 1 | 1.00 | 0.00 | −0.04 | 2.00 | 2.05 |
| OsFe@NSV | 4 | 3 | 1 | 1.52 | 3 | 2.74 | 0.26 | 0.06 | 1.26 | 1.45 |
| NiIr@NDV | 2 | 1 | 1 | 1.00 | 1 | 1.00 | 0.00 | 0.19 | 1.00 | 0.80 |
| PtPt@SV | 2 | 0 | 2 | 0.00 | 0 | 1.00 | −1.00 | 0.00 | 1.00 | 0.00 |
| FeFe@NSV | 4 | 3 | 1 | 2.90 | 3 | 2.05 | 0.95 | −0.27 | 1.95 | 3.17 |
| NiCo@NSV | 2 | 2 | 0 | 4.00 | 2 | 0.00 | 2.00 | 2.67 | 2.00 | 1.33 |
| PdIr@NDV | 2 | 1 | 1 | 0.88 | 1 | 1.06 | −0.06 | 0.48 | 0.94 | 0.41 |

are presented more on TM↑, which in turn lowers its magnetic moment. $N_{rel}$ may have two different origins: I) a spin-dependent charge transfer between both TM atoms; II) a formation of donor-acceptor bonds. The first option can be searched by Bader charge analysis, results are discussed in **Sec. III D**, but it was found that it is not as easy to trace. The latter is hard to distinguish as the only difference between a classical covalent bond and the donor-acceptor bond is in the mechanism of their creation. A more thorough discussion with PtPt@SV as an example can be found on **Page 50**.

The derivation of $N_{rel}$ is following. We want to obtain magnetic moments on the TM↓ together with defective graphene ($\mu_{\mathrm{VG+TM}\downarrow,calc}$) and on the TM↑ ($\mu_{\mathrm{TM}\uparrow,calc}$) by a simple subtraction (addition):

$$\begin{aligned} \mu_{\mathrm{VG+TM}\downarrow,calc} &= \mu_{\mathrm{VG+TM}\downarrow,pred} - N_{rel} \cdot 1\ \mu_{\mathrm{B}}, \\ \mu_{\mathrm{TM}\uparrow,calc} &= \mu_{\mathrm{TM}\uparrow,pred} + N_{rel} \cdot 1\ \mu_{\mathrm{B}}. \end{aligned} \tag{39}$$

So far we kept the magnetic moment of defective graphene and the TM↓ merged. Nevertheless, at this point it may be beneficial to split them to two independent variables: $\mu_{\mathrm{VG},calc}$ and $\mu_{\mathrm{TM}\downarrow,calc}$:

$$\mu_{\mathrm{VG+TM}\downarrow,calc} = \mu_{\mathrm{VG},calc} + \mu_{\mathrm{TM}\downarrow,calc}. \tag{40}$$

$N_{rel}$ is now in the same situation as $N_{bor}$. If we knew it or if we could somehow estimate its value, we could also predict local magnetic moments according to **Eq. 39** without the DFT calculations. If we do not have a possibility to assess it, we can calculate it by using following procedure leading to **Eq. 43**.

For the direct evaluation of $N_{rel}$ we need another thought process. $\mu_{tot,\mathrm{DFT}}$ of the supercell is calculated as the difference in occupations of the spin-up and -down channels within the whole supercell, which is therefore exact. VASP projects the local magnetic moments onto spheres around each given atom (Wigner-Seitz cells), it is very improbable to cover all local magnetic moments, their sum ($\mu_{sum,\mathrm{DFT}}$) is usually slightly smaller than $\mu_{tot,\mathrm{DFT}}$. In systems with non-zero magnetic moments, we can introduce a scaling factor ($\mu_{\mathrm{WS}}$):

$$\mu_{\mathrm{WS}} = \frac{\mu_{tot,\mathrm{DFT}}}{\mu_{sum,\mathrm{DFT}}}. \tag{41}$$

If we multiply $\mu_{sum,\mathrm{DFT}}$ (that is not fully exact) by $\mu_{\mathrm{WS}}$, we get the exact $\mu_{tot,\mathrm{DFT}}$. Straightforwardly, if we multiply each local magnetic moment (not fully precise) by $\mu_{\mathrm{WS}}$ and then we sum these scaled local magnetic moments, we once again obtain $\mu_{tot,\mathrm{DFT}}$. Therefore,

we can approximate that the contribution of each atom to the total magnetic moment is:

$$\begin{aligned} \mu_{\mathrm{VG},calc} &= \mu_{\mathrm{VG,WS}} \cdot \mu_{\mathrm{WS}}, \\ \mu_{\mathrm{TM}\downarrow,calc} &= \mu_{\mathrm{TM}\downarrow,\mathrm{WS}} \cdot \mu_{\mathrm{WS}}, \\ \mu_{\mathrm{TM}\uparrow,calc} &= \mu_{\mathrm{TM}\uparrow,\mathrm{WS}} \cdot \mu_{\mathrm{WS}}, \end{aligned} \tag{42}$$

where we need to know the local magnetic moments within the atoms' Wigner-Seitz cells obtained by the SR calculations. As these local moments inherently are not absolutely precise, our approximation cannot be precise either, but it is as close as we can reasonably get. Thanks to that we are now able to calculate $N_{rel}$ by a substitution of the calculated values to the **Eq. 39**, *e.g.*:

$$N_{rel} = \frac{\mu_{\mathrm{TM}\uparrow,\mathrm{WS}} \cdot \frac{\mu_{tot,\mathrm{DFT}}}{\mu_{sum,\mathrm{DFT}}} - \mu_{\mathrm{TM}\uparrow,pred}}{1\ \mu_{\mathrm{B}}}. \tag{43}$$

The value of $N_{rel}$ is another important quantity representing the TM dimer, it allows distinguishing donor-acceptor bonds, and for future calculations it would be advantageous to know its trends with respect to both TM atoms and the defect.

### *5. Summary of the Proposed Model*

In summary, we were able to construct a theoretical model that elucidates the bonding mechanism within the TM dimer and in the rest of the system. TM↓ is bound by a similar mechanism as it was bound in the corresponding system with only a single adsorbed TM atom at defective graphene, *i.e.*, by a maximal number of possible covalent bonds; this may leave unpaired electrons on the TM atom ($N_{ue,\mathrm{SA}}$, *cf.*, **Sec. III A** or Ref. 13). The unpaired electrons are then able to form bonds with TM↑. The primitive initial model would predict the bond order ($N_{bom,coval}$) within the TM dimer to be determined again as the minimal number of electrons (on TM↑ or TM↓) that can pair. This would allow us to determine the total magnetic moment of the supercell as the total number of the unpaired electrons (after the bonding) multiplied by 1 $\mu_{\mathrm{B}}$. A similar local magnetic moment could be expected on the TM atom that would have initially more unpaired electrons. So far, this model is very simple and does not require any additional parameters except the number of the electrons within the valence shell of the TM atoms.

The discrepancies between the predictions of the simple model and the results obtained by the DFT calculations forced us to introduce additional parameters (real bond order, $N_{bor}$, and number of relocated electrons, $N_{rel}$) that significantly improve the model quality.

The former allows us to include the cases where the bond within the TM dimer does not achieve the maximal predicted bond order. The latter gives an account of the systems where the spin density within the TM dimer is significantly shifted in comparison with the predicted case. The values of both parameters are unknown without the results from the DFT calculations, but we thoroughly examined them and their trends and now we are able to approximate their value, *vide infra*. We can conclude that $N_{bor} < N_{bom,coval}$ is typical mainly for the TM atoms from earlier periods, similarly as their tendency to achieve higher magnetic moments which is then numerically included in $N_{rel}$. The proposed model provides us with a valuable insight, but it cannot fully replace the DFT calculations.

### C. Stability of Upright Dimers

TM dimers that are perpendicular to the substrate achieve the greatest values of MAE[10,11] because TM↑ retains better its free-atom-like properties. The interaction of TM↑ with the substrate often leads to the quenching or a significant lowering of the MAE. We are therefore interested only in the systems that preserve the TM dimer in the perpendicular orientation.

Many TM dimers are stable in the perpendicular geometry at the SV, NSV, and NDV defects. All values of $E_{perp}$ are summarized in **Table III** together with the most favourable tilted geometries that are described by the adsorption site of the TM↑ according to **Fig. 5**. Values of $E_{perp}$ are graphically represented in **Fig. 6**.

Dimers at SV are in most cases tilted (TM↓ from Fe and Ru groups); dimers with TM↓ from Os group are, in contrast, in many cases perpendicular to the graphene plane (Fe-,

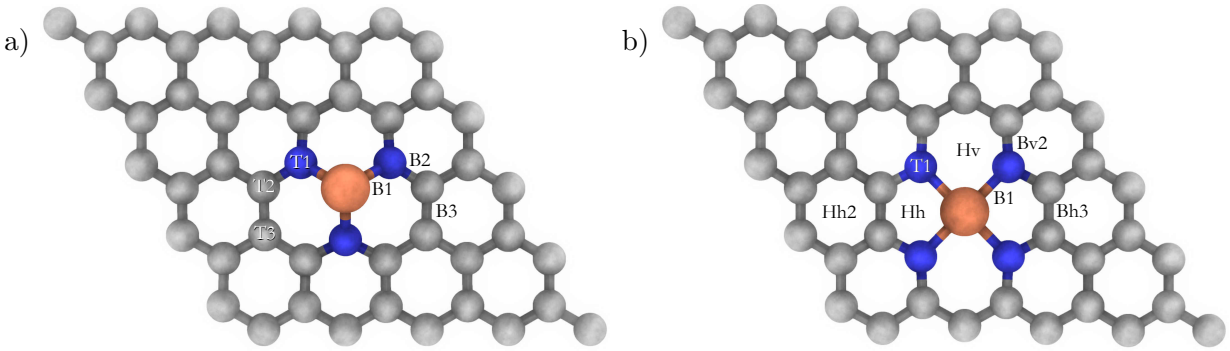


**FIG. 5:** Different adsorption sites above graphene of the upper TM atom when the dimer is tilted. T denotes "top", B "bridge", H "hollow". a) SV (blue spheres represent C atoms) and NSV, b) NDV. C/N/TM atoms are represented by grey/blue/orange spheres.

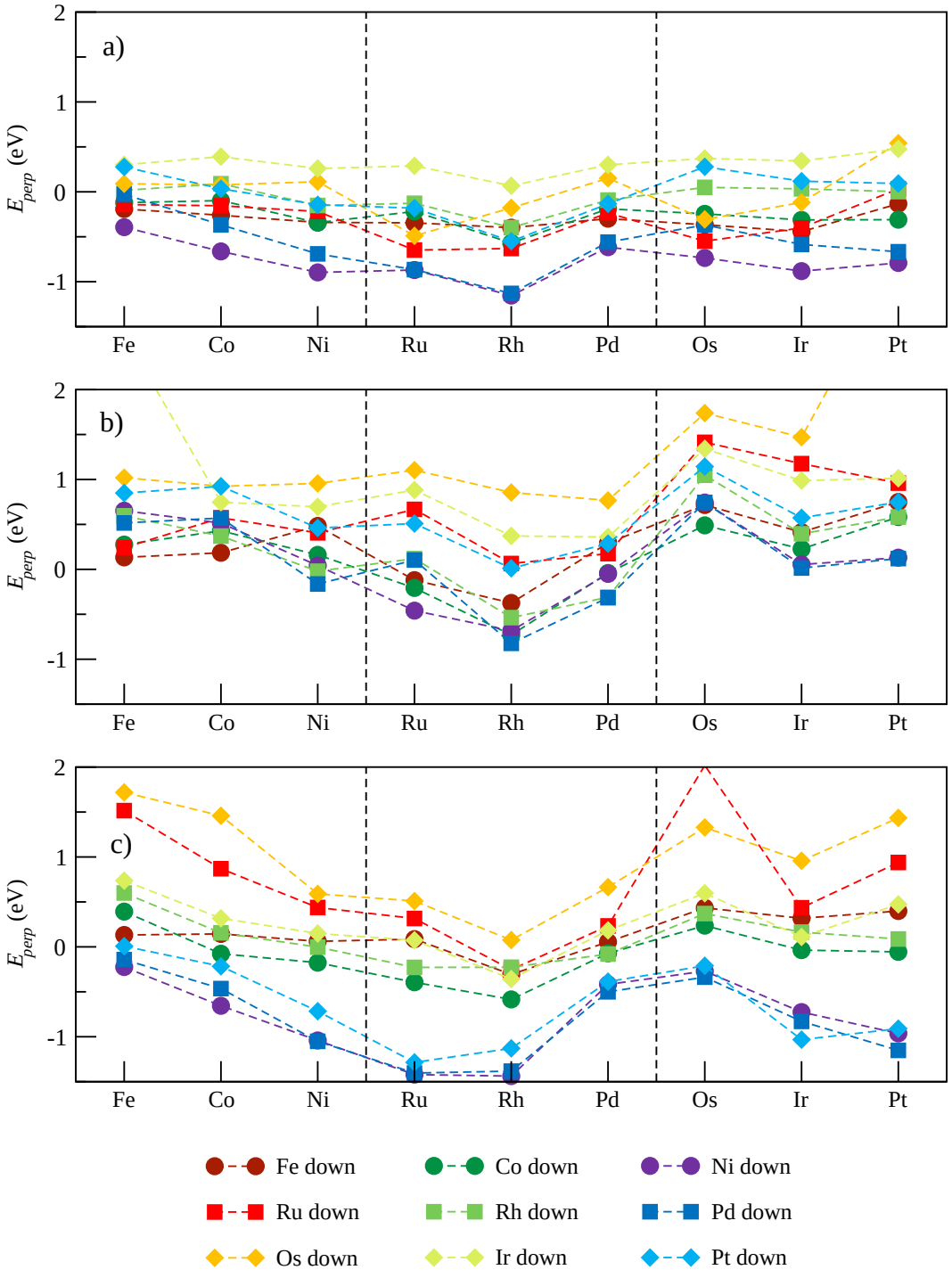


**FIG. 6:** Perpendicular stabilities (expressed by $E_{perp}$) of TM dimers at defective graphene: a) SV, b) NSV, c) NDV. Series show systems with one given TM↓ (as shown in the legend), the elements at $x$-axis represent TM↑. Dashed lines serve as the guide to the eye. For a better readability, circle, square, and diamond symbols correspond to Fe, Ru, and Os groups, respectively, as TM↓.

**TABLE III:** Perpendicular stabilities (expressed by $E_{perp}$) of TM dimers at defective graphene together with the abbreviations denoting the most stable adsorption site of TM↑ of the tilted dimer as was shown in **Fig. 5**.

| Lower | Upper TM atom | | | | | | | | | | | | | | | | | | | | | | | | | | |
|---|---|---|---|---|---|---|---|---|---|---|---|---|---|---|---|---|---|---|---|---|---|---|---|---|---|---|---|
| TM | SV Graphene | | | | | | | | | NSV Graphene | | | | | | | | | NDV Graphene | | | | | | | | |
| Atom | Fe | Co | Ni | Ru | Rh | Pd | Os | Ir | Pt | Fe | Co | Ni | Ru | Rh | Pd | Os | Ir | Pt | Fe | Co | Ni | Ru | Rh | Pd | Os | Ir | Pt |
| Fe | −0.2 | −0.3 | −0.3 | −0.3 | −0.4 | −0.3 | −0.4 | −0.4 | −0.1 | 0.1 | 0.2 | 0.5 | −0.1 | −0.4 | 0.3 | 0.7 | 0.4 | 0.7 | 0.1 | 0.1 | 0.1 | 0.1 | −0.3 | 0.1 | 0.4 | 0.3 | 0.4 |
| | T1 | T1 | B2 | T1 | T1 | T1 | T1 | T1 | T1 | B3 | T3 | B2 | T3 | B3 | T1 | T3 | B3 | T3 | Hh | B1 | B1 | Hh | Hh | B1 | Hh | B1 | Bh3 |
| Co | −0.1 | −0.1 | −0.3 | −0.2 | −0.6 | −0.2 | −0.2 | −0.3 | −0.3 | 0.3 | 0.4 | 0.2 | −0.2 | −0.7 | 0.0 | 0.5 | 0.2 | 0.6 | 0.4 | −0.1 | −0.2 | −0.4 | −0.6 | −0.1 | 0.2 | 0.0 | −0.1 |
| | T1 | T1 | B2 | T1 | T2 | B2 | T1 | T1 | T1 | T2 | B2 | T3 | T3 | T3 | B3 | B3 | B3 | T3 | Hh2 | Hv | B1 | Hv | Hh | B1 | Hh | Hh | Bh3 |
| Ni | −0.4 | −0.7 | −0.9 | −0.9 | −1.2 | −0.6 | −0.7 | −0.9 | −0.8 | 0.7 | 0.5 | 0.0 | −0.5 | −0.7 | −0.1 | 0.7 | 0.1 | 0.1 | −0.2 | −0.7 | −1.0 | −1.4 | −1.4 | −0.4 | −0.3 | −0.7 | −1.0 |
| | T1 | T1 | T1 | B2 | B2 | T1 | T1 | T1 | T1 | T2 | B3 | T3 | T3 | T3 | B3 | T2 | B3 | B3 | Hv | Hv | Hh2 | Hh2 | Hh2 | Bh3 | Bh3 | Bh3 | Bh3 |
| Ru | −0.1 | −0.2 | −0.2 | −0.6 | −0.6 | −0.2 | −0.5 | −0.4 | 0.0 | 0.2 | 0.6 | 0.4 | 0.7 | 0.1 | 0.2 | 1.4 | 1.2 | 1.0 | 1.5 | 0.9 | 0.4 | 0.3 | −0.3 | 0.2 | 2.0 | 0.4 | 0.9 |
| | T1 | T1 | B2 | B2 | B2 | B2 | T1 | B2 | T1 | B2 | B3 | B3 | B3 | B3 | T3 | B3 | T2 | T3 | Hh2 | Hh | Hh | Hh | Hh | Hh | Hh2 | Hh | Hh |
| Rh | 0.0 | 0.1 | −0.2 | −0.1 | −0.4 | −0.1 | 0.0 | 0.0 | 0.0 | 0.6 | 0.4 | 0.0 | 0.1 | −0.5 | −0.3 | 1.0 | 0.4 | 0.6 | 0.6 | 0.2 | 0.0 | −0.2 | −0.2 | −0.1 | 0.4 | 0.2 | 0.1 |
| | T1 | B2 | B2 | T2 | T2 | B2 | T1 | T1 | T1 | T3 | B3 | B3 | B3 | B3 | T2 | B3 | B3 | T3 | Hh2 | Hh | B1 | Hh | T1 | Hh | Hh | Hh | Hh |
| Pd | 0.0 | −0.4 | −0.7 | −0.9 | −1.1 | −0.6 | −0.4 | −0.6 | −0.7 | 0.5 | 0.6 | −0.2 | 0.1 | −0.8 | −0.3 | 0.7 | 0.0 | 0.1 | −0.1 | −0.5 | −1.1 | −1.4 | −1.4 | −0.5 | −0.3 | −0.8 | −1.2 |
| | T1 | T1 | T1 | T2 | B2 | T1 | T1 | T1 | T1 | T3 | T3 | B3 | T3 | B3 | B3 | T3 | B3 | B3 | Hv | Hv | Hh2 | Hh2 | Hh2 | Bh3 | Bh3 | Bh3 | Bh3 |
| Os | 0.1 | 0.1 | 0.1 | −0.5 | −0.2 | 0.2 | −0.3 | −0.1 | 0.5 | 1.0 | 0.9 | 1.0 | 1.1 | 0.9 | 0.8 | 1.7 | 1.5 | 3.4 | 1.7 | 1.5 | 0.6 | 0.5 | 0.1 | 0.7 | 1.3 | 1.0 | 1.4 |
| | T1 | T1 | B2 | B2 | T1 | T1 | T1 | T1 | T1 | T3 | T2 | T2 | B3 | T3 | T3 | T3 | T2 | far | Hh2 | Hh2 | Hh | Hh | Hh | Hh | Hh | Hh | Hh |
| Ir | 0.3 | 0.4 | 0.3 | 0.3 | 0.1 | 0.3 | 0.4 | 0.3 | 0.5 | 2.6 | 0.7 | 0.7 | 0.9 | 0.4 | 0.4 | 1.3 | 1.0 | 1.0 | 0.7 | 0.3 | 0.1 | 0.1 | −0.4 | 0.2 | 0.6 | 0.1 | 0.5 |
| | T1 | B2 | B2 | T1 | B3 | B2 | T1 | T1 | T1 | far | B3 | T3 | B3 | B3 | T2 | B3 | B3 | T3 | Hh2 | T1 | B1 | Hv | Hh | Hh | Hh | Hh | Hh |
| Pt | 0.3 | 0.0 | −0.1 | −0.2 | −0.5 | −0.1 | 0.3 | 0.1 | 0.1 | 0.8 | 0.9 | 0.5 | 0.5 | 0.0 | 0.3 | 1.1 | 0.6 | 0.7 | 0.0 | −0.2 | −0.7 | −1.3 | −1.1 | −0.4 | −0.2 | −1.0 | −0.9 |
| | T1 | B2 | T1 | T2 | B2 | T1 | T1 | T1 | T1 | T3 | B3 | B3 | B3 | B3 | T3 | T3 | B3 | T3 | Hv | Bv2 | Hh2 | Hh2 | Hv | Bh3 | Bh3 | Bh3 | Bh3 |

Co-, Ni-, Pd-, PtOs@SV; all TMIr@SV; Fe-, Co-, Os-, Ir-, PtPt@SV), that is in a good agreement with predictions in **Sec. III B**. It has to be emphasized, that in most cases the energy difference of the perpendicular and tilted geometry of the dimer is very low.

Examined defects decorated by pyridinic nitrogen atoms (NSV, NDV) leave unpaired electrons on the single adsorbed TM atom and it supports the creation of the upright TM dimer. The only systematic exceptions are TM10@NDV systems (*c.f.* **Sec. III B**), from which the only stable perpendicular derived dimer is FePt@NDV (but the stability is very low), in some other analogous systems the TM↑ is even strongly pushed away from the TM↓ adsorbed at the defect. Other significant exceptions are in dimers where a Rh atom is up, there are much fewer stable perpendicular cases in comparison with the other TM atoms. Among the considered defects, dimers at NSV prefer the upright geometry the most. Exceptions are in some cases with TM atom from Ru group as TM↑, they are attracted by graphene more.

The affinity of TM↑ towards the graphene plane (*i.e.*, the dimer's compulsion to be tilted) can be partially justified by TM↑'s adsorption energy at pristine graphene. For following considerations, we take the adsorption energies of TM atoms at pristine graphene from Ref. 37, but in negative values to be consistent with our work. Correlation coefficients with adsorption energies at pristine graphene are calculated for every set (given TM↓ adsorbed at given defective graphene; TM↑ differs). Correlation coefficients are in most cases positive, which means that the TM dimer is in the perpendicular position less stable as the adsorption energy of TM↑ at pristine graphene increases (is more negative). The correlation coefficients of sets with TM↓ from Co and Ni groups correlate more strongly than with TM↓ from Fe group. Moreover, the correlation averaged among all sets at NDV ($0.75\pm0.14$) is greater and more consistent than at SV ($0.48\pm0.32$) and NSV ($0.46\pm0.26$). Probably there are also additional factors influencing the perpendicular stability.

Perpendicular TM dimers at DV are unstable and the TM↑ is strongly attracted by the defect, *c.f.*, **Sec. III B**, in line with Ref. 17. In most cases, none of the calculations of a given system converged to the upright geometry of the dimer, so we could not determine their $E_{perp}$. Dimers can be tilted (**Fig. 7a**), or in a specific (through) position, where one TM atom is placed under the graphene plane and the second one is placed above the plane (**Fig. 7b**). Dimers in such configurations do not possess high magnetic moments, and thus are not important for the aims of this thesis and will not be considered further.

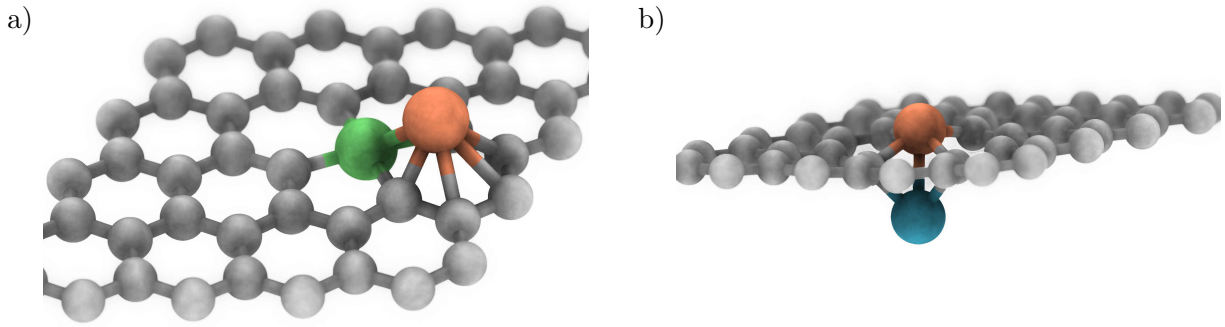


**FIG. 7:** Different examples of structures of adsorbed TM dimers at DV: a) tilted dimer (FeNi@DV), b) dimer through graphene (PdFe@DV).

### D. Scalar-relativistic Properties of Stable Transition-metal Dimers

#### *1. TM Dimers at Single Vacancy*

TM dimers at SV require as TM↓ an element that has great polarizability (*c.f.*, **Sec. III B**). From our examined elements, only Os, Ir, and Pt are suitable. In **Table IV** it is clearly visible that the element of TM↑ has a low impact on the geometry properties related mostly with the TM↓ ($d_{van}$, $d_{vag}$, and $d_{ba}$). The given properties are also only slightly larger than at the corresponding systems with single TM atoms at defective graphene.[13] $E_{ad2}$ of the elements from the later periods is generally larger than from those from the earlier periods. The only exception is Pd that is bound overall weaker; the reason is the full $d$ shell groundstate in its free atomic state. $d_d$ slightly differ without any observable trend. $q_{\mathrm{TM}\uparrow}$ systematically decreases in all horizontal groups of TM↑, which is not surprising, as the electronegativity of TM↑ increases similarly. At the same time, $q_{\mathrm{TM}\downarrow}$ increases. It is worth mentioning that in TMOs@SV and TMIr@SV the $q_{\mathrm{TM}\downarrow}$ are closest to the values of $q_{\mathrm{TM}}$ in the corresponding systems with a single adsorbed TM atom, *e.g.*, Os@SV and Ir@SV[13], respectively, when $q_{\mathrm{TM}\uparrow}$ is the closest to 0. In TMPt@SV the closest value of $q_{\mathrm{TM}\downarrow}$ to $q_{\mathrm{TM}}$ is obtained in OsPt@SV where $q_{\mathrm{TM}\uparrow} = -0.08$ e.

Before we start the discussion of the electronic properties by following **Sec. III B**, we need to make a description of a donor-acceptor bond in an exemplary system PtPt@SV, because the only bond within the TM dimer is (according to our predictions) of a donor-acceptor origin and the explanation is therefore as simple as it can be (without any additional bond). There are two possible explanations (*c.f.*, **Fig. 8**). I) Pt↑ accepts one electron in the spin-down channel ($N_{rel} = -1$). Then the unpaired electron at Pt↑ changes its spin (*i.e.*, the spin-flip), which preserves the absolute value of the local magnetic

**TABLE IV:** SR properties of stable perpendicular TM dimers at SV. Distance of TM atoms within the TM dimer ($d_d$), vertical distance of TM↓ above its neighbours ($d_{van}$), vertical distance of TM↓ above average graphene $z$ coordinate ($d_{vag}$), graphene buckling amplitude ($d_{ba}$), all in Å. Adsorption energy of the second TM atom ($E_{ad2}$, in eV). Maximal number of covalent bonds within the TM dimer ($N_{bom,coval}$), real bond order within the TM dimer ($N_{bor}$, **Eq. 37**), number of relocated electrons in the minority spin channel from TM↑ to TM↓ ($N_{rel}$, **Eq. 39**). Total magnetic moment of the supercell ($\mu_{tot}$), sum of all local magnetic moments within the supercell ($\mu_{sum}$), calculated magnetic moment of defective graphene ($\mu_{\mathrm{VG},calc}$, **Eq. 42**), of TM↓ ($\mu_{\mathrm{TM}\downarrow,calc}$, **Eq. 42**), and of TM↑ ($\mu_{\mathrm{TM}\uparrow,calc}$, **Eq. 42**), all in $\mu_\mathrm{B}$. Bader charge located on TM↓ ($\mu_{\mathrm{TM}\downarrow}$) and on TM↑ ($\mu_{\mathrm{TM}\uparrow}$), in e.

| System | $d_d$ | $d_{van}$ | $d_{vag}$ | $d_{ba}$ | $E_{ad2}$ | $N_{bom,coval}$ | $N_{bor}$ | $N_{rel}$ | $\mu_{tot}$ | $\mu_{sum}$ | $\mu_{\mathrm{VG},calc}$ | $\mu_{\mathrm{TM}\downarrow,calc}$ | $\mu_{\mathrm{TM}\uparrow,calc}$ | $q_{\mathrm{TM}\downarrow}$ | $q_{\mathrm{TM}\uparrow}$ |
|---|---|---|---|---|---|---|---|---|---|---|---|---|---|---|---|
| FeOs@SV | 2.43 | 1.08 | 1.66 | 0.59 | −2.0 | 0 | 0.09 | −0.37 | 3.82 | 3.47 | 0.04 | 0.24 | 3.54 | 0.54 | 0.11 |
| CoOs@SV | 2.36 | 1.09 | 1.66 | 0.57 | −2.2 | 0 | 0.18 | −0.52 | 2.65 | 2.45 | 0.03 | 0.32 | 2.31 | 0.58 | 0.00 |
| NiOs@SV | 2.30 | 1.09 | 1.65 | 0.57 | −2.4 | 0 | 0.08 | −0.86 | 1.84 | 1.70 | 0.14 | 0.64 | 1.06 | 0.70 | −0.19 |
| PdOs@SV | 2.47 | 1.09 | 1.66 | 0.57 | −1.9 | 0 | 0.30 | −0.91 | 1.40 | 0.91 | 0.15 | 0.46 | 0.79 | 0.71 | −0.21 |
| PtOs@SV | 2.35 | 1.12 | 1.66 | 0.54 | −3.5 | 0 | 0.12 | −1.26 | 1.77 | 1.55 | 0.20 | 0.94 | 0.62 | 0.88 | −0.47 |
| FeIr@SV | 2.38 | 1.10 | 1.65 | 0.56 | −2.1 | 1 | 1.00 | 0.24 | 3.00 | 2.78 | −0.11 | −0.13 | 3.24 | 0.28 | 0.13 |
| CoIr@SV | 2.38 | 1.10 | 1.64 | 0.55 | −2.3 | 1 | 1.00 | 0.05 | 2.00 | 2.02 | −0.06 | 0.02 | 2.05 | 0.34 | −0.01 |
| NiIr@SV | 2.33 | 1.09 | 1.63 | 0.54 | −2.6 | 1 | 1.08 | −0.06 | 0.83 | 0.85 | −0.02 | 0.00 | 0.86 | 0.43 | −0.14 |
| RuIr@SV | 2.41 | 1.12 | 1.66 | 0.54 | −2.6 | 1 | 1.00 | −0.02 | 3.00 | 2.55 | −0.05 | 0.08 | 2.98 | 0.37 | 0.03 |
| RhIr@SV | 2.42 | 1.11 | 1.65 | 0.54 | −2.7 | 1 | 1.05 | −0.09 | 1.90 | 1.44 | −0.02 | 0.06 | 1.86 | 0.42 | −0.06 |
| PdIr@SV | 2.46 | 1.09 | 1.63 | 0.54 | −2.2 | 1 | 1.02 | −0.23 | 0.95 | 0.56 | 0.08 | 0.12 | 0.74 | 0.45 | −0.15 |
| OsIr@SV | 2.37 | 1.14 | 1.68 | 0.55 | −3.0 | 1 | 1.05 | −0.10 | 2.91 | 2.51 | 0.04 | 0.02 | 2.85 | 0.41 | −0.06 |
| IrIr@SV | 2.35 | 1.13 | 1.67 | 0.53 | −3.1 | 1 | 1.16 | −0.26 | 1.67 | 1.57 | −0.02 | 0.11 | 1.58 | 0.55 | −0.32 |
| PtIr@SV | 2.38 | 1.12 | 1.65 | 0.53 | −3.5 | 1 | 1.22 | −0.27 | 0.56 | 0.52 | 0.01 | 0.04 | 0.51 | 0.58 | −0.44 |
| FePt@SV | 2.22 | 1.18 | 1.68 | 0.50 | −1.9 | 0 | 1.00 | −0.43 | 2.00 | 2.33 | −0.44 | −0.13 | 2.57 | 0.20 | 0.05 |
| CoPt@SV | 2.27 | 1.19 | 1.68 | 0.49 | −2.2 | 0 | 1.00 | −0.62 | 1.00 | 1.36 | −0.29 | −0.09 | 1.38 | 0.15 | 0.01 |
| OsPt@SV | 2.34 | 1.19 | 1.70 | 0.50 | −3.0 | 0 | 1.00 | −0.69 | 2.00 | 2.02 | −0.27 | −0.04 | 2.31 | 0.27 | −0.08 |
| IrPt@SV | 2.33 | 1.18 | 1.67 | 0.49 | −3.4 | 0 | 1.00 | −0.84 | 1.00 | 1.02 | −0.13 | −0.03 | 1.16 | 0.35 | −0.28 |
| PtPt@SV | 2.32 | 1.16 | 1.66 | 0.50 | −3.6 | 0 | 1.00 | −1.00 | 0.00 | 0.00 | 0.00 | 0.00 | 0.00 | 0.41 | −0.46 |

moment on Pt↑. The spin-flip is supported by the following energetically-advantageous formation of a covalent bond with an unpaired electron at Pt↓ ($N_{bor} = 1$). II) One of the unpaired electrons at Pt↑ changes its spin and pairs with another unpaired electron at Pt↑ and therefore it decreases magnetic moment on Pt↑ from 2 $\mu_\mathrm{B}$ to 0. We did not considered these cases in **Sec. III B** as it seemingly violates the Hund's rule of the maximal multiplicity but here it is caused by the interaction with another TM atom. We

could introduce a new quantity (similar to $N_{rel}$ but local only for Pt↑) that would have value $-2$, *i.e.*, the change in the local magnetic moment of Pt↑ is similar as it would accept 2 electrons in the spin-down channel. Then Pt↑ accepts whole electron pair to the emptied orbital; one bond is formed ($N_{bor} = 1$). This donation can be thoughtfully divided to two steps. Pt↑ virtually accepts an electron in the spin-up channel ($N_{rel,virtual} = 1$) and thanks to that it is able to form covalent bond with Pt↓ that posses an unpaired electron with spin down. Combined $N_{rel}$ (as we used in the rest of the thesis) is then $N_{rel} = -2 + 1 = -1$ which is the same as in the explanation I) and calculated by the equations from **Sec. III B**. Although the explanation I) seems to be more straightforward as it strictly follows the derived equations, the explanation II) is more preferred in the coordination chemistry. The formation of the coordination-covalent bond is an excellent opportunity to fill up the $d$ shell of Pt↑ which is clearly visible on the value of $E_{ad2}$.

As it was shown in **Sec. III B**, examined dimers (TMOs@SV and TMPt@SV) cannot be created by the simple formation of covalent bonds ($N_{bom,coval} = 0$). According to $N_{bor}$ in TMOs@SV, it is apparent that no real bond is formed. $N_{rel}$ indicates that the interaction has mainly an electrostatic origin. $q_{\mathrm{TM}\uparrow}$ supports this statement only at the later TM↑ atoms but it strongly depends on the Bader's definition of an atom. We may

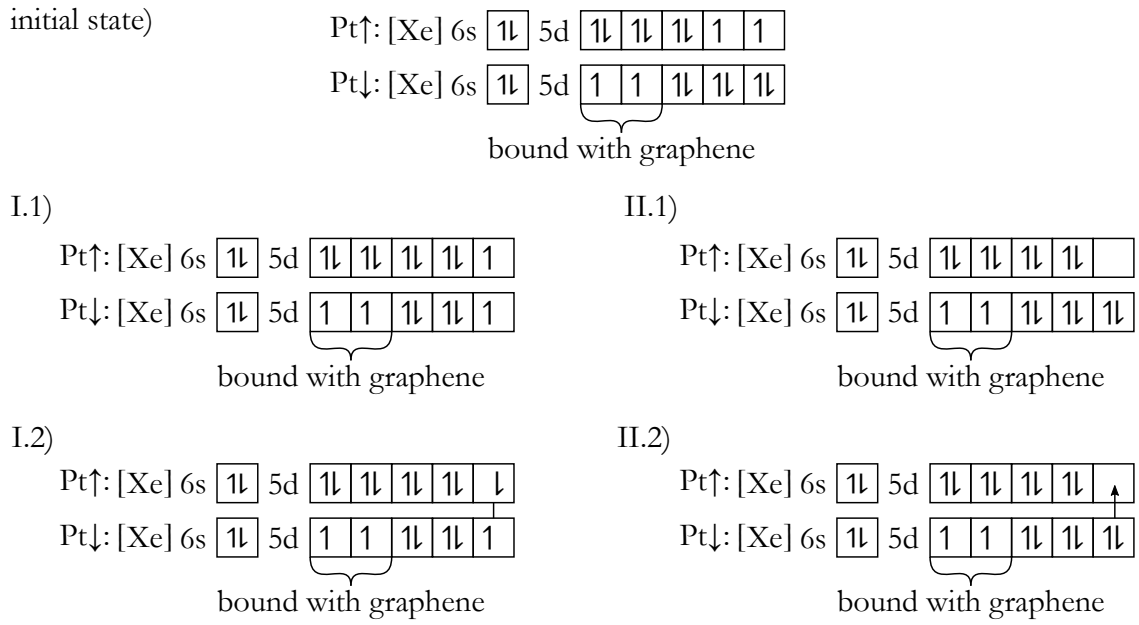


**FIG. 8:** Schemes of possible bond formations in PtPt dimer in PtPt@SV. The explanation is developed in the main text. All schemes are simplified and do not consider the real energy of different $d$ orbitals, similarly the bonds with graphene are here pictured as strictly localized. Given $d$ orbitals are not ordered by their magnetic quantum number because now it is not necessary. An arrow in II.2 represents the donor-acceptor bond.

therefore expect that the shift of charge occurs only in a small region and is therefore poorly perceptible by the Bader charge analysis. It also needs to be highlighted that the presence of TM↑ induces magnetism in the rest of the initially non-magnetic TM@SV system[13], in PtOs@SV there is even a higher magnetic moment presented on Os than on Pt.

Properties of TMIr@SV are similar to the ones predicted in **Sec. III B**. Real bond order in all such systems is similar to the maximal number of classical covalent bonds (1) and $N_{rel}$ is small. $\mu_{tot}$ is mostly implied by TM↑ which is decreased by $\sim 1$ $\mu_{\mathrm{B}}$ with respect to the unbound state of TM↑, while magnetic moments of TM↓ and graphene are negligible.

In TMPt@SV, again, the number of covalent bonds that can be created is zero but there is a significant difference of Os@SV and Pt@SV. The latter has one additional electron pair (*c.f.*, **Eq. 33**) that is rather delocalized. Values of $N_{bor}$ (**Table IV**) suggest that all TM dimers in mentioned TMPt@SV systems have one single bond while $N_{rel}$ points out that these bonds are mostly of the donor-acceptor origin. Donor-acceptor character of bonds increases from Fe to Pt as TM↑ which is not surprising because the acceptance of the electron pair in Pt↑ leads to the completely filled 5 *d* shell.

The magnetic moments (both total and local) presented in this subchapter are in a very good agreement with the values reported in the supporting information of Ref. 17.

### *2. TM Dimers at Single Vacancy Decorated by Pyridinic Nitrogen Atoms*

**Systems TMTM8@NSV** are summarized in **Table V**. The geometry parameters are rather diverse and depend on both TM↓ and TM↑ (in contrast with TMTM@SV). $d_{ba}$ is the only quantity that remains similar with only a small increment from TMFe@NSV to TMOs@NSV by $\sim$ 0.1 Å. The interaction with the second TM atom in Fe@NSV averagely decreases $d_{vag}$ and increases $d_{van}$ (with respect to Fe@NSV) which gives rise to a significantly lowered graphene buckling. Although the values of $d_{vag}$ are similar in TMRu@NSV and TMOs@NSV and also very close to those of Ru@NSV and Os@NSV[13], $d_{van}$ are similar in TMRu@NSV and TMOs@NSV but they are longer than in the corresponding systems with a single adsrobed TM atom by $\sim$ 0.2 Å which implies that graphene is less buckled. Values of $d_d$ are rather diverse and generally do not correlate with $E_{ad2}$. The only exception is Pd as its interaction with TM↓ is overall the weakest and $d_d$ are the longest. $E_{ad2}$ systematically increases from the systems with TM↑ from

earlier periods to the systems with TM↑ from later periods (similarly as in TMTM@SV).

Although theoretically $N_{bom,coval} = 3$ in triads FeTM8@NSV and CoTM8@NSV, the small TM↑ atoms are not capable of forming triple bonds (when they are TM↑) and prefer the creation of double bonds instead. It would leave an unpaired electron on TM↓ which is probably unfavourable. Therefore, the second bond is of a donor-acceptor origin (*c.f.*, **Page 50**) but now TM↑ is the donor. *d* shell of TM↓ is thus filled and the highest

**TABLE V:** SR properties of stable perpendicular TM dimers (TM8 as TM↓) at NSV. *Cf.,* **Table IV** for the description of the included properties.

| System | $d_d$ | $d_{van}$ | $d_{vag}$ | $d_{ba}$ | $E_{ad2}$ | $N_{bom,}$ $_{coval}$ | $N_{bor}$ | $N_{rel}$ | $\mu_{tot}$ | $\mu_{sum}$ | $\mu_{\mathrm{VG},}$ $_{calc}$ | $\mu_{\mathrm{TM}\downarrow,}$ $_{calc}$ | $\mu_{\mathrm{TM}\uparrow,}$ $_{calc}$ | $q_{\mathrm{TM}\downarrow}$ | $q_{\mathrm{TM}\uparrow}$ |
|---|---|---|---|---|---|---|---|---|---|---|---|---|---|---|---|
| FeFe@NSV | 2.06 | 1.01 | 1.35 | 0.35 | −2.0 | 3 | 2.05 | 1.22 | 2.90 | 2.84 | −0.06 | −0.21 | 3.17 | 0.72 | −0.12 |
| CoFe@NSV | 2.06 | 0.98 | 1.32 | 0.34 | −2.2 | 3 | 2.06 | 1.05 | 1.89 | 1.88 | −0.04 | −0.06 | 1.99 | 0.81 | −0.26 |
| NiFe@NSV | 2.10 | 1.28 | 1.60 | 0.32 | −2.5 | 2 | 0.00 | −0.77 | 5.00 | 4.75 | 0.23 | 3.54 | 1.23 | 0.80 | −0.29 |
| PdFe@NSV | 2.25 | 0.87 | 1.22 | 0.35 | −1.9 | 2 | 2.50 | 0.50 | 0.00 | 0.00 | 0.00 | 0.00 | 0.00 | 0.95 | −0.33 |
| OsFe@NSV | 1.99 | 1.03 | 1.36 | 0.33 | −3.7 | 3 | 2.74 | 0.19 | 1.52 | 1.47 | −0.12 | 0.18 | 1.45 | 0.85 | −0.29 |
| IrFe@NSV | 2.04 | 0.99 | 1.31 | 0.33 | −3.8 | 3 | 2.85 | 0.15 | 0.30 | 0.32 | −0.05 | 0.05 | 0.30 | 0.90 | −0.47 |
| PtFe@NSV | 2.15 | 0.98 | 1.30 | 0.32 | −3.8 | 2 | 2.00 | 0.14 | 1.00 | 0.90 | 0.02 | 0.85 | 0.14 | 0.97 | −0.60 |
| FeRu@NSV | 2.12 | 1.22 | 1.61 | 0.39 | −2.5 | 3 | 2.14 | 1.11 | 2.73 | 2.68 | −0.12 | −0.13 | 2.97 | 0.56 | −0.08 |
| CoRu@NSV | 2.03 | 1.17 | 1.58 | 0.41 | −2.6 | 3 | 2.25 | 0.82 | 1.50 | 1.50 | −0.08 | 0.01 | 1.57 | 0.81 | −0.27 |
| NiRu@NSV | 2.13 | 1.13 | 1.55 | 0.42 | −2.8 | 2 | 2.34 | 0.49 | 0.32 | 0.27 | 0.04 | 0.13 | 0.15 | 0.79 | −0.26 |
| RuRu@NSV | 2.04 | 1.26 | 1.64 | 0.38 | −3.5 | 3 | 2.86 | 0.24 | 1.27 | 1.14 | −0.10 | 0.00 | 1.38 | 0.80 | −0.34 |
| RhRu@NSV | 2.11 | 1.18 | 1.58 | 0.41 | −3.3 | 3 | 2.74 | 0.24 | 0.53 | 0.32 | −0.04 | 0.06 | 0.51 | 0.86 | −0.34 |
| PdRu@NSV | 2.33 | 1.08 | 1.52 | 0.43 | −2.2 | 2 | 2.50 | 0.50 | 0.00 | 0.00 | 0.00 | 0.00 | 0.00 | 0.88 | −0.36 |
| OsRu@NSV | 2.07 | 1.28 | 1.66 | 0.38 | −4.6 | 3 | 2.89 | 0.13 | 1.23 | 1.19 | −0.11 | 0.10 | 1.24 | 0.76 | −0.23 |
| IrRu@NSV | 2.11 | 1.22 | 1.61 | 0.39 | −4.7 | 3 | 3.00 | 0.00 | 0.00 | 0.00 | 0.00 | 0.00 | 0.00 | 0.89 | −0.47 |
| PtRu@NSV | 2.23 | 1.16 | 1.56 | 0.41 | −4.3 | 2 | 2.24 | 0.38 | 0.51 | 0.42 | 0.08 | 0.30 | 0.14 | 0.95 | −0.53 |
| FeOs@NSV | 2.14 | 1.23 | 1.66 | 0.43 | −3.3 | 3 | 2.26 | 1.01 | 2.48 | 2.46 | −0.12 | −0.15 | 2.75 | 0.77 | −0.10 |
| CoOs@NSV | 2.16 | 1.20 | 1.64 | 0.44 | −3.4 | 3 | 2.18 | 0.84 | 1.64 | 1.64 | −0.05 | 0.02 | 1.66 | 0.83 | −0.21 |
| NiOs@NSV | 2.16 | 1.14 | 1.60 | 0.46 | −3.6 | 2 | 2.50 | 0.50 | 0.00 | 0.00 | 0.00 | 0.00 | 0.00 | 0.89 | −0.26 |
| RuOs@NSV | 2.10 | 1.30 | 1.70 | 0.40 | −4.4 | 3 | 2.92 | 0.18 | 1.15 | 1.12 | −0.13 | 0.03 | 1.26 | 0.78 | −0.22 |
| RhOs@NSV | 2.13 | 1.25 | 1.67 | 0.42 | −4.2 | 3 | 3.00 | 0.00 | 0.00 | 0.00 | 0.00 | 0.00 | 0.00 | 0.97 | −0.46 |
| PdOs@NSV | 2.30 | 1.12 | 1.58 | 0.46 | −3.0 | 2 | 2.50 | 0.50 | 0.00 | 0.00 | 0.00 | 0.00 | 0.00 | 1.07 | −0.52 |
| OsOs@NSV | 2.14 | 1.27 | 1.69 | 0.42 | −5.4 | 3 | 2.84 | 0.18 | 1.32 | 1.28 | −0.13 | 0.11 | 1.34 | 0.87 | −0.24 |
| IrOs@NSV | 2.16 | 1.23 | 1.65 | 0.43 | −5.6 | 3 | 3.00 | 0.00 | 0.00 | 0.00 | 0.00 | 0.00 | 0.00 | 1.02 | −0.46 |
| PtOs@NSV | 2.26 | 1.16 | 1.61 | 0.45 | −5.2 | 2 | 2.47 | 0.48 | 0.06 | 0.04 | 0.01 | 0.03 | 0.01 | 1.07 | −0.51 |

contributions to the total magnetic moment come from TM↑.

Ru and Os as TM↑ have the expected properties without significant $N_{rel}$. Total magnetic moment is implied mostly by TM↑ ($\sim$ 1 $\mu_B$) whereas a contribution of graphene is slightly negative. Rh and Ir as TM↑ should form a triple bond and the resulting system should be non-magnetic. This is true in most cases or the solution is very close to it, $N_{rel}$ is equal or close to 0.

A special attention needs to be devoted to the Ni, Pd, and Pt as TM↑. According to the proposed model, the total magnetic moment (initially predicted to be $\sim$ 1 $\mu_B$) should be located mainly on TM↓. Fe and Co as TM↑ have already pointed out that this is energetically unfavourable and the electrons tend to relocate in order to lower the magnetic moment on TM↓ and increase it on TM↑, which can be observed in the values of $N_{rel}$. Nevertheless, $N_{bor}$ is in many cases higher than $N_{bom,coval}$ which implies the formation of a donor-acceptor bond. $\mu_{tot}$ in these systems lies in an interval $\langle 0, 1\ \mu_B \rangle$ and $N_{bor}$ in an interval $\langle 2,\ 2.5 \rangle$. The lowest $N_{bor}$ is in the PtFe@NSV system with $N_{rel}$ close to 0; Fe as TM↓ has among all the examined TM atoms the greatest potential to hold an unpaired electron. NiFe@NSV is a very special case that is hold together only by the electrostatic interactions (although other local minima with higher $N_{bor}$ may exist) because the formation of higher-order bonds is energetically unfavourable.

SR properties of **Systems TMTM9@NSV** are shown in **Table VI**. $d_d$ within groups with the same TM↓ are similar, the only exceptions are with Pd and Pt as TM↑ where $d_d$ is usually longer. $d_{vag}$, $d_{van}$, and $d_{ba}$ are similar within TMRh@NSV and TMIr@NSV groups, they are also very close to the values of the corresponding single adsorbed TM atom at NSV[13]. The average value of $d_{vag}$ in TMCo@NSV is comparable with that of Co@NSV but the value of $d_{van}$ is higher by $\sim$ 0.2 Å which gives rise to a smaller graphene buckling. The difference in $E_{ad2}$ is more modest than in TMTM8@NSV, follows the similar trend (the higher the period of TM↑, the stronger the binding), and PdTM9@NSV is again bound weakest.

$N_{bom,coval}$ in all given systems is 2. It is advantageous to divide the description of the electronic properties to two branches. I) systems in which $N_{bor} \sim N_{bom,coval}$ and $N_{rel}$ is close to 0. Total magnetic moments are close to the integer numbers and if the system is magnetic, the largest magnetic moment is located on TM↑. II) the most pronounced exceptions are in systems with Co as TM↓ and with Fe and Co as TM↑ as they tend to preserve the high magnetic moments at the mentioned atoms. $N_{bor}$ are usually

significantly smaller than $N_{bom,coval}$ and $N_{rel}$ has such value that enhances the magnetic moment on the Fe or Co atom. Surprisingly, electrons in many TMCo@NSV systems are relocated in the manner that magnetic moment of Co↓ is further enhanced, even in CoCo@NSV. It is also important to note that the magnetic moment of Fe in FeRh@NSV and FeIr@NSV is of the opposite direction than that of TM↓ and the rest of graphene.

**Table VII** lists the SR properties of **TMTM10@NSV systems**. $d_d$ in TMNi@NSV are similar and by $\sim 0.1$ Å shorter than in TMPd@NSV and TMPt@NSV. Alike as in the

**TABLE VI:** SR properties of stable perpendicular TM dimers (TM9 as TM↓) at NSV. *Cf.,* **Table IV** for the description of the included properties.

| System | $d_d$ | $d_{van}$ | $d_{vag}$ | $d_{ba}$ | $E_{ad2}$ | $N_{bom,}$ $_{coval}$ | $N_{bor}$ | $N_{rel}$ | $\mu_{tot}$ | $\mu_{sum}$ | $\mu_{\mathrm{VG},}$ $_{calc}$ | $\mu_{\mathrm{TM}\downarrow,}$ $_{calc}$ | $\mu_{\mathrm{TM}\uparrow,}$ $_{calc}$ | $q_{\mathrm{TM}\downarrow}$ | $q_{\mathrm{TM}\uparrow}$ |
|---|---|---|---|---|---|---|---|---|---|---|---|---|---|---|---|
| FeCo@NSV | 2.08 | 1.10 | 1.40 | 0.30 | −1.7 | 2 | 1.00 | 0.48 | 3.99 | 3.80 | 0.01 | 0.51 | 3.47 | 0.59 | −0.07 |
| CoCo@NSV | 2.09 | 1.20 | 1.53 | 0.33 | −2.1 | 2 | 0.00 | −0.56 | 5.00 | 4.76 | 0.24 | 2.31 | 2.44 | 0.70 | −0.17 |
| NiCo@NSV | 2.13 | 1.15 | 1.48 | 0.33 | −2.1 | 2 | 0.00 | −0.67 | 4.00 | 3.78 | 0.28 | 2.39 | 1.33 | 0.77 | −0.26 |
| RuCo@NSV | 2.10 | 1.07 | 1.37 | 0.31 | −2.2 | 2 | 2.00 | 0.48 | 2.00 | 1.73 | −0.20 | −0.28 | 2.48 | 0.67 | −0.18 |
| PdCo@NSV | 2.32 | 1.09 | 1.45 | 0.36 | −1.6 | 2 | 0.00 | −1.08 | 4.00 | 3.31 | 0.33 | 2.75 | 0.92 | 0.85 | −0.28 |
| OsCo@NSV | 2.07 | 1.07 | 1.37 | 0.31 | −3.1 | 2 | 1.98 | 0.01 | 2.04 | 1.89 | −0.11 | 0.12 | 2.03 | 0.69 | −0.26 |
| IrCo@NSV | 2.08 | 1.04 | 1.33 | 0.29 | −3.2 | 2 | 1.93 | −0.30 | 1.14 | 1.06 | −0.02 | 0.40 | 0.77 | 0.79 | −0.46 |
| PtCo@NSV | 2.17 | 1.05 | 1.34 | 0.29 | −3.1 | 2 | 1.12 | −0.60 | 1.76 | 1.59 | 0.19 | 1.28 | 0.28 | 0.87 | −0.55 |
| FeRh@NSV | 2.19 | 1.31 | 1.64 | 0.32 | −2.4 | 2 | 1.81 | 0.91 | 2.39 | 2.41 | −0.29 | −0.43 | 3.10 | 0.47 | −0.06 |
| CoRh@NSV | 2.15 | 1.31 | 1.61 | 0.30 | −2.4 | 2 | 1.09 | 0.42 | 2.81 | 2.63 | 0.13 | 0.35 | 2.33 | 0.49 | −0.10 |
| NiRh@NSV | 2.20 | 1.28 | 1.62 | 0.35 | −2.5 | 2 | 1.92 | 0.29 | 0.16 | 0.31 | −0.07 | −0.13 | 0.37 | 0.53 | −0.21 |
| RuRh@NSV | 2.15 | 1.33 | 1.66 | 0.33 | −2.9 | 2 | 2.00 | 0.09 | 2.00 | 1.81 | −0.15 | 0.07 | 2.09 | 0.53 | −0.18 |
| OsRh@NSV | 2.16 | 1.33 | 1.68 | 0.34 | −3.9 | 2 | 2.00 | −0.11 | 2.00 | 1.84 | −0.07 | 0.18 | 1.89 | 0.54 | −0.19 |
| IrRh@NSV | 2.17 | 1.30 | 1.64 | 0.34 | −4.0 | 2 | 1.96 | −0.26 | 1.08 | 1.01 | −0.03 | 0.33 | 0.78 | 0.65 | −0.36 |
| PtRh@NSV | 2.28 | 1.25 | 1.59 | 0.34 | −3.8 | 2 | 2.00 | 0.00 | 0.00 | 0.00 | 0.00 | 0.00 | 0.00 | 0.70 | −0.48 |
| FeIr@NSV | 2.18 | 1.33 | 1.69 | 0.36 | −3.5 | 2 | 1.80 | 0.75 | 2.40 | 2.37 | −0.24 | −0.31 | 2.95 | 0.44 | 0.03 |
| CoIr@NSV | 2.11 | 1.30 | 1.68 | 0.38 | −3.5 | 2 | 1.70 | 0.44 | 1.61 | 1.58 | −0.10 | −0.04 | 1.74 | 0.48 | −0.01 |
| NiIr@NSV | 2.17 | 1.29 | 1.67 | 0.38 | −3.7 | 2 | 2.00 | 0.00 | 0.00 | 0.00 | 0.00 | 0.00 | 0.00 | 0.53 | −0.19 |
| RuIr@NSV | 2.19 | 1.36 | 1.73 | 0.37 | −4.3 | 2 | 2.00 | 0.01 | 2.00 | 1.75 | −0.07 | 0.06 | 2.01 | 0.45 | −0.06 |
| RhIr@NSV | 2.20 | 1.33 | 1.70 | 0.37 | −4.1 | 2 | 2.00 | −0.18 | 1.00 | 0.83 | −0.01 | 0.19 | 0.82 | 0.64 | −0.30 |
| PdIr@NSV | 2.32 | 1.27 | 1.65 | 0.38 | −3.0 | 2 | 2.00 | 0.00 | 0.00 | 0.00 | 0.00 | 0.00 | 0.00 | 0.60 | −0.34 |
| OsIr@NSV | 2.16 | 1.36 | 1.73 | 0.37 | −5.1 | 2 | 1.96 | −0.18 | 2.08 | 1.90 | −0.10 | 0.32 | 1.86 | 0.63 | −0.18 |
| IrIr@NSV | 2.20 | 1.31 | 1.69 | 0.38 | −5.1 | 2 | 2.00 | −0.31 | 1.00 | 0.89 | 0.00 | 0.31 | 0.69 | 0.67 | −0.32 |
| PtIr@NSV | 2.29 | 1.28 | 1.66 | 0.38 | −5.1 | 2 | 2.00 | 0.00 | 0.00 | 0.00 | 0.00 | 0.00 | 0.00 | 0.71 | −0.43 |

previously discussed systems, $d_{vag}$ and $d_{van}$ in TMPd@NSV and TMPt@NSV are similar and slightly larger than in the corresponding systems with single adsorbed TM atom at NSV[13] and $d_{ba}$ is only quite lower. Analogously to TMFe@NSV and TMCo@NSV, $d_{van}$ in TMNi@NSV is significantly longer than in Ni@NSV while $d_{vag}$ is comparable; this implies a smaller graphene buckling. $E_{ad2}$ are similar within TMNi@NSV, TMPd@NSV, and TMPt@NSV systems; TM↑ from the later periods are generally bound stronger.

Values of $\mu_{tot}$ point out that only sparse covalent bonds are formed despite $N_{bom,coval}$ is equal to 1 in all cases. $N_{rel}$ suggest that the prevailing bonding mechanism is of an electrostatic origin, in all cases with $N_{bor} = 0$ the magnetic moment of TM↑ is suppressed

**TABLE VII:** SR properties of stable perpendicular TM dimers (TM10 as TM↓) at NSV. *Cf.,* **Table IV** for the description of the included properties.

| System | $d_d$ | $d_{van}$ | $d_{vag}$ | $d_{ba}$ | $E_{ad2}$ | $N_{bom,coval}$ | $N_{bor}$ | $N_{rel}$ | $\mu_{tot}$ | $\mu_{sum}$ | $\mu_{VG,calc}$ | $\mu_{TM\downarrow,calc}$ | $\mu_{TM\uparrow,calc}$ | $q_{TM\downarrow}$ | $q_{TM\uparrow}$ |
|---|---|---|---|---|---|---|---|---|---|---|---|---|---|---|---|
| FeNi@NSV | 2.12 | 1.20 | 1.51 | 0.31 | −2.2 | 1 | 0.00 | −0.38 | 5.00 | 4.73 | 0.21 | 1.16 | 3.62 | 0.50 | 0.03 |
| CoNi@NSV | 2.12 | 1.19 | 1.49 | 0.30 | −2.2 | 1 | 0.00 | −0.52 | 4.00 | 3.80 | 0.27 | 1.25 | 2.48 | 0.54 | −0.07 |
| NiNi@NSV | 2.16 | 1.16 | 1.46 | 0.31 | −2.1 | 1 | 0.00 | −0.67 | 3.00 | 2.86 | 0.31 | 1.35 | 1.33 | 0.61 | −0.19 |
| OsNi@NSV | 2.20 | 1.22 | 1.51 | 0.30 | −2.9 | 1 | 0.00 | −0.60 | 5.00 | 4.60 | 0.26 | 1.33 | 3.40 | 0.63 | −0.16 |
| IrNi@NSV | 2.21 | 1.19 | 1.49 | 0.29 | −3.1 | 1 | 0.00 | −0.74 | 4.00 | 3.70 | 0.33 | 1.41 | 2.26 | 0.71 | −0.31 |
| PtNi@NSV | 2.21 | 1.18 | 1.46 | 0.29 | −3.0 | 1 | 0.00 | −0.90 | 3.00 | 2.77 | 0.40 | 1.51 | 1.10 | 0.79 | −0.47 |
| FePd@NSV | 2.21 | 1.56 | 1.82 | 0.26 | −2.3 | 1 | 0.00 | −0.17 | 5.00 | 4.65 | 0.37 | 0.80 | 3.83 | 0.24 | 0.15 |
| CoPd@NSV | 2.21 | 1.54 | 1.81 | 0.27 | −2.3 | 1 | 0.00 | −0.34 | 4.00 | 3.73 | 0.44 | 0.90 | 2.66 | 0.34 | 0.00 |
| RuPd@NSV | 2.32 | 1.57 | 1.85 | 0.28 | −2.1 | 1 | 0.00 | −0.42 | 5.00 | 4.25 | 0.42 | 1.00 | 3.58 | 0.32 | 0.09 |
| OsPd@NSV | 2.26 | 1.50 | 1.78 | 0.28 | −2.4 | 1 | 2.00 | −0.63 | 1.00 | 0.91 | −0.21 | −0.15 | 1.37 | 0.38 | 0.04 |
| IrPd@NSV | 2.33 | 1.53 | 1.79 | 0.26 | −2.9 | 1 | 0.00 | −0.52 | 4.00 | 3.62 | 0.48 | 1.04 | 2.48 | 0.46 | −0.14 |
| PtPd@NSV | 2.33 | 1.44 | 1.69 | 0.26 | −2.8 | 1 | 1.00 | −0.49 | 1.00 | 0.92 | 0.18 | 0.31 | 0.51 | 0.56 | −0.43 |
| FePt@NSV | 2.20 | 1.57 | 1.84 | 0.26 | −3.4 | 1 | 0.00 | −0.17 | 5.00 | 4.53 | 0.36 | 0.81 | 3.83 | 0.15 | 0.24 |
| CoPt@NSV | 2.20 | 1.55 | 1.82 | 0.27 | −3.3 | 1 | 0.00 | −0.37 | 4.00 | 3.62 | 0.44 | 0.92 | 2.63 | 0.22 | 0.12 |
| NiPt@NSV | 2.22 | 1.49 | 1.74 | 0.25 | −3.2 | 1 | 1.00 | −0.15 | 1.00 | 0.95 | 0.06 | 0.09 | 0.85 | 0.26 | −0.03 |
| RuPt@NSV | 2.27 | 1.54 | 1.80 | 0.26 | −3.2 | 1 | 1.96 | −0.31 | 1.09 | 0.93 | −0.33 | −0.32 | 1.74 | 0.25 | 0.07 |
| RhPt@NSV | 2.27 | 1.51 | 1.77 | 0.27 | −3.2 | 1 | 1.00 | −0.57 | 2.00 | 1.63 | 0.18 | 0.38 | 1.43 | 0.33 | −0.06 |
| PdPt@NSV | 2.44 | 1.51 | 1.75 | 0.24 | −2.3 | 1 | 0.00 | −0.98 | 3.00 | 2.30 | 0.72 | 1.26 | 1.02 | 0.33 | −0.04 |
| OsPt@NSV | 2.24 | 1.44 | 1.76 | 0.32 | −4.0 | 1 | 1.80 | −0.59 | 1.40 | 1.27 | −0.11 | −0.09 | 1.61 | 0.43 | −0.09 |
| IrPt@NSV | 2.25 | 1.44 | 1.75 | 0.31 | −4.2 | 1 | 2.00 | −1.00 | 0.00 | 0.00 | 0.00 | 0.00 | 0.00 | 0.46 | −0.27 |
| PtPt@NSV | 2.32 | 1.45 | 1.72 | 0.27 | −4.1 | 1 | 1.00 | −0.62 | 1.00 | 0.86 | 0.26 | 0.36 | 0.38 | 0.52 | −0.35 |

while the magnetic moment of TM↓ is enhanced, sum of a magnetic moments of TM↓ and of graphene is higher then $\mu_{tot}$ of the corresponding system with a single adsorbed TM atom[13]. Systems that form covalent bonds within the TM dimer generally cannot be systematically summarized. Systems with $N_{bor} = N_{bom,coval} = 1$ usually posses high negative values of $N_{rel}$; contributions to the total magnetic moment come also from TM↓ and from graphene. Systems with TM8 as TM↑ tend to have higher values of $N_{bor}$, magnetic moments of TM↓ and graphene have an opposite orientations than that of TM↑. The remaining system, IrPt@NSV, contains a double bond within the TM dimer, one is a classical covalent bond, the second one is of a donor-acceptor origin with Pt as a donor (*c.f.*, **Page 50**) and the whole structure is non-magnetic.

### *3. TM Dimers at Double Vacancy Decorated by Pyridinic Nitrogen Atoms*

SR properties of **TMTM8@NDV systems** are presented in **Table VIII**. $d_d$ are dependent of both TM↓ and TM↑ with the highest values when Pd and Pt are present as TM↑. Values of $d_{van}$ are similar in TMFe@NDV with TM↑ from Fe- and Ru groups ($d_{van} \simeq 0.20$ Å), and in TMRu@NDV with TM↑ from Fe- and Ru groups ($d_{van} \simeq 0.34$ Å). Values of both TMFe@NDV and TMRu@NDV with TM↑ from the Os group are by $\sim$ 0.1 Å higher than that of the previously discussed cases. A similar shift of values can be observed between TMOs@NDV systems with TM↑ from Fe- and Ru groups, and from Ru- and Os groups. We need to highlight the value of $d_{van}$ of OsRu@NDV which is significantly higher than the other values of TMRu@NDV; $d_d$ in the given system is, on the other hand, the smallest and it is the only TMRu@NDV system that has $N_{bor} \simeq 2$ while the values of the other systems are much smaller. Higher $N_{bor}$ thus presumably causes the closer distance within the TM dimer and it is also responsible for the dimer's shift farther from the graphene plane. Values of $d_{ba}$ are comparable with the corresponding values in systems with a single TM@NDV. Adsorption energies within TMTM8@NDV systems with the same TM↓ are similar, again with an exception of the PdTM8@NDV systems where the binding is again the weakest.

Although $N_{bom,coval} = 2$ in all given systems, $N_{bor}$ achieves this value only in systems with Os as TM↓ and concurrently TM↑ from Ru- or Os group. It is in line with the previous results where we observed that atoms from the earlier periods do not tend to form higher-order bonds. In TMFe@NDV, magnetic moment of Fe↓ is decreased when TM↑ is Fe, Co, or Os; in other cases the magnetic moment is increased. Contributions

to the total magnetic moment from graphene are in all TMFe@NDV systems slightly negative. As in TMFe@NDV, the magnetic moment of Ru↓ is decreased if TM↑ is Fe, Co, Ni, Ru, or Ir; in TMOs@NDV the magnetic moment of Os↓ is decreased when TM↑ is Fe, Co, or Ni. Generally, if TM↑ is an element that commonly tends to have high spin moments, the magnetic moment of TM↑ is increased and the magnetic moment of TM↓ is decreased. PdOs@NDV and PtOs@NDV are strictly following the presumptions

**TABLE VIII:** SR properties of stable perpendicular TM dimers (TM8 as TM↓) at NDV. *Cf.,* **Table IV** for the description of the included properties.

| System | $d_d$ | $d_{van}$ | $d_{vag}$ | $d_{ba}$ | $E_{ad2}$ | $N_{bom}$, $_{coval}$ | $N_{bor}$ | $N_{rel}$ | $\mu_{tot}$ | $\mu_{sum}$ | $\mu_{\mathrm{VG}}$, $_{calc}$ | $\mu_{\mathrm{TM}\downarrow}$, $_{calc}$ | $\mu_{\mathrm{TM}\uparrow}$, $_{calc}$ | $q_{\mathrm{TM}\downarrow}$ | $q_{\mathrm{TM}\uparrow}$ |
|---|---|---|---|---|---|---|---|---|---|---|---|---|---|---|---|
| FeFe@NDV | 2.09 | 0.21 | 0.30 | 0.09 | −1.5 | 2 | 0.98 | 0.35 | 4.04 | 3.76 | −0.04 | 0.71 | 3.37 | 0.80 | 0.28 |
| CoFe@NDV | 2.10 | 0.22 | 0.30 | 0.08 | −1.7 | 2 | 1.00 | 0.06 | 3.00 | 3.01 | −0.07 | 1.01 | 2.06 | 0.86 | 0.13 |
| NiFe@NDV | 2.12 | 0.20 | 0.27 | 0.07 | −1.8 | 2 | 1.00 | −0.11 | 2.01 | 2.05 | −0.06 | 1.18 | 0.90 | 0.91 | 0.05 |
| RuFe@NDV | 2.17 | 0.22 | 0.32 | 0.10 | −1.9 | 2 | 1.00 | −0.07 | 4.00 | 3.48 | −0.05 | 1.12 | 2.93 | 0.94 | 0.10 |
| RhFe@NDV | 2.19 | 0.19 | 0.27 | 0.08 | −1.9 | 2 | 0.99 | −0.42 | 3.02 | 2.72 | −0.08 | 1.51 | 1.59 | 0.93 | 0.07 |
| PdFe@NDV | 2.33 | 0.19 | 0.25 | 0.06 | −1.3 | 2 | 1.00 | −0.61 | 2.00 | 1.99 | −0.01 | 1.62 | 0.39 | 0.97 | −0.07 |
| OsFe@NDV | 2.21 | 0.29 | 0.38 | 0.09 | −2.1 | 2 | 1.00 | 0.05 | 4.00 | 3.70 | −0.03 | 0.98 | 3.05 | 0.92 | −0.06 |
| IrFe@NDV | 2.21 | 0.31 | 0.38 | 0.08 | −2.4 | 2 | 1.00 | −0.12 | 3.00 | 2.85 | −0.08 | 1.20 | 1.88 | 0.97 | −0.22 |
| PtFe@NDV | 2.24 | 0.29 | 0.35 | 0.06 | −2.4 | 2 | 1.00 | −0.30 | 2.00 | 1.97 | −0.09 | 1.39 | 0.70 | 1.02 | −0.33 |
| FeRu@NDV | 2.20 | 0.34 | 0.56 | 0.22 | −2.5 | 2 | 1.00 | 0.53 | 4.00 | 3.61 | 0.07 | 0.40 | 3.53 | 0.72 | 0.26 |
| CoRu@NDV | 2.17 | 0.34 | 0.55 | 0.20 | −2.6 | 2 | 1.00 | 0.27 | 3.00 | 2.80 | 0.09 | 0.64 | 2.27 | 0.81 | 0.10 |
| NiRu@NDV | 2.18 | 0.34 | 0.54 | 0.20 | −2.7 | 2 | 1.00 | 0.08 | 2.00 | 1.82 | 0.14 | 0.78 | 1.08 | 0.85 | 0.04 |
| RuRu@NDV | 2.26 | 0.36 | 0.58 | 0.22 | −2.8 | 2 | 1.00 | 0.15 | 4.00 | 3.28 | 0.16 | 0.69 | 3.15 | 0.89 | 0.09 |
| PdRu@NDV | 2.39 | 0.32 | 0.53 | 0.20 | −1.8 | 2 | 1.10 | −0.32 | 1.80 | 1.61 | 0.18 | 1.04 | 0.58 | 0.89 | −0.08 |
| OsRu@NDV | 2.13 | 0.58 | 0.78 | 0.20 | −3.4 | 2 | 2.07 | −0.27 | 1.85 | 1.58 | 0.17 | 0.03 | 1.65 | 0.94 | −0.12 |
| IrRu@NDV | 2.27 | 0.42 | 0.62 | 0.20 | −3.4 | 2 | 1.00 | 0.01 | 3.00 | 2.64 | 0.17 | 0.82 | 2.01 | 0.90 | −0.13 |
| PtRu@NDV | 2.30 | 0.42 | 0.59 | 0.17 | −3.3 | 2 | 1.00 | −0.16 | 1.99 | 1.73 | 0.19 | 0.96 | 0.84 | 1.05 | −0.36 |
| FeOs@NDV | 2.23 | 0.39 | 0.66 | 0.27 | −2.7 | 2 | 1.00 | 0.51 | 4.00 | 3.58 | 0.13 | 0.36 | 3.51 | 0.84 | 0.22 |
| CoOs@NDV | 2.22 | 0.40 | 0.65 | 0.25 | −2.9 | 2 | 1.00 | 0.26 | 3.00 | 2.74 | 0.16 | 0.57 | 2.26 | 0.91 | 0.09 |
| NiOs@NDV | 2.21 | 0.39 | 0.64 | 0.24 | −2.9 | 2 | 1.09 | 0.09 | 1.83 | 1.60 | 0.18 | 0.64 | 1.00 | 0.97 | 0.01 |
| RuOs@NDV | 2.20 | 0.51 | 0.75 | 0.25 | −3.2 | 2 | 1.98 | −0.16 | 2.03 | 1.71 | 0.16 | 0.02 | 1.85 | 1.15 | −0.16 |
| RhOs@NDV | 2.22 | 0.49 | 0.72 | 0.23 | −3.1 | 2 | 2.05 | −0.41 | 0.90 | 0.69 | 0.27 | 0.09 | 0.54 | 1.17 | −0.25 |
| PdOs@NDV | 2.38 | 0.37 | 0.63 | 0.25 | −2.3 | 2 | 2.00 | 0.00 | 0.00 | 0.00 | 0.00 | 0.00 | 0.00 | 1.14 | −0.15 |
| OsOs@NDV | 2.16 | 0.64 | 0.84 | 0.21 | −4.1 | 2 | 2.20 | −0.38 | 1.60 | 1.34 | 0.21 | −0.03 | 1.42 | 1.15 | −0.20 |
| IrOs@NDV | 2.17 | 0.64 | 0.83 | 0.20 | −4.1 | 2 | 2.33 | −0.54 | 0.33 | 0.22 | 0.18 | 0.03 | 0.12 | 1.19 | −0.33 |
| PtOs@NDV | 2.30 | 0.48 | 0.73 | 0.25 | −3.8 | 2 | 2.00 | 0.00 | 0.00 | 0.00 | 0.00 | 0.00 | 0.00 | 1.28 | −0.37 |

from **Sec. III B**, form double bonds within the TM dimer and are non-magnetic. Os↓ in RhOs@NDV and IrOs@NDV shows a similar tendency to completely fill the $d$ shell of TM↑ and the 'additional' bond is partly of a donor-acceptor origin. It also needs to be highlighted that $q_{\mathrm{TM}\downarrow}$ follows the opposite trend than in a corresponding system with a single adsorbed TM atom: while the $q_{\mathrm{Fe}\downarrow}$ in any system does not achieve the value of $q_{\mathrm{Fe}}$ in Fe@NDV, most of the systems with Os↓ have higher $q_{\mathrm{Os}\downarrow}$ than is the value of $q_{\mathrm{Os}}$ in Os@NDV.[13]

**Table IX** lists the SR properties of **TMTM9@NDV systems** and of **FePt@NDV**. Let us start with the description of FePt@NDV. Values of $d_d$, $E_{ad2}$, $N_{bor}$, and $N_{rel}$ clearly show that no bond is formed and the dimer truly is not stable (*c.f.*, **Sec. III B**). The presence of Fe slightly induces magnetism in the initially non-magnetic Pt@NDV system[13] but the overall interaction is weak.

$d_d$ in TMTM9@NDV systems is reliant on both TM↑ and TM↓. The highest observed values are in systems with a Pd atom as TM↑. $d_{van}$ and $d_{vag}$ are higher than in the corresponding TM@NDV systems[13], $d_{ba}$ is greater in TMCo@NDV and TMIr@NDV, while it is nearly equal in TMRh@NDV as in the systems with a single adsorbed TM atom. The interaction of TM↓ with TM↑ from the Os group is generally stronger and pushes the whole dimer farther from graphene (both $d_{van}$ and $d_{vag}$ are greater) while $d_{ba}$ remains nearly constant. The interaction with other TM↑ is overall weak (with a Pd atom is again the weakest).

In all given systems $N_{bom,coval} = 1$. With only few exceptions, $N_{bor} \simeq 1$ and $N_{rel}$ is close to 0. $N_{bor}$ is low in FeCo@NDV, OsCo@NDV, and IrCo@NDV where both TM↑ and TM↓ prefer to remain magnetic instead of forming the bond. Significant values of $N_{rel}$ are present in the systems with Pd or Pt as TM↑ which leads to their nearly fully occupied $d$ shell. A similar tendency is also perspicuous in systems with Rh or Ir as TM↑ but with a smaller magnitude. $\mu_{\mathrm{TM}\downarrow}$ is rather high in TMCo@NDV while it is modest in TMRh@NDV and TMIr@NDV. Magnetic moments of graphene are negligible. Charge located on TM↓ remains high, $q_{\mathrm{TM}\uparrow}$ differs similarly as in the other above discussed systems.

The total and local magnetic moments reported in this subchapter significantly agree with the values presented in the supporting information of Ref. 17.

*4. General Summary of Trends in Scalar-relativistic Properties*

Values of $d_d$ are dependent on all 3 main factors: TM↑, TM↓, and a type of defective graphene. In TMTM@SV, $d_{van}$, $d_{vag}$, and $d_{ba}$ are determined only by TM↓. In TMTM@NSV and TMTM@NDV, all the geometry properties are related to the combination of all 3 main factors. In TMTM@NSV, the formation of the TM dimer pushes the neighbouring N atoms closer to the graphene plane while $d_{vag}$ remains similar as in the

**TABLE IX:** SR properties of stable perpendicular TM dimers (TM9 as TM↓) at NDV and of FePt@NDV. *Cf.,* **Table IV** for the description of the included properties.

| System | $d_d$ | $d_{van}$ | $d_{vag}$ | $d_{ba}$ | $E_{ad2}$ | $N_{bom}$, $_{coval}$ | $N_{bor}$ | $N_{rel}$ | $\mu_{tot}$ | $\mu_{sum}$ | $\mu_{\mathrm{VG}}$, $_{calc}$ | $\mu_{\mathrm{TM}\downarrow}$, $_{calc}$ | $\mu_{\mathrm{TM}\uparrow}$, $_{calc}$ | $q_{\mathrm{TM}\downarrow}$ | $q_{\mathrm{TM}\uparrow}$ |
|---|---|---|---|---|---|---|---|---|---|---|---|---|---|---|---|
| FeCo@NDV | 2.26 | 0.14 | 0.20 | 0.06 | −1.4 | 1 | 0.03 | 0.20 | 4.94 | 4.21 | 0.02 | 0.74 | 4.18 | 0.70 | 0.30 |
| CoCo@NDV | 2.24 | 0.12 | 0.16 | 0.04 | −1.3 | 1 | 0.99 | −0.09 | 2.02 | 2.13 | −0.08 | 0.18 | 1.92 | 0.76 | 0.19 |
| NiCo@NDV | 2.22 | 0.12 | 0.17 | 0.05 | −1.5 | 1 | 0.99 | −0.21 | 1.03 | 1.16 | −0.06 | 0.28 | 0.80 | 0.80 | 0.12 |
| RuCo@NDV | 2.35 | 0.13 | 0.18 | 0.05 | −1.3 | 1 | 0.91 | −0.18 | 3.19 | 2.84 | −0.09 | 0.36 | 2.91 | 0.78 | 0.17 |
| PdCo@NDV | 2.45 | 0.07 | 0.10 | 0.03 | −1.1 | 1 | 1.01 | −0.61 | 0.97 | 0.89 | 0.03 | 0.57 | 0.37 | 0.86 | 0.04 |
| OsCo@NDV | 2.35 | 0.22 | 0.28 | 0.06 | −1.5 | 1 | 0.38 | −0.09 | 4.24 | 3.88 | −0.05 | 0.76 | 3.53 | 0.78 | −0.02 |
| IrCo@NDV | 2.32 | 0.24 | 0.29 | 0.05 | −1.7 | 1 | 0.24 | −0.28 | 3.51 | 3.20 | −0.02 | 1.05 | 2.47 | 0.84 | −0.16 |
| PtCo@NDV | 2.35 | 0.17 | 0.21 | 0.04 | −1.8 | 1 | 1.00 | −0.42 | 1.00 | 1.05 | −0.08 | 0.49 | 0.58 | 0.88 | −0.22 |
| FeRh@NDV | 2.36 | 0.18 | 0.32 | 0.14 | −1.6 | 1 | 0.80 | 0.11 | 3.41 | 3.30 | −0.05 | 0.15 | 3.31 | 0.60 | 0.25 |
| CoRh@NDV | 2.32 | 0.19 | 0.32 | 0.13 | −1.6 | 1 | 0.99 | −0.02 | 2.03 | 2.06 | −0.08 | 0.12 | 1.99 | 0.65 | 0.20 |
| NiRh@NDV | 2.29 | 0.18 | 0.31 | 0.13 | −1.8 | 1 | 1.00 | −0.16 | 1.00 | 1.07 | −0.01 | 0.17 | 0.84 | 0.70 | 0.13 |
| OsRh@NDV | 2.41 | 0.27 | 0.39 | 0.12 | −1.8 | 1 | 0.74 | −0.02 | 3.53 | 3.21 | −0.05 | 0.34 | 3.24 | 0.69 | 0.00 |
| IrRh@NDV | 2.43 | 0.23 | 0.34 | 0.11 | −1.9 | 1 | 1.00 | −0.16 | 2.00 | 1.86 | −0.06 | 0.22 | 1.84 | 0.80 | −0.15 |
| PtRh@NDV | 2.43 | 0.21 | 0.32 | 0.11 | −2.0 | 1 | 1.00 | −0.33 | 1.00 | 0.94 | 0.02 | 0.31 | 0.67 | 0.80 | −0.20 |
| FeIr@NDV | 2.33 | 0.25 | 0.43 | 0.19 | −1.7 | 1 | 0.82 | 0.05 | 3.36 | 3.27 | −0.03 | 0.16 | 3.23 | 0.66 | 0.26 |
| CoIr@NDV | 2.29 | 0.25 | 0.43 | 0.18 | −1.8 | 1 | 0.96 | −0.06 | 2.08 | 2.11 | −0.09 | 0.19 | 1.98 | 0.73 | 0.20 |
| NiIr@NDV | 2.29 | 0.22 | 0.38 | 0.16 | −2.0 | 1 | 1.00 | −0.20 | 1.00 | 1.05 | −0.02 | 0.21 | 0.80 | 0.77 | 0.14 |
| RuIr@NDV | 2.46 | 0.23 | 0.42 | 0.18 | −1.7 | 1 | 0.97 | −0.14 | 3.07 | 2.69 | −0.09 | 0.26 | 2.89 | 0.77 | 0.13 |
| RhIr@NDV | 2.47 | 0.21 | 0.37 | 0.17 | −1.9 | 1 | 1.00 | −0.33 | 2.00 | 1.79 | 0.02 | 0.30 | 1.67 | 0.83 | 0.07 |
| PdIr@NDV | 2.52 | 0.16 | 0.30 | 0.14 | −1.4 | 1 | 1.06 | −0.53 | 0.88 | 0.79 | 0.11 | 0.37 | 0.41 | 0.85 | −0.03 |
| OsIr@NDV | 2.39 | 0.32 | 0.50 | 0.18 | −2.0 | 1 | 0.83 | −0.15 | 3.34 | 3.01 | 0.00 | 0.32 | 3.02 | 0.86 | −0.07 |
| IrIr@NDV | 2.42 | 0.29 | 0.47 | 0.18 | −1.9 | 1 | 0.98 | −0.23 | 2.03 | 1.90 | −0.07 | 0.32 | 1.79 | 0.91 | −0.15 |
| PtIr@NDV | 2.42 | 0.25 | 0.41 | 0.16 | −2.3 | 1 | 1.00 | −0.40 | 1.00 | 0.93 | 0.03 | 0.37 | 0.60 | 0.97 | −0.27 |
| FePt@NDV | 2.62 | 0.11 | 0.20 | 0.08 | −0.6 | 0 | −0.09 | −0.06 | 4.19 | 3.65 | 0.02 | 0.14 | 4.03 | 0.64 | 0.15 |

corresponding TM@NSV system; that gives rise to a smaller graphene buckling. There are also cases with the whole TM dimer shifted farther from graphene ($d_{van}$ and $d_{vag}$ increase similarly) which preserves the graphene buckling; some systems indicate that this can be caused by the stronger interaction within the TM dimer. $E_{ad2}$ is the lowest for Pd atoms as TM↑. In general, TM↑ from the earlier periods are bound weaker than those from the later periods. A similar effect is apparent when values of $E_{ad2}$ are inspected with respect to TM↓.

$N_{bor}$ often follows the predicted value ($N_{bom,coval}$, *c.f.*, **Sec. III B**). Higher bond-orders are mostly achieved in systems containing TM atoms from the later periods as they are bigger and also according to the following reasons. Systems with TM atoms from earlier periods tend to have small $N_{bor}$ and thus they preserve higher magnetic moments. The magnetic moment of TM↓ is usually decreased but the TM atoms from the Fe group incline to preserve higher magnetic moments than TM↓ in the analogical systems with TM↓ from Ru- and Os groups. Magnetic moments located in graphene are overall small but in some cases not negligible. The presence of TM↑ induces magnetism also in some initially non-magnetic TM@SV and TM@NSV systems. If the only unpaired electron should be located on TM↓, the electronic structure undergoes such relocation that the unpaired electron is in the result delocalized or used to increase $N_{bor}$. Structures with an excess number of electrons on TM↓ tend to form donor-acceptor bonds (*c.f.*, **Page 50**) and thus to fill the *d* shell of TM↑. It is also worth mentioning that we observed also the formation of donor-acceptor bonds with TM↑ as the donor in order to lower the charge density on TM↑ and thus to achieve higher local magnetic moments on TM↑. Some bonds within the TM dimer are mainly of the electrostatic origin without any significant overlap of states on both TM atoms.

It needs to be highlighted that the above described charge transitions in some cases were not supported by the Bader charge analysis. That may be caused by the Bader's definition of an atom. TM↑ in our setup occupy a very large space in comparison with the other atoms which may introduce inaccuracies. $q_{\mathrm{TM}\downarrow}$ is always positive, mainly because of the interaction with defective graphene[13]. $q_{\mathrm{TM}\uparrow}$ decreases in all horizontal groups in systems with the same TM↓ and defective graphene. As $q_{\mathrm{TM}\uparrow}$ decreases, $q_{\mathrm{TM}\downarrow}$ increases but with a smaller magnitude (the sum of $q_{\mathrm{TM}\downarrow}$ and $q_{\mathrm{TM}\uparrow}$ decreases), which means that the lowering charge of TM↓ is partly compensated by the shift of charge in graphene.

### E. Magnetic Anisotropy Energy

We performed NCL calculations of the perpendicularly stable TM dimers with non-zero magnetic moments obtained in the SR mode. All calculated results are presented in **Tables X-XVI**. Following the $k$-point convergence tests from Ref. 13 and the additional tests in systems IrIr@NSV, OsIr@NSV, OsPd@NSV, and IrRh@NDV, we found that the $k$-point mesh containing 6 x 6 x 1 $k$-points is sufficient to calculate MAE that differs only by $< 2$ meV from the value obtained with 11 x 11 x 1 $k$-points and therefore we decided to use the former to calculate all presented systems.

The calculations are also stable against the electron relaxation algorithm (preconditioned conjugate gradient algorithm or the combination of the Davidson and RMM-DIIS algorithms) in the systems with sparse local minima. Their choice can affect the found

**TABLE X:** NCL properties of stable perpendicular TMOs@SV dimers that have non-zero magnetic moments in the SR mode. Initial orientation (Or.) of magnetization ($x$ or $y$ and $z$), spin magnetic moment of TM↓ ($\mu_{S,\mathrm{TM}\downarrow}$), an increment of ($\Delta\mu_{S,\mathrm{TM}\downarrow}$) when magnetization changes from the parallel to the perpendicular to the graphene plane. Analogous properties of spin magnetic moment of TM↑ ($\mu_{S,\mathrm{TM}\uparrow}$, $\Delta\mu_{S,\mathrm{TM}\uparrow}$), orbital magnetic moment of TM↓ ($\mu_{L,\mathrm{TM}\downarrow}$, $\Delta\mu_{L,\mathrm{TM}\downarrow}$), and of orbital magnetic moment of TM↑ ($\mu_{L,\mathrm{TM}\uparrow}$, $\Delta\mu_{L,\mathrm{TM}\uparrow}$), all in $\mu_\mathrm{B}$. Magnetic anisotropy energy (MAE) in meV, a positive value corresponds to the easy magnetic axis perpendicular to the graphene plane. Difference in spin-orbit coupling energies of TM↓ ($\Delta E_{SOC,\mathrm{TM}\downarrow}$) and of TM↑ ($\Delta E_{SOC,\mathrm{TM}\uparrow}$), both in meV, a positive value corresponds to the stronger spin-orbit interaction while the magnetization is perpendicular to graphene. The last part assesses the contribution of pairs of $d$ orbitals that contribute the most ($1^{st}+$) and the second most ($2^{nd}+$) to the positive value of $\Delta E_{SOC,\mathrm{TM}\uparrow}$ and that contribute the most ($1^{st}-$) and the second most ($2^{nd}-$) to the negative value of $\Delta E_{SOC,\mathrm{TM}\uparrow}$, the upper part describes the pair of $d$ orbitals ($-2$ is $d_{xy}$, $-1$ is $d_{yz}$, 0 is $d_{z^2}$, 1 is $d_{xz}$, and 2 is $d_{x^2-y^2}$), the lower quantifies their contribution in meV.

| System | Or. | $\mu_{S,\mathrm{TM}\downarrow}$ | $\Delta\mu_{S,\mathrm{TM}\downarrow}$ | $\mu_{S,\mathrm{TM}\uparrow}$ | $\Delta\mu_{S,\mathrm{TM}\uparrow}$ | $\mu_{L,\mathrm{TM}\downarrow}$ | $\Delta\mu_{L,\mathrm{TM}\downarrow}$ | $\mu_{L,\mathrm{TM}\uparrow}$ | $\Delta\mu_{L,\mathrm{TM}\uparrow}$ | MAE | $\Delta E_{SOC}$ TM↓ | $\Delta E_{SOC}$ TM↑ | Contrib. to $\Delta E_{SOC,\mathrm{TM}\uparrow}$ $1^{st}+$ | $2^{nd}+$ | $1^{st}-$ | $2^{nd}-$ |
|---|---|---|---|---|---|---|---|---|---|---|---|---|---|---|---|---|
| FeOs@SV | $y$ | 0.19 | 0.07 | 3.20 | 0.00 | 0.01 | 0.20 | 0.17 | −0.02 | −0.6 | −0.3 | 0.1 | −2, 2 | −2, 0 | 0, 1 | −1, 1 |
| | $z$ | 0.26 | | 3.20 | | 0.21 | | 0.14 | | | | | 1.1 | 0.0 | −0.4 | −0.2 |
| CoOs@SV | $y$ | 0.29 | 0.00 | 2.12 | 0.00 | 0.03 | 0.08 | 0.31 | −0.12 | −10.2 | −6.2 | −2.4 | −1, 1 | −2, 1 | 0, 1 | 1, 2 |
| | $z$ | 0.29 | | 2.12 | | 0.11 | | 0.19 | | | | | 1.1 | 0.1 | −2.4 | −0.6 |
| NiOs@SV | $y$ | 0.54 | 0.03 | 0.96 | 0.01 | 0.02 | 0.16 | 0.21 | −0.08 | −13.9 | −15.5 | −2.2 | −1, 1 | −2, 1 | −2, 2 | 0, 1 |
| | $z$ | 0.58 | | 0.97 | | 0.18 | | 0.12 | | | | | 2.1 | 0.2 | −2.5 | −1.3 |
| PdOs@SV | $x$ | 0.20 | 0.23 | 0.50 | 0.02 | 0.01 | 0.32 | 0.10 | −0.07 | 3.5 | 2.1 | 0.3 | −2, 2 | −2, 1 | −1, 0 | −1, 1 |
| | $z$ | 0.43 | | 0.52 | | 0.34 | | 0.03 | | | | | 0.7 | 0.0 | −0.2 | −0.1 |
| PtOs@SV | $x$ | 0.68 | −0.61 | 0.38 | −0.16 | 0.03 | 0.08 | 0.24 | 0.11 | −27.6 | 22.0 | 4.1 | −2, 2 | 0, 1 | −1, 1 | −1, 2 |
| | $z$ | 0.07 | | 0.22 | | 0.10 | | 0.35 | | | | | 27.8 | 4.0 | −10.4 | −5.2 |

**TABLE XI:** NCL properties of stable perpendicular TMIr@SV and TMPt@SV dimers that have non-zero magnetic moments in the SR mode. *Cf.,* **Table X** for the description of the included properties.

| System | Or. | $\mu_{S,\text{TM}\downarrow}$ | $\Delta\mu_{S,\text{TM}\downarrow}$ | $\mu_{S,\text{TM}\uparrow}$ | $\Delta\mu_{S,\text{TM}\uparrow}$ | $\mu_{L,\text{TM}\downarrow}$ | $\Delta\mu_{L,\text{TM}\downarrow}$ | $\mu_{L,\text{TM}\uparrow}$ | $\Delta\mu_{L,\text{TM}\uparrow}$ | MAE | $\Delta E_{SOC}$ TM↓ | $\Delta E_{SOC}$ TM↑ | Contrib. to $\Delta E_{SOC,\text{TM}\uparrow}$ $1^{st}+$ | $2^{nd}+$ | $1^{st}-$ | $2^{nd}-$ |
|---|---|---|---|---|---|---|---|---|---|---|---|---|---|---|---|---|
| FeIr@SV | $y$ | 0.12 | 0.00 | 3.00 | 0.00 | 0.00 | 0.00 | 0.16 | −0.10 | −1.3 | 0.1 | −1.2 | −1, 1 | −2, 1 | −2, 2 | −2, −1 |
| | $z$ | 0.12 | | 3.00 | | 0.01 | | 0.06 | | | | | 0.1 | 0.0 | −0.7 | −0.2 |
| CoIr@SV | $x$ | 0.08 | 0.00 | 1.96 | 0.00 | 0.00 | 0.00 | 0.25 | 0.03 | 0.3 | −0.2 | 0.5 | −2, 2 | 0, 1 | −1, 0 | −2, 1 |
| | $z$ | 0.08 | | 1.96 | | 0.01 | | 0.27 | | | | | 2.9 | 0.1 | −1.8 | −0.4 |
| NiIr@SV | $x$ | 0.00 | 0.02 | 0.87 | −0.03 | 0.00 | 0.05 | 0.16 | 0.88 | −15.8 | 5.5 | 16.3 | −2, 2 | 0, 1 | −1, 1 | −2, 1 |
| | $z$ | 0.03 | | 0.83 | | 0.06 | | 1.05 | | | | | 20.3 | 0.9 | −1.9 | −1.3 |
| RuIr@SV | $y$ | 0.06 | 0.00 | 2.49 | 0.00 | 0.01 | 0.01 | 0.34 | −0.03 | −5.8 | −4.7 | −3.1 | −1, 1 | −2, 1 | −2, 2 | −2, −1 |
| | $z$ | 0.06 | | 2.49 | | 0.02 | | 0.30 | | | | | 1.7 | 0.2 | −2.5 | −1.0 |
| RhIr@SV | $y$ | 0.05 | 0.03 | 1.37 | −0.04 | 0.00 | 0.06 | 0.27 | 1.04 | −10.5 | 5.7 | 31.8 | −2, 2 | −1, 0 | 1, 2 | −1, 2 |
| | $z$ | 0.07 | | 1.33 | | 0.06 | | 1.30 | | | | | 39.1 | 0.7 | −2.4 | −2.0 |
| PdIr@SV | $y$ | 0.07 | 0.00 | 0.44 | −0.01 | 0.01 | −0.01 | 0.10 | −0.09 | 0.0 | 0.0 | 0.0 | −1, 0 | 1, 2 | 0, 1 | −2, 2 |
| | $z$ | 0.07 | | 0.43 | | 0.00 | | 0.01 | | | | | 0.0 | 0.0 | 0.0 | 0.0 |
| OsIr@SV | $x$ | 0.02 | −0.02 | 2.28 | −0.05 | 0.02 | 0.02 | 0.80 | −0.27 | −52.6 | −5.1 | −25.7 | −1, 1 | −2, −1 | −2, 2 | −1, 0 |
| | $z$ | 0.00 | | 2.23 | | 0.03 | | 0.53 | | | | | 10.6 | 6.5 | −49.6 | −5.4 |
| IrIr@SV | $x$ | 0.08 | −0.07 | 1.16 | 0.13 | 0.01 | 0.01 | 0.68 | 0.97 | 10.9 | −6.3 | 18.9 | −2, 2 | 0, 1 | −2, 1 | −2, −1 |
| | $z$ | 0.01 | | 1.29 | | 0.01 | | 1.64 | | | | | 55.6 | 17.2 | −17.7 | −16.6 |
| PtIr@SV | $y$ | 0.00 | 0.05 | 0.03 | 0.50 | 0.00 | 0.08 | 0.05 | 0.88 | 1.1 | 0.5 | 1.9 | −2, 2 | −1, 2 | −2, 1 | −2, −1 |
| | $z$ | 0.05 | | 0.53 | | 0.08 | | 0.92 | | | | | 1.6 | 0.4 | −0.5 | −0.4 |
| FePt@SV | $x$ | 0.15 | 0.00 | 3.00 | 0.00 | 0.00 | 0.00 | 0.14 | −0.12 | −4.4 | −2.3 | −1.8 | −2, 0 | 0, 1 | −2, 2 | −1, 2 |
| | $z$ | 0.15 | | 2.99 | | 0.00 | | 0.02 | | | | | 0.0 | 0.0 | −1.1 | −0.2 |
| CoPt@SV | $x$ | 0.12 | 0.00 | 1.86 | 0.00 | 0.00 | 0.00 | 0.15 | 0.11 | −0.1 | −1.7 | 1.7 | −2, 2 | 0, 1 | −1, 0 | −1, 1 |
| | $z$ | 0.12 | | 1.86 | | 0.00 | | 0.26 | | | | | 3.0 | 0.0 | −0.7 | −0.3 |
| OsPt@SV | $y$ | 0.04 | 0.01 | 2.12 | 0.00 | 0.02 | −0.01 | 0.55 | −0.18 | −76.9 | −3.7 | −51.6 | −2, 1 | −1, 2 | −2, 2 | −2, 0 |
| | $z$ | 0.05 | | 2.11 | | 0.01 | | 0.37 | | | | | 7.3 | 7.3 | −84.6 | 0.0 |
| IrPt@SV | $y$ | 0.01 | 0.01 | 0.48 | 0.65 | 0.00 | 0.01 | 0.15 | 1.56 | 39.4 | −0.4 | 11.2 | −2, 2 | −2, −1 | −1, 2 | 1, 2 |
| | $z$ | 0.02 | | 1.13 | | 0.01 | | 1.71 | | | | | 16.7 | 3.3 | −5.5 | −5.3 |

electronic groundstate in systems with plenty of local minima as well as it can be influenced by the size of the initial magnetic moments. Presented results thus need to be perceived with care. The systems with high values of MAE will be deeply examined in the future research.

VASP assesses the contribution to the spin-orbit coupling energy ($E_{SOC}$) of each pair of orbitals (with the same orbital angular momentum number) of each atom and prints them

**TABLE XII:** NCL properties of stable perpendicular TM dimers (TM8 as TM↓) at NSV that have non-zero magnetic moments in the SR mode. *Cf.,* **Table X** for the description of the included properties.

| System | Or. | $\mu_{S,}$ TM↓ | $\Delta\mu_{S,}$ TM↓ | $\mu_{S,}$ TM↑ | $\Delta\mu_{S,}$ TM↑ | $\mu_{L,}$ TM↓ | $\Delta\mu_{L,}$ TM↓ | $\mu_{L,}$ TM↑ | $\Delta\mu_{L,}$ TM↑ | MAE | $\Delta E_{SOC}$ TM↓ | $\Delta E_{SOC}$ TM↑ | Contrib. to $\Delta E_{SOC,\text{TM}\uparrow}$ $1^{st}+$ | $2^{nd}+$ | $1^{st}-$ | $2^{nd}-$ |
|---|---|---|---|---|---|---|---|---|---|---|---|---|---|---|---|---|
| FeFe@NSV | $x$ | 0.19 | 0.00 | 3.10 | 0.00 | 0.00 | 0.06 | 0.10 | −0.08 | −2.3 | −0.8 | −1.4 | $-2,-1$ | $1,2$ | $-2,2$ | $-1,1$ |
| | $z$ | 0.19 | | 3.10 | | 0.06 | | 0.02 | | | | | 0.0 | 0.0 | −1.4 | −0.1 |
| CoFe@NSV | $y$ | 0.03 | 0.05 | 1.98 | −0.02 | 0.01 | 0.04 | 0.13 | 1.33 | −106.3 | 0.8 | 24.3 | $-2,2$ | $-2,1$ | $-1,1$ | $0,1$ |
| | $z$ | 0.09 | | 1.96 | | 0.05 | | 1.46 | | | | | 25.4 | 0.0 | −0.4 | −0.3 |
| NiFe@NSV | $y$ | 3.36 | 0.00 | 1.16 | 0.01 | 0.09 | −0.06 | 0.14 | 0.11 | −1.9 | −2.6 | 0.4 | $-2,2$ | $-1,0$ | $0,1$ | $-2,-1$ |
| | $z$ | 3.36 | | 1.17 | | 0.02 | | 0.25 | | | | | 2.6 | 0.0 | −0.7 | −0.6 |
| OsFe@NSV | $y$ | 0.20 | −0.16 | 0.96 | 0.30 | 0.11 | −0.07 | 0.23 | 0.91 | 15.4 | −1.9 | −3.4 | $-2,1$ | $-2,-1$ | $-2,2$ | $-1,0$ |
| | $z$ | 0.03 | | 1.26 | | 0.04 | | 1.14 | | | | | 2.9 | 2.8 | −8.2 | −3.3 |
| IrFe@NSV | $x$ | 0.55 | 0.12 | 0.31 | 0.53 | 0.16 | 0.05 | 0.05 | 0.99 | 44.4 | 0.8 | 5.2 | $-2,2$ | $-1,2$ | $0,1$ | $-1,0$ |
| | $z$ | 0.66 | | 0.84 | | 0.21 | | 1.04 | | | | | 15.2 | 0.3 | −5.1 | −3.4 |
| PtFe@NSV | $x$ | 0.79 | −0.05 | 0.10 | 0.05 | 0.12 | −0.09 | 0.03 | 0.01 | −3.3 | 0.5 | −2.5 | $-2,2$ | $0,1$ | $-1,0$ | $-1,1$ |
| | $z$ | 0.74 | | 0.15 | | 0.03 | | 0.03 | | | | | 3.1 | 0.2 | −3.0 | −0.9 |
| FeRu@NSV | $y$ | 0.12 | 0.00 | 2.91 | 0.00 | 0.03 | 0.00 | 0.12 | −0.11 | −3.6 | −1.7 | −1.8 | $-2,1$ | $-1,2$ | $-2,2$ | $-2,-1$ |
| | $z$ | 0.12 | | 2.91 | | 0.04 | | 0.01 | | | | | 0.0 | 0.0 | −1.8 | 0.0 |
| CoRu@NSV | $y$ | 0.01 | 0.05 | 1.55 | −0.24 | 0.02 | 0.04 | 0.09 | 1.01 | −46.8 | 1.3 | 18.1 | $-2,2$ | $-1,0$ | $-1,1$ | $-2,-1$ |
| | $z$ | 0.06 | | 1.31 | | 0.05 | | 1.10 | | | | | 18.5 | 0.2 | −0.3 | −0.3 |
| NiRu@NSV | $y$ | 0.12 | 0.00 | 0.15 | 0.01 | 0.00 | 0.00 | 0.03 | −0.01 | −0.1 | 0.0 | 0.1 | $-2,2$ | $-1,1$ | $0,1$ | $1,2$ |
| | $z$ | 0.13 | | 0.16 | | 0.00 | | 0.02 | | | | | 0.1 | 0.0 | 0.0 | 0.0 |
| RuRu@NSV | $y$ | 0.01 | 0.00 | 1.14 | 0.05 | 0.01 | 0.06 | 0.05 | 0.62 | 8.5 | 0.4 | 7.8 | $-2,2$ | $0,1$ | $-2,1$ | $-2,0$ |
| | $z$ | 0.01 | | 1.18 | | 0.07 | | 0.67 | | | | | 7.6 | 0.1 | 0.0 | 0.0 |
| RhRu@NSV | $y$ | 0.07 | 0.00 | 0.34 | 0.00 | 0.00 | 0.00 | 0.03 | −0.01 | 0.5 | 0.0 | 0.6 | $-2,2$ | $0,1$ | $-2,0$ | $-2,0$ |
| | $z$ | 0.07 | | 0.34 | | 0.01 | | 0.03 | | | | | 0.3 | 0.2 | 0.0 | 0.0 |
| OsRu@NSV | $x$ | 0.06 | −0.04 | 0.69 | 0.32 | 0.03 | 0.01 | 0.06 | 1.12 | 6.0 | −2.7 | 4.1 | $-2,1$ | $-2,-1$ | $-2,2$ | $-2,0$ |
| | $z$ | 0.02 | | 1.01 | | 0.04 | | 1.18 | | | | | 1.2 | 1.1 | −1.3 | 0.0 |
| PtRu@NSV | $y$ | 0.26 | −0.01 | 0.12 | 0.00 | 0.05 | −0.04 | 0.02 | −0.01 | 0.0 | −0.1 | 0.3 | $0,1$ | $-2,2$ | $-1,1$ | $-1,2$ |
| | $z$ | 0.26 | | 0.12 | | 0.01 | | 0.01 | | | | | 0.2 | 0.1 | 0.0 | 0.0 |
| FeOs@NSV | $x$ | 0.15 | −0.01 | 2.72 | 0.00 | 0.12 | −0.09 | 0.21 | −0.06 | −12.7 | −8.4 | −4.2 | $-2,-1$ | $1,2$ | $-2,2$ | $-1,0$ |
| | $z$ | 0.14 | | 2.73 | | 0.03 | | 0.15 | | | | | 0.1 | 0.1 | −3.7 | −0.4 |
| CoOs@NSV | $y$ | 0.03 | 0.06 | 1.66 | −0.06 | 0.08 | −0.01 | 0.18 | 1.00 | −71.4 | 3.1 | 18.6 | $-2,2$ | $-1,0$ | $0,1$ | $-1,1$ |
| | $z$ | 0.09 | | 1.60 | | 0.07 | | 1.18 | | | | | 20.4 | 0.2 | −0.8 | −0.5 |
| RuOs@NSV | $y$ | 0.01 | −0.01 | 1.11 | 0.01 | 0.01 | 0.08 | 0.09 | 0.56 | −1.4 | −4.2 | 5.4 | $-2,2$ | $-1,1$ | $-1,2$ | $1,2$ |
| | $z$ | 0.00 | | 1.12 | | 0.09 | | 0.65 | | | | | 5.0 | 0.2 | 0.0 | 0.0 |
| OsOs@NSV | $x$ | 0.08 | −0.02 | 0.79 | 0.16 | 0.03 | −0.01 | 0.11 | 0.96 | −15.4 | −11.6 | 5.3 | $-1,2$ | $-2,1$ | $-2,2$ | $-2,0$ |
| | $z$ | 0.05 | | 0.95 | | 0.01 | | 1.07 | | | | | 1.3 | 1.2 | −1.0 | 0.0 |

**TABLE XIII:** NCL properties of stable perpendicular TM dimers (TM9 as TM↓) at NSV that have non-zero magnetic moments in the SR mode. *Cf.,* **Table X** for the description of the included properties.

| System | Or. | $\mu_{S,}$ TM↓ | $\Delta\mu_{S,}$ TM↓ | $\mu_{S,}$ TM↑ | $\Delta\mu_{S,}$ TM↑ | $\mu_{L,}$ TM↓ | $\Delta\mu_{L,}$ TM↓ | $\mu_{L,}$ TM↑ | $\Delta\mu_{L,}$ TM↑ | MAE | $\Delta E_{SOC}$ TM↓ | $\Delta E_{SOC}$ TM↑ | Contrib. to $\Delta E_{SOC,\text{TM}\uparrow}$ $1^{st}+$ | $2^{nd}+$ | $1^{st}-$ | $2^{nd}-$ |
|---|---|---|---|---|---|---|---|---|---|---|---|---|---|---|---|---|
| FeCo@NSV | $x$ | 2.20 | 0.00 | 2.32 | 0.00 | 0.11 | 0.00 | 0.17 | 0.06 | −1.0 | −0.7 | −0.2 | −2, 2 | 0, 1 | −1, 0 | −1, 1 |
| | $z$ | 2.20 | | 2.32 | | 0.11 | | 0.23 | | | | | 1.9 | 0.0 | −1.1 | −0.6 |
| CoCo@NSV | $x$ | 2.20 | 0.00 | 2.32 | 0.00 | 0.11 | 0.00 | 0.17 | 0.06 | −1.0 | −0.7 | −0.2 | −2, 2 | 0, 1 | −1, 0 | −1, 1 |
| | $z$ | 2.20 | | 2.32 | | 0.11 | | 0.23 | | | | | 1.9 | 0.0 | −1.1 | −0.6 |
| NiCo@NSV | $x$ | 2.26 | 0.00 | 1.25 | 0.00 | 0.10 | 0.14 | 0.23 | 0.21 | 5.2 | 1.8 | 3.2 | −2, 2 | 0, 1 | −1, 2 | −1, 0 |
| | $z$ | 2.26 | | 1.25 | | 0.24 | | 0.44 | | | | | 7.7 | 0.2 | −1.5 | −1.4 |
| RuCo@NSV | $x$ | 0.23 | 0.00 | 2.11 | 0.01 | 0.02 | 0.03 | 0.12 | 0.44 | 10.3 | −0.2 | 10.7 | −2, 2 | −1, 0 | −1, 1 | −1, 2 |
| | $z$ | 0.23 | | 2.12 | | 0.05 | | 0.55 | | | | | 9.0 | 1.2 | −0.2 | −0.2 |
| PdCo@NSV | $y$ | 2.27 | 0.00 | 0.76 | −0.01 | 0.09 | 0.01 | 0.13 | −0.10 | −1.2 | −0.7 | −0.4 | 0, 1 | −2, 2 | −1, 1 | 1, 2 |
| | $z$ | 2.27 | | 0.76 | | 0.10 | | 0.03 | | | | | 0.2 | 0.1 | −0.4 | −0.2 |
| OsCo@NSV | $x$ | 0.24 | −0.03 | 1.36 | 0.37 | 0.22 | −0.21 | 0.04 | 1.30 | 66.9 | −0.7 | 38.3 | −2, 2 | −2, 1 | 0, 1 | 1, 2 |
| | $z$ | 0.21 | | 1.72 | | 0.01 | | 1.34 | | | | | 24.7 | 11.0 | −2.3 | −1.4 |
| IrCo@NSV | $x$ | 0.35 | 0.10 | 0.28 | 0.58 | 0.05 | −0.01 | 0.06 | 0.81 | 17.8 | 0.9 | −0.9 | −2, 2 | −2, 1 | −2, −1 | 1, 2 |
| | $z$ | 0.45 | | 0.87 | | 0.04 | | 0.87 | | | | | 13.0 | 10.0 | −10.6 | −10.1 |
| PtCo@NSV | $x$ | 0.02 | 0.00 | 0.00 | 0.00 | 0.00 | 0.00 | 0.00 | 0.00 | 0.0 | 0.0 | 0.0 | −2, 0 | −2, 1 | 0, 1 | −1, 0 |
| | $z$ | 0.02 | | 0.00 | | 0.00 | | 0.00 | | | | | 0.0 | 0.0 | 0.0 | 0.0 |
| FeRh@NSV | $x$ | 0.42 | −0.32 | 3.13 | 0.11 | 0.08 | 0.01 | 0.12 | 0.32 | −57.0 | 2.3 | 5.9 | −2, 2 | −1, 2 | −1, 0 | 0, 1 |
| | $z$ | 0.10 | | 3.24 | | 0.09 | | 0.44 | | | | | 5.6 | 0.2 | −0.2 | −0.2 |
| CoRh@NSV | $x$ | 0.34 | 0.01 | 2.17 | 0.00 | 0.01 | 0.06 | 0.14 | 0.13 | 3.5 | 1.6 | 2.1 | −2, 2 | −2, 0 | −1, 0 | −1, 1 |
| | $z$ | 0.35 | | 2.17 | | 0.07 | | 0.28 | | | | | 3.2 | 0.0 | −0.7 | −0.2 |
| NiRh@NSV | $x$ | 0.26 | 0.01 | 0.68 | −0.01 | 0.03 | 0.01 | 0.25 | −0.09 | −4.0 | −0.5 | −1.7 | −1, 0 | 0, 1 | −2, 2 | −1, 1 |
| | $z$ | 0.26 | | 0.68 | | 0.04 | | 0.15 | | | | | 0.4 | 0.1 | −1.7 | −0.6 |
| RuRh@NSV | $x$ | 0.07 | 0.04 | 1.85 | 0.00 | 0.01 | 0.04 | 0.10 | 1.52 | −64.5 | 0.9 | 49.3 | −2, 2 | −2, 1 | −1, 1 | −2, 0 |
| | $z$ | 0.11 | | 1.85 | | 0.05 | | 1.62 | | | | | 46.1 | 0.9 | −0.3 | 0.0 |
| OsRh@NSV | $x$ | 0.21 | −0.02 | 1.28 | 0.34 | 0.17 | −0.11 | 0.02 | 1.43 | 57.4 | −0.3 | 42.4 | −2, 2 | −2, 1 | 0, 1 | 1, 2 |
| | $z$ | 0.18 | | 1.61 | | 0.05 | | 1.45 | | | | | 33.7 | 7.1 | −1.7 | −0.9 |
| IrRh@NSV | $y$ | 0.30 | 0.00 | 0.47 | 0.35 | 0.11 | −0.08 | 0.08 | 0.55 | 25.5 | 2.5 | −9.5 | −2, 2 | −2, 0 | 0, 1 | −1, 0 |
| | $z$ | 0.30 | | 0.82 | | 0.03 | | 0.63 | | | | | 7.7 | 0.0 | −6.2 | −6.1 |
| FeIr@NSV | $y$ | 0.18 | 0.02 | 2.99 | −0.01 | 0.16 | −0.01 | 0.24 | 0.22 | 11.1 | −1.0 | 4.1 | −2, 2 | −1, 0 | 0, 1 | 1, 2 |
| | $z$ | 0.20 | | 2.98 | | 0.14 | | 0.46 | | | | | 5.9 | 0.1 | −1.1 | −0.4 |
| CoIr@NSV | $x$ | 0.02 | −0.01 | 1.72 | −0.08 | 0.08 | −0.01 | 0.10 | 1.07 | −41.1 | −7.4 | 20.0 | −2, 2 | 0, 1 | −1, 2 | −1, 1 |
| | $z$ | 0.01 | | 1.65 | | 0.07 | | 1.17 | | | | | 20.2 | 1.4 | −0.8 | −0.8 |
| RuIr@NSV | $x$ | 0.05 | 0.05 | 1.74 | −0.01 | 0.08 | −0.01 | 0.22 | 1.16 | −41.0 | 3.2 | 36.2 | −2, 2 | 1, 2 | −2, −1 | −2, 1 |
| | $z$ | 0.10 | | 1.73 | | 0.07 | | 1.38 | | | | | 36.5 | 0.3 | −0.5 | −0.4 |
| RhIr@NSV | $y$ | 0.15 | 0.01 | 0.69 | 0.02 | 0.04 | −0.03 | 0.18 | −0.05 | 3.6 | −0.6 | 2.7 | −2, 2 | −2, 0 | 0, 1 | −2, 1 |
| | $z$ | 0.15 | | 0.71 | | 0.01 | | 0.13 | | | | | 3.1 | 0.0 | −0.1 | −0.1 |
| OsIr@NSV | $x$ | 0.23 | −0.03 | 1.22 | 0.21 | 0.05 | 0.02 | 0.15 | 1.27 | 50.1 | −3.5 | 41.5 | −2, 2 | −2, 1 | 0, 1 | −2, 0 |
| | $z$ | 0.19 | | 1.43 | | 0.07 | | 1.41 | | | | | 35.0 | 2.7 | −0.1 | 0.0 |
| IrIr@NSV | $y$ | 0.30 | 0.01 | 0.48 | 0.30 | 0.06 | 0.00 | 0.15 | 0.52 | 36.3 | 4.1 | 4.4 | −2, 2 | 1, 2 | −1, 0 | 0, 1 |
| | $z$ | 0.31 | | 0.78 | | 0.06 | | 0.68 | | | | | 12.6 | 0.1 | −2.7 | −2.5 |

**TABLE XIV:** NCL properties of stable perpendicular TM dimers (TM10 as TM↓) at NSV that have non-zero magnetic moments in the SR mode. *Cf.,* **Table X** for the description of the included properties.

| System | Or. | $\mu_{S,\text{TM}\downarrow}$ | $\Delta\mu_{S,\text{TM}\downarrow}$ | $\mu_{S,\text{TM}\uparrow}$ | $\Delta\mu_{S,\text{TM}\uparrow}$ | $\mu_{L,\text{TM}\downarrow}$ | $\Delta\mu_{L,\text{TM}\downarrow}$ | $\mu_{L,\text{TM}\uparrow}$ | $\Delta\mu_{L,\text{TM}\uparrow}$ | MAE | $\Delta E_{SOC}$ TM↓ | $\Delta E_{SOC}$ TM↑ | Contrib. to $\Delta E_{SOC,\text{TM}\uparrow}$ $1^{st}+$ | $2^{nd}+$ | $1^{st}-$ | $2^{nd}-$ |
|---|---|---|---|---|---|---|---|---|---|---|---|---|---|---|---|---|
| FeNi@NSV | $y$ | 1.10 | 0.00 | 3.43 | 0.00 | 0.10 | −0.05 | 0.13 | −0.11 | −3.8 | −1.4 | −2.3 | −2, 1 | −1, 2 | −2, 2 | 0, 1 |
| | $z$ | 1.10 | | 3.43 | | 0.05 | | 0.02 | | | | | 0.0 | 0.0 | −1.6 | −0.4 |
| CoNi@NSV | $x$ | 1.19 | 0.00 | 2.35 | 0.00 | 0.12 | −0.05 | 0.17 | 0.13 | 0.4 | −1.1 | 1.5 | −2, 2 | 0, 1 | −1, 0 | −2, 1 |
| | $z$ | 1.19 | | 2.36 | | 0.07 | | 0.30 | | | | | 3.1 | 0.0 | −1.1 | −0.2 |
| NiNi@NSV | $x$ | 1.29 | 0.01 | 1.26 | 0.01 | 0.10 | −0.01 | 0.22 | 0.24 | −19.1 | 0.0 | 3.6 | −2, 2 | 0, 1 | −1, 0 | −1, 2 |
| | $z$ | 1.29 | | 1.27 | | 0.09 | | 0.46 | | | | | 6.9 | 0.2 | −2.0 | −0.6 |
| OsNi@NSV | $y$ | 1.17 | −0.21 | 2.89 | −0.32 | 0.20 | −0.17 | 0.51 | 0.05 | 53.6 | −12.2 | 93.4 | 1, 2 | −2, −1 | −2, 2 | −2, 0 |
| | $z$ | 0.96 | | 2.57 | | 0.04 | | 0.56 | | | | | 31.5 | 30.9 | −28.0 | 0.0 |
| IrNi@NSV | $y$ | 1.25 | 0.02 | 1.74 | 0.21 | 0.14 | −0.02 | 0.59 | 1.23 | 74.1 | −7.1 | 51.6 | −2, 2 | 0, 1 | −1, 1 | −2, 1 |
| | $z$ | 1.27 | | 1.95 | | 0.11 | | 1.81 | | | | | 85.1 | 23.3 | −17.0 | −14.4 |
| PtNi@NSV | $x$ | 1.31 | 0.00 | 0.77 | 0.07 | 0.02 | 0.09 | 0.48 | 0.11 | 4.8 | −2.9 | −0.5 | −1, 0 | −2, 2 | 0, 1 | −1, 1 |
| | $z$ | 1.32 | | 0.84 | | 0.10 | | 0.59 | | | | | 16.2 | 15.7 | −12.5 | −8.8 |
| FePd@NSV | $y$ | 0.74 | 0.00 | 3.56 | 0.00 | 0.12 | −0.06 | 0.14 | −0.14 | −6.1 | −2.3 | −3.6 | −2, 1 | −1, 2 | −2, 2 | 0, 1 |
| | $z$ | 0.74 | | 3.56 | | 0.05 | | 0.00 | | | | | 0.0 | 0.0 | −1.7 | −0.9 |
| CoPd@NSV | $y$ | 0.83 | 0.01 | 2.47 | 0.00 | 0.14 | −0.05 | 0.18 | 1.61 | −157.9 | −0.1 | 28.1 | −2, 2 | −1, 0 | 0, 1 | −1, 1 |
| | $z$ | 0.84 | | 2.47 | | 0.09 | | 1.79 | | | | | 32.0 | 0.1 | −1.9 | −0.9 |
| RuPd@NSV | $y$ | 0.83 | −0.01 | 3.02 | −0.01 | 0.12 | −0.09 | 0.21 | 0.24 | −0.2 | −5.8 | 6.4 | −2, 2 | 1, 2 | −1, 1 | −1, 0 |
| | $z$ | 0.82 | | 3.01 | | 0.04 | | 0.45 | | | | | 6.3 | 1.4 | −2.8 | 0.0 |
| OsPd@NSV | $x$ | 0.68 | −0.19 | 2.82 | −0.29 | 0.14 | −0.05 | 0.39 | 0.50 | 170.4 | −11.7 | 120.4 | −1, 2 | −1, 0 | −2, −1 | −2, 0 |
| | $z$ | 0.49 | | 2.53 | | 0.09 | | 0.89 | | | | | 38.2 | 34.6 | −16.1 | 0.0 |
| IrPd@NSV | $x$ | 0.77 | 0.06 | 1.76 | 0.22 | 0.08 | −0.01 | 0.64 | 0.83 | 50.8 | −14.6 | 12.9 | −2, 2 | −1, 0 | −1, 1 | −2, −1 |
| | $z$ | 0.83 | | 1.97 | | 0.07 | | 1.47 | | | | | 49.7 | 27.8 | −23.4 | −18.6 |
| PtPd@NSV | $y$ | 0.25 | 0.06 | 0.27 | 0.19 | 0.05 | 0.11 | 0.06 | 0.58 | 6.0 | −1.0 | 3.9 | 0, 1 | −1, 1 | −2, 2 | −1, 0 |
| | $z$ | 0.31 | | 0.46 | | 0.16 | | 0.64 | | | | | 2.9 | 1.7 | −2.1 | −1.7 |
| FePt@NSV | $x$ | 0.69 | −0.01 | 3.44 | 0.00 | 0.23 | −0.09 | 0.22 | −0.17 | −12.0 | −1.0 | −9.9 | 0, 1 | −2, 0 | −1, 0 | −2, 2 |
| | $z$ | 0.68 | | 3.44 | | 0.15 | | 0.05 | | | | | 0.1 | 0.0 | −2.7 | −2.5 |
| CoPt@NSV | $y$ | 0.76 | 0.00 | 2.35 | 0.01 | 0.27 | −0.11 | 0.18 | 0.13 | −8.3 | −6.7 | −4.0 | −2, 2 | −1, 0 | 0, 1 | −1, 1 |
| | $z$ | 0.75 | | 2.35 | | 0.16 | | 0.31 | | | | | 3.5 | 0.7 | −4.8 | −2.3 |
| NiPt@NSV | $x$ | 0.16 | −0.05 | 0.82 | −0.02 | 0.14 | −0.04 | 0.12 | 0.01 | 3.7 | −0.4 | 2.0 | −2, 2 | −1, 0 | −1, 2 | −1, 1 |
| | $z$ | 0.11 | | 0.80 | | 0.10 | | 0.13 | | | | | 1.2 | 0.6 | −1.1 | −0.4 |
| RuPt@NSV | $x$ | 0.16 | 0.01 | 2.31 | 0.02 | 0.08 | 0.06 | 0.22 | 0.20 | 14.4 | 8.1 | 12.2 | −2, 2 | −1, 1 | 0, 1 | −1, 2 |
| | $z$ | 0.17 | | 2.33 | | 0.14 | | 0.42 | | | | | 9.5 | 0.7 | −0.2 | −0.2 |
| RhPt@NSV | $x$ | 0.27 | 0.01 | 1.15 | 0.02 | 0.02 | 0.06 | 0.22 | −0.14 | 12.4 | 6.5 | 4.2 | −2, 2 | −1, 1 | 1, 2 | 0, 1 |
| | $z$ | 0.29 | | 1.17 | | 0.09 | | 0.08 | | | | | 4.3 | 0.4 | −0.4 | −0.4 |
| PdPt@NSV | $y$ | 0.82 | 0.04 | 0.73 | 0.03 | 0.34 | −0.14 | 0.08 | −0.07 | −34.7 | −27.3 | −7.3 | −1, 0 | −2, 2 | −1, 1 | 0, 1 |
| | $z$ | 0.87 | | 0.76 | | 0.20 | | 0.02 | | | | | 5.4 | 0.2 | −5.6 | −5.2 |
| OsPt@NSV | $y$ | 0.02 | 0.23 | 1.10 | 0.85 | 0.05 | 0.03 | 0.32 | 0.94 | 119.4 | −3.2 | 54.8 | −2, 2 | −2, −1 | −1, 0 | −1, 2 |
| | $z$ | 0.25 | | 1.95 | | 0.08 | | 1.26 | | | | | 21.5 | 11.6 | −10.3 | −1.4 |
| PtPt@NSV | $y$ | 0.20 | 0.11 | 0.23 | 0.04 | 0.10 | 0.00 | 0.24 | −0.12 | 0.9 | 0.6 | −0.2 | 1, 2 | −2, −1 | −1, 0 | 0, 1 |
| | $z$ | 0.31 | | 0.27 | | 0.10 | | 0.13 | | | | | 0.2 | 0.1 | −0.3 | −0.2 |

**TABLE XV:** NCL properties of stable perpendicular TM dimers (TM8 as TM↓) at NDV that have non-zero magnetic moments in the SR mode. *Cf.,* **Table X** for the description of the included properties.

| System | Or. | $\mu_{S,\text{TM}\downarrow}$ | $\Delta\mu_{S,\text{TM}\downarrow}$ | $\mu_{S,\text{TM}\uparrow}$ | $\Delta\mu_{S,\text{TM}\uparrow}$ | $\mu_{L,\text{TM}\downarrow}$ | $\Delta\mu_{L,\text{TM}\downarrow}$ | $\mu_{L,\text{TM}\uparrow}$ | $\Delta\mu_{L,\text{TM}\uparrow}$ | MAE | $\Delta E_{SOC}$ TM↓ | $\Delta E_{SOC}$ TM↑ | Contrib. to $\Delta E_{SOC,\text{TM}\uparrow}$ $1^{st}+$ | $2^{nd}+$ | $1^{st}-$ | $2^{nd}-$ |
|---|---|---|---|---|---|---|---|---|---|---|---|---|---|---|---|---|
| FeFe@NDV | $y$ | 0.64 | 0.00 | 3.14 | 0.00 | 0.00 | 0.00 | 0.12 | 0.01 | −0.8 | −0.4 | −0.3 | $-2,2$ | $-2,-1$ | $1,2$ | $-1,1$ |
| | $z$ | 0.64 | | 3.14 | | 0.00 | | 0.13 | | | | | 0.4 | 0.2 | −0.4 | −0.4 |
| CoFe@NDV | $y$ | 1.01 | 0.00 | 2.07 | 0.00 | 0.03 | −0.02 | 0.17 | 0.13 | 0.7 | −0.8 | 1.4 | $-2,2$ | $-1,0$ | $0,1$ | $-1,1$ |
| | $z$ | 1.01 | | 2.07 | | 0.00 | | 0.30 | | | | | 3.2 | 0.0 | −1.0 | −0.5 |
| NiFe@NDV | $x$ | 1.19 | 0.01 | 0.91 | 0.00 | 0.03 | −0.02 | 0.22 | −0.15 | −3.7 | −1.0 | −2.4 | $-2,2$ | $1,2$ | $-2,1$ | $-1,1$ |
| | $z$ | 1.20 | | 0.91 | | 0.01 | | 0.07 | | | | | 0.9 | 0.1 | −1.6 | −0.9 |
| RuFe@NDV | $x$ | 0.97 | 0.00 | 2.53 | 0.01 | 0.08 | −0.07 | 0.19 | 0.32 | 5.9 | −1.9 | 7.4 | $-2,2$ | $-1,0$ | $-1,1$ | $-2,1$ |
| | $z$ | 0.97 | | 2.53 | | 0.01 | | 0.51 | | | | | 8.4 | 2.1 | −2.2 | −1.7 |
| RhFe@NDV | $y$ | 1.35 | 0.01 | 1.41 | 0.00 | 0.03 | −0.02 | 0.29 | −0.11 | −2.0 | −2.0 | −0.7 | $-2,2$ | $0,1$ | $1,2$ | $-1,1$ |
| | $z$ | 1.36 | | 1.41 | | 0.01 | | 0.19 | | | | | 4.2 | 3.4 | −3.4 | −3.0 |
| PdFe@NDV | $y$ | 1.61 | 0.00 | 0.39 | −0.01 | 0.02 | −0.01 | 0.21 | −0.17 | −5.3 | −1.5 | −3.1 | $-1,0$ | $-2,2$ | $0,1$ | $-1,1$ |
| | $z$ | 1.61 | | 0.38 | | 0.01 | | 0.04 | | | | | 0.6 | 0.0 | −1.6 | −1.6 |
| OsFe@NDV | $y$ | 0.83 | −0.19 | 2.49 | −0.23 | 0.21 | −0.06 | 0.40 | 0.21 | 39.7 | −0.6 | 50.9 | $-2,-1$ | $1,2$ | $-2,2$ | $0,1$ |
| | $z$ | 0.64 | | 2.26 | | 0.15 | | 0.61 | | | | | 43.0 | 29.7 | −29.0 | −14.1 |
| IrFe@NDV | $y$ | 1.09 | 0.00 | 1.42 | 0.28 | 0.16 | −0.11 | 0.46 | 1.18 | 32.6 | −2.3 | 2.5 | $-2,2$ | $-1,0$ | $-1,1$ | $-1,2$ |
| | $z$ | 1.09 | | 1.70 | | 0.05 | | 1.64 | | | | | 55.1 | 3.7 | −20.8 | −10.9 |
| PtFe@NDV | $y$ | 1.28 | 0.07 | 0.62 | 0.01 | 0.03 | 0.01 | 0.41 | −0.15 | −23.5 | −3.4 | −15.3 | $-2,2$ | $0,1$ | $-1,1$ | $1,2$ |
| | $z$ | 1.35 | | 0.62 | | 0.04 | | 0.26 | | | | | 15.7 | 9.7 | −22.3 | −8.2 |
| FeRu@NDV | $x$ | 0.36 | 0.00 | 3.18 | 0.00 | 0.00 | 0.00 | 0.11 | 0.01 | −2.0 | −2.3 | 0.3 | $-2,1$ | $-2,2$ | $-1,1$ | $-1,0$ |
| | $z$ | 0.36 | | 3.18 | | 0.00 | | 0.12 | | | | | 0.4 | 0.3 | −0.6 | 0.0 |
| CoRu@NDV | $x$ | 0.60 | 0.00 | 2.11 | 0.00 | 0.02 | −0.02 | 0.17 | 0.11 | −1.6 | −2.7 | 1.0 | $-2,2$ | $0,1$ | $-1,1$ | $-1,0$ |
| | $z$ | 0.60 | | 2.11 | | 0.01 | | 0.27 | | | | | 3.1 | 0.1 | −1.1 | −0.5 |
| NiRu@NDV | $x$ | 0.69 | 0.02 | 0.97 | 0.01 | 0.02 | −0.02 | 0.23 | −0.22 | −9.4 | −4.2 | −5.1 | $0,1$ | $-2,2$ | $-1,1$ | $-2,1$ |
| | $z$ | 0.70 | | 0.97 | | 0.01 | | 0.01 | | | | | 0.2 | 0.2 | −2.6 | −1.8 |
| RuRu@NDV | $x$ | 0.56 | 0.00 | 2.56 | 0.01 | 0.05 | −0.03 | 0.19 | 0.27 | 2.7 | −4.8 | 7.0 | $-2,2$ | $-1,0$ | $-1,1$ | $-2,1$ |
| | $z$ | 0.56 | | 2.57 | | 0.02 | | 0.47 | | | | | 8.0 | 3.7 | −3.8 | −1.9 |
| PdRu@NDV | $y$ | 0.72 | 0.17 | 0.40 | 0.09 | 0.02 | −0.02 | 0.14 | −0.11 | −29.2 | −13.5 | −9.6 | $0,1$ | $-1,0$ | $-1,1$ | $-2,-1$ |
| | $z$ | 0.90 | | 0.49 | | 0.00 | | 0.03 | | | | | 2.9 | 2.1 | −10.5 | −1.5 |
| OsRu@NDV | $x$ | 0.03 | 0.04 | 1.02 | 0.39 | 0.01 | 0.13 | 0.12 | 1.01 | 41.5 | 0.3 | 33.1 | $-2,2$ | $-1,2$ | $0,1$ | $-1,0$ |
| | $z$ | 0.07 | | 1.41 | | 0.13 | | 1.13 | | | | | 18.6 | 6.2 | −2.9 | −1.2 |
| IrRu@NDV | $y$ | 0.46 | 0.01 | 1.17 | 0.12 | 0.13 | −0.01 | 0.54 | 0.29 | 18.4 | −3.6 | −12.6 | $1,2$ | $-2,2$ | $-2,1$ | $-1,1$ |
| | $z$ | 0.47 | | 1.29 | | 0.12 | | 0.84 | | | | | 29.3 | 17.6 | −20.7 | −15.3 |
| PtRu@NDV | $x$ | 0.58 | −0.58 | 0.49 | −0.49 | 0.09 | −0.09 | 0.32 | −0.32 | −33.0 | 5.0 | 29.2 | $-1,1$ | $-2,-1$ | $0,1$ | $-2,2$ |
| | $z$ | 0.00 | | 0.00 | | 0.00 | | 0.00 | | | | | 21.3 | 8.9 | −10.4 | −2.9 |
| FeOs@NDV | $x$ | 0.30 | 0.00 | 3.14 | −0.01 | 0.06 | −0.04 | 0.22 | −0.16 | −14.0 | −11.9 | −1.1 | $-2,1$ | $0,1$ | $-1,1$ | $-1,0$ |
| | $z$ | 0.30 | | 3.13 | | 0.02 | | 0.06 | | | | | 0.4 | 0.1 | −1.3 | −0.7 |
| CoOs@NDV | $x$ | 0.48 | 0.01 | 2.05 | 0.00 | 0.02 | 0.01 | 0.26 | −0.04 | −15.6 | −13.3 | −2.0 | $-2,2$ | $0,1$ | $-1,1$ | $-1,2$ |
| | $z$ | 0.49 | | 2.06 | | 0.02 | | 0.22 | | | | | 3.1 | 0.4 | −2.8 | −1.4 |
| NiOs@NDV | $x$ | 0.34 | −0.34 | 0.70 | −0.66 | 0.01 | −0.01 | 0.23 | −0.19 | −29.3 | 7.5 | 0.6 | $-1,1$ | $-2,-1$ | $-2,1$ | $-1,2$ |
| | $z$ | 0.01 | | 0.03 | | 0.00 | | 0.04 | | | | | 1.5 | 1.5 | −1.4 | −1.1 |
| RuOs@NDV | $y$ | 0.02 | 0.01 | 1.54 | 0.03 | 0.00 | 0.08 | 0.23 | 0.15 | 8.2 | 3.5 | 4.4 | $-2,2$ | $1,2$ | $0,1$ | $-1,0$ |
| | $z$ | 0.03 | | 1.57 | | 0.08 | | 0.38 | | | | | 4.7 | 1.6 | −2.3 | −1.0 |
| RhOs@NDV | $y$ | 0.07 | 0.02 | 0.42 | 0.03 | 0.01 | 0.06 | 0.23 | −0.17 | 1.1 | 2.4 | −0.8 | $-2,2$ | $-2,1$ | $0,1$ | $1,2$ |
| | $z$ | 0.08 | | 0.46 | | 0.06 | | 0.06 | | | | | 1.2 | 0.2 | −1.4 | −0.8 |
| OsOs@NDV | $x$ | 0.01 | −0.01 | 0.86 | 0.32 | 0.01 | 0.06 | 0.12 | 1.02 | 15.9 | −0.7 | 15.4 | $-2,2$ | $-1,2$ | $0,1$ | $-2,1$ |
| | $z$ | 0.01 | | 1.18 | | 0.07 | | 1.15 | | | | | 10.0 | 2.2 | −0.8 | −0.2 |
| IrOs@NDV | $x$ | 0.02 | 0.01 | 0.08 | −0.01 | 0.03 | 0.00 | 0.01 | 0.00 | 8.9 | 1.7 | 8.5 | $-2,2$ | $-1,1$ | $-2,1$ | $0,1$ |
| | $z$ | 0.03 | | 0.07 | | 0.03 | | 0.00 | | | | | 12.8 | 1.4 | −2.3 | −2.2 |

**TABLE XVI:** NCL properties of stable perpendicular TM dimers (TM9 as TM↓) at NDV that have non-zero magnetic moments in the SR mode. *Cf.,* **Table X** for the description of the included properties.

| System | Or. | $\mu_{S,\text{TM}\downarrow}$ | $\Delta\mu_{S,\text{TM}\downarrow}$ | $\mu_{S,\text{TM}\uparrow}$ | $\Delta\mu_{S,\text{TM}\uparrow}$ | $\mu_{L,\text{TM}\downarrow}$ | $\Delta\mu_{L,\text{TM}\downarrow}$ | $\mu_{L,\text{TM}\uparrow}$ | $\Delta\mu_{L,\text{TM}\uparrow}$ | MAE | $\Delta E_{SOC}$ TM↓ | $\Delta E_{SOC}$ TM↑ | Contrib. to $\Delta E_{SOC,\text{TM}\uparrow}$ $1^{st}+$ | $2^{nd}+$ | $1^{st}-$ | $2^{nd}-$ |
|---|---|---|---|---|---|---|---|---|---|---|---|---|---|---|---|---|
| FeCo@NDV | $y$ | 0.63 | 0.00 | 3.56 | 0.00 | 0.02 | −0.02 | 0.11 | 0.05 | 0.3 | −0.4 | 0.7 | −2, 2 | 0, 1 | 1, 2 | −1, 1 |
| | $z$ | 0.63 | | 3.56 | | 0.01 | | 0.16 | | | | | 1.3 | 0.3 | −0.7 | −0.5 |
| CoCo@NDV | $x$ | 0.18 | 0.01 | 2.02 | 0.01 | 0.00 | 0.01 | 0.24 | 0.08 | 1.2 | 0.0 | 1.3 | −2, 2 | −1, 1 | −2, 1 | −1, 0 |
| | $z$ | 0.19 | | 2.02 | | 0.01 | | 0.32 | | | | | 2.8 | 0.8 | −0.8 | −0.8 |
| NiCo@NDV | $y$ | 0.31 | 0.00 | 0.88 | 0.00 | 0.02 | 0.05 | 0.36 | 0.02 | 1.8 | 0.8 | 1.3 | −1, 1 | −1, 2 | −2, −1 | −1, 0 |
| | $z$ | 0.31 | | 0.88 | | 0.06 | | 0.38 | | | | | 4.3 | 1.3 | −3.8 | −0.9 |
| RuCo@NDV | $y$ | 0.28 | 0.00 | 2.61 | 0.01 | 0.02 | −0.02 | 0.43 | 0.11 | 0.2 | −0.1 | 0.2 | −2, 2 | −2, −1 | 0, 1 | −1, 1 |
| | $z$ | 0.28 | | 2.61 | | 0.00 | | 0.54 | | | | | 8.4 | 2.2 | −5.6 | −2.8 |
| PdCo@NDV | $y$ | 0.52 | 0.00 | 0.34 | 0.00 | 0.08 | 0.00 | 0.23 | −0.01 | −0.1 | 0.1 | −0.1 | −1, 1 | −1, 0 | 0, 1 | −2, 0 |
| | $z$ | 0.52 | | 0.34 | | 0.08 | | 0.22 | | | | | 0.1 | 0.0 | −0.3 | 0.0 |
| OsCo@NDV | $x$ | 0.62 | 0.05 | 2.93 | 0.07 | 0.14 | −0.13 | 0.64 | 0.21 | −26.4 | −4.1 | 0.9 | −1, 2 | −1, 0 | −2, 2 | −1, 1 |
| | $z$ | 0.67 | | 3.01 | | 0.02 | | 0.85 | | | | | 24.8 | 16.1 | −23.6 | −10.6 |
| IrCo@NDV | $x$ | 0.76 | −0.04 | 1.86 | 0.11 | 0.02 | 0.06 | 1.16 | 0.74 | 63.2 | −6.3 | 52.7 | −2, 2 | −1, 0 | −2, 1 | −1, 2 |
| | $z$ | 0.72 | | 1.97 | | 0.08 | | 1.90 | | | | | 91.6 | 8.1 | −23.3 | −16.0 |
| PtCo@NDV | $y$ | 0.19 | 0.14 | 0.32 | 0.13 | 0.04 | 0.16 | 0.47 | 0.31 | 2.5 | 0.4 | −6.2 | −1, 2 | 1, 2 | −2, 2 | −2, −1 |
| | $z$ | 0.34 | | 0.46 | | 0.20 | | 0.77 | | | | | 17.1 | 15.4 | −17.1 | −13.2 |
| FeRh@NDV | $y$ | 0.31 | 0.04 | 3.47 | 0.07 | 0.01 | −0.01 | 0.12 | 0.31 | −97.7 | 0.6 | 3.9 | −2, 2 | 1, 2 | −1, 1 | −2, −1 |
| | $z$ | 0.34 | | 3.54 | | 0.01 | | 0.43 | | | | | 5.3 | 0.2 | −0.6 | −0.3 |
| CoRh@NDV | $x$ | 0.11 | 0.00 | 2.02 | 0.00 | 0.01 | 0.00 | 0.24 | 0.09 | 1.4 | −0.1 | 1.3 | −2, 2 | −1, 1 | −1, 0 | −1, 2 |
| | $z$ | 0.11 | | 2.02 | | 0.01 | | 0.32 | | | | | 2.6 | 0.9 | −0.8 | −0.8 |
| NiRh@NDV | $y$ | 0.18 | 0.00 | 0.88 | 0.00 | 0.01 | 0.04 | 0.36 | −0.01 | 0.9 | 1.0 | 0.2 | −1, 1 | −1, 2 | −2, −1 | −1, 0 |
| | $z$ | 0.18 | | 0.88 | | 0.05 | | 0.35 | | | | | 4.0 | 1.5 | −4.1 | −0.9 |
| OsRh@NDV | $x$ | 0.29 | −0.01 | 2.66 | 0.12 | 0.12 | −0.11 | 0.67 | 0.58 | 5.8 | −1.9 | −3.8 | −2, 2 | −1, 2 | −1, 1 | −2, 1 |
| | $z$ | 0.28 | | 2.78 | | 0.02 | | 1.25 | | | | | 26.1 | 17.3 | −22.5 | −12.6 |
| IrRh@NDV | $y$ | 0.18 | 0.06 | 1.37 | 0.34 | 0.00 | 0.10 | 1.07 | 1.11 | 70.0 | −4.4 | 56.8 | −2, 2 | −1, 1 | 1, 2 | −2, −1 |
| | $z$ | 0.25 | | 1.71 | | 0.10 | | 2.19 | | | | | 89.4 | 15.2 | −35.2 | −19.7 |
| PtRh@NDV | $y$ | 0.15 | 0.07 | 0.35 | 0.11 | 0.02 | 0.12 | 0.45 | 0.27 | −1.4 | 0.2 | −4.0 | −1, 2 | 1, 2 | −2, 2 | −2, −1 |
| | $z$ | 0.21 | | 0.46 | | 0.14 | | 0.72 | | | | | 14.9 | 11.4 | −13.4 | −9.9 |
| FeIr@NDV | $x$ | 0.38 | −0.24 | 3.55 | −0.43 | 0.07 | −0.06 | 0.17 | −0.02 | 1.2 | 3.1 | −1.3 | −2, 2 | 0, 1 | −1, 1 | −1, 0 |
| | $z$ | 0.14 | | 3.11 | | 0.01 | | 0.14 | | | | | 1.3 | 0.4 | −1.0 | −0.8 |
| CoIr@NDV | $x$ | 0.18 | 0.00 | 2.00 | 0.00 | 0.00 | 0.02 | 0.22 | 0.16 | −0.1 | −0.3 | 1.1 | −2, 2 | −1, 1 | −1, 0 | −1, 2 |
| | $z$ | 0.18 | | 2.00 | | 0.02 | | 0.38 | | | | | 2.9 | 1.0 | −1.8 | −0.4 |
| NiIr@NDV | $y$ | 0.21 | 0.00 | 0.82 | 0.01 | 0.01 | 0.05 | 0.29 | 0.06 | 2.9 | 3.5 | 0.6 | −1, 1 | −2, 2 | −2, −1 | 0, 1 |
| | $z$ | 0.21 | | 0.83 | | 0.06 | | 0.35 | | | | | 3.2 | 1.0 | −2.6 | −0.8 |
| RuIr@NDV | $y$ | 0.22 | 0.04 | 2.55 | −0.01 | 0.01 | 0.03 | 0.48 | 0.24 | −44.9 | 5.8 | 0.1 | −2, 2 | −1, 1 | 0, 1 | −2, −1 |
| | $z$ | 0.26 | | 2.53 | | 0.04 | | 0.71 | | | | | 7.9 | 2.7 | −8.3 | −1.9 |
| RhIr@NDV | $y$ | 0.26 | 0.00 | 1.45 | 0.01 | 0.02 | 0.03 | 0.53 | 0.07 | 0.6 | 0.5 | −1.1 | −2, 2 | −1, 0 | 0, 1 | 1, 2 |
| | $z$ | 0.25 | | 1.47 | | 0.05 | | 0.60 | | | | | 8.1 | 0.9 | −3.9 | −2.8 |
| PdIr@NDV | $y$ | 0.30 | 0.03 | 0.30 | 0.07 | 0.01 | 0.12 | 0.08 | 0.19 | 1.9 | 0.7 | 0.5 | −1, 1 | −1, 2 | −1, 0 | −2, −1 |
| | $z$ | 0.33 | | 0.37 | | 0.13 | | 0.27 | | | | | 0.5 | 0.3 | −0.4 | −0.1 |
| OsIr@NDV | $x$ | 0.26 | −0.02 | 2.42 | 0.11 | 0.10 | −0.06 | 0.62 | 0.61 | −5.1 | −7.5 | 0.3 | −2, 2 | −1, 2 | −1, 1 | −2, 1 |
| | $z$ | 0.25 | | 2.53 | | 0.04 | | 1.23 | | | | | 28.5 | 17.0 | −29.1 | −10.0 |
| IrIr@NDV | $y$ | 0.25 | −0.01 | 1.33 | 0.21 | 0.01 | 0.07 | 1.00 | 0.93 | 37.5 | −5.7 | 35.6 | −2, 2 | −2, 1 | 1, 2 | −1, 2 |
| | $z$ | 0.25 | | 1.54 | | 0.07 | | 1.93 | | | | | 79.6 | 20.9 | −50.6 | −24.1 |
| PtIr@NDV | $y$ | 0.21 | 0.04 | 0.35 | 0.08 | 0.03 | 0.10 | 0.35 | 0.19 | −0.8 | 1.2 | −2.9 | −1, 2 | 1, 2 | −2, 2 | −1, 0 |
| | $z$ | 0.25 | | 0.43 | | 0.13 | | 0.54 | | | | | 4.0 | 2.9 | −4.7 | −3.1 |

in the matrices. Changes in the $E_{SOC}$ between two orientations of magnetization should be responsible for the major part of the MAE. We therefore present the difference of $E_{SOC}$ ($\Delta E_{SOC}$) of TM↓ and of TM↑. As we discussed in the previous chapter, magnetic moments of TM↓ are significantly quenched by the adsorption of TM↑. TM↓ has only a limited direct contribution to the MAE in the sense that its magnetic moments significantly differ with different orientations of magnetization. TM↓ has a crucial indirect impact by influencing the electronic structure of TM↑. Similar conclusions can be derived for the rest of graphene, its contribution is again mostly indirect. We therefore decided to briefly inspect $\Delta E_{SOC}$ of TM↓ and to deeply examine $\Delta E_{SOC}$ of TM↑ in the sense that we focus on the pairs of $d$ orbitals that contribute the most to the positive or negative value of $\Delta E_{SOC}$.

As expected, TM dimers with TM↑ from the Fe- and Ru group do not posses high positive values of MAE (MAE $<$ 15 meV), on the other hand, the value of the MAE is significantly negative in some cases. Interestingly, systems with the most negative values of MAE undergo a high increment of the orbital magnetic moment of TM↑ when the magnetization changes from in-plane to the perpendicular to the graphene plane and the value of the $\Delta E_{SOC}$ is positive as well. Such elements thus presumably favour the configuration that keeps low values of the orbital magnetic moment and the value of the MAE is imposed by other factors that we have not sufficiently identified yet. As anticipated, TM↓ has generally only a small positive impact on MAE or the negative contribution is always greater (*i.e.,* less negative) than $-15$ meV.

Our results can be compared with the systematical study presented in Ref. 17 that includes also perpendicularly unstable dimers. The overall comparison of their and our MAE predictions is shown in **Table XVII**. It needs to be noted that all the systems with Pt as TM↑ in our calculations exhibit only negligible values of MAE, or they are negative, which is strictly different from their results. The source of the discrepancies remains unclear because the authors predicted the total and local magnetic moments in the SR mode very similar to ours and also the authors do not report any parameters in the NCL mode that would significantly differ from ours. The only visible difference is in the used mechanism of determining of the MAE. The authors used a torque method but their tests showed that it is quantitatively comparable with the procedure of determining MAE from the total energies as we used in our present work. To the best of our knowledge, only few other authors examined the MAE of the TM dimers at graphene with the same

defects as we did: the MAE of IrIr@NSV was estimated to be 18.5 meV[78] and 37.9 meV[79].

Our results indicate that triads have similar NCL properties. In the first approximation, the most influencing property of TM↓ is the number of valence electrons. In **Sec. III D** we showed that TM atoms from the earlier periods tend to form lower-order bonds than that from the later ones and the bonding mechanism within the TM dimer may slightly differ. The hybridization within the TM dimer may have a crucial impact on $\Delta E_{SOC}$. That is also the reason why the NCL properties within the triads slightly differ.

Several authors[80–83] derived that $E_{SOC}$ can be predicted from DOS obtained in the SR mode. The SOC occurs between the occupied and unoccupied orbitals (with the magnetic quantum number $m_l$) that must fulfil conditions $\Delta|m_l| \leq 1$ and $\Delta m_l \neq 0$. The effect is inversely proportional to the energetical difference of both orbitals, we are therefore most interested in the states in the vicinity of the $E_F$. The authors also derived that from all the possible SOC effects that occur in a single spin channel, just $\Delta|m_l| = 0$ contribute to the perpendicular easy axis (along $z$-axis), while the rest contributes to a parallel easy axis. If the SOC effect takes part between both spin channels, the rules are opposite, *i.e.*, $\Delta|m_l| = 0$ contribute to the parallel easy axis and the rest to the perpendicular easy axis. It needs to be emphasized that this is a very crude approximation, in contrast with the self-consistent NCL calculations, and it can serve only as a support for the obtained values. It is also impossible to judge the contributions by a simple observation of DOS by eye. The message that needs to be remarked is that the closer distance to $E_F$ of any

**TABLE XVII:** Predicted values of MAE (meV) compared with the paper by Hu and Wu[17].

| System | Pres. | Ref. 17 | System | Pres. | Ref. 17 |
|---|---|---|---|---|---|
| PtOs@SV | −28 | −23 | OsOs@NDV | 16 | 38 |
| OsIr@SV | −53 | < −60 | OsCo@NDV | −26 | −7 |
| IrIr@SV | 11 | 27 | IrCo@NDV | 63 | 75 |
| PtIr@SV | 1 | 85 | PtCo@NDV | 3 | 38 |
| OsFe@NDV | 40 | −8 | OsRh@NDV | 6 | −17 |
| IrFe@NDV | 33 | 28 | IrRh@NDV | 70 | 52 |
| PtFe@NDV | −24 | 6 | PtRh@NDV | −1 | 28 |
| OsRu@NDV | 42 | 62 | OsIr@NDV | −5 | −20 |
| IrRu@NDV | 18 | 14 | IrIr@NDV | 38 | 30 |
| PtRu@NDV | −33 | −52 | PtIr@NDV | −1 | 25 |

state results in its greater contribution to MAE (regardless if it is positive or negative), *e.g.*, if one state is split to two parts, one is above $E_F$ and the second one below, its contribution to $E_{SOC}$ will be greater at a weaker hybridization within the TM dimer (stronger hybridization separates the states more than the weaker one). In the states that are whole placed below (above) $E_F$ their hybridization pushes one of their part closer to $E_F$. The impact of hybridization on the overall MAE is therefore not completely straightforward.

MAE values in systems with Os or Ir as TM↑ often follow the trend of $\Delta E_{SOC}$. Systems with high values ($\geq$ 15 meV) of MAE are (for a brief summary) listed in **Table XVIII**. Values of the MAE in the given triads correlate with $E_{ad2}$ strongly proportionally (*i.e.*, the weaker binding corresponds with a higher MAE, *e.g.*, in OsTM9@NSV), strongly inverse-proportionally (IrTM9@NSV), and somewhere between. That range confirms that MAE cannot be easily assessed by the strength of the interaction within the TM dimer. The highest contribution to $\Delta E_{SOC}$ of TM↑ most often comes from the spin-orbit coupling interaction between $d_{xy}$ and $d_{x^2-y^2}$ orbitals and then from the interaction between $|m_l| = 2$ and $|m_l| = 1$ $d$ orbitals. High values of MAE are in these systems always accompanied by a substantial anisotropy of orbital magnetic moments of TM↑ (it always increases) and also by a modest anisotropy of spin magnetic moment of TM↑ (it increases in most cases). The anisotropy of magnetic moments of TM↓ is not always negligible but it never reaches the magnitude of the anisotropies of TM↑.

**TABLE XVIII:** A brief summary of the systems with rounded MAE values (in meV) greater or equal to 15 meV

| System | MAE | System | MAE | System | MAE | System | MAE |
|---|---|---|---|---|---|---|---|
| IrPt@SV | 39 | IrRh@NSV | 26 | IrPd@NSV | 51 | OsOs@NDV | 16 |
| OsFe@NSV | 15 | OsIr@NSV | 50 | OsPt@NSV | 119 | IrCo@NDV | 63 |
| IrFe@NSV | 44 | IrIr@NSV | 36 | OsFe@NDV | 40 | IrRh@NDV | 70 |
| OsCo@NSV | 67 | OsNi@NSV | 54 | IrFe@NDV | 33 | IrIr@NDV | 38 |
| IrCo@NSV | 18 | IrNi@NSV | 74 | OsRu@NDV | 42 | | |
| OsRh@NSV | 57 | OsPd@NSV | 170 | IrRu@NDV | 18 | | |

As we mentioned above, the aim of our research is to find a material that would be able to preserve the information to the temperature of liquid nitrogen (77 K) that is

commercially affordable. The naive energy barrier can be estimated as

$$E_T = k_B T, \tag{44}$$

where $k_B$ is the Boltzmann constant and $T$ is the thermodynamic temperature. $E_T$ is the energy difference of the precise magnetic groundstate and the saddle point of the energy hypersurface between the two valleys of different orientations of magnetization. If MAE = $E_T$, the system is able to withstand one such thermal excitation. According to the **Eq. 44**, it would be sufficient to have MAE $\sim$ 32 meV to reliably store the information up to 100 °C. We have found many systems that possess higher MAE values. Unfortunately, for a long-time data storage, we need to incorporate also statistical effects. One of the most used formulas for this purpose is the one proposed by Néel:

$$\mathrm{MAE} = T_B \cdot k_B \cdot \ln \frac{\tau_N}{\tau_0}, \tag{45}$$

where $T_B$ is the aimed temperature to be withstood (blocking temperature), $\tau_N$ is the aimed relaxation time (we decided to calculate with 10 years), and $\tau_0$ is an attempt period that is characteristic for each magnetic material (usually in the order of $10^{-10}$ s, we used directly $10^{-10}$ s). According to **Eq. 45**, we need to achieve MAE higher than 285 meV. We have not discovered a system with such MAE but we have made great progress in contrast with the single adsorbed TM atoms, *e.g.*, $T_B$ of OsPd@NSV is $\sim$ 44 K. Our future research will deeply examine the systems presented in **Table XVIII** to precisely elucidate the mechanisms determining the high values of MAE. We can use this knowledge in the future to engineer the systems with a greater potential to have desired values of MAE. We will also consider the role of the substrate under graphene because, *e.g.*, the presence of Cu(111) substrate even enhanced the high MAE of the IrCo dimer initially standing on pristine graphene[11].

### F. Techniques Beyond the Presented NCL Calculations

Now we could use many other techniques that are able to farther elucidate the NCL properties of a given system, but we would get far beyond the scope of the present thesis. Now we will briefly sum up the techniques and results that we already published.[13] These techniques will be soon applied on the other systems with high values of MAE discovered in the present work.

The tests with bigger supercells with the same area density of TM atoms (dimers) showed that the MAE per one magnetic centre remains the same in Ir@DV in 5 x 5

(that is the supercell used in the rest of this thesis), 5 x 10, and 10 x 10 supercells. Similarly, MAE per magnetic centre is nearly the same in 5 x 5 and 5 x 10 supercell in IrIr@NDV. The usage of a non-local correlation functional optB86b-vdW[57] leads to a slightly decreased MAE of Ir@DV and to a slight increment in MAE of IrIr@NDV.

The usage of the magnetic force theorem (FT)[49,84] proved itself to be very useful. It is generally an adequate approximation but it may badly fail in the calculations of the MAE in some systems and therefore it needs to be handled with care. If MAEs obtained by both SC and FT calculations are similar, FT allows us to quantify the contribution of each single orbital (and the values of energy below $E_F$ where the contribution is the most dominant) to the total MAE by the integration of difference of DOS from the calculations with a different orientation of magnetization. Here we accentuate that the sum of the obtained values cannot in principle be the same as the total MAE because of the mechanism how VASP projects DOS around each atom on spheres (their radius is a parameter entering the calculations as a Wigner-Seitz radius) surrounding each atom.

Another aspect to be examined is the additional orbital-dependent on-site Coulomb repulsion $U$.[51,52] As we do not know the real measured values yet, we can only calculate the systems with arbitrarily chosen values of $U - J$. In the previous work[13] we showed that the choice of $U - J$ may have a crucial impact on the values of the MAE. $U - J = 4$ led to an enhancement of the MAE in Ir@DV from 6.6 meV to 18.7 meV. In Ir@NSV it even reversed the sign of the MAE, starting at $-9.8$ meV and ending at 16.9 meV. Nevertheless, the value of $U - J = 4$ may be too high and we will not know for sure unless the real values are measured. $U - J = 2$ in IrIr@SV and in the metastable dimer IrIr@DV had no impact on MAE, in IrIr@NSV and IrIr@NDV it led to a further enhancement of MAE by $\sim$ 10 meV.

It is possible to combine FT calculations with an additional $U$ parameter and see the direct impact of the additional electron repulsion on resulting MAE. The effect should be virtually similar to the strength of hybridization within the TM dimer (it can have both positive or negative impact on MAE) but it cannot be generalized. It will be thoroughly discussed in the future.

## IV. SUMMARY

We have significantly extended our previous work[13] that considered only single TM atoms and TMIr dimers adsorbed at defective graphene. We were able to use and extend the simple equations describing the number of unpaired electrons in systems with a single adsorbed TM atom and to predict the bond order of the newly created TM dimer by the adsorption of the second TM atom. It allowed us to elucidate the perpendicular stability of TM dimers and to explain the perpendicular instability of TM dimers in all TMTM@DV and in most TMTM8@SV, TMTM9@SV, TMTM10@SV, and TMTM10@NDV systems. Many TM dimers are perpendicularly very stable, their reluctance to be tilted is higher than 1 eV.

A thorough discussion of the SR properties led to the adjustment of the initial simple thoughts. Now we consider not just the pairing of the initially unpaired electrons but also their spin-dependent relocation. Thanks to that we were able to observe also the formation of donor-acceptor bonds. Many TM dimers in the examined systems do not form the predicted maximal number of the covalent bonds. In these cases the electrons are often relocated in that manner to keep the magnetic moment of TM↓ the lowest while the magnetic moment of TM↑ is even enhanced. We defined so called triads: systems with the same TM↑, defective graphene, and differing in TM↓ within the same vertical group. Triads have similar SR properties, although there is a small development of the values from systems with TM↓ from an earlier period to the one with TM↓ from later periods. Heavier elements tend to form higher-order bonds while the lighter elements prefer the formation of single bonds. Heavier elements are also able to adapt their electronic structure more easily to their bonding partner and their binding is therefore stronger. DOS of triads are also very similar and may slightly differ only in the concrete positions of the states.

The Bader charge analysis has a limited applicability in these systems (definition of an atom by Bader in our systems attributes unphysical large space to TM↑) but shows clear trends. Charge of TM↓ is always positive due to the interaction with graphene but its value is significantly affected by TM↑. The attraction of electrons of TM↑ in general in our systems increases within both the horizontal and vertical group (*e.g.*, Fe attracts electrons the weakest and thus forms cations while Pt attracts electrons the most and therefore it possesses a negative charge). Charge within the TM dimer is partly compensated by the charge shift between TM↓ and graphene.

NCL calculations confirmed that elements from the earlier periods as TM↑ are not

suitable to achieve high values of MAE. The MAE of systems with Pt as TM↑ are mostly close to 0, in a sharp contrast with Ref. 17 which predicts a high MAE in these systems; the reason remains unclear because their total and local magnetic moments in the SR mode are similar to ours and the authors do not report any different parameter that should have such an impact. Os and Ir are the only examined elements that achieve high MAE values as TM↑. Members of the triads are often similar and a trend in MAE in some triads is also clear. Nevertheless, this trend is not always the same, which points to the limitations of predictions of the MAE by a comparison with similar systems. A high MAE is always accompanied by a high orbital anisotropy and a modest spin anisotropy of TM↑ while the anisotropies of TM↓ remain of a lower magnitude. A more thorough research of NCL properties in the promising systems is necessary, but it is beyond the scope of the present thesis and will be made in the future. According to the best of our knowledge, most of the systems were calculated for the very first time. We highlight our MAE values of TM dimers at NSV, that were calculated by other authors only for the IrIr dimer, but they are also very high in many other dimers that were firstly calculated by us.

We aimed to found a material that would be suitable as a novel magnetic recording medium with an information density $\sim 490$ Tb·inch$^{-2}$. In contrast with a single adsorbed TM atoms, we have found many adsorbed TM dimers that would withstand a single thermal excitation up to 100 °C (MAE $>$ 32 meV) but they would not be able to hold the information for a long time. To achieve the information lifetime of 10 years at 77 K, we need to have MAE $>$ 285 meV; the most promising system is OsPd@NSV with the MAE of 170 meV. We will examine the impact of the substrate under graphene in the future, and we may also include other TM atoms to our research.

# V. ZÁVĚR

Touto prací jsme zásadně rozšířili svůj článek[13], ve kterém jsme se zabývali pouze atomy přechodných kovů (PK) a dimery PK s atomy Ir adsorbovaných na defektním grafenu. Podařilo se nám vhodně rozšířit jednoduché rovnice použité pro popis samostatných adsorbovaných PK a následně predikovat řád vazby v nových dimerech PK, které vznikly adsorpcí druhého atomu PK na již adsorbovaný PK. Díky tomu jsme byli schopni posoudit stabilitu kolmé geometrie daného dimeru a také jsme byli schopni zdůvodnit nestabilitu dimerů PK ve všech systémech PKPK@DV a ve většině systémů PKPK8@SV, PKPK9@SV, PKPK10@SV a PKPK10@NDV. Většina dimerů je v této geometrii velmi stabilní, jejich odpor vůči jiné geometrii je větší než 1 eV.

Pečlivá diskuse spočítaných vlastností systémů nás vedla k úpravě původních jednoduchých myšlenek. Nyní už neuvažujeme pouze párování původně nespárovaných elektronů, ale také jejich přemístění v závislosti na spinu. Díky tomu se nám podařilo také popsat vytvoření donor-akceptorových vazeb. Spousta dimerů PK netvoří maximální predikovaný počet kovalentních vazeb. V těchto případech jsou pak elektrony přemístěny tak, aby byl magnetický moment na spodním atomu PK co nejmenší, zatímco magnetický moment na horním atomu PK je tímto ještě zvýšen. Definovali jsme takzvané triády: systémy se stejným horním atomem PK, stejným defektním grafenem, ale různým spodním atomem PK (všechny spodní atomy PK jsou ze stejné skupiny). Triády mají obecně podobné vlastnosti, ale i v nich můžeme pozorovat postupný vývoj hodnot těchto vlastností od spodního atomu PK z dřívějších period do pozdějších period. Těžší prvky častěji tvoří vícenásobné vazby zatímco lehčí prvky preferují jednoduché vazby. Těžší prvky jsou navíc schopné lépe přizpůsobit svůj elektronový obal svému vazebnému partnerovi a jejich vazba je tedy silnější. Hustota stavů triád je velmi podobná a většinou se pouze drobně liší pozice jednotlivých stavů.

Baderova analýza nábojů má v těchto systémech pouze omezenou aplikovatelnost (Bade-rova definice atomu přisuzuje hornímu atomu PK příliš velký prostor), ale trendy, které predikuje, jsou jasné. Náboj na spodním atomu PK je vždy kladný kvůli interakci s defektním grafenem, ale jeho hodnota je silně závislá na horním atomu PK. Přitahování elektronů horním atomem PK obecně roste s horizontální i vertikální skupinou daného atomu PK (tedy Fe přitahuje elektrony nejméně, a tudíž preferuje tvorbu kationtů, zatímco Pt nejvíce, takže tvoří především anionty). Náboj v rámci dimeru je částečně kompenzován přesunem náboje mezi spodním atomem PK a defektním grafenem.

Nekolineární (NCL) kalkulace potvrdily, že lehčí PK jako horní atomy nejsou vhodné k dosažení vysokých hodnot magnetické anizotropní energie (MAE). Hodnoty MAE Pt jako horního atomu PK jsou často blízké 0, což je v ostrém rozporu s referencí 17, která v těchto systémech predikuje vysoké hodnoty MAE. Důvod tohoto nesouladu je nejasný, protože autoři uvádí velmi podobné hodnoty magnetických momentů a také neuvádí žádný parametr, který by měl výsledky takto ovlivnit. Jediné atomy PK, které jako horní atomy dosahují vysokých hodnot MAE, jsou Os a Ir. Jejich triády jsou často podobné a některé dokonce vykazují jasný trend. Tyto trendy se nicméně liší, což poukazuje na limitaci odhadu MAE na základě srovnání s jinými systémy. Vysoká hodnota MAE je vždy doprovázena velkou anizotropií orbitálního magnetického momentu na horním atomu PK a také o trochu menší anizotropií spinového magnetického momentu. Anizotropie magnetických momentů na ostatních atomech jsou zanedbatelné. Je nezbytné provést další analýzy NCL vlastností dimerů se slibnými hodnotami MAE, ale takový výzkum přesahuje rozsah této práce a bude proveden v budoucnu. Pokud je nám známo, většina systémů byla spočítána úplně poprvé. Chtěli bychom zdůraznit hlavně MAE dimerů PK adsorbovaných na monovakanci dekorované atomy dusíku, které byly spočítány ostatními autory pouze pro dimer IrIr, ale které mají velmi vysoké hodnoty ve spoustě dalších dimerů, které byly prvně spočítány námi.

Cílem naší práce bylo nalezení materiálu, který by byl vhodný jako nové magnetické záznamové médium s kapacitou $\sim$ 490 Tb·inch$^{-2}$. Objevili jsme, že ve srovnání se samostatnými adsorbovanými atomy PK existuje mnoho dimerů PK, které by byly schopné odolat jediné termální excitaci do 100 °C (MAE $>$ 32 meV), ale nedokázaly by udržet informaci po delší dobu. Potřebovali bychom MAE $>$ 285 meV, abychom dosáhli průměrné doby života informace 10 let při teplotě kapalného dusíku (77 K). Nejvíce jsme se této hodnotě přiblížili v systému OsPd@NSV s hodnotou MAE 170 meV. V budoucnu posoudíme také vliv substrátu umístěného pod grafenem a možná zkusíme zahrnout i další atomy PK.

[1] R. Wood, IEEE Transactions on Magnetics **36**, 36 (2000).
[2] R. E. Fontana and G. M. Decad, AIP Advances **8**, 056506 (2018).
[3] Y. Shiroishi, K. Fukuda, I. Tagawa, H. Iwasaki, S. Takenoiri, H. Tanaka, H. Mutoh, and N. Yoshikawa, IEEE Transactions on Magnetics **45**, 3816 (2009).
[4] Seagate, Heat Assisted Magnetic Recording (HAMR), [online] https://www.seagate.com/innovation/hamr/ (2020).
[5] P. Gambardella, S. Rusponi, M. Veronese, S. S. Dhesi, C. Grazioli, A. Dallmeyer, I. Cabria, R. Zeller, P. H. Dederichs, K. Kern, C. Carbone, and H. Brune, Science **300**, 1130 (2003).
[6] R. Baltic, M. Pivetta, F. Donati, C. Wäckerlin, A. Singha, J. Dreiser, S. Rusponi, and H. Brune, Nano Letters **16**, 7610 (2016).
[7] F. Donati, S. Rusponi, S. Stepanow, C. Wackerlin, A. Singha, L. Persichetti, R. Baltic, K. Diller, F. Patthey, E. Fernandes, J. Dreiser, . ljivan anin, K. Kummer, C. Nistor, P. Gambardella, and H. Brune, Science **352**, 318 (2016).
[8] F. D. Natterer, K. Yang, W. Paul, P. Willke, T. Choi, T. Greber, A. J. Heinrich, and C. P. Lutz, Nature **543**, 226 (2017).
[9] P. Błoński and J. Hafner, Physical Review B **79**, 224418 (2009).
[10] P. Błoński and J. Hafner, Journal of Physics: Condensed Matter **26**, 146002 (2014).
[11] P. Błoński and J. Hafner, Journal of Physics: Condensed Matter **26**, 256001 (2014).
[12] A. W. Robertson, C. S. Allen, Y. A. Wu, K. He, J. Olivier, J. Neethling, A. I. Kirkland, and J. H. Warner, Nature Communications **3**, 1144 (2012).
[13] J. Navrátil, P. Błoński, and M. Otyepka, Nanotechnology **32**, 230001 (2021).
[14] Wikipedia, Hard disk drive. [online] https://en.wikipedia.org/wiki/Hard_disk_drive (2021).
[15] Wikipedia, Solid-state drive. [online] https://en.wikipedia.org/wiki/Solid-state-drive (2021).
[16] Fujifilm; IBM, Fujifilm develops technology to deliver the world's highest 580TB storage capacity for magnetic tapes using strontium ferrite (SrFe) magnetic particles, [online] https://techxplore.com/news/2020-12-fujifilm-ibm-unveil-terabyte-magnetic.html (2020).
[17] J. Hu and R. Wu, Nano Letters **14**, 1853 (2014).
[18] G.-X. Ge, Y.-B. Li, G.-H. Wang, and J.-G. Wan, Physical Chemistry Chemical Physics **18**, 11550 (2016).
[19] M. Tanveer, J. Dorantes-Dávila, and G. M. Pastor, Physical Review B **96**, 224413 (2017).
[20] Z. Meng, G. Li, S.-M. Ng, H.-F. Wong, S.-C. Yiu, C.-L. Ho, C.-W. Leung, and W.-Y. Wong, Polymer Chemistry **7**, 4467 (2016).
[21] Q. Dong, Z. Meng, C.-L. Ho, H. Guo, W. Yang, I. Manners, L. Xu, and W.-Y. Wong, Chemical Society Reviews **47**, 4934 (2018).
[22] Z. Meng, C.-L. Ho, H.-F. Wong, Z.-Q. Yu, N. Zhu, G. Li, C.-W. Leung, and W.-Y. Wong, Science China Materials **62**, 566 (2019).
[23] A. W. Robertson, B. Montanari, K. He, C. S. Allen, Y. A. Wu, N. M. Harrison, A. I. Kirkland, and J. H. Warner, ACS Nano **7**, 4495 (2013).
[24] Y.-C. Lin, P.-Y. Teng, C.-H. Yeh, M. Koshino, P.-W. Chiu, and K. Suenaga, Nano Letters **15**, 7408 (2015).
[25] F. D. Natterer, F. Donati, F. Patthey, and H. Brune, Physical Review Letters **121**, 027201 (2018).
[26] K. S. Novoselov, Science **306**, 666 (2004).
[27] J. Tuček, P. Błoński, J. Ugolotti, A. K. Swain, T. Enoki, and R. Zbořil, Chemical Society Reviews **47**, 3899 (2018).
[28] R. Zbořil, F. Karlický, A. B. Bourlinos, T. A. Steriotis, A. K. Stubos, V. Georgakilas,

K. Šafářová, D. Jančík, C. Trapalis, and M. Otyepka, Small **6**, 2885 (2010).
[29] R. R. Nair, W. Ren, R. Jalil, I. Riaz, V. G. Kravets, L. Britnell, P. Blake, F. Schedin, A. S. Mayorov, S. Yuan, M. I. Katsnelson, H.-M. Cheng, W. Strupinski, L. G. Bulusheva, A. V. Okotrub, I. V. Grigorieva, A. N. Grigorenko, K. S. Novoselov, and A. K. Geim, Small **6**, 2877 (2010).
[30] D. Zaoralová, V. Hrubý, V. Šedajová, R. Mach, V. Kupka, J. Ugolotti, A. Bakandritsos, M. Medved', and M. Otyepka, ACS Sustainable Chemistry and Engineering (2020), 10.1021/acssuschemeng.9b07161.
[31] A. Bakandritsos, M. Pykal, P. Błoński, P. Jakubec, D. D. Chronopoulos, K. Poláková, V. Georgakilas, K. Čépe, O. Tomanec, V. Ranc, A. B. Bourlinos, R. Zbořil, and M. Otyepka, ACS Nano **11**, 2982 (2017).
[32] A. Bakandritsos, R. G. Kadam, P. Kumar, G. Zoppellaro, M. Medved', J. Tuček, T. Montini, O. Tomanec, P. Andrýsková, B. Drahoš, R. S. Varma, M. Otyepka, M. B. Gawande, P. Fornasiero, and R. Zbořil, Advanced Materials **31**, 1900323 (2019).
[33] A. Hashimoto, K. Suenaga, A. Gloter, K. Urita, and S. Iijima, Nature **430**, 870 (2004).
[34] F. Banhart, J. Kotakoski, and A. V. Krasheninnikov, ACS Nano **5**, 26 (2011).
[35] S. T. Pantelides, Y. Puzyrev, L. Tsetseris, and B. Wang, MRS Bulletin **37**, 1187 (2012).
[36] Y. Gan, L. Sun, and F. Banhart, Small **4**, 587 (2008).
[37] M. Manadé, F. Viñes, and F. Illas, Carbon **95**, 525 (2015).
[38] X. Q. Dai, J. H. Zhao, M. H. Xie, Y. N. Tang, Y. H. Li, and B. Zhao, The European Physical Journal B **80**, 343 (2011).
[39] Y. Fujimoto and S. Saito, Physical Review B **84**, 245446 (2011).
[40] Z. Hou, X. Wang, T. Ikeda, K. Terakura, M. Oshima, M.-a. Kakimoto, and S. Miyata, Physical Review B **85**, 165439 (2012).
[41] Z. Hou, X. Wang, T. Ikeda, K. Terakura, M. Oshima, and M.-a. Kakimoto, Physical Review B **87**, 165401 (2013).
[42] A. Groß, *Theoretical Surface Science* (Springer Berlin Heidelberg, Berlin, Heidelberg, 2009).
[43] J. P. Perdew, International Journal of Quantum Chemistry **28**, 497 (1986).
[44] P. Hohenberg and W. Kohn, Physical Review **136**, B864 (1964).
[45] W. Kohn and L. J. Sham, Physical Review **140**, A1133 (1965).
[46] C. Fiolhais and F. Nogueira, *A primer in density functional theory* (Springer, Berlin, 2003).
[47] D. Hobbs, G. Kresse, and J. Hafner, Physical Review B **62**, 11556 (2000).
[48] S. Steiner, S. Khmelevskyi, M. Marsmann, and G. Kresse, Physical Review B **93**, 224425 (2016).
[49] A. Liechtenstein, M. Katsnelson, V. Antropov, and V. Gubanov, Journal of Magnetism and Magnetic Materials **67**, 65 (1987).
[50] V. I. Anisimov, J. Zaanen, and O. K. Andersen, Physical Review B **44**, 943 (1991).
[51] H. J. Kulik, M. Cococcioni, D. A. Scherlis, and N. Marzari, Physical Review Letters **97**, 103001 (2006).
[52] S. L. Dudarev, G. A. Botton, S. Y. Savrasov, C. J. Humphreys, and A. P. Sutton, Physical Review B **57**, 1505 (1998).
[53] A. Rohrbach, J. Hafner, and G. Kresse, Journal of Physics: Condensed Matter **15**, 979 (2003).
[54] M. Dion, H. Rydberg, E. Schröder, D. C. Langreth, and B. I. Lundqvist, Physical Review Letters **92**, 246401 (2004).
[55] G. Román-Pérez and J. M. Soler, Physical Review Letters **103**, 096102 (2009).
[56] J. Klimeš, D. R. Bowler, and A. Michaelides, Journal of Physics: Condensed Matter **22**, 022201 (2010).

[57] J. Klimeš, D. R. Bowler, and A. Michaelides, Physical Review B **83**, 195131 (2011).
[58] A. D. Becke, The Journal of Chemical Physics **85**, 7184 (1986).
[59] G. Kresse and J. Hafner, Physical Review B **47**, 558 (1993).
[60] G. Kresse and J. Hafner, Physical Review B **49**, 14251 (1994).
[61] G. Kresse and J. Furthmüller, Computational Materials Science **6**, 15 (1996).
[62] G. Kresse and J. Furthmüller, Physical Review B **54**, 11169 (1996).
[63] G. Kresse and D. Joubert, Physical Review B **59**, 1758 (1999).
[64] P. E. Blöchl, Physical Review B **50**, 17953 (1994).
[65] J. P. Perdew, K. Burke, and M. Ernzerhof, Physical Review Letters **77**, 3865 (1996); Physical Review Letters **78**, 1396 (1997).
[66] J. P. Perdew, J. A. Chevary, S. H. Vosko, K. A. Jackson, M. R. Pederson, D. J. Singh, and C. Fiolhais, Physical Review B **46**, 6671 (1992); Physical Review B **48**, 4978 (1993).
[67] N. O. Weiss, H. Zhou, L. Liao, Y. Liu, S. Jiang, Y. Huang, and X. Duan, Advanced Materials **24**, 5782 (2012).
[68] G. Lehmann, P. Rennert, M. Taut, and H. Wonn, physica status solidi (b) **37**, K27 (1970).
[69] O. Jepson and O. Anderson, Solid State Communications **9**, 1763 (1971).
[70] G. Lehmann and M. Taut, Physica Status Solidi (b) **54**, 469 (1972).
[71] P. E. Blöchl, O. Jepsen, and O. K. Andersen, Physical Review B **49**, 16223 (1994).
[72] R. Bader and T. Nguyen-Dang, in *Advances in Quantum Chemistry*, Vol. 14 (Academic Press, 1981) pp. 63–124, iSSN: 0065-3276.
[73] R. F. W. Bader, Accounts of Chemical Research **18**, 9 (1985).
[74] G. Henkelman, A. Arnaldsson, and H. Jónsson, Computational Materials Science **36**, 354 (2006).
[75] L. Kleinman, Physical Review B **21**, 2630 (1980).
[76] A. H. MacDonald, W. E. Picket, and D. D. Koelling, Journal of Physics C: Solid State Physics **13**, 2675 (1980).
[77] M. Marsman and J. Hafner, Physical Review B - Condensed Matter and Materials Physics **66**, 1 (2002).
[78] M. Guo, X. Liang, H. Wang, and J. Zhang, Physical Chemistry Chemical Physics **22**, 238 (2020).
[79] Y. Han, G.-X. Ge, J.-G. Wan, J.-J. Zhao, F.-Q. Song, and G.-H. Wang, Physical Review B **87**, 155408 (2013).
[80] M.-H. Whangbo, E. E. Gordon, H. Xiang, H.-J. Koo, and C. Lee, Accounts of Chemical Research **48**, 3080 (2015).
[81] J. Zhou, Q. Wang, Q. Sun, Y. Kawazoe, and P. Jena, Physical Chemistry Chemical Physics **17**, 17182 (2015).
[82] K. C. Zhang, Y. F. Li, Y. Liu, Y. Zhu, and L. B. Shi, Physical Chemistry Chemical Physics **19**, 13245 (2017).
[83] X. Chen, S. Zhang, B. Liu, F. Hu, B. Shen, and J. Sun, Physical Review B **100**, 144413 (2019).
[84] V. Heine, in *Solid State Physics - Advances in Research and Applications*, Vol. 35 (1980) pp. 1–127, issue: C ISSN: 00811947.

# APPENDICES

## A1. Our Paper Published in *Nanotechnology*

IOP Publishing Nanotechnology

Nanotechnology **32** (2021) 230001 (13pp) https://doi.org/10.1088/1361-6528/abe966

# Large magnetic anisotropy in an OsIr dimer anchored in defective graphene

**Jan Navrátil[1], Piotr Błoński[2] and Michal Otyepka[2]**

[1] Department of Physical Chemistry, Faculty of Science, Palacký University Olomouc, tř. 17 listopadu 12, 771 46 Olomouc, Czech Republic
[2] Regional Centre of Advanced Technologies and Materials, Faculty of Science, Palacký University Olomouc, Šlechtitelů 27, 783 71 Olomouc, Czech Republic

E-mail: piotr.blonski@upol.cz

Received 25 November 2020, revised 10 February 2021
Accepted for publication 24 February 2021
Published 19 March 2021

**Abstract**

Single-atom magnets represent the ultimate limit of magnetic data storage. The identification of substrates that anchor atom-sized magnets firmly and, thus, prevent their diffusion and large magnetic anisotropy has been at the centre of intense research efforts for a long time. Using density functional theory we show the binding of transition metal (TM) atoms in defect sites in the graphene lattice: single vacancy and double vacancy, both pristine and decorated by pyridinic nitrogen atoms, are energetically more favourable than away from the centre of defects, which could be used for engineering the position of TMs with atomic precision. Relativistic calculations revealed magnetic anisotropy energy (MAE) of ~10 meV for Ir@NSV with an easy axis parallel to the graphene plane. MAE can be remarkably boosted to 50 meV for OsIr@NSV with the easy axis perpendicular to the graphene plane, which paves the way to the storage density of ~490 Tb/inch$^2$ with the blocking temperature of 14 K assuming the relaxation time of 10 years. Magnetic anisotropy is discussed based on the relativistic electronic structures. The influence of an orbital-dependent on-site Coulomb repulsion $U$ and a non-local correlation functional optB86b-vdW on MAE is also discussed.

Supplementary material for this article is available online

Keywords: magnetic anisotropy energy, information storage, defective graphene, transition metal atoms and dimers

(Some figures may appear in colour only in the online journal)

### 1. Introduction

The big-data phenomenon challenges the storage capacity of data centres. Consequently, there is a quest for novel materials with ultimate storage density. A fundamental constraint for the minimal size of a bit for classical information storage is imposed by the magnetic anisotropy energy (MAE) of the storage material, i.e. the barrier to magnetization reversal due to thermal excitations. If a system was to be found with MAE corresponding to at least the temperature of liquid nitrogen (77 K), applications in data centres could become feasible.

Magnetic anisotropy is a relativistic effect stemming from spin–orbit coupling (SOC), i.e. the coupling of the charge's angular momentum to its spin. Free transition metal (TM) atoms display large spin (**S**) and orbital (**L**) magnetic moments. However, in most magnetic compounds, electron delocalization and crystal field effects compete with the intra-atomic Coulomb interactions, triggering a decrease in **S** and quenching of **L** with implications for a value of MAE. Theoretical calculations predict such effects to be diminished at surfaces [1–4] and in low-symmetry nanostructures [5–7] owing to the reduced coordination of TM atoms, which may also imply a substantial MAE [8, 9]. However, if dimensions of the bit were reduced to the atomic scale, thermal effects may affect the rate of magnetization switching and quantum-mechanical excitations may play an important role. Thus, besides the technological challenges, the question of where downscaling of the information bit ends from fundamental

 

physics has motivated intense research towards an improved understanding of the fundamental properties of magnetic nanostructures [10–19].

Giant MAE of 9 meV found for Co atoms on a Pt(111) substrate [20] has shown that the surface-adsorbed single-atom storing bit of information may represent the ultimate limit of the classical approach to high-density magnetic storage of data. Indeed, magnetic remanence up to a temperature of 30 K, allowing for storage and processing of information and long relaxation times, was measured on an ensemble of Ho atoms on ultra-thin MgO(100) films coating Ag(100) [21]. Also, the reading and writing of the magnetic state of individual Ho atoms on MgO/Ag was demonstrated using a spin-polarized scanning tunnelling microscope, and showed that they retain their magnetic information over many hours [17]. Magnetic hysteresis and a spin lifetime of 1000 s at 2.5 K were measured for a self-assembled superlattice of non-interacting Dy atoms on graphene/Ir(111) substrate [22]. The lattice mismatch between graphene and iridium led to a periodic moiré pattern, allowing for a highly ordered array of the most favourable Dy adsorption sites.

Atomic vacancies in the graphene lattice can be created unintentionally, due to the growth conditions, or intentionally, e.g. by irradiation [23–25]. TM atoms, which are mobile on the pristine graphene layer, can be trapped by lattice defects [26, 27], e.g. single (SV) and double (DV) vacancies, which may lead to collective phenomena such as ferromagnetism (FM). The incorporation of pyridinic nitrogen atoms into the graphene lattice at SV and DV defects was demonstrated experimentally by using scanning transmission electron microscopy [28]. The N-decorated vacancy defects were shown to trap metals (Mg, Al, Ca, Ti, Cr, Mn, and Fe) as single atoms. Very recently, a combined experimental and theoretical work reported FM in graphene up to room temperature due to Cu single atoms anchored in phthalocyanine-like moieties, Cu-$N_4$ [29].

An abundance of theoretical literature has been devoted to the structural, electronic, and magnetic properties of TM atoms on defective graphene (see section S 1 in the supporting information stacks.iop.org/NANO/32/230001/mmedia (SI), and references cited therein). However, to the best of our knowledge, only a few have attempted to determine the MAE [30–32]. A large MAE of ∼20 meV was predicted for Ir@DV, [30] whereas Co and Fe at SV exhibited MAE below 1 meV [31, 32]. The MAE can be remarkably enlarged up to 85 meV for TM dimers bound in an upright geometry at the vacancy defects in the graphene lattice. [33]

In addition, TM atoms dispersed onto a graphene support have been extensively studied as an ultimate limit to the downsizing of heterogeneous metal catalysts, termed single-atom catalysts (SAC) [34–42]. Stabilizing the individual TM atoms on graphene remains a significant challenge in the further development of efficient and stable SACs. Therefore, understanding structural and electronic properties of TM@graphene systems is of paramount importance both for data storage applications and in heterogeneous catalysis.

In this work, we employed density functional theory (DFT)-based calculations including SOC to systematically investigate the structural, electronic, and magnetic properties of nine TM atoms of the Fe- (TM8: Fe, Ru, Os), Co- (TM9: Co, Rh, Ir), and Ni-groups (TM10: Ni, Pd, Pt) embedded in defective graphene containing SV and DV, both pristine and decorated by pyridinic nitrogen atoms (NSV and NDV). Relativistic calculations showed a perpendicular easy magnetic axis for Ir@DV with MAE of 7 meV, comparable to the giant MAE reported for Co atoms on Pt(111) in the seminal work by Gambardella *et al* [20]. Adsorption of a second Ir atom on top of the already adsorbed Ir atom at NSV and NDV increased the MAE to ∼37 meV with the easy axis perpendicular to the graphene plane. Adsorption of an Os atom on top of the Ir atom at NSV enhanced the perpendicular MAE to 50 meV. For selected systems, the origin of magnetic anisotropy is discussed based on relativistic electronic structures. We compared MAEs determined in terms of fully self-consistent (SC) independent total-energy calculations for different magnetic-moments directions with MAE obtained using the magnetic force theorem (FT) [43] as the difference in the band energies at a frozen potential and charge density. The influence of an orbital-dependent on-site Coulomb repulsion $U$ [44, 45] and a non-local correlation functional (optB86b-vdW) [46] on MAE was also investigated.

## 2. Computational details

DFT-based calculations were performed using a Vienna *ab-initio* simulation package (VASP) [47–50] that implements a projected augmented wave method [51, 52] to describe an electron–ion interaction. A generalized gradient approximation (GGA), [53] specifically the functional of Perdew, Burke, and Ernzerhof (PBE), [54] was used for an evaluation of the electronic exchange and correlation effects. The plane wave basis set contained waves with kinetic energy smaller than 400 eV, which was sufficient to obtain converged adsorption characteristics [26].

The graphene layer with the lattice constant of 2.47 Å (the experimental value is 2.46 Å) [55] was represented by a $5 \times 5$ supercell containing 50 C atoms. A vacuum layer of length 14 Å was deployed along the off-planar direction to ward off spurious interactions between graphene sheets due to the periodic boundary conditions. Defective graphene contained one SV, DV, NSV, and NDV defects in the supercell (figure 1). To explore the influence of lateral interactions between the adsorbed TM atoms and dimers on MAE for selected systems the size of the supercell was doubled either in one direction or in two directions, so that there were two defects and four defects in the supercell, respectively.

Full structural optimizations were performed in a scalar-relativistic (SR) mode until the forces acting on all atoms were reduced to less than 10 meV/Å. Simultaneously, the electronic and magnetic degrees of freedom were relaxed until

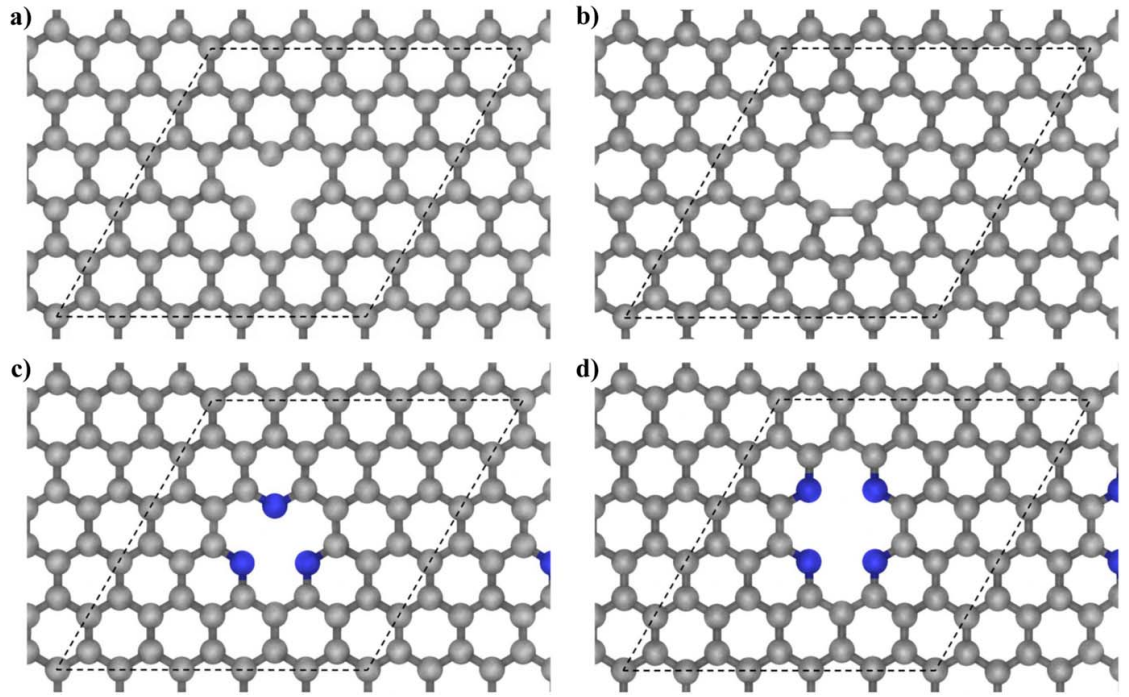


**Figure 1.** Relaxed defective graphene: (a) SV, (b) DV, (c) SV decorated by pyridinic nitrogen atoms (NSV), (d) DV decorated by pyridinic nitrogen atoms (NDV). Supercells are marked by broken lines. C/N atoms are represented by grey/blue spheres.

the change in total energy between successive iteration steps was smaller than $10^{-6}$ eV. The Brillouin zone was sampled by using Γ point-centred $12 \times 12 \times 1$ *k*-point mesh. The Gaussian smearing of width 0.02 eV for partial occupancies of orbitals was used. For the relaxed structures, static calculations were performed with the tetrahedron method [56–58] with Blöchel corrections [59] with the width of smearing and the *k*-point mesh unchanged.

Single TM atoms were initially placed 2.1 Å directly above the centre of the vacancy and the entire system was re-optimized. To assess an affinity of each TM atom to imperfect regions of defective graphene, we also studied the migration of TM atoms toward defects. More than 20 initial positions of TM atoms in the vicinity to the defect were considered for each combination of a defect and a TM atom, and each system was relaxed according to the scheme described in section S 2 in the SI.

The binding of TM atoms to defective graphene was quantified by the adsorption energy ($E_{ad}$) defined as

$$E_{ad} = E_{(\mathrm{VG+TM})} - (E_{\mathrm{VG}} + E_{\mathrm{TM}}), \quad (1)$$

where $E_{\mathrm{VG+TM}}$ ($E_{\mathrm{VG}}$) and $E_{\mathrm{TM}}$ are, respectively, the ground state (GS) energy of defective graphene with (without) a TM atom and of the single TM atom in the vacuum. Adsorption energy of the second TM atom (TM2) in systems with the pre-adsorbed TM atom is defined as

$$E_{ad2} = E_{(\mathrm{VG+TM+TM2})} - (E_{\mathrm{VG+TM}} + E_{\mathrm{TM2}}). \quad (2)$$

Negative adsorption energy means that the adsorption of TM is energetically favourable.

Bader charge analysis [60–62] was performed to evaluate the charge located on each atom ($q$) as the difference between the number of valence electrons in a free atom and the computed number of valence electrons in the atom in the system, $q = N_{val} - N_{Bader}$.

Static SC relativistic calculations including SOC [63–66] with the cut-off energy enhanced to 600 eV were executed on all systems with non-zero SR magnetic moments. Following the convergence test (see the SI for details), $9 \times 9 \times 1$ *k*-point mesh was used for the calculations of MAE defined as

$$\mathrm{MAE} = \min(E_x, E_y) - E_z \quad (3)$$

where $E_x$, $E_y$, and $E_z$ are the total energies of systems with different initial orientation of the magnetization. In this convention, the positive MAE corresponds to the perpendicular ($z$) easy axis.

In addition to the GGA-PBE calculations, we performed, for selected systems, calculations with the orbital-dependent exchange-correlation potential using Dudarev's approach [44] to the DFT+$U$ method, to see the effect of the Hubbard $U$ ($U - J$ was in the range of 0 and 4 eV) on the MAE, and with a non-local correlation functional that approximately accounts for dispersion interactions (optB86b-vdW) [46].

## 3. Results and discussion

### *3.1. Adsorption energies and structures*

To assess the stability of TM atoms in the vicinity of the defects, we studied energetics and migration of TM atoms in various configurations. We found that from many initial positions TM atoms moved toward defects and, moreover, the binding there was energetically more favourable than away from the centre of the defects. The affinity of TM atoms to the vacancy defects could be used for engineering the position of TMs with atomic precision, since they would be mobile unless pinned by the defects (see section S2 in the SI).

The adsorption energy (figure 2(a)), decreased in the sequence $3d > 4d > 5d$ TM atoms from the Fe- and Co-group bound in the SV and DV defects. For NDV the order changed to $4d > 3d > 5d$, whereas for the NSV defect $E_{ad}$ followed the sequence $3d > 5d > 4d$ and $5d > 4d > 3d$ for TM8 and TM9, respectively. Among TM atoms from the Ni-group, the highest $E_{ad}$ was found for the Pd atom—which is not surprising, as it has a closed-shell $d^{10}$ GS—followed by Ni and Pt atoms. However, for the atoms of the Ni-group at the NSV defect the order was $4d > 5d > 3d$. The binding was the weakest at NSV and the strongest at the SV (for TM8 and Rh, and Ir) or NDV (TM10 and the Co atom), followed by the DV, (cf section 3.2 and equation (4)).

One might expect in general that shorter TM–C(N) bonds ($d_{bl}$, figure 2(b)) would correspond to a lower $E_{ad}$ (figure 2(a)). Indeed, the shortest $d_{bl}$ were found for TM8 and TM9 at the SV, where the binding was the strongest. Although a separate inspection of the relation between $d_{bl}$ and $E_{ad}$ for each defect type and TM atom revealed that it also holds for SV and NSV defects, the correlation between the TM–C(N) length and $E_{ad}$ was not at all straightforward (see section S 3 in the SI), as the shortest bond lengths were obtained for TM10@SV, whereas the lowest $E_{ad}$ corresponded to the adsorption at NDV, where the charge transfer from the TM atoms to the substrate was the greatest (cf figure 2(f) and section 3.2). At the same time, $d_{bl}$ hardly changes for the groups of TM atoms at the NDV and DV defects, as it seems mostly determined by the radii of TM atoms, whereas $E_{ad}$ varied quite considerably and, for TM@DV, it is mostly determined by the number of newly created bonds (cf equation 4).

TM atoms sank deeply into the NDV defect, the vertical distance of a TM atom above its neighbours ($d_{van}$, figure 2(c)) and the vertical distance of a TM atom above the average graphene $z$-coordinate ($d_{vag}$, figure 2(d)) were both ordered as $\mathrm{NDV} < \mathrm{DV} < \mathrm{SV} < \mathrm{NSV}$ or $\mathrm{NDV} < \mathrm{DV} < \mathrm{NSV} < \mathrm{SV}$. However, the values of $d_{van}$ and $d_{vag}$ differed significantly with respect to each other because the TM atom's neighbours were lifted out of the plane of the graphene lattice, which let their $sp^2$ orbitals orient toward the TM atom. This caused buckling of the graphene layer ($d_{ba}$, figure 2(e)), which was the most pronounced for the NSV and SV defective graphene. Figure 2(e) also reveals that the stronger interaction between the TM and SV led to more distorted graphene layer.

### *3.2. Bader charge analysis and magnetism*

The Bader charge analysis revealed that all examined TM atoms donated electrons to the graphene lattice (figure 2(f)). Due to the higher electronegativity of the N atom than the C atom, N-decorated vacancies attracted electrons more than the bare defects, and the electron transfer decreased in the order $\mathrm{NDV} > \mathrm{NSV} > \mathrm{DV} > \mathrm{SV}$. At the same time, following an increasing electronegativity of the TM atoms grouped according to the period of the periodic table, the electron transfer from the TM atoms to the substrate increased in the order $3d < 5d < 4d$ or $3d < 4d < 5d$ (see table S3). Due to a lower electronegativity of the $3d$ atoms as compared to the $5d$ and $4d$ elements, the former lost electrons more easily and did not attract electrons so strongly. More significant electron back-donation from nitrogen lone pairs can be seen for the $5d$ and $4d$ TMs.

The TM atoms studied in this work were magnetic when adsorbed on at least one type of the defect in graphene (figure 2(h)) and can also induce magnetism in graphene (figure 2(i)). Regions of high-spin density were primarily located in the vicinity of a TM atom. Generally, a larger moment on TM induced a larger moment in graphene. Nevertheless, the value of induced moments differed among different defective graphene systems; the greatest effects were in SV and NSV systems, and very modest in NDV systems. One should note that the magnetic moment on Fe, Co, and Os and the induced moments in graphene for Fe@NSV, Fe@NDV, Co@DV, and Os@NDV were anti-parallel (table S4).

The number of unpaired electrons ($N_{ue}$) in defective graphene with a TM atom can be estimated as [26, 67]

$$N_{ue} = \begin{cases} 2O - G - D & \text{if } (2O - G) \geqslant D, \\ |2O - G - D| (\mathrm{mod}\ 2) & \text{otherwise,} \end{cases} \quad (4)$$

where $O$ stands for the number of TM atom's involved orbitals (i.e. one for $s$ and five for $d$, six in total in this paper), $G$ is the number corresponding to the TM atom's group in the periodic table, and $D$ represents the maximal number of electrons that can be used for bonding the TM atom to the defect.

Equation (4) is based on the Hund's rule of the maximal multiplicity. It assumes that the TM atom uses its unpaired electrons to form all possible bonds with the defect and remaining electrons remain unpaired. If the number of preliminary unpaired electrons of the TM atom is lower than the number of possible bonds, the TM atom uses all its unpaired electrons to form the bonds and some electrons in graphene get paired; moreover, if the total number of electrons in such a system is odd, the unpaired electron should be significantly delocalized in the vicinity of the TM atom. One should note that equation 4 is valid in this paper (with some exceptions discussed below). Its universality would need to be tested (and its form probably adjusted) in systems with other defect types and other TM atoms, e.g. it cannot be valid if $G < 6$.

In an unreconstructed SV defect two C atoms have one electron each that is not involved in bonding, and the remaining C atom possesses two electrons not involved in

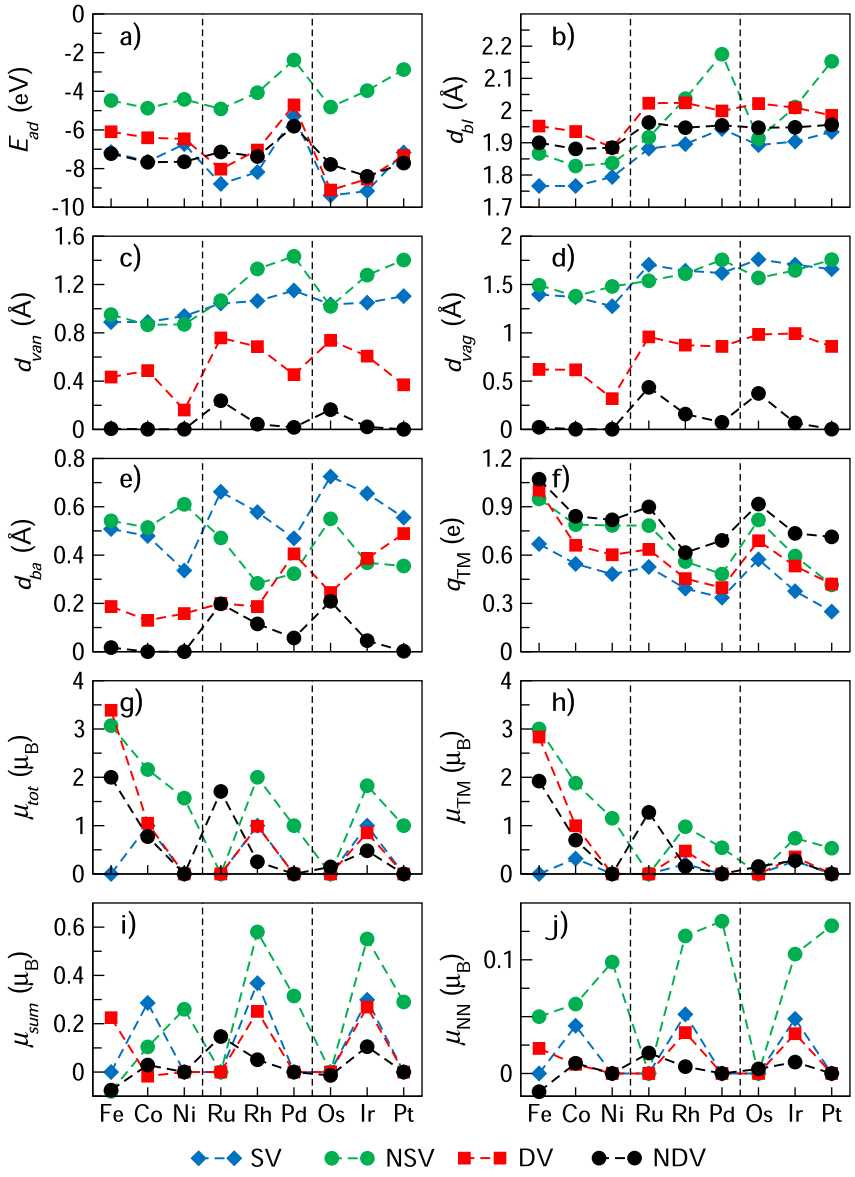


**Figure 2.** Properties of defective graphene systems with adsorbed TM atoms: (a) adsorption energy ($E_{ad}$), (b) the average bond length of the TM atom to the neighbouring C(N) atoms in graphene ($d_{bl}$), (c) the vertical distance between the TM atom and its neighbours ($d_{van}$), (d) the vertical distance between the TM atom and an average height of C atoms in the graphene layer ($d_{vag}$), (e) graphene buckling amplitude ($d_{ba}$), (f) the charge on TM atoms ($q_{TM}$), (g) the magnetic moment of the supercell ($\mu_{tot}$), (h) the magnetic moment of a TM atom ($\mu_{TM}$), (i) a sum of local magnetic moments ($\mu_{sum}$) of all atoms of the defective graphene layer (minus $\mu_{TM}$), and (j) magnetic moments on the nearest-neighbour atoms to a TM atom ($\mu_{NN}$). Dashed lines are a guide to the eye.

bonding; $D = 4$. In agreement with equation 4, the total magnetic moment was 1 $\mu_B$ for the Co-group's atoms and 0 for the remaining systems. Due to the $C_{3v}$ symmetry in TM@SV the degeneracy of $d$ orbitals was broken into three groups, $d_{z^2}$ and 2-fold degenerate $d_{x^2-y^2}/d_{xy}$, $d_{xz}/d_{yz}$ orbitals (figures S7–S9). [68] The major contribution to the total magnetic moment of TM9@SV came from the $d_{z^2}$ states with the same magnitude as from the $p$ states of the C atoms (table S6).

The boundary of the NSV defect is formed by three pyridinic nitrogen atoms. Without a TM atom, one would expect two N atoms to have three electrons involved in bonding with graphene and the remaining two electrons to form lone pairs heading to the vacancy; the third N atom uses

two electrons to form bonds with graphene, two electrons form a lone pair, and one electron is left unpaired; $D = 1$. Except for Ru@NSV and Os@NSV, whose magnetic moment was zero, all the other TM@NSV systems were magnetic (table S4). Thus, equation 4 is not valid for Ru@NSV and Os@NSV, as it predicted the magnetic moment of 3 $\mu_B$; fixed-moment calculations further confirmed the non-magnetic GS for the two systems (section S5 in the SI). Fe, Co, and Ni are well known for their ability to preserve high-spin moments, whereas atoms from the later periods are not good at it. Three unpaired electrons were unfavourable for Ru and Os, while two unpaired electrons on Rh and Ir were sustainable. In TM@NSV, the degeneracy of $d$ orbitals of a TM atom was lifted similarly as in TM@SV into $d_{x^2-y^2}/d_{xy}$, $d_{xz}/d_{yz}$, and $d_{z^2}$, although the difference in density of states (DOS) between the pairs was slightly more pronounced (figures S10–S12). For Fe@NSV and Ni@NSV, narrow peaks close to the Fermi level ($E_F$) corresponded to the minority (Fe@NSV) and majority (Ni@NSV) $d_{x^2-y^2}/d_{xy}$ and $d_{xz}/d_{yz}$ states, whereas $d_{z^2}$ was located at least $-1$ eV below $E_F$ and further broadened by the hybridization with the substrate. In the partial density of states (PDOS) of Co@NSV, a narrow peak at $E_F$ arose from the majority $d_{z^2}$ states. Both Rh@NSV and Ir@NSV exhibited, close to $E_F$ in the spin-up channel, a narrow peak of $d_{xz}/d_{yz}$ and $d_{x^2-y^2}/d_{xy}$ character; $d_{z^2}$ was shifted deeper into the binding energy. A dominant contribution to the narrow peak at $E_F$ in PDOS of the Pd@NSV and Pt@NSV systems came from the $d_{xz}/d_{yz}$ minority states. However, integrated differences in spin-up and spin-down PDOS showed that the important contribution to the magnetic moments of TM@NSV can also originate from the states deeper in binding energies (table S6).

It is also interesting to note that generally a smaller electron density located on the TM atom corresponded to a higher-spin system of TM@NSV (figure 2(f)). The quenching of the TM's magnetic moment followed a similar sequence to the increase in their electronegativity within groups of the periodic table. Particularly, electron back-donation from nitrogen lone pairs to Ru and Os may lead to electron pairing and, accordingly, the complete disappearance of magnetism.

The removal of two neighbouring C atoms from graphene leaves one unpaired electron on each of the atoms surrounding the defect. Four unpaired electrons in an unreconstructed DV are available to form bonds with a TM atom (similarly to in the SV defect); $D = 4$ and the magnetic moments on TMs were similar in the corresponding TM@SV and TM@DV systems (except for Fe, see table S3 and S4), i.e. TM9@DV (and Fe@DV) were magnetic; the remaining TM@DV systems were non-magnetic. In the DV the local symmetry was reduced to $C_{2v}$ and the degeneracy of the $d$ orbitals was further lifted (figures S13–S15). The electron charge on Fe@DV was lower compared to Fe@SV (also, in comparison to Ru and Os), therefore it can more easily preserve the high-spin state. Inspection of PDOS revealed a peak located at $E_F$ arising from $d_{z^2}$ minority spin states and, deeper in binding energies, two narrow peaks corresponding to the $d_{xz}$ states, at about $-0.3$ eV in the spin-up channel and at about $-1.15$ eV in the spin-down channel. The other $d$ states were broadened by the hybridization with the substrate in the range of binding energies between $-4$ eV and $-1.75$ eV and exhibited a strong spin-asymmetry. In this range, the spin-up PDOS of the $d_{z^2}$ and $d_{x^2-y^2}$ states were more sharply peaked. In the PDOS of the Co@DV system, the spin-up $d_{xz}/d_{yz}$ states coincided in $E_F$. The $d_{x^2-y^2}$ states formed narrow peaks located at binding energies of about $-0.95$ eV and $-0.35$ eV, arising from majority and minority spin, respectively. The other $d$ states were also spin-split, although more broadened, especially in the majority-spin channel. For Rh@DV and Ir@DV, the vicinity of $E_F$ consisted of the $d_{xz}$ and $d_{yz}$ states; whereas for Rh@DV, the majority $d_{yz}$ states were occupied and the corresponding peak of the minority $d_{yz}$ states pushed above $E_F$, as well as the $d_{xz}$ states. For Ir@DV the occupied spin-up $d_{xz}$ states were strongly peaked just below $E_F$ and the spin-down component was pushed just above $E_F$, and $d_{yz}$ was more broadened and coincided with $E_F$. The $d_{x^2-y^2}$ states were peaked between $-1.7$ eV and $-1.4$ eV in both Rh@DV and Ir@DV PDOS, and the other $d$ states were broadened deeper in the binding energies.

Each N atom in the pristine NDV uses three electrons to form bonds with neighbouring C atoms and the two remaining electrons form a lone pair heading to the vacancy. Fe@NDV and Ru@NDV carried the magnetic moment of $\sim 2\,\mu_B$. The magnetic moment of Os@NDV was much smaller, $0.15\,\mu_B$. Additional calculations considering the effect of $U$, with $U - J = 2$ and 4, both led to the magnetic moment of 2 $\mu_B$. To fulfill the form of equation 4, one needed to assign to $D$ a value of 2. In the SR approximation, magnetic moments of the defective graphene complexes with TMs were determined by the electronic GS of the isolated atom and the bonding–antibonding, and exchange splittings. The isolated Fe (and Os) have $s^2d^6$ GS; in NDV the formation of the coordinate-covalent bonds required Fe to lose two electrons primarily from the $s$ orbital and accept four lone pairs primarily to orbitals $d_{x^2-y^2}$, $s$, $p_x$, and $p_y$; thus, 6 electrons were in 4 remaining 3$d$ orbitals, two were occupied by two electrons each, two possessed one electron each, and that induced the magnetic moment of $\sim 2\,\mu_B$. A similar mechanism was valid for the remaining TM@NDV systems. However, a fully occupied $d$ orbital shell is energetically advantageous; therefore, TM9@NDV and TM10@NDV had magnetic moments significantly smaller than 1 $\mu_B$ or null, respectively. Inspection of PDOS (figure S16–S18) of Fe@NDV revealed a very narrow peak of spin-down $d_{x^2-y^2}$ states about $-0.45$ eV below $E_F$ and its spin-up counterpart at about $-1.5$ eV. Somewhat deeper in the binding energies the spin-majority $d_{xz}/d_{yz}$ and $d_{x^2-y^2}/d_{z^2}$ states were peaked; the spin-down $d_{z^2}$ and $d_{yz}$ counterpart was pushed just above $E_F$. The partial DOS of Ru@NDV exhibited a narrow peak of the minority $d_{z^2}$ states at $E_F$, whereas its majority counterpart was peaked at about $-1.3$ eV. Also, the $d_{x^2-y^2}$ and $d_{xz}$ states of both spin-up and spin-down character were sharply peaked between $-0.95$ eV and $-0.37$ eV. The partial DOS of TM9@NDV exhibited a rather broad $d_{yz}$ peak at $E_F$; for Co@NDV of spin-minority character and for Rh@NDV and Ir@NDV of both spin channels, the $d_{x^2-y^2}$ and $d_{z^2}$ states were more sharply peaked, although deeper in the binding energies.

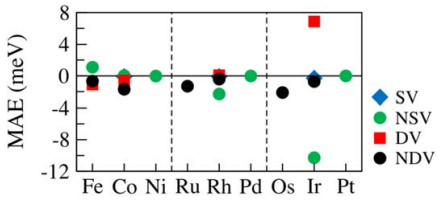


**Figure 3.** MAE determined from SC non-collinear calculations for a single TM atom embedded in defects in graphene. The positive MAE corresponds to an easy magnetic axis perpendicular to the graphene plane.

**Table 1.** Fully SC MAE and MAE from the FT (in meV) for different $U-J$ values for Ir@DV and Ir@NSV.

| $U-J$ | Ir@DV | | Ir@NSV | |
|---|---|---|---|---|
| | MAE | MAE(FT) | MAE | MAE(FT) |
| 0 | 6.6 | 11.0 | −9.8 | −8.1 |
| 1 | 8.9 | 13.9 | −6.4 | −6.9 |
| 2 | 12.0 | 19.3 | −0.2 | −5.9 |
| 3 | 15.2 | 24.5 | 9.3 | −5.2 |
| 4 | 18.7 | 25.8 | 16.9 | −4.6 |

### *3.3. MAE of TM@Defects*

Calculated MAEs are shown in figure 3, in table 1, and in table S9.

Two remarkable values of MAE were found, ∼7 meV for Ir@DV and ∼ − 10 meV for Ir@NSV (the negative MAE corresponds to an in-plane easy magnetic axis), comparable to the giant MAE (∼9 meV) reported for Co atoms on a Pt(111) substrate, [20] and accompanied by an orbital moment anisotropy (0.126 $\mu_B$ and −0.170 $\mu_B$, respectively; the positive value corresponds to a greater spin/orbital moment in the direction perpendicular to the graphene plane).

The MAE of Ir@DV was hardly influenced by the size of the computational cell; we found an MAE of 6.9 meV per single defect for both the $5\times10$ and $10\times10$ supercells. A larger MAE of 20.8 meV was reported for the Ir@DV system. [30] The origin of this discrepancy is unclear as they also used the VASP code; it may be related to the applied cut-off energy for the plane wave basis set (not shown therein) or the $k$-point mesh of $3\times3\times1$ for the $6\times6$ computational cell. We showed that at least $6\times6\times1$ $k$-point mesh for the $5\times5$ computational cell is necessary to have converged MAE (see section S7 in the SI for details).

The MAE of Ir@DV corresponds to the thermal energy of ∼80 K according to $E_T = k_B T$. If the Néel relaxation theory was considered, the blocking temperature ($T_B$) is only ∼2 K according to

$$T_B = \frac{\mathrm{MAE}}{k_B \cdot \ln\left(\frac{\tau_N}{\tau_0}\right)}, \tag{5}$$

where $\tau_N$ is an aimed relaxation time (10 years) and $\tau_0$ is an attempt period typical for the material (usually between $10^{-9}$ s and $10^{-10}$ s, here we used $10^{-10}$ s).

One may expect significant changes in the partial densities of states of Ir@DV and Ir@NSV associated with a reorientation of the magnetization direction (figure 4(a), (b); the orbital-resolved PDOS of the Ir atom from SC calculations for both orientations of the magnetic moments are shown in figure S29). The individual PDOS are, however, rather noisy, which makes a visual assessment of the MAE origin difficult. The FT permitted us to elucidate the electronic origin of the MAE and the contribution from different angular momentum states $m_l$ at the site $i$ (equation 6). This approximation required the integration of the difference in orbital-decomposed PDOS ($\Delta n^i_{m_l}$) from the bottom of the valence band ($E_B$) to $E_F$ for perpendicular and in-plane magnetization,

$$\mathrm{MAE} = \sum_i \sum_{m_l} \int_{E_B}^{E_F} (E - E_F)\Delta n^i_{m_l}(E)\,dE. \tag{6}$$

At this point, it must be emphasized that the decomposition of the MAE may have semi-quantitative validity, because the FT is already an approximation and the plane wave components of the eigenfunctions were projected onto spherical waves within atomic spheres. Indeed, the integrated differences in PDOS of all atoms of individual systems yielded a maximum up to ∼65% of the MAE from FT calculations.

For Ir@DV, the decomposition of the MAE showed that the positive MAE has a double origin, a leading contribution from the $d_{x^2-y^2}$ and $d_{z^2}$ states of Ir, respectively, at ∼−1.3 eV and ∼−1.8 eV below the Fermi level (figure 4(c)), and from the graphene sheet, together 4.1 meV, which is in good agreement with the MAE from total-energy differences. Contributions from the $d_{yz}$ and $d_{xz}$ states of Ir were of opposite signs and restricted to the peaks just below the $E_F$, whereas the contribution from the $d_{xy}$ states was an order of magnitude smaller and thus negligible. The explanation for this orbital dependence of the MAE must be sought in subtle differences in the hybridization between the $d$ states of the Ir atom and the substrate orbitals. The bandwidth of the Ir $d$ states is a measure of the strength of this hybridization (figure 4(a), (b)); it decreases in the sequence $d_{xy} \rightarrow d_{xz}, d_{yz} \rightarrow d_{x^2-y^2}, d_{z^2}$.

For Ir@NSV, the contribution from the N atoms (0.7 meV) and the Ir atom is of opposite signs (−5.7 meV) such that the negative MAE was caused by the Ir atom (figure 4(d)). The leading contributions came from the states forming narrow peaks at −1.3 eV ($d_\pi$ and $d_\delta$) and −0.65 eV ($d_{z^2}$), and the peaks close to the Fermi edge.

Fully SC MAE with the MAE from FT calculations for different $U-J$ values is compared in table 1. For Ir@DV, MAE increased with increasing $U-J$, reaching a remarkable value of ∼19 meV (SC) and ∼26 meV (FT) for $U-J=4$; the FT yielded higher MAE by 38%–66%. The non-local correlation functional optB86b-vdW had a smaller impact on the MAE (5.3 meV).

In turn the impact of $U-J$ on MAE of the Ir@NSV system was more complex; the FT predicted MAE decreases with the increasing $U-J$ term, from ∼ −8 meV to −4.6 meV, whereas SC predicted MAE decreases from ∼ −10 meV for $U-J=0$ to only −0.2 meV for $U-J=2$. Further increasing the $U-J$ value reversed the

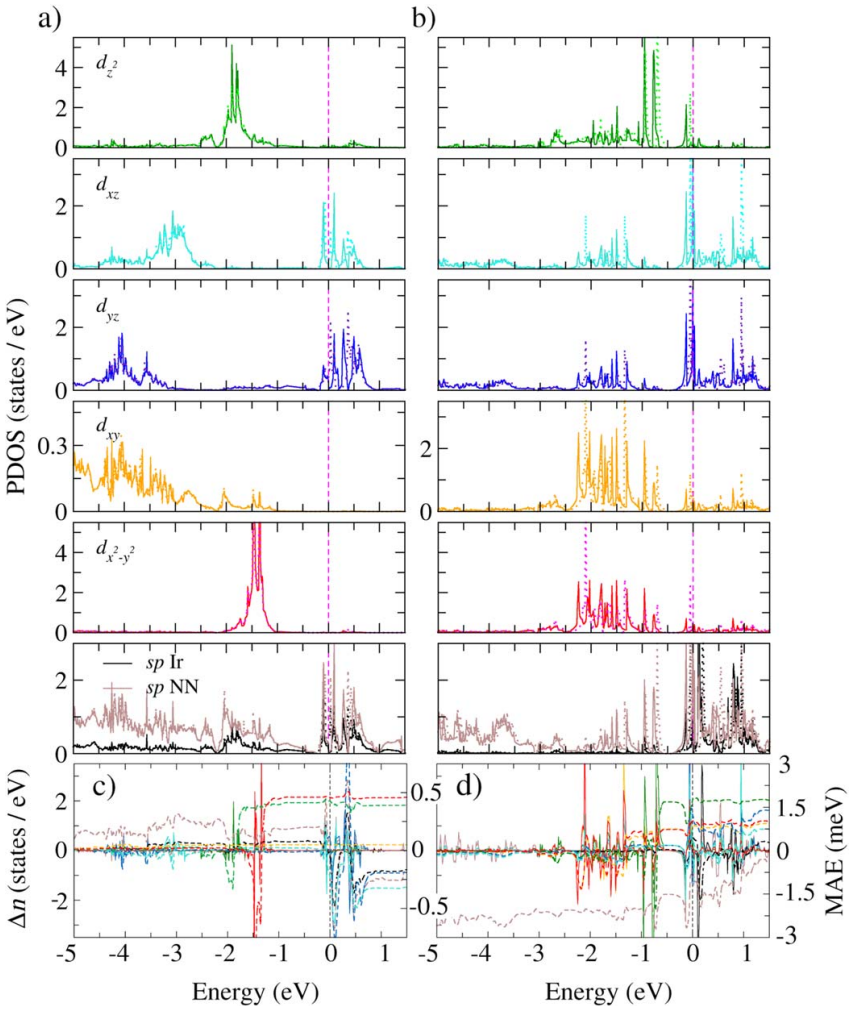


**Figure 4.** Relativistic partial densities of states for (a) Ir@DV and (b) Ir@NSV for perpendicular (solid lines) and in-plane (dashed lines) magnetization (cf figure S29). (c, d) Corresponding changes in the orbital-decomposed PDOS with reorientation of the magnetization direction from the easy to hard direction (solid lines and left-hand scale) and integrated contributions to the MAE (dashed lines and right-hand scale), cf equation (6).

sign of the MAE, which reached the value comparable to the MAE of Ir@DV. Similarly, the change in the sign of the MAE has been reported for gas-phase TM dimers [69]. Thus, care must be taken when a GGA + $U$ Hamiltonian is employed, because realistic MAE in line with conventional DFT calculations can be achieved only if moderate values of the on-site Coulomb repulsion are admitted.

### *3.4. MAE of $TM_2$@Defects*

Motivated by previous reports showing an enhanced MAE in (bi)metallic dimers on (defective)graphene, [8, 33] we investigated the MAE of Ir dimers and (TM)Ir heteroatomic dimers (Ir down, i.e. closer to graphene) embedded in the centre of the defects in graphene.

The energetically most favourable geometry for $Ir_2$ was an upright dimer bound in the centre of the SV, NSV, and NDV defect (figure 5). Only in the relaxed configuration of $Ir_2$@DV, the dimer axis was tilted by 45° with respect to the surface normal. In this configuration, the dimer was, however, non-magnetic. A meta-stable upright $Ir_2$@DV, higher in energy by 0.3 eV than the GS, was magnetic and considered in further discussions. The adsorption energy (equation 2) of a second Ir atom on the Ir atom already anchored in the centre of the defect was strong, exceeding −2 eV, and for NSV it even reached −5.3 eV (table 2); thus, the formation of the Ir dimer is energetically favourable.

SR magnetic moments are listed in table 2. The magnetism of the Ir atom binding to graphene was strongly quenched, and the magnetic moment on the upper Ir atom

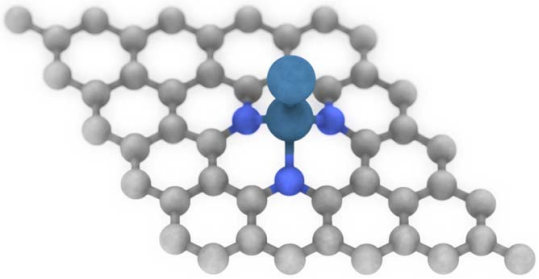

**Figure 5.** An upright Ir dimer (shown as large blue spheres) bound in the centre of the NSV defect seen from an oblique direction.

varied between 0.6 $\mu_B$ (NSV) and ∼1.7 $\mu_B$ (NDV). The free Ir atom has three unpaired electrons ($N_{ue2}$). The bond between Ir atoms in $Ir_2$ on defective graphene was created by a maximal possible coupling of their unpaired electrons. The total number of unpaired electrons can be estimated as

$$N_{ue} = N_{ue2} - N_{ue1}, \tag{7}$$

where $N_{ue1}$ is the number of unpaired electrons in the systems with single Ir atoms (cf equation 4). Equation (7) is qualitatively valid for systems with localized unpaired electrons and, accordingly, with the integer magnetic moments. For the other systems the agreement between the calculated magnetic moment and equation 7 is at least semi-qualitative (see tables 2 and 3).

Relativistic calculations including SOC predicted enhanced MAE of $Ir_2$ compared to the Ir atom binding to the defects in graphene (table 2). The lowest MAE was found for the $Ir_2$@SV system (∼11 meV). An increased MAE to ∼18 meV of $Ir_2$@SV was predicted for a larger graphene supercell (7 × 7). [70] Using a torque method, an even larger MAE of ∼25 meV was calculated for the 7 × 7 supercell of $Ir_2$@SV. [33] For $Ir_2$@DV, the MAE increased to ∼30 meV. For the N-decorated vacancy defects, the MAE increased even further to ∼36–37 meV, which agrees well with the MAE reported for $Ir_2$@NDV [33]. The highest MAE corresponds to $T_B$ of 10 K or $E_T$ of 435 K. Both the local spin and orbital magnetic moments on the upper Ir atom exhibited a strong anisotropy.

It is worth mentioning that the size of the computational cell hardly affected the MAE of $Ir_2$@NDV; we found an MAE of 36.8 meV per single defect in the 5 × 10 supercell.

FT calculations yielded a higher MAE than the SC calculations for $Ir_2$@DV (51%) and $Ir_2$@NSV (311%), and a lower MAE for $Ir_2$@NDV (11%) (table 2), or even a change in the sign of MAE for $Ir_2$@SV, which points to the limitations of this method.

Figure 6(a) reveals significant changes in the *d* states of the upper Ir atom of the $Ir_2$@NDV system associated with the reorientation of the magnetization direction and restricted to a rather narrow range of binding energies from $E_F$ to −1.15 eV (see also figure S30). Specifically, the narrow peak lying just below $E_F$ in the $d_{xz}$ spectra for the perpendicular magnetization was pushed above $E_F$ for the in-plane direction. A similar effect can be seen for the $d_{xy}$; here, however, also deeper in the binding energy (−0.8 eV). Indeed, the decomposition of the MAE of $Ir_2$@NDV into the atom partial contributions indicated roughly an order of magnitude larger contribution to the MAE from the upper Ir atom (6.9 meV) than from the lower one (<1 meV), and a small contribution from N atoms (0.6 meV). Inspection of the partial orbital contribution to the MAE (figure 6(c)) revealed leading positive contributions from the $d_{xz}$ (5.4 meV) and $d_{xy}$ (2.2 meV) states of the upper Ir atom, and negative contributions from the $d_{z^2}$ states (−1.4 meV). Here, it must be noted that the decomposition of the MAE has a semi-quantitative value, as the integrated differences in the PDOS of all the atoms yielded 9.2 meV.

The influence of the support on the magnetic properties of the adsorbed dimers depends on the overlap of their PDOS with those of the substrate. The strong interaction of the upper Ir atom in the meta-stable $Ir_2$@DV system suppressed its magnetism (table 2). The $d_{xz}$ states were broadened due to the stronger hybridization with the Ir@DV system and pushed deeper into the binding energies (figure S31), which caused the lower MAE of $Ir_2$@DV compared to $Ir_2$@NDV.

For $Ir_2$@NSV the FT yielded only a qualitative agreement with the SC MAE, therefore the decomposition of the MAE has a qualitative value too. Nonetheless, it suggested the contributions from the Ir atoms and the N atoms were of opposite signs, and the leading contribution to the MAE was imposed by the $d_\delta$ states of the upper Ir atom (figures 6(b), (d)).

The effect of the moderate $U - J = 2$ parameter on MAE was investigated for the $Ir_2$ dimer. The MAE of $Ir_2$@SV and $Ir_2$@DV remained almost unaffected (∼9 meV and ∼33 meV, respectively), whereas a larger effect on MAE was predicted for $Ir_2$@NDV (∼47 meV). The $Ir_2$@NSV systems with initial in-plane magnetic moments converged to a nearly non-magnetic solution, and perpendicular magnetic moments remained unaffected by $U - J$; the energy barrier against this non-magnetic–magnetic transition was ∼44 meV.

The optB86b-vdW functional was applied to $Ir_2$@NDV; the MAE increased to 43.2 meV.

The interaction of Fe, Co, Ni, Ru, Rh, Pd, Os, and Pt atoms with the Ir atom pre-adsorbed in the defects in the graphene lattice was also investigated. Except for RhIr@NDV and the DV system, where the (TM)Ir dimer adopted a tilted configuration (the angle between an axis along the dimer bond and the axis perpendicular to the graphene plane varied between 46° and 89°, see table S12), in all the other systems an upright dimer was energetically preferred. The binding of a TM atom to the Ir@defects in graphene was strong reaching for OsIr@NSV −5.1 eV (table 3).

The magnetic moment on the Ir atom was strongly quenched and much more pronounced on the upper TM atom (table 3). Relativistic calculations predicted an in-plane easy axis with a large MAE for CoIr@NSV (∼−41 meV), RuIr@NSV (∼−41 meV), RuIr@NDV (∼−45 meV), and OsIr@SV (∼−53 meV). For OsIr@NSV a perpendicular easy axis was preferred with a large MAE of ∼50 meV corresponding to $T_B$ of 14 K or $E_T$ of 580 K. The large MAE was, in many cases, accompanied with a quite pronounced spin and, especially, orbital moment anisotropy. However, the sign of the spin and orbital anisotropy did not always follow the sign

**Table 2.** Adsorption energy of the Ir atom ($E_{ad2}$, in eV) on defective graphene with a pre-adsorbed Ir atom, the number of unpaired electrons ($N_{ue}$, equation 7), and SR magnetic moments of Ir dimers in defective graphene (in $\mu_B$): the magnetic moment of the supercell ($\mu_{tot}$), the magnetic moment on the Ir atom closer to graphene ($\mu_{Ir1}$), the magnetic moment on the upper Ir atom ($\mu_{Ir2}$), anisotropy of the spin ($\Delta\mu_S$) and orbital ($\Delta\mu_L$) magnetic moments of Ir atoms (positive values correspond to the increased moment for the perpendicular direction of magnetization), SC MAE and from FT (MAE(FT)) (both in meV).

| | $E_{ad2}$ | $N_{ue}$ | $\mu_{tot}$ | $\mu_{Ir1}$ | $\mu_{Ir2}$ | $\Delta\mu_{S,Ir1}$ | $\Delta\mu_{S,Ir2}$ | $\Delta\mu_{L,Ir1}$ | $\Delta\mu_{L,Ir2}$ | MAE | MAE(FT) |
|---|---|---|---|---|---|---|---|---|---|---|---|
| $Ir_2$@SV | −3.4 | 2 | 1.67 | 0.10 | 1.48 | −0.07 | 0.13 | 0.01 | 0.97 | 10.9 | −5.8 |
| $Ir_2$@NSV | −5.3 | 1 | 1.00 | 0.28 | 0.61 | 0.01 | 0.30 | 0.00 | 0.52 | 36.3 | 113.0 |
| $Ir_2$@DV | −3.7 | 2 | 1.22 | 0.03 | 1.17 | 0.00 | 0.54 | −0.01 | 1.41 | 29.6 | 44.8 |
| $Ir_2$@NDV | −2.1 | 2 | 2.04 | 0.30 | 1.67 | −0.01 | 0.21 | 0.07 | 0.93 | 37.5 | 33.3 |

of the MAE. Our results indicate that the picture of the MAE based on perturbation theory relating the MAE to the product of the SOC strength and the orbital anisotropy (with the largest orbital moment always corresponding to the easy-axis magnetization) at isotropic spin moments [71] has a limited applicability or even does not hold for (TM)Ir dimers on defective graphene.

A large magnetic anisotropy in the TM dimers occurs when a singly occupied highest occupied molecular orbital (HOMO) has a two-fold orbital degeneracy in the absence of SOC, implying a GS with angular momentum along the $z$-axis equal to $\pm m_l$ (see reference 69 and references therein). However, the interaction with the substrate may significantly affect the character of the eigenstates of the dimer. In the SR limit, the $d_\delta$ states of the Os atom in the OsIr@NSV system are degenerate and coincide with $E_F$ (figure S22), while the $d_\pi$ states are deeper in the binding energies. The MAE of OsIr@NSV is determined by changes in the partial $d$-band DOS close to $E_F$ with the rotation of the direction of magnetization (figure S33). The decomposition of the MAE of OsIr@NSV (figure 7(a), (c); see also figure S28) revealed opposite contributions from the N atoms and the OsIr dimer such that the positive MAE was caused by the dimer with a roughly six times larger contribution of the Os than the Ir atom. Specifically, a large positive contribution from $d_\delta$ seems associated with the down-shift of the narrow peaks in the $d_\delta$ spectra for the perpendicular magnetization, which coincided with $E_F$ for the in-plane direction (figures 7(a), (c) and figure S32). A similar effect was observed in the PDOS of the $d_\pi$, however, with a much smaller effect on the MAE. The opposite effect in the partial DOS of the $d_{z^2}$ brought about the negative contribution to the MAE. Needless to say, the large MAE is also accompanied by a strongly anisotropic orbital moment on Os at the largest SOC constant among the elements considered [69]. The lower Ir atom, whose spin and orbital moments were largely quenched, acts like an anchor for the Os atom pointing away from the defect and, thus, has no significant direct impact on MAE.

For OsIr@SV we also found opposite contributions of the dimer and the nearest-neighbour C atoms of the graphene layer. Here, the negative MAE was imposed by the IrOs dimer, again with a leading contribution from the upper atom. The decomposition of the MAE into the orbital partial contributions indicated leading negative contributions from the $d_\pi$ brought about by a down-shift of the narrow peaks at $\sim -0.5$ eV corresponding to the in-plane magnetization (figure 7(b), (d) and figure S32).

For both the homoatomic Ir dimer and the heteroatomic TMIr dimers the leading contribution to the MAE is provided by the upper TM atom, which retained a substantial spin and orbital magnetic moments (table S10) and was accompanied by their large anisotropy (table 2 and table 3). The magnetism of the lower Ir atom is largely suppressed and, accordingly, its contribution to the MAE is less significant. Also, the effect of the substrate atoms, both N and C, are not directly decisive for the sign of the MAE, although they indirectly affect the MAE via the influence on the electronic structure of the TM atom/dimer.

## 4. Summary and outlook

Vacancy defects in graphene can be created intentionally, by irradiation. While TM atoms tend to aggregate on a defect-free graphene layer, vacancy defects may create spots that anchor TM atoms and dimers firmly, preventing their diffusion and conserving their size, symmetry and, accordingly, large magnetic anisotropy.

In this work, we theoretically showed that vacancy defects in graphene can anchor TM atoms. The interaction energy of the second TM atom with the Ir atom already pinned by the defect in graphene is strong; the formation of the dimers should be energetically favourable.

While Ir@NSV exhibited an MAE of ∼10 meV with an easy axis parallel to the graphene plane, adsorption of the Os atom on top of the Ir atom boosted the MAE to 50 meV and changed the easy axis to the axial direction. The MAE of 50 meV corresponds to $T_B$ of 14 K or $E_T$ of 580 K. The magnetism of the Ir atom closer to graphene was strongly quenched and the upper TM atom retained a substantial magnetic moment. The large MAE was accompanied by a substantial orbital anisotropy at anisotropic spin moments on the upper TM atom, which provided a significant contribution to the MAE.

A highly ordered array of the NSV defects in graphene anchoring OsIr dimers may allow us to realize ultra-high-density atomic-scale information storage. Indeed, the Ir@NSV system corresponds to the storage density of ∼490 Tb/inch$^2$. However, for practical applications of graphene-supported magnetic dimers, the carbon sheet must be

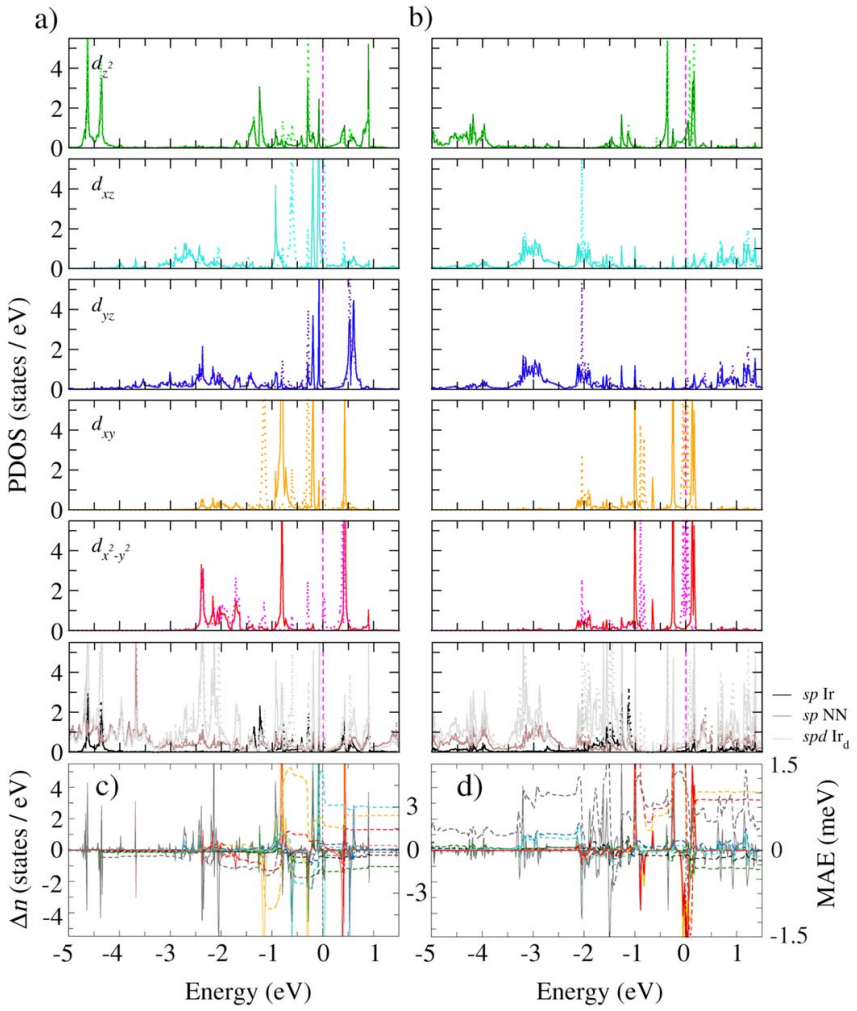


**Figure 6.** Partial densities of states for (a) $Ir_2$@NDV and (b) $Ir_2$@NSV. (c, d) Corresponding changes in the orbital-decomposed PDOS with reorientation of the magnetization direction from the easy to hard direction and integrated contributions to the MAE: cf figure 4 and figure S30. $Ir_d$ denotes the Ir atom closer to graphene.

**Table 3.** Adsorption energies of a TM atom ($E_{ad2}$) on defective graphene with a pre-adsorbed Ir atom, the number of unpaired electrons, SR magnetic moments, anisotropy of the spin and orbital magnetic moments, MAE and MAE(FT). Cf table 2.

| | $E_{ad2}$ | $N_{ue}$ | $\mu_{tot}$ | $\mu_{\mathrm{Ir}}$ | $\mu_{\mathrm{TM}}$ | $\Delta\mu_{S,\mathrm{Ir}}$ | $\Delta\mu_{S,\mathrm{TM}}$ | $\Delta\mu_{L,\mathrm{Ir}}$ | $\Delta\mu_{L,\mathrm{TM}}$ | MAE | MAE(FT) |
|---|---|---|---|---|---|---|---|---|---|---|---|
| NiIr@SV | −2.6 | 1 | 0.83 | 0.00 | 0.88 | 0.02 | −0.03 | 0.04 | 0.87 | −15.8 | 4.0 |
| RuIr@SV | −2.6 | 3 | 3.00 | 0.06 | 2.53 | 0.00 | 0.00 | 0.01 | −0.03 | −5.8 | −9.3 |
| RhIr@SV | −2.7 | 2 | 1.90 | 0.04 | 1.41 | 0.03 | −0.04 | 0.06 | 1.04 | −10.5 | 11.9 |
| OsIr@SV | −3.0 | 3 | 2.91 | 0.01 | 2.46 | −0.02 | −0.05 | 0.02 | −0.27 | −52.6 | −60.0 |
| FeIr@NSV | −3.5 | 2 | 2.40 | −0.30 | 2.92 | 0.02 | −0.01 | −0.01 | 0.22 | 11.1 | −5.2 |
| CoIr@NSV | −3.5 | 1 | 1.61 | −0.04 | 1.71 | −0.01 | −0.08 | −0.01 | 1.07 | −41.1 | 15.1 |
| RuIr@NSV | −4.3 | 2 | 2.00 | 0.05 | 1.76 | 0.05 | −0.01 | −0.01 | 1.16 | −41.0 | 6.4 |
| OsIr@NSV | −5.1 | 2 | 2.08 | 0.30 | 1.69 | −0.03 | 0.21 | 0.02 | 1.27 | 50.1 | 41.4 |
| RuIr@NDV | −1.7 | 3 | 3.07 | 0.23 | 2.54 | 0.04 | −0.01 | 0.03 | 0.24 | −44.9 | −8.4 |
| OsIr@NDV | −2.0 | 3 | 3.34 | 0.29 | 2.72 | −0.02 | 0.11 | −0.06 | 0.61 | −5.1 | −15.5 |

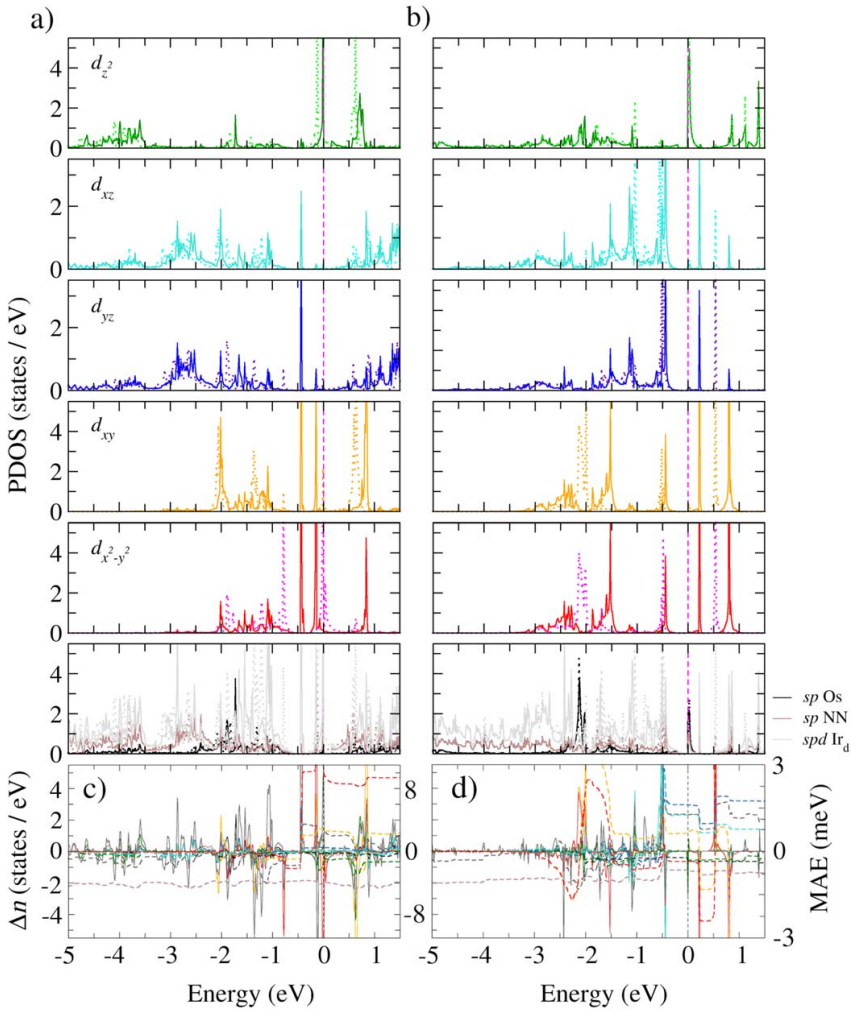


**Figure 7.** Partial densities of states for (a) OsIr@NSV and (b) OsIr@SV. (c, d) Corresponding changes in the orbital-decomposed PDOS with reorientation of the magnetization direction from the easy to hard direction and integrated contributions to the MAE: cf figure 4 and figure S32.

deposited on a solid substrate. Theoretical relativistic calculations for IrCo@graphene/Cu(111) reported an enormous MAE of 204 meV [9], corresponding to the theoretical $T_B$ of 56 K. An enhancement of the MAE to 285 meV would lead to $T_B$ of ∼78 K, that of liquid nitrogen. Further study is needed to address the effect of substrates on the MAE of TM dimers anchored by defects in graphene.

## Acknowledgments

The authors gratefully acknowledge the support of the Operational Programme for Research, Development and Education of the European Regional Development Fund (Project No. CZ.02.1.01/0.0/0.0/16_019/0000754). MO acknowledges the ERC grant (683024) from the EU Horizon 2020 Research and Innovation Programme. JN acknowledges support by Palacký University Olomouc (project IGA_PrF_2021_031).

## ORCID iDs

Piotr Błoński https://orcid.org/0000-0002-7072-232X
Michal Otyepka https://orcid.org/0000-0002-1066-5677

## References

[1] Nonas B, Cabria I, Zeller R, Dederichs P H, Huhne T and Ebert H 2001 *Phys. Rev. Lett.* **86** 2146–9
[2] Błoński P and Hafner J 2009 *J. Phys. Condens. Matter* **21** 426001

[3] Błoński P, Lehnert A, Dennler S, Rusponi S, Etzkorn M, Moulas G, Bencok P, Gambardella P, Brune H and Hafner J 2010 *Phys. Rev.* B **81** 104426
[4] Lehnert A, Dennler S, Błoński P, Rusponi S, Etzkorn M, Moulas G, Bencok P, Gambardella P, Brune H and Hafner J 2010 *Phys. Rev.* B **82** 094409
[5] Błoński P, Dennler S and Hafner J J 2011 *Chem. Phys.* **134** 034107
[6] Błoński P and Hafner J 2011 *J. Phys. Condens. Matter* **23** 136001
[7] Błoński P and Hafner J 2015 *J. Phys. Condens. Matter* **27** 046002
[8] Błoński P and Hafner J 2014 *J. Phys. Condens. Matter* **26** 146002
[9] Błoński P and Hafner J 2014 *J. Phys. Condens. Matter* **26** 256001
[10] Gambardella P, Dallmeyer A, Maiti K, Malagoli M C, Rusponi S, Ohresser P, Eberhardt eiss, Carbone C and Kern K 2004 *Phys. Rev. Lett.* **93** 7–10
[11] Weiss N *et al* 2005 *Phys. Rev. Lett.* **95** 157204
[12] Brune H and Gambardella P 2009 *Surf. Sci* **603** 1812–30
[13] Khajetoorians A A, Lounis S, Chilian B, Costa A T, Zhou L, Mills D L, Wiebe J and Wiesendanger R 2011 *Phys. Rev. Lett.* **106** 037205
[14] Khajetoorians A A, Schlenk T, Schweflinghaus B, dos Santos Dias M, Steinbrecher M, Bouhassoune M, Lounis S, Wiebe J and Wiesendanger R 2013 *Phys. Rev. Lett.* **111** 157204
[15] Heinrich B W, Braun L, Pascual J I and Franke K 2013 *J. Nat. Phys.* **9** 765–8
[16] Paul W, Yang K, Baumann S, Romming N, Choi T, Lutz C P and Heinrich A 2017 *J. Nat. Phys.* **13** 403–7
[17] Natterer F D, Yang K, Paul W, Willke P, Choi T, Greber T, Heinrich A J and Lutz C P 2017 *Nature* **543** 226–8
[18] Hermenau J, Ternes M, Steinbrecher M, Wiesendanger R and Wiebe J 2018 *Nano Lett.* **18** 1978–83
[19] Natterer F D, Donati F, Patthey F and Brune H 2018 *Phys. Rev. Lett* **121** 027201
[20] Gambardella P *et al* 2003 *Science* **300** 1130–3
[21] Donati F *et al* 2016 *Science* **352** 318–21
[22] Baltic R, Pivetta M, Donati F, Wäckerlin C, Singha A, Dreiser J, Rusponi S and Brune H 2016 *Nano Lett.* **16** 7610–5
[23] Hashimoto A, Suenaga K, Gloter A, Urita K and Iijima S 2004 *Nature* **430** 870–3
[24] Banhart F, Kotakoski J and Krasheninnikov A V 2011 *ACS Nano* **5** 26–41
[25] Pantelides S T, Puzyrev Y, Tsetseris L and Wang B 2012 *MRS Bull.* **37** 1187–94
[26] Krasheninnikov A V, Lehtinen P O, Foster A S, Pyykkö P and Nieminen R M 2009 *Phys. Rev. Lett.* **102** 126807
[27] Cretu O, Krasheninnikov A V, Rodríguez-Manzo J A, Sun L, Nieminen R M and Banhart F 2010 *Phys. Rev. Lett.* **105** 196102
[28] Lin Y-C, Teng P-Y, Yeh C-H, Koshino M, Chiu P-W and Suenaga K 2015 *Nano Lett.* **15** 7408–13
[29] Xia B, Liao Z, Liu Y, Chi X, Xiao W, Ding J, Wang T, Gao D and Xue D 2020 *Appl. Phys. Lett.* **116** 113102
[30] Ge G-X, Li Y-B, Wang G-H and Wan J-G 2016 *Phys. Chem. Chem. Phys.* **18** 11550–5
[31] Kandpal H C, Koepernik K and Richter M 2012 *Phys. Rev.* B **86** 235430
[32] Haldar S, Pujari B S, Bhandary S, Cossu F, Eriksson O, Kanhere D G and Sanyal B 2014 *Phys. Rev.* B **89** 205411
[33] Hu J and Wu R 2014 *Nano Lett.* **14** 1853–8
[34] Langer R, Fako E, Błoński P, Vavrečka M, Bakandritsos A, Otyepka M and López N 2020 *Appl. Mater. Today* **18** 100462
[35] Bakandritsos A *et al* 2019 *Adv. Mater.* **31** 1900323
[36] Fei H *et al* 2018 *Adv. Mater.* **30** 1802146
[37] Liu J 2017 *ACS Catal.* **7** 34–59
[38] Liu L and Corma A 2018 *Chem. Rev.* **118** 4981–5079
[39] Fei H *et al* 2018 *Nat. Catal* **1** 63–72
[40] Deng D *et al* 2015 *Sci. Adv.* **1** e1500462
[41] Yan H *et al* 2017 *Nat. Commun.* **8** 1070
[42] Yang X-F, Wang A, Qiao B, Li J, Liu J and Zhang T 2013 *Acc. Chem. Res.* **46** 1740–8
[43] Heine V 1980 *In Solid State Phys. - Adv. Res. Appl. C* **35** 1–127
[44] Dudarev S L, Botton G A, Savrasov S Y, Humphreys C J and Sutton A P 1998 *Phys. Rev.* B **57** 1505–9
[45] Kulik H J, Cococcioni M, Scherlis D A and Marzari N 2006 *Phys. Rev. Lett.* **97** 103001
[46] Klimeš J, Bowler D R and Michaelides A 2011 *Phys. Rev.* B **83** 195131
[47] Kresse G and Hafner J 1993 *Phys. Rev.* B **47** 558–61
[48] Kresse G and Hafner J 1994 *Phys. Rev.* B **49** 14251
[49] Kresse G and Furthmüller J 1996 *Comput. Mater. Sci.* **6** 15–50
[50] Kresse G and Furthmüller J 1996 *Phys. Rev.* B **54** 11169–86
[51] Kresse G and Joubert D 1999 *Phys. Rev.* B **59** 1758–75
[52] Blöchl P E 1994 *Phys. Rev.* B **50** 17953–79
[53] Perdew J P, Chevary J A, Vosko S H, Jackson K A, Pederson M R, Singh D J and Fiolhais C 1992 *Phys. Rev.* B **46** 6671
Perdew J P, Chevary J A, Vosko S H, Jackson K A, Pederson M R, Singh D J and Fiolhais C 1993 Erratum *Phys. Rev.* B **48** 4978
[54] Perdew J P, Burke K and Ernzerhof M 1996 *Phys. Rev. Lett.* **77** 3865–8
Perdew J P, Burke K and Ernzerhof M 1997 Erratum: *Phys. Rev. Lett.* **78** 1396
[55] Weiss N O, Zhou H, Liao L, Liu Y, Jiang S, Huang Y and Duan X 2012 *Adv. Mater.* **24** 5782–825
[56] Lehmann G, Rennert P, Taut M and Wonn H 1970 *Phys. Stat. Sol.* **37** K27
[57] Jepson O and Anderson O 1971 *Solid State Commun.* **9** 1763–7
[58] Lehmann G and Taut M 1972 *Phys. Status Solidi.* **54** 469–77
[59] Blöchl P E, Jepsen O and Andersen O K 1994 *Phys. Rev.* B **49** 16223–33
[60] Bader R F W and Nguyen-Dang T T 1981 *Adv. Quantum Chem.* **14** 63–124
[61] Bader R F W 1985 *Acc. Chem. Res.* **18** 9–15
[62] Henkelman G, Arnaldsson A and Jonsson H 2006 *Comput. Mater. Sci.* **36** 354–60
[63] Kleinman L 1980 *Phys. Rev.* B **21** 2630
[64] MacDonald A H, Pickett W E and Koelling D D 1980 *J. Phys. C* **13** 2675
[65] Hobbs D, Kresse G and Hafner J 2000 *Phys. Rev.* B **62** 11556–70
[66] Marsman M and Hafner J 2002 *Phys. Rev.* B **66** 1–13
[67] Sńtos E J G, Ayuela A and Sanchez-Portal D 2010 *New J. Phys.* **12** 053012
[68] Sun M, Ren Q, Zhao Y, Chou J-P, Yu J and Tang W 2017 *Carbon* **120** 265–73
[69] Błoński P and Hafner J 2009 *Phys. Rev.* B **79** 224418
[70] Guo M, Liang X, Wang H and Zhang J 2020 *Phys. Chem. Chem. Phys.* **22** 238–44
[71] Bruno P 1989 *Phys. Rev.* B **39** 865–8

## A2. Density of States Plots

This appendix includes DOS plots of all perpendicularly stable TM dimers. Plots are ordered as follows: by TM↓, then by a type of the defect, then by a horizontal group of TM↑, *e.g.*, TM8Fe@NSV are first, then TM9Fe@NSV, later TM8Fe@NDV, later TM8Co@NSV, and so on. We decided to keep the structure even if the plot does not include all systems (we show a free space instead of showing DOS of systems that are not perpendicularly stable) to keep the natural flow of the figures without any irregularities in the ordering.

All the plots were achieved by using custom Python script called DosPlotter. It is programmed to be very universal and could be useful for anyone that is struggling with DOS plotting from VASP outputs. DosPlotter accepts many parameters that can influence its output. Then it reads DOSCAR file that includes all DOS of given system (or more DOSCARs from more systems) and outputs it to the grace-type format. Any software able to read grace format is then able to graphically plot the data without any additional effort. We used QtGrace software and the included PdfHaru library to plot grace files directly to Pdf.

DosPlotter is now available upon request. It may be significantly developed and adapted in the future and therefore we decided not to print its actual version in the Thesis. Once its final form is achieved, we may make it public.

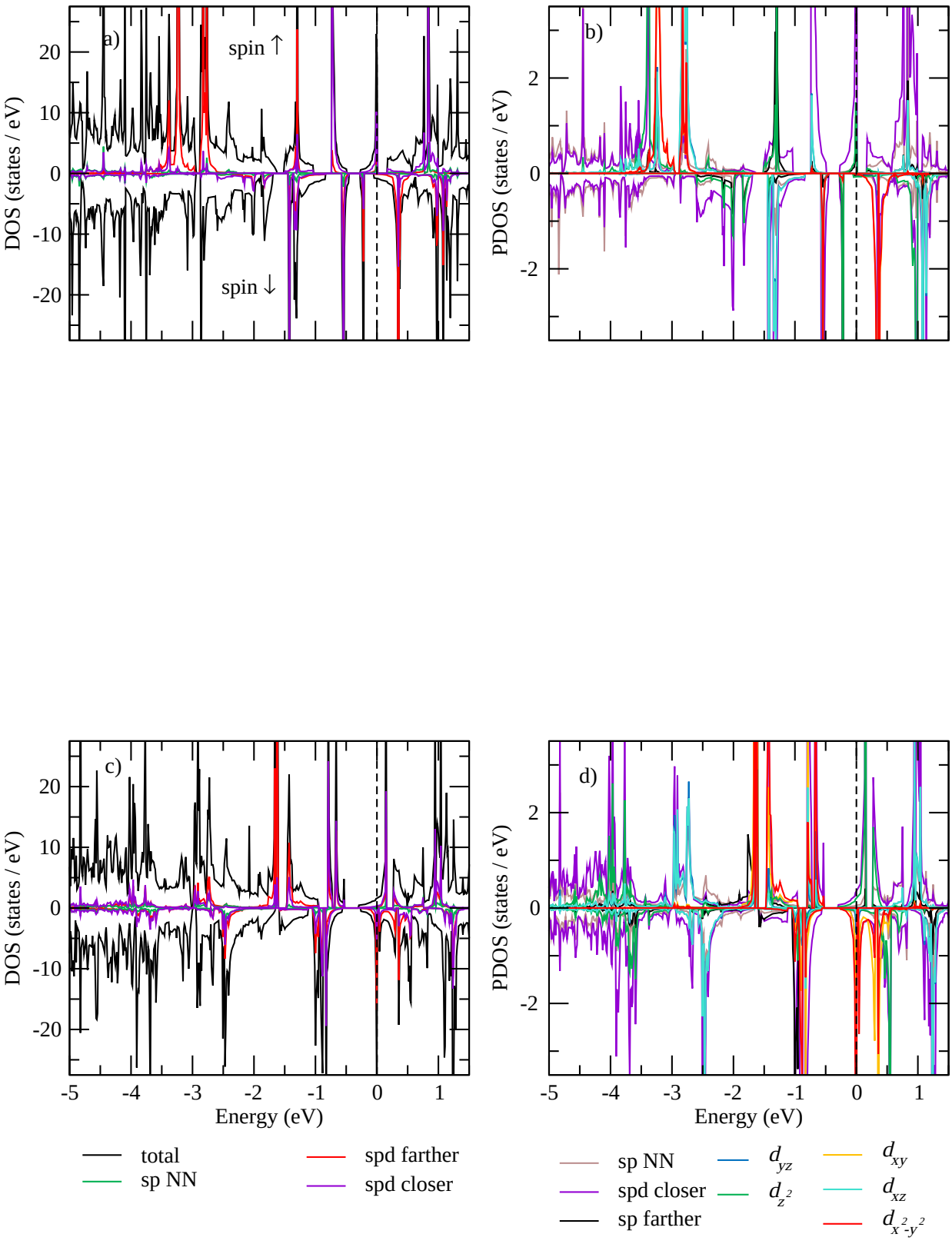


**FIG. A1:** DOS and PDOS plots. FeFe@NSV (a) and (b); OsFe@NSV (c) and (d).

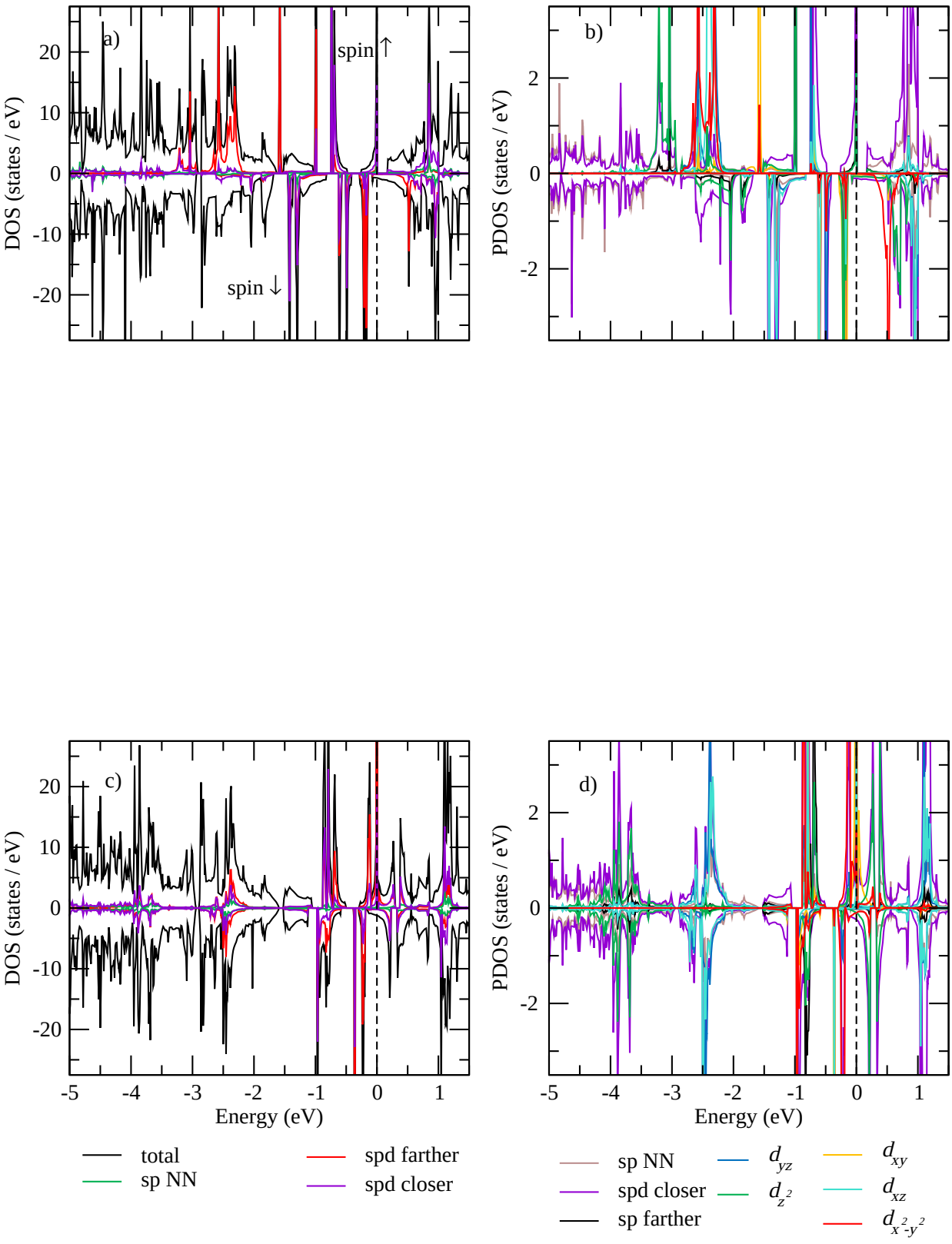


**FIG. A2:** DOS and PDOS plots. CoFe@NSV (a) and (b); IrFe@NSV (c) and (d).

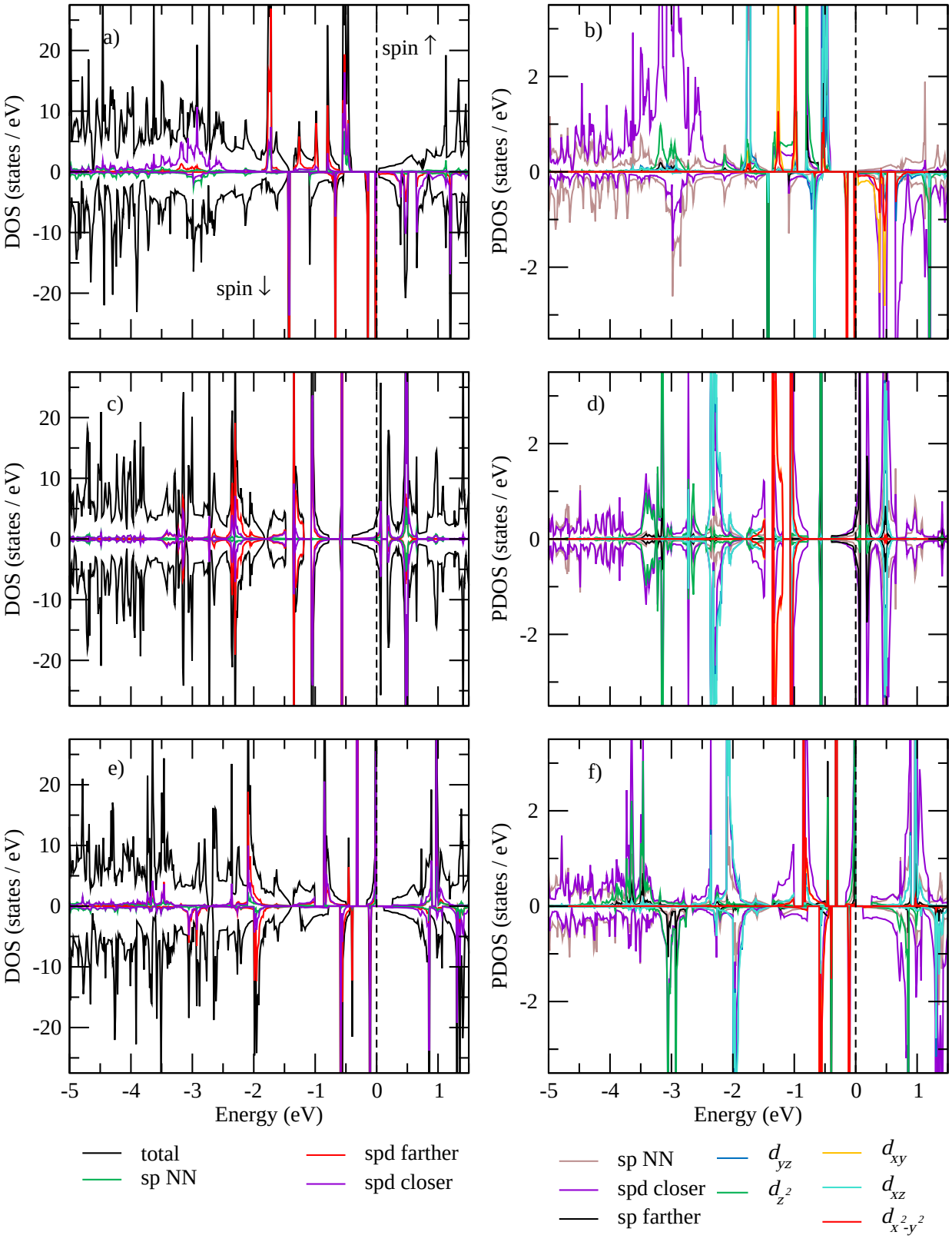


**FIG. A3:** DOS and PDOS plots. NiFe@NSV (a) and (b); PdFe@NSV (c) and (d); PtFe@NSV (e) and (f).

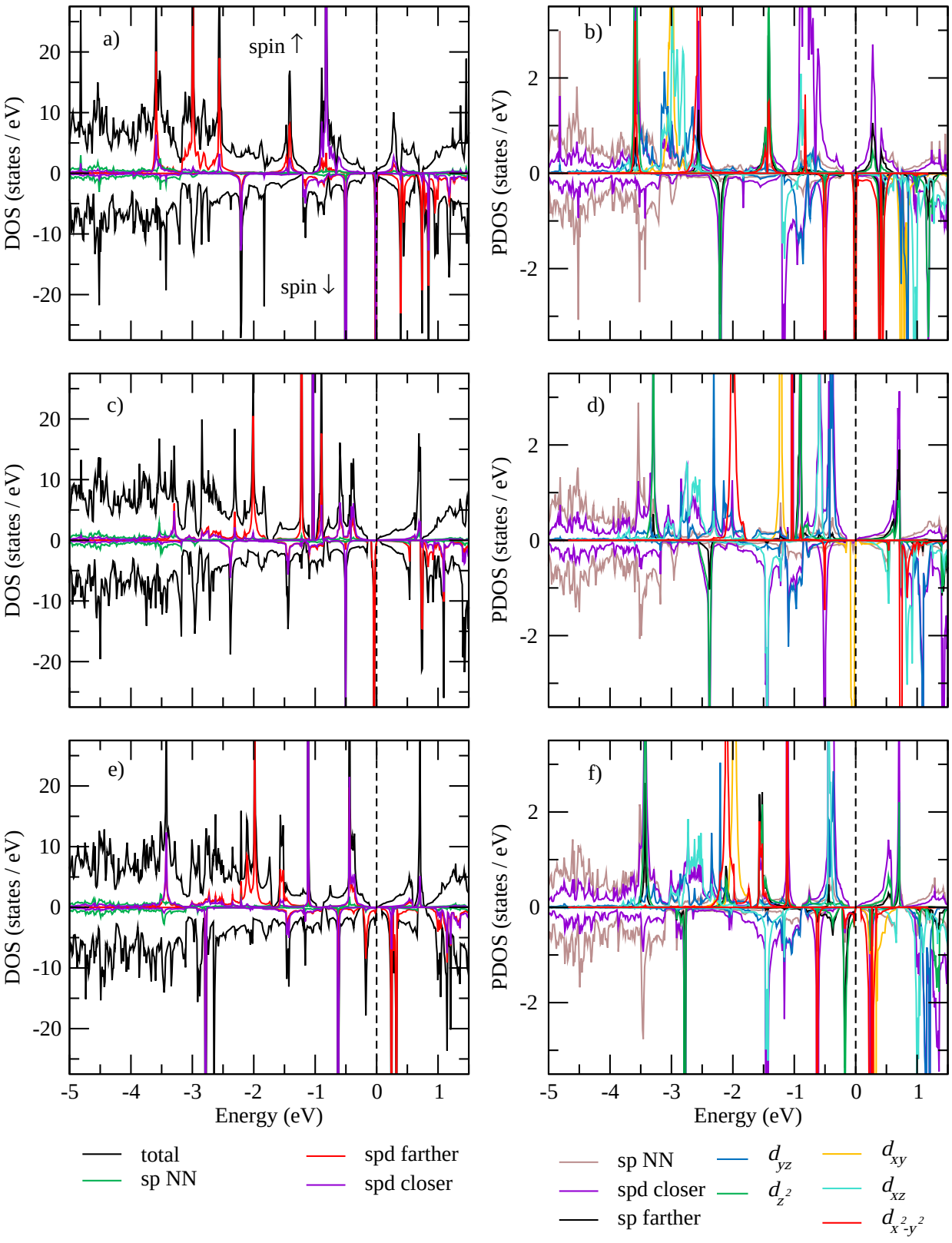


**FIG. A4:** DOS and PDOS plots. FeFe@NDV (a) and (b); RuFe@NDV (c) and (d); OsFe@NDV (e) and (f).

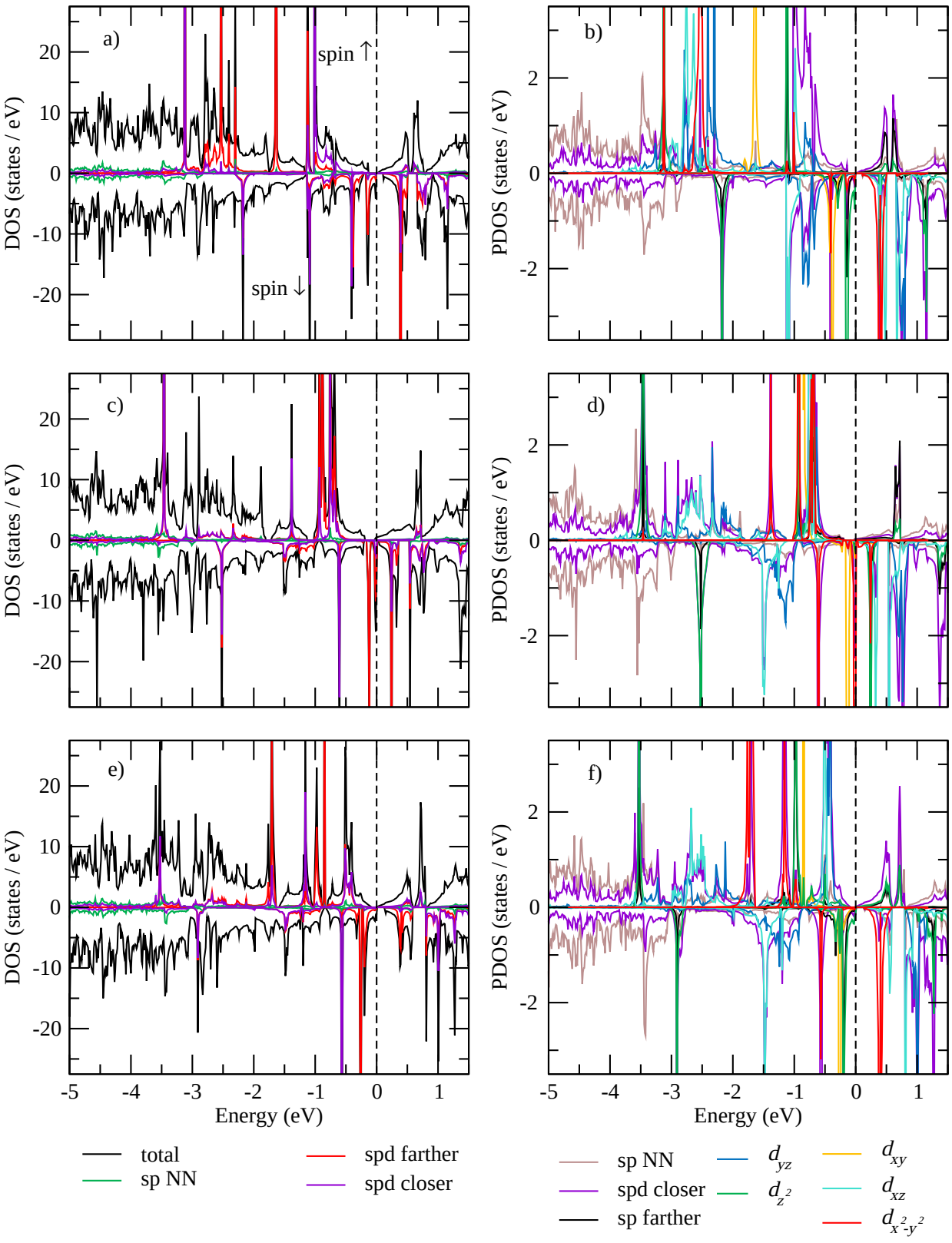


**FIG. A5:** DOS and PDOS plots. CoFe@NDV (a) and (b); RhFe@NDV (c) and (d); IrFe@NDV (e) and (f).

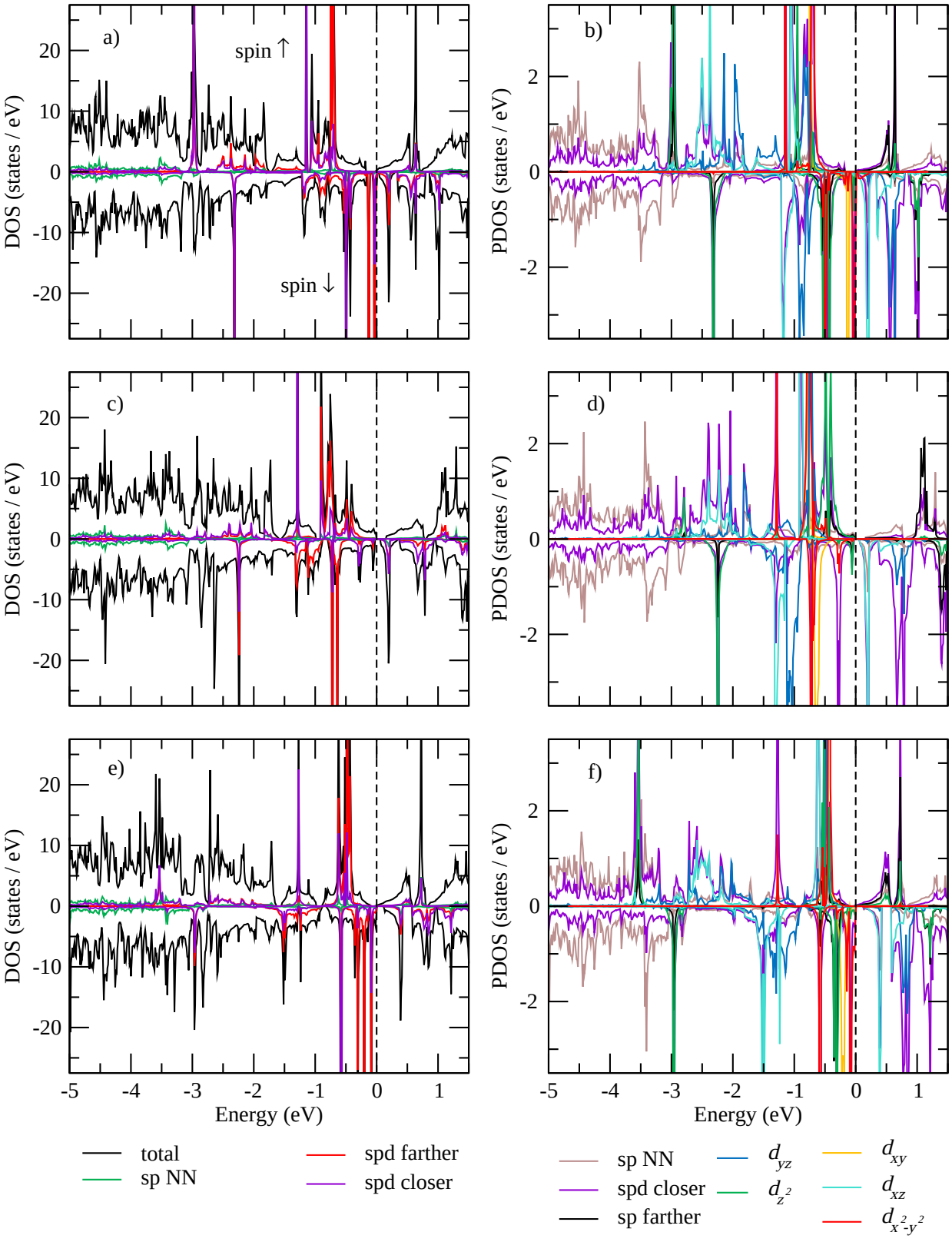


**FIG. A6:** DOS and PDOS plots. NiFe@NDV (a) and (b); PdFe@NDV (c) and (d); PtFe@NDV (e) and (f).

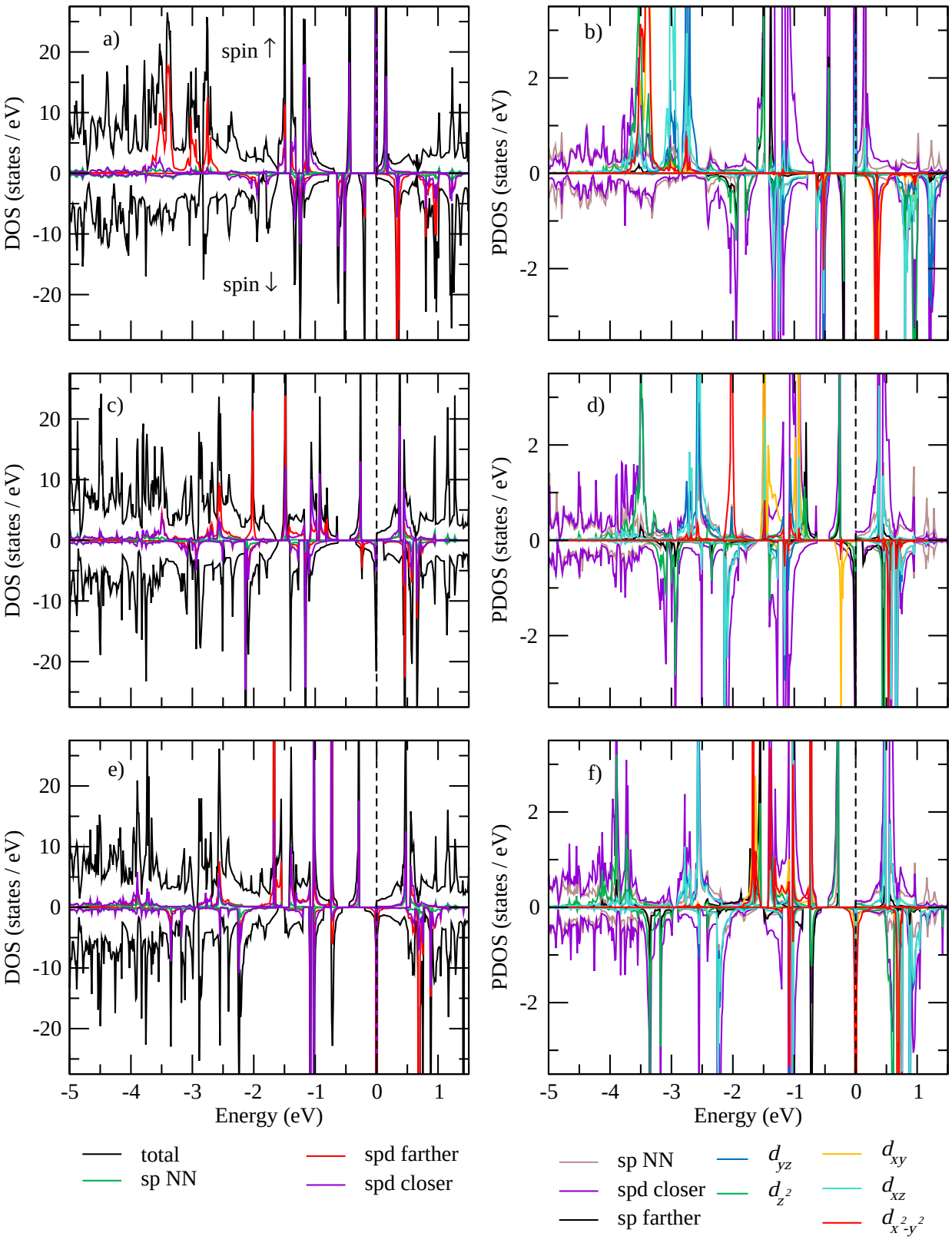


**FIG. A7:** DOS and PDOS plots. FeCo@NSV (a) and (b); RuCo@NSV (c) and (d); OsCo@NSV (e) and (f).

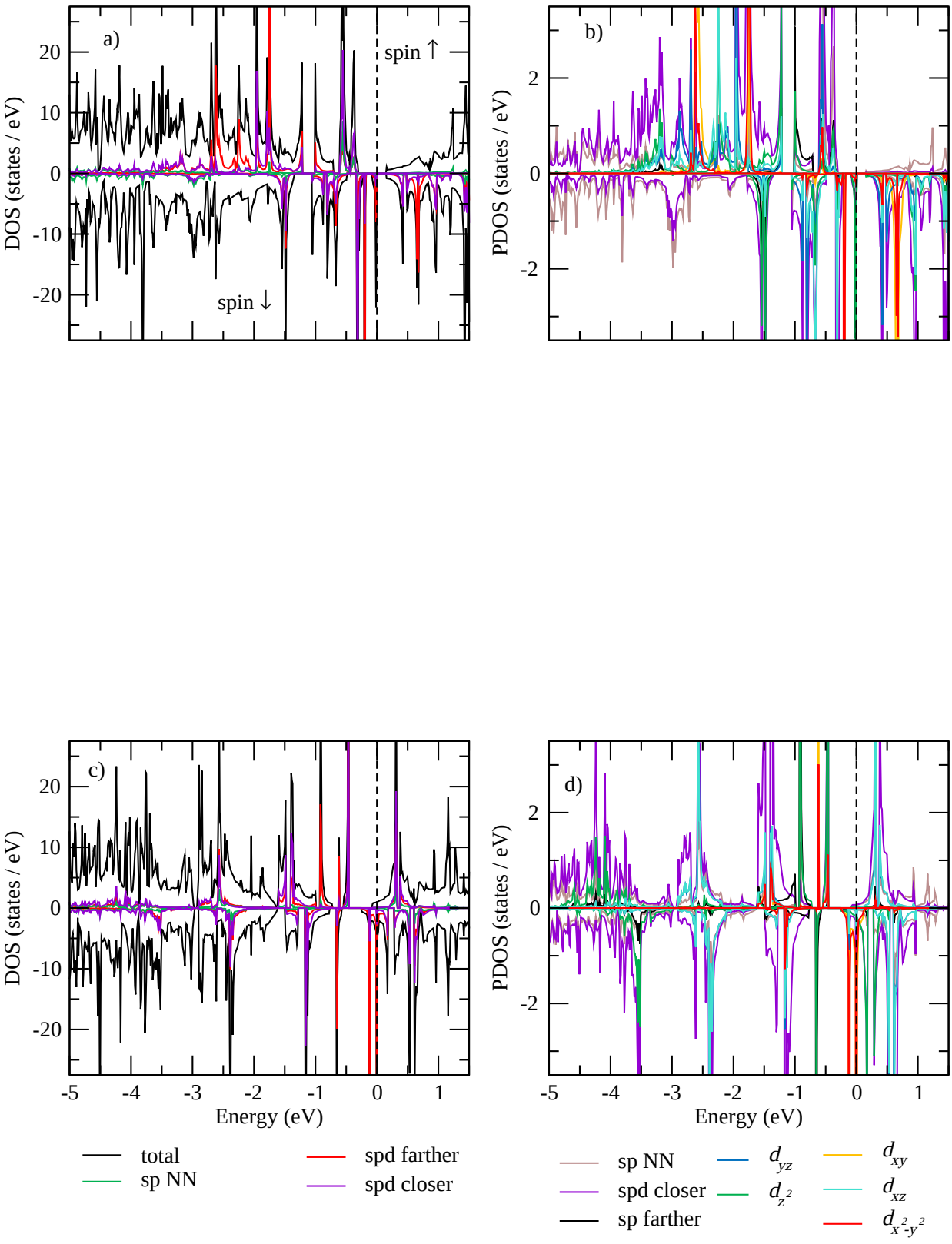


**FIG. A8:** DOS and PDOS plots. CoCo@NSV (a) and (b); IrCo@NSV (c) and (d).

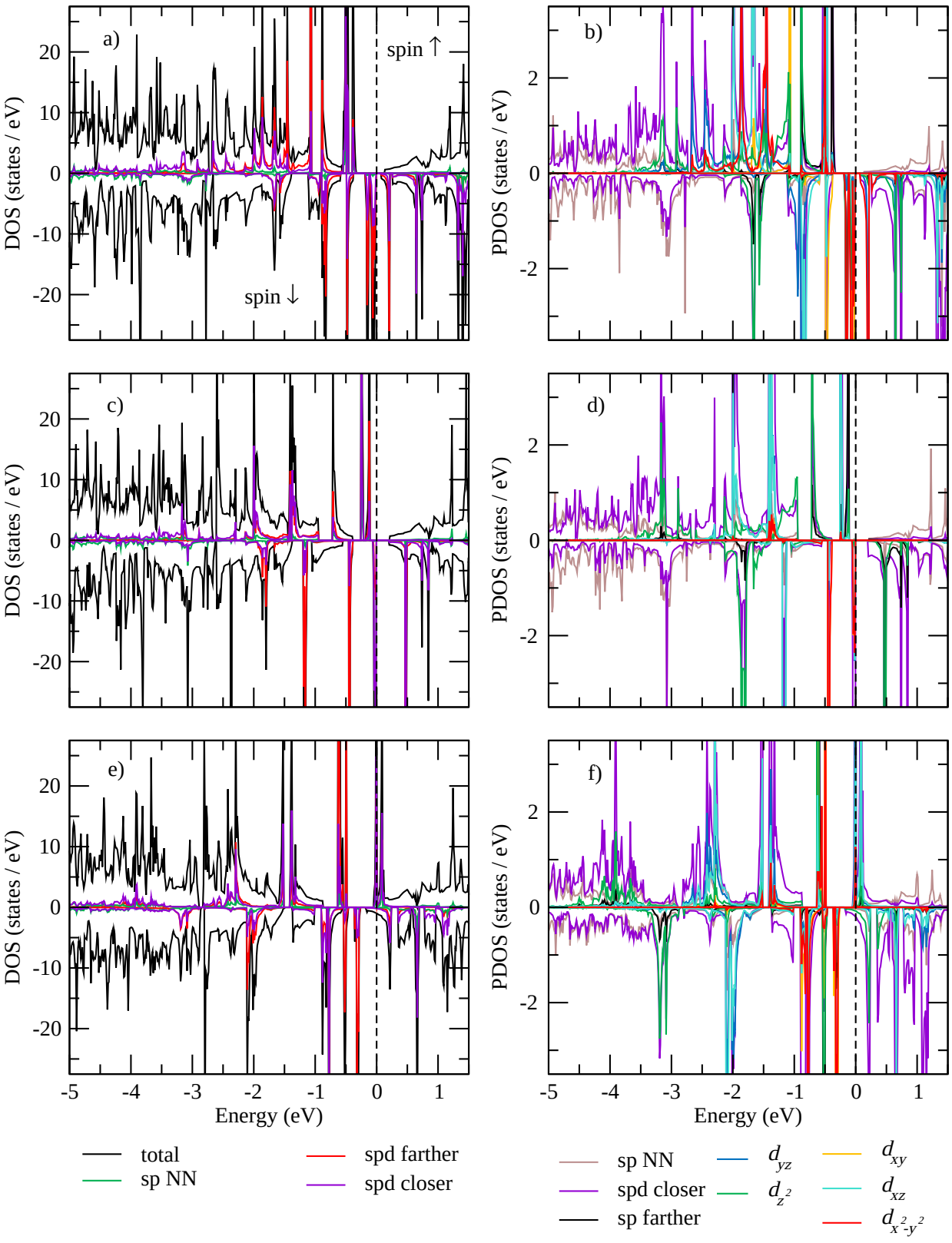


**FIG. A9:** DOS and PDOS plots. NiCo@NSV (a) and (b); PdCo@NSV (c) and (d); PtCo@NSV (e) and (f).

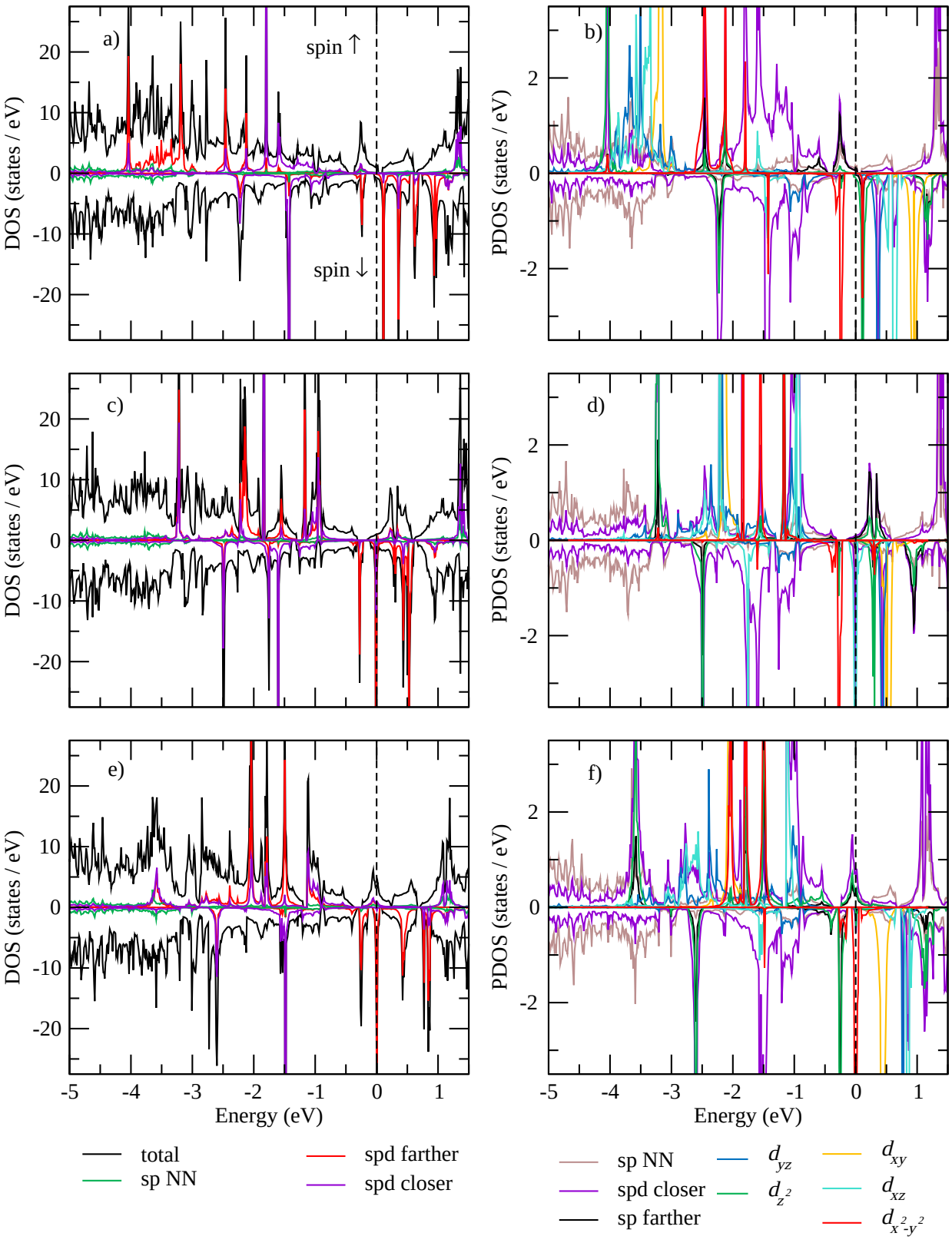


**FIG. A10:** DOS and PDOS plots. FeCo@NDV (a) and (b); RuCo@NDV (c) and (d); OsCo@NDV (e) and (f).

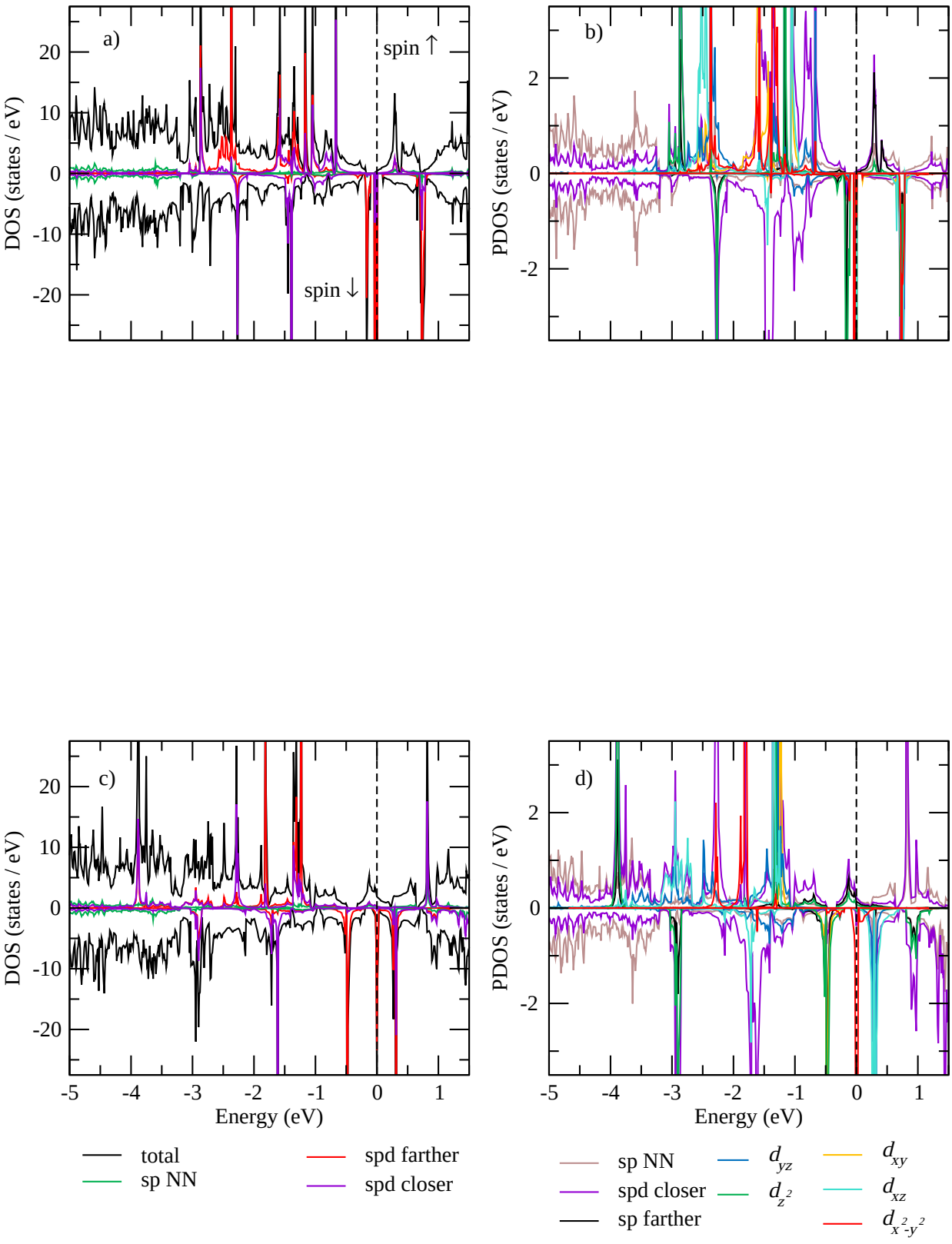


**FIG. A11:** DOS and PDOS plots. CoCo@NDV (a) and (b); IrCo@NDV (c) and (d).

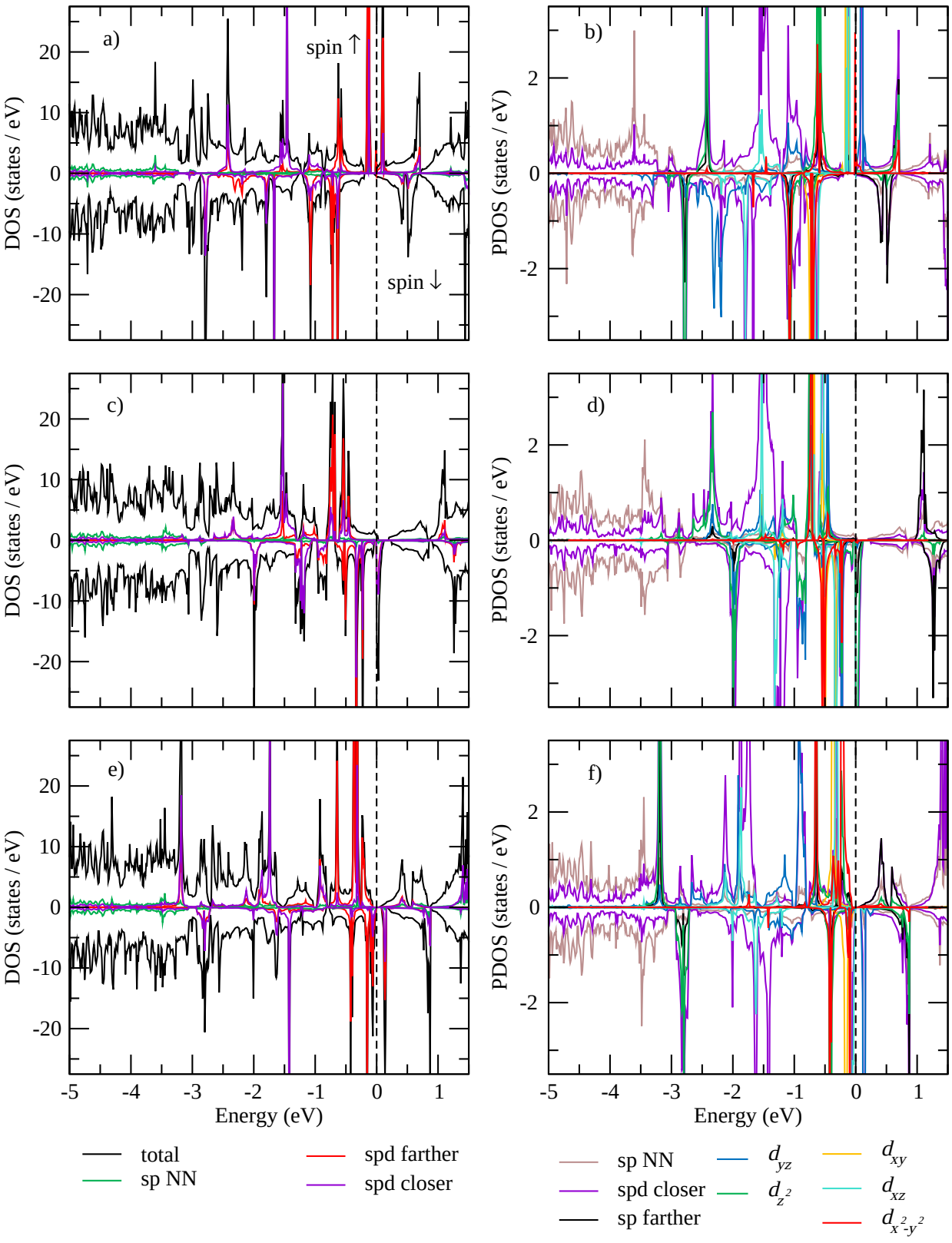


**FIG. A12:** DOS and PDOS plots. NiCo@NDV (a) and (b); PdCo@NDV (c) and (d); PtCo@NDV (e) and (f).

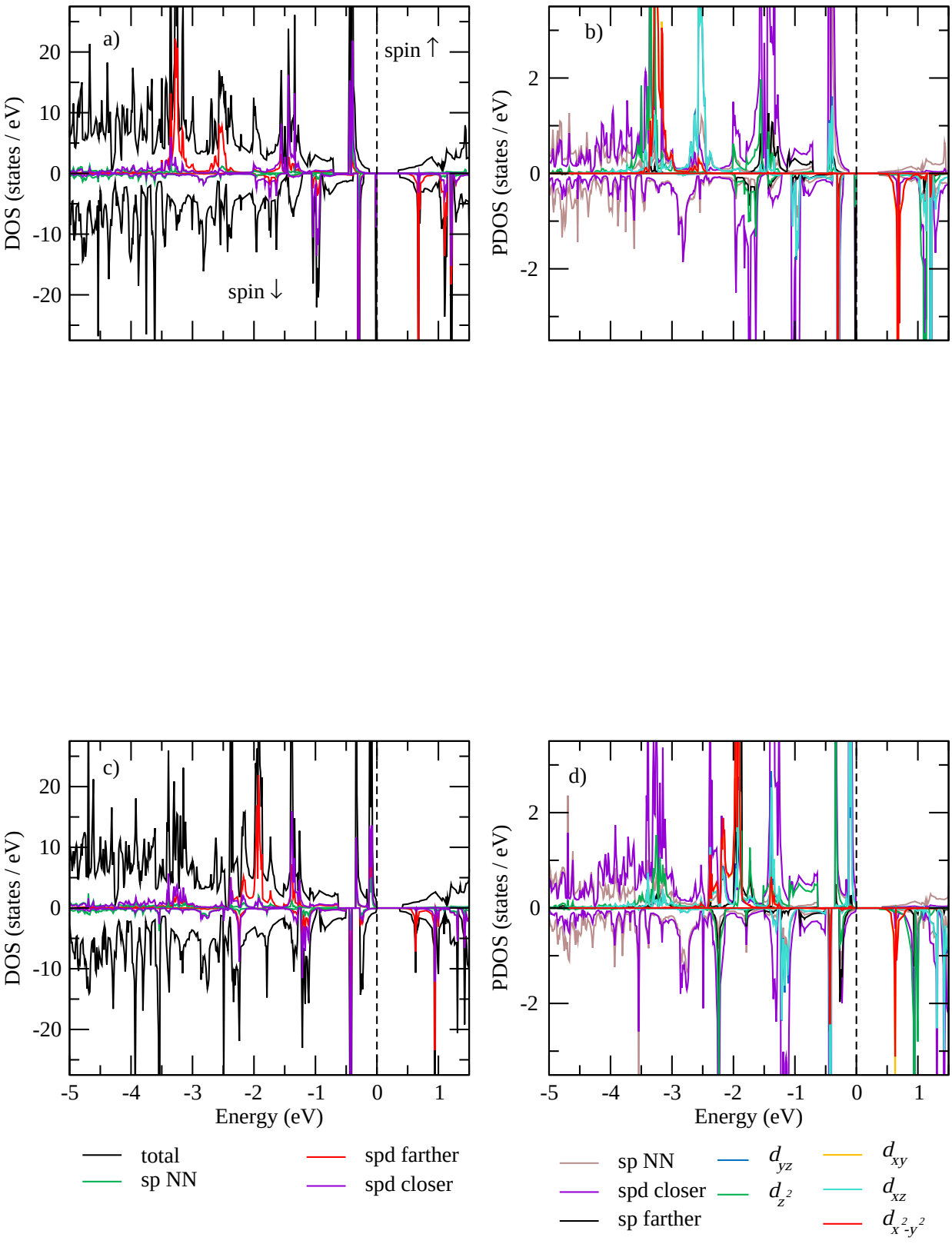


**FIG. A13:** DOS and PDOS plots. FeNi@NSV (a) and (b); OsNi@NSV (c) and (d).

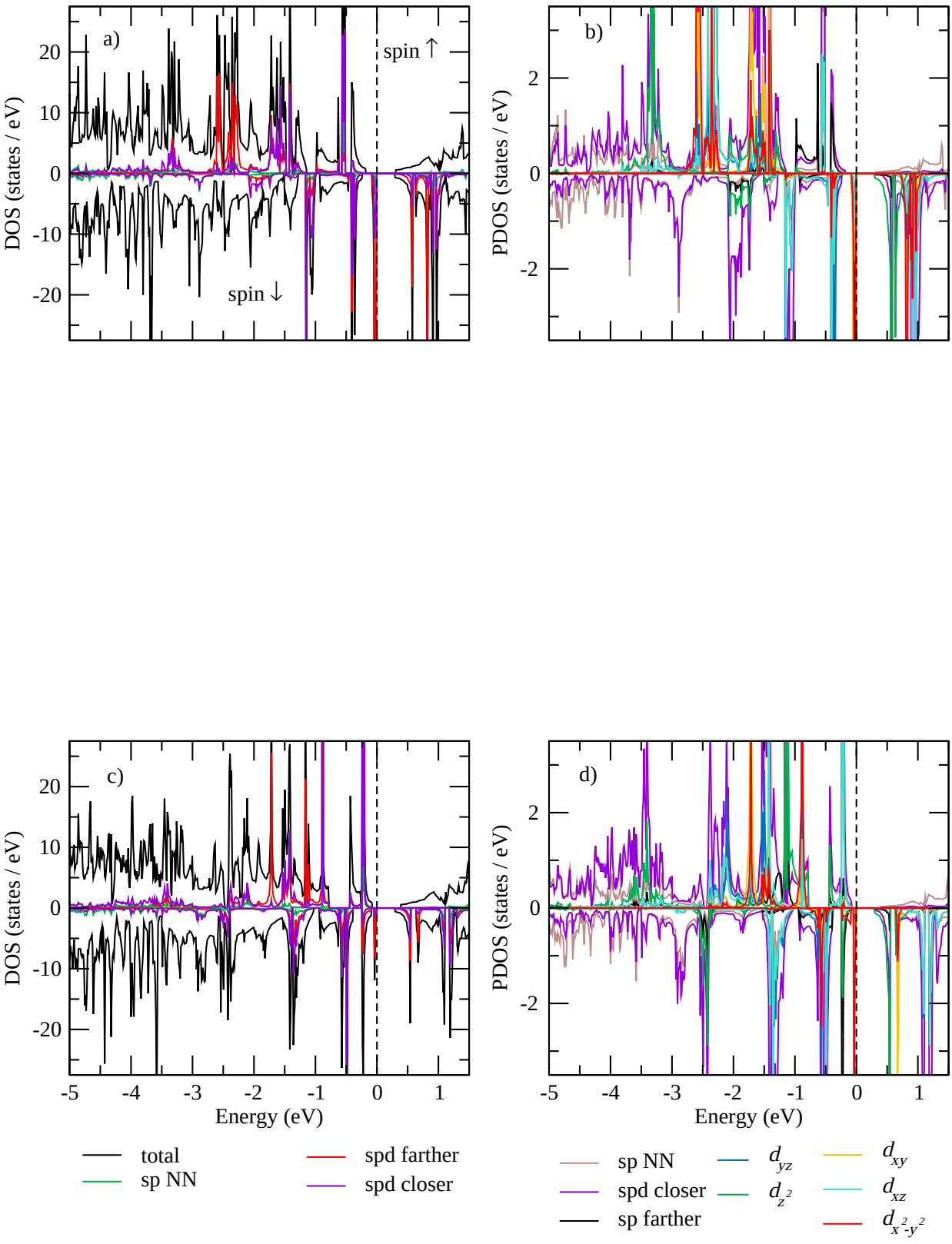


**FIG. A14:** DOS and PDOS plots. CoNi@NSV (a) and (b); IrNi@NSV (c) and (d).

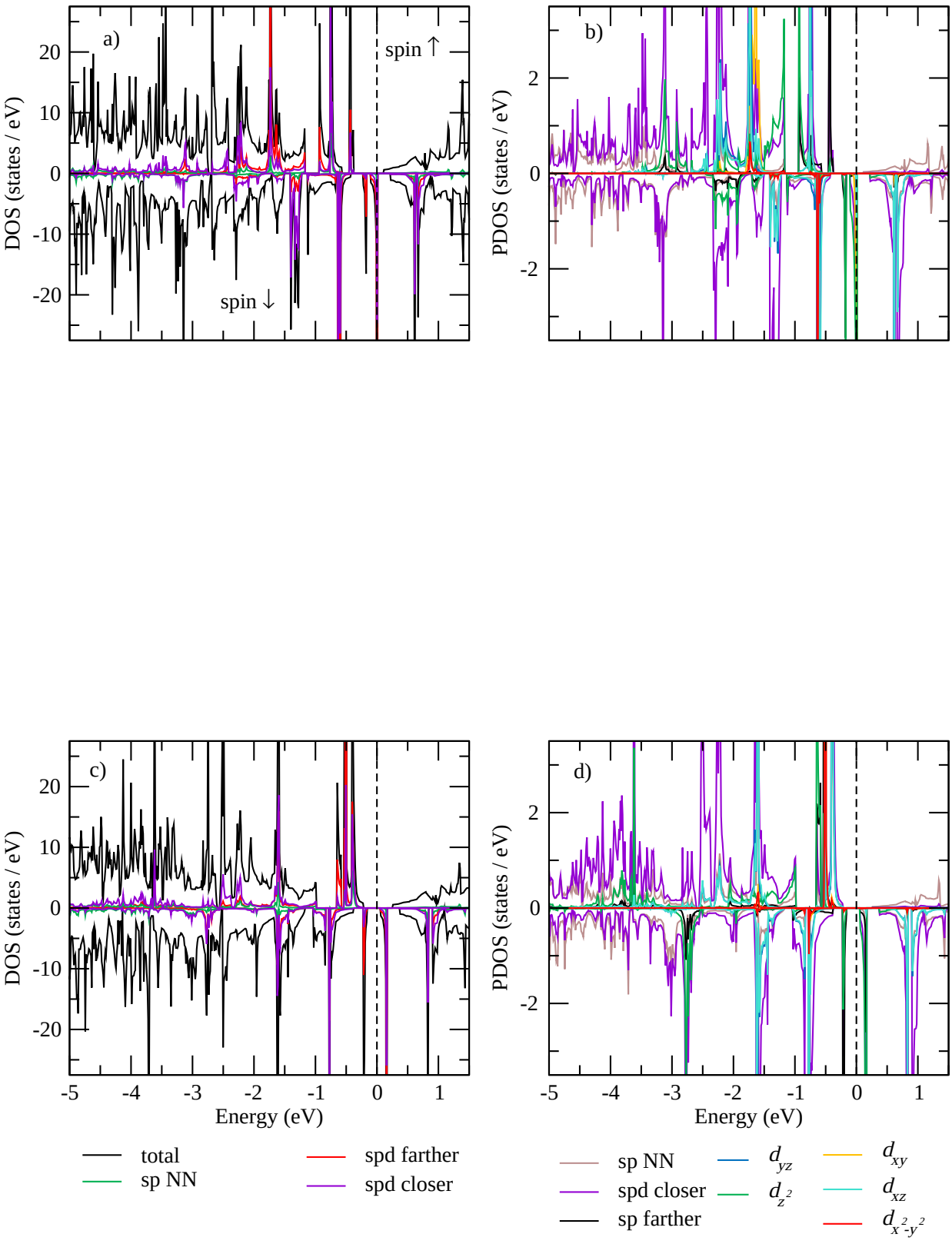


**FIG. A15:** DOS and PDOS plots. NiNi@NSV (a) and (b); PtNi@NSV (c) and (d).

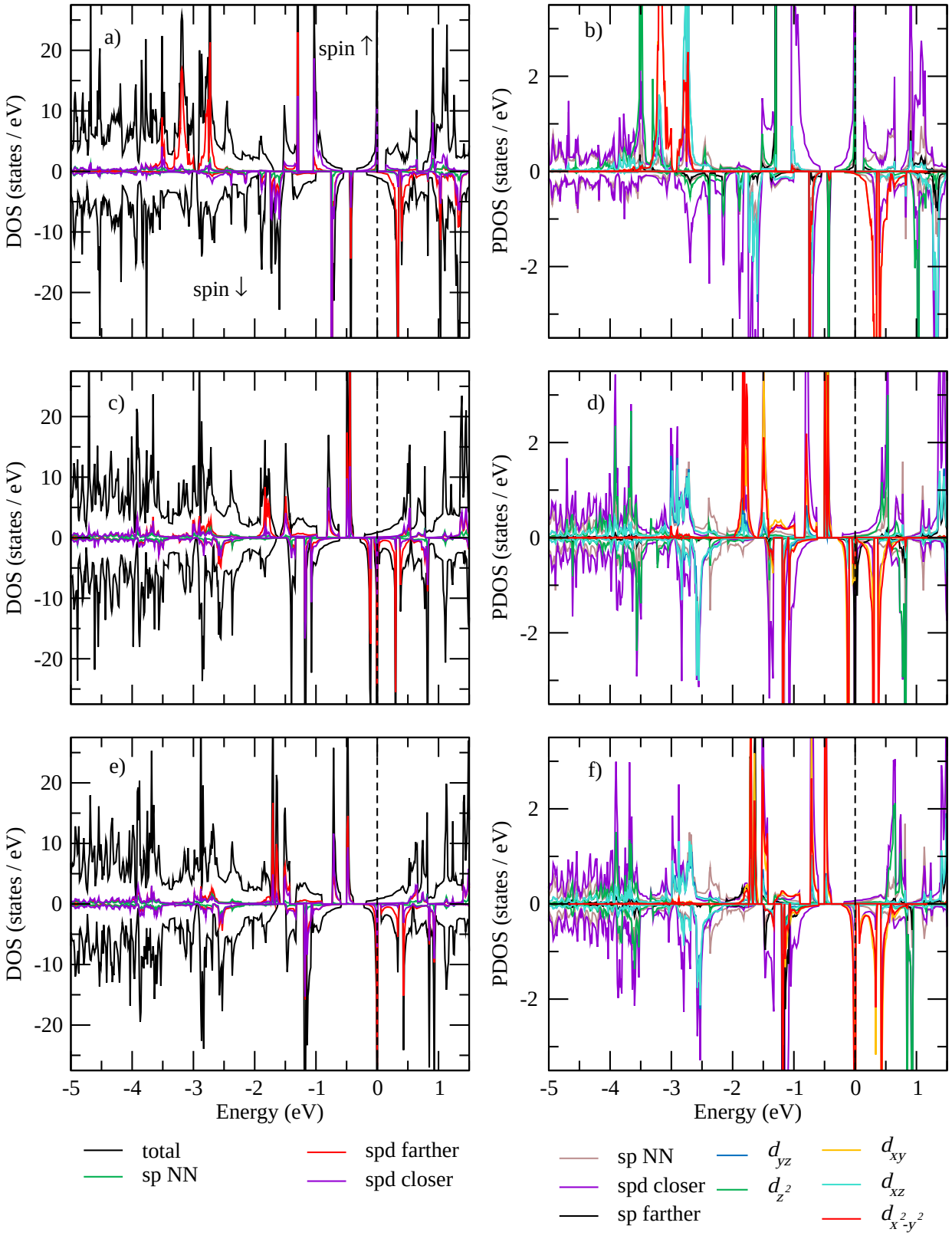


**FIG. A16:** DOS and PDOS plots. FeRu@NSV (a) and (b); RuRu@NSV (c) and (d); OsRu@NSV (e) and (f).

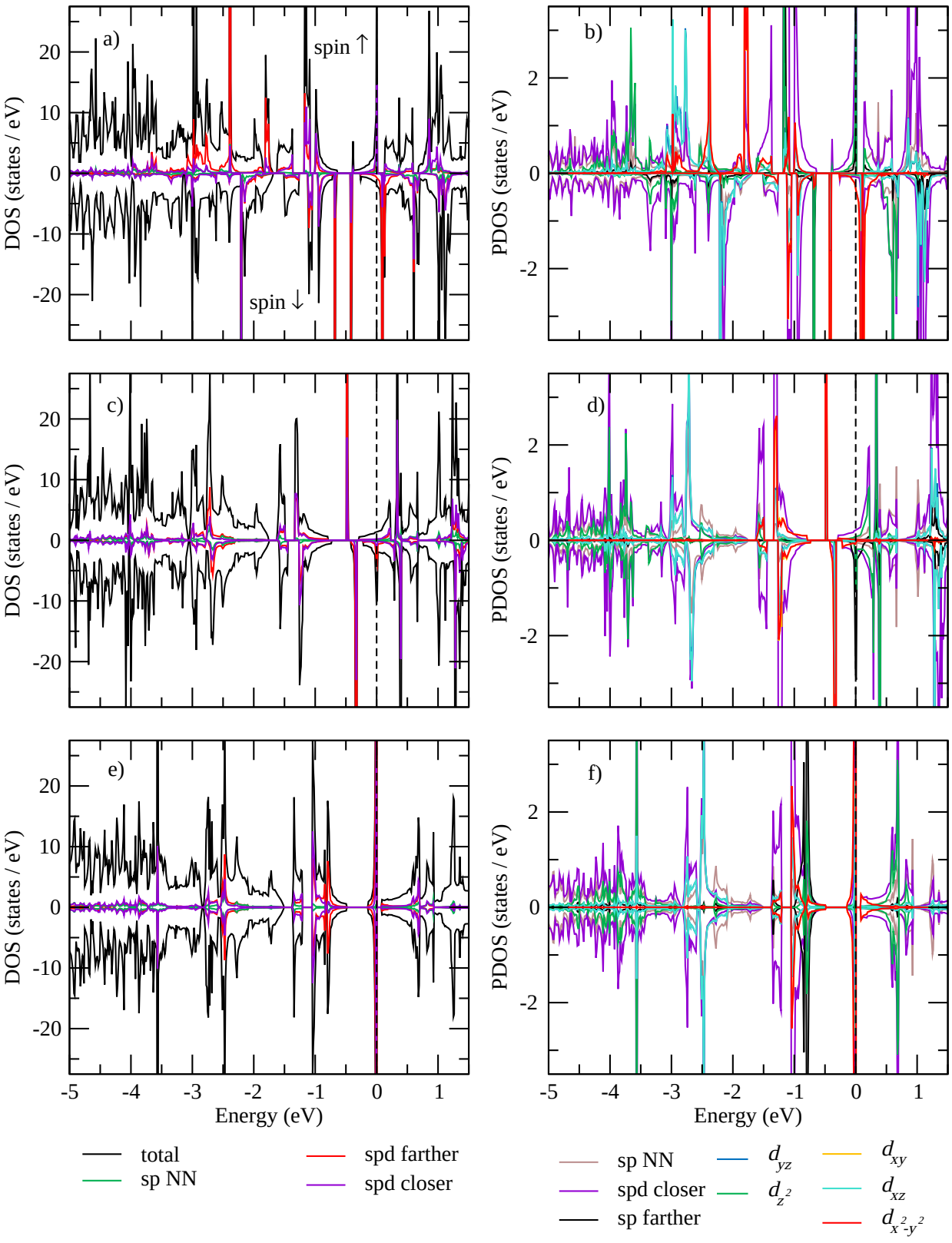


**FIG. A17:** DOS and PDOS plots. CoRu@NSV (a) and (b); RhRu@NSV (c) and (d); IrRu@NSV (e) and (f).

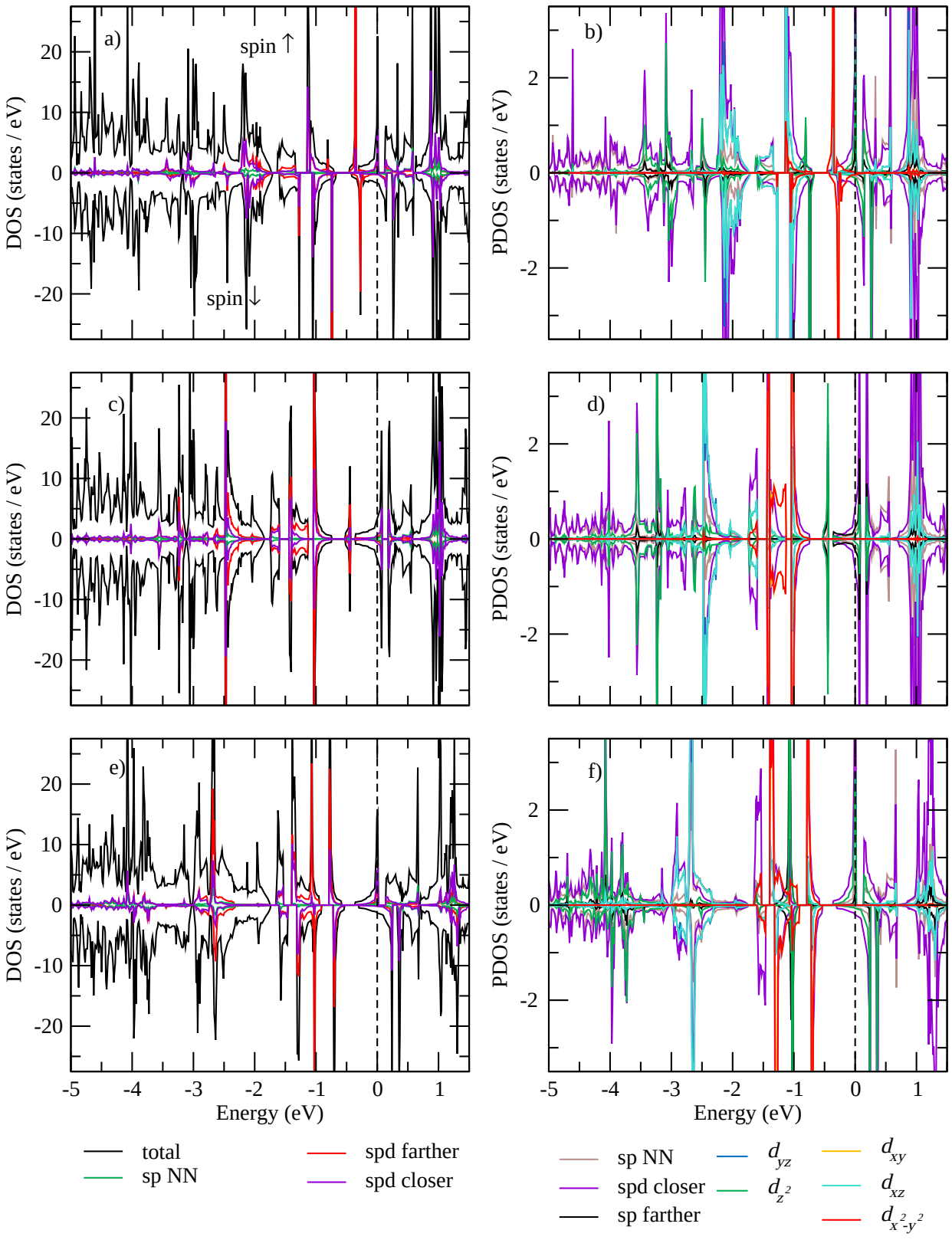


**FIG. A18:** DOS and PDOS plots. NiRu@NSV (a) and (b); PdRu@NSV (c) and (d); PtRu@NSV (e) and (f).

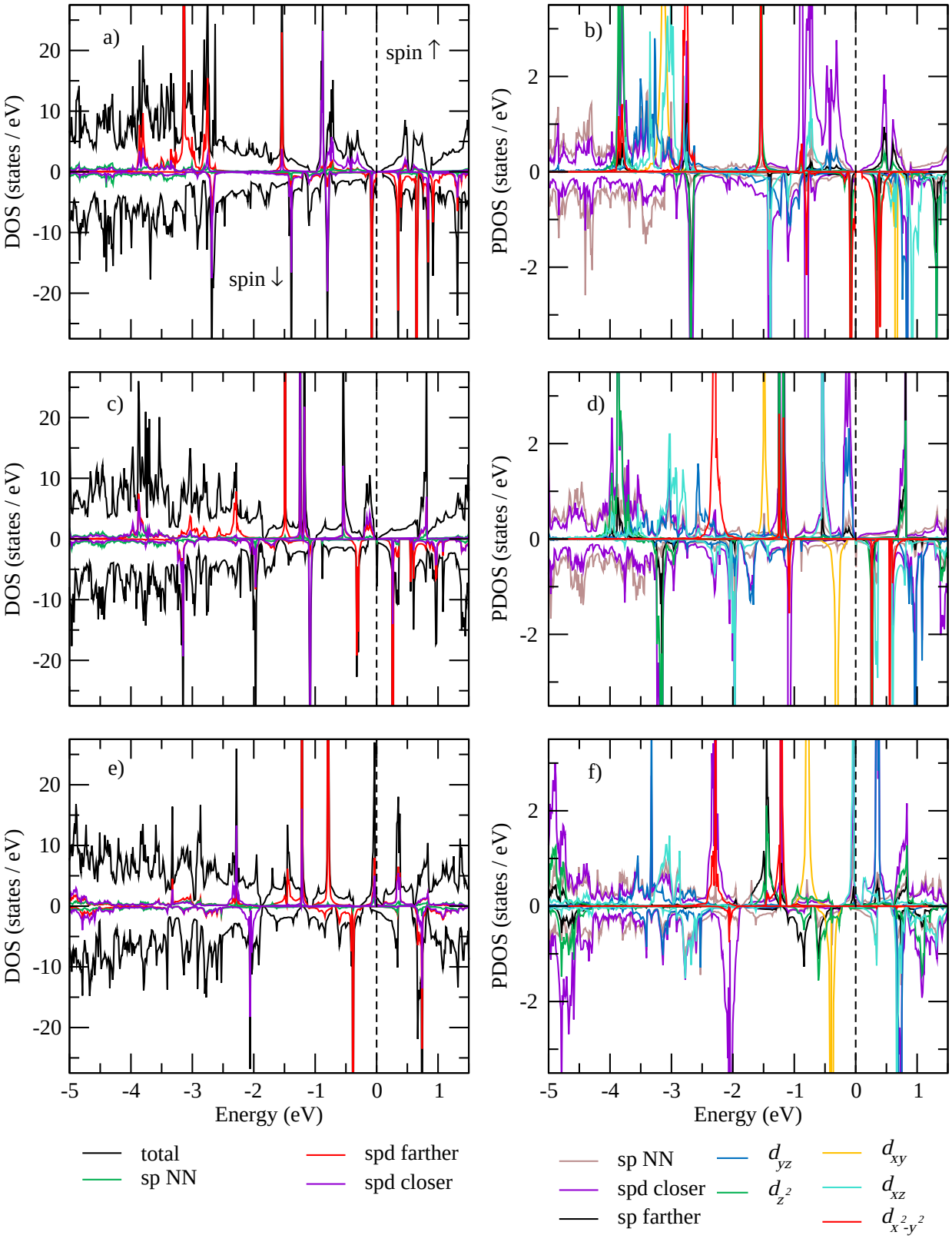


**FIG. A19:** DOS and PDOS plots. FeRu@NDV (a) and (b); RuRu@NDV (c) and (d); OsRu@NDV (e) and (f).

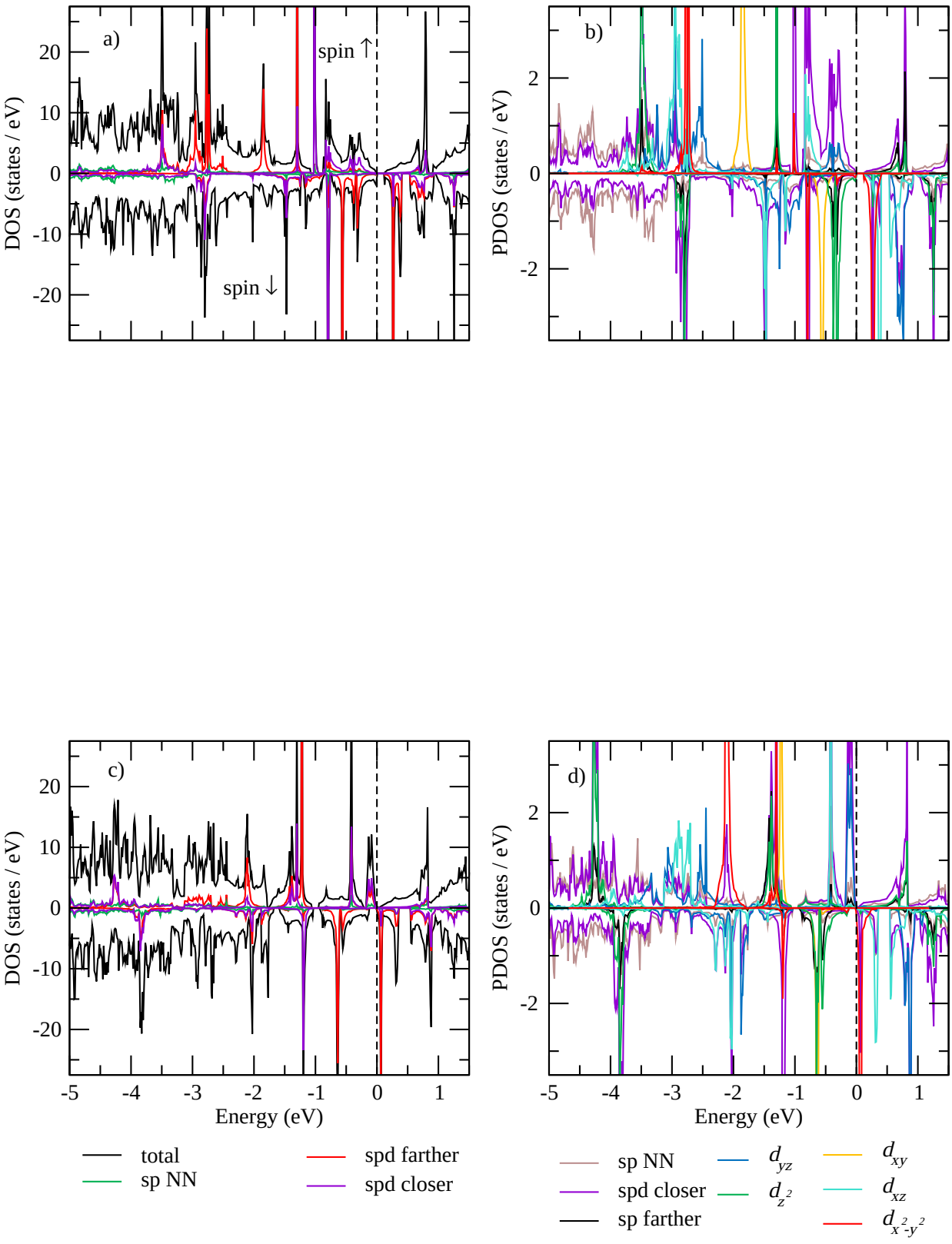


**FIG. A20:** DOS and PDOS plots. CoRu@NDV (a) and (b); IrRu@NDV (c) and (d).

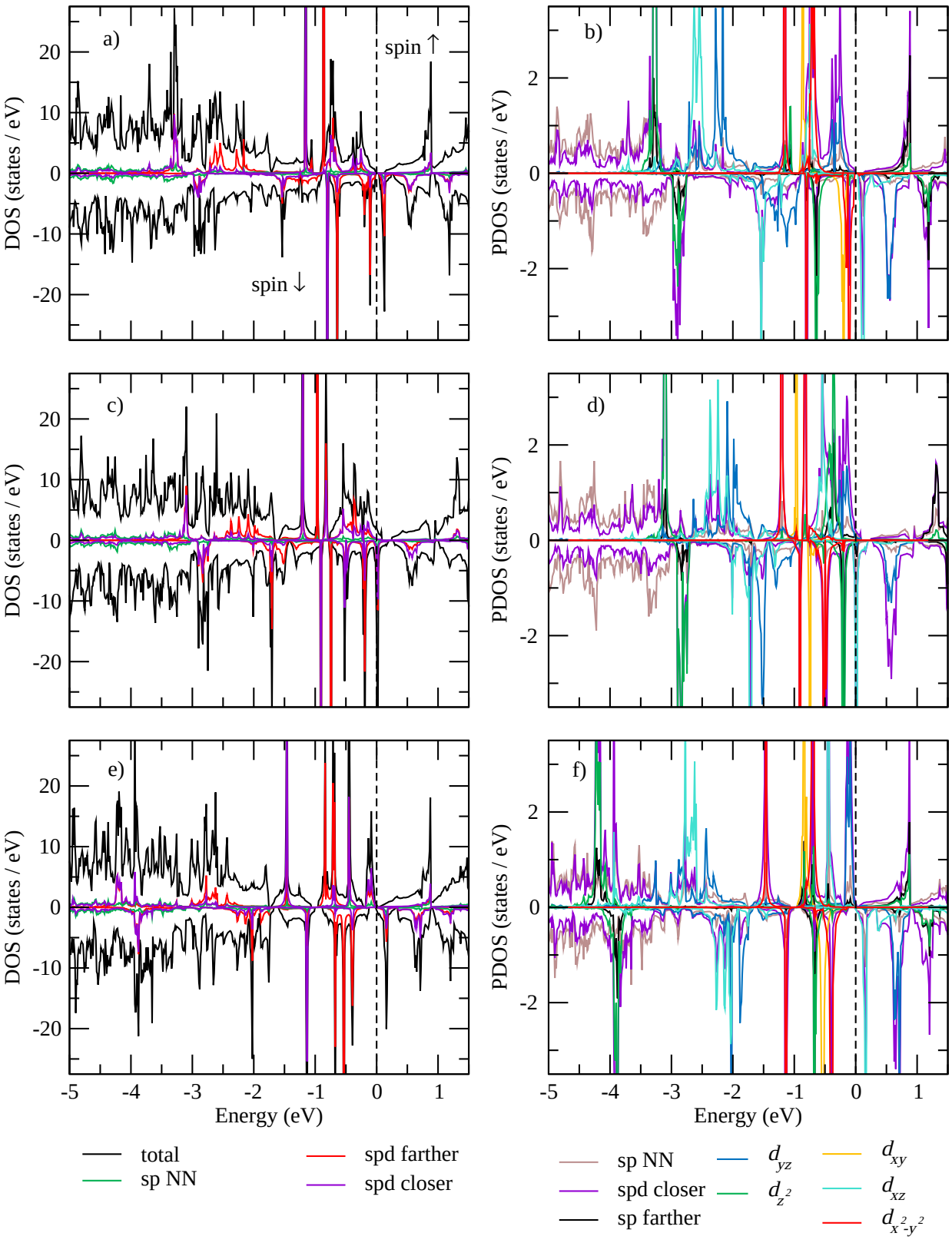


**FIG. A21:** DOS and PDOS plots. NiRu@NDV (a) and (b); PdRu@NDV (c) and (d); PtRu@NDV (e) and (f).

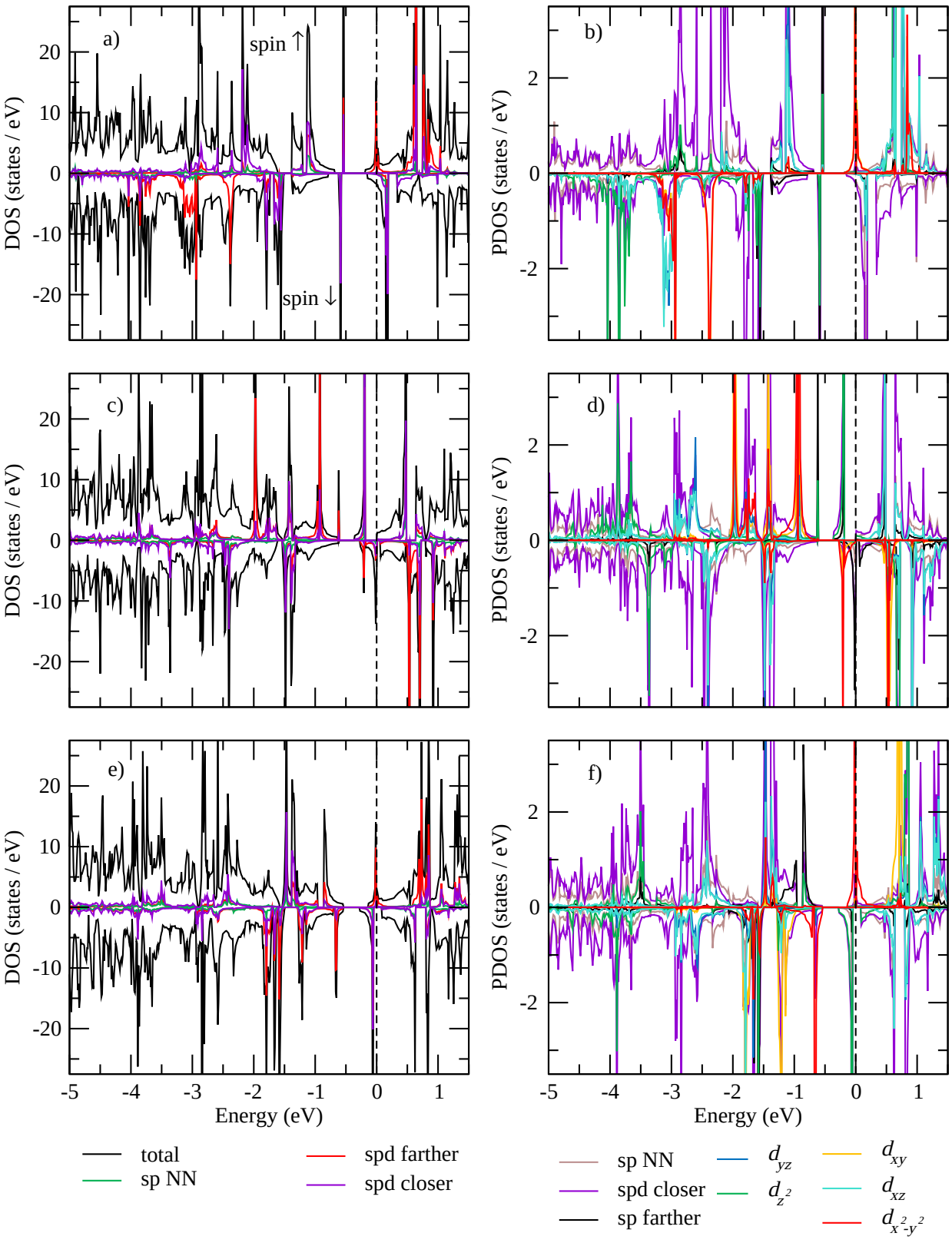


**FIG. A22:** DOS and PDOS plots. FeRh@NSV (a) and (b); RuRh@NSV (c) and (d); OsRh@NSV (e) and (f).

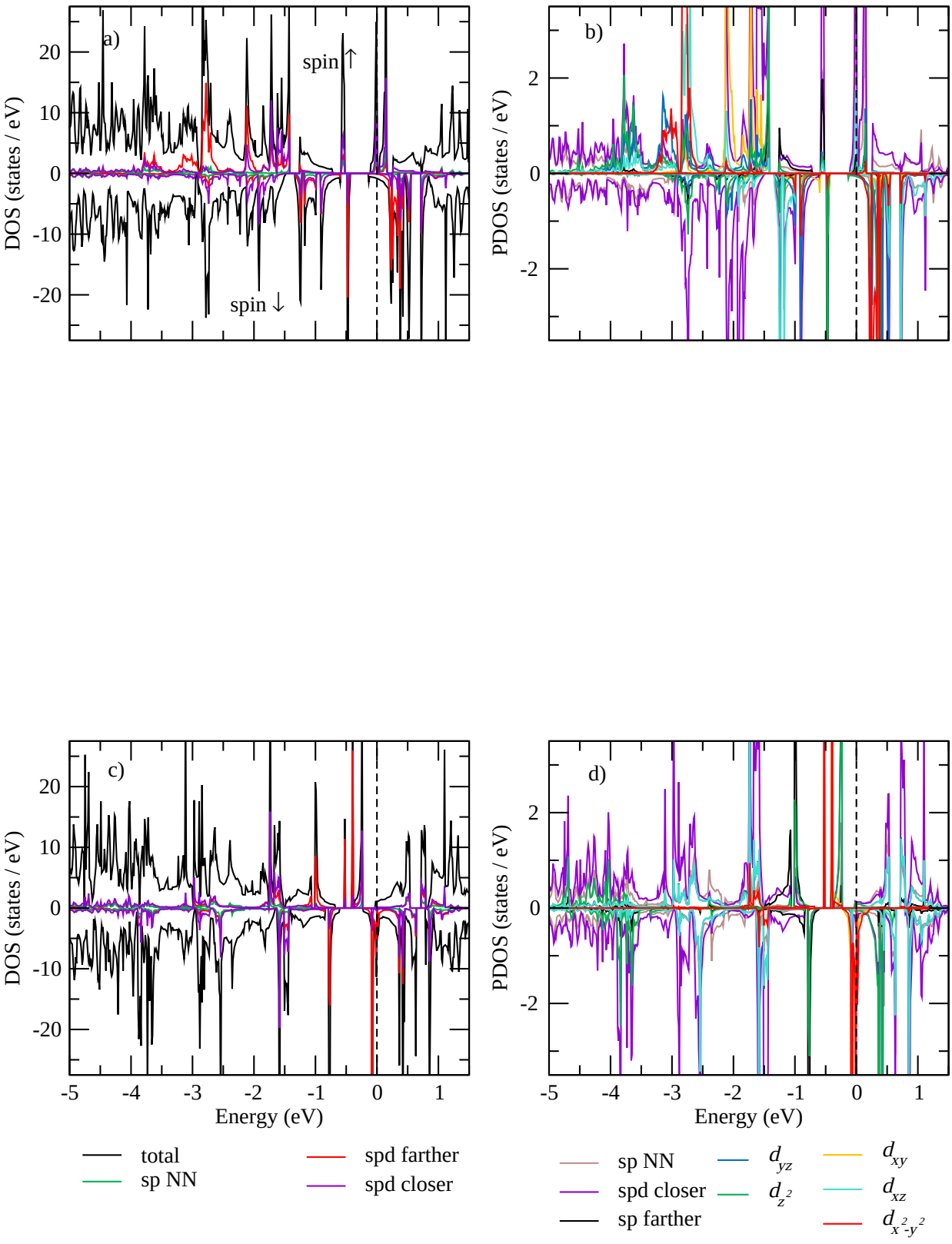


**FIG. A23:** DOS and PDOS plots. CoRh@NSV (a) and (b); IrRh@NSV (c) and (d).

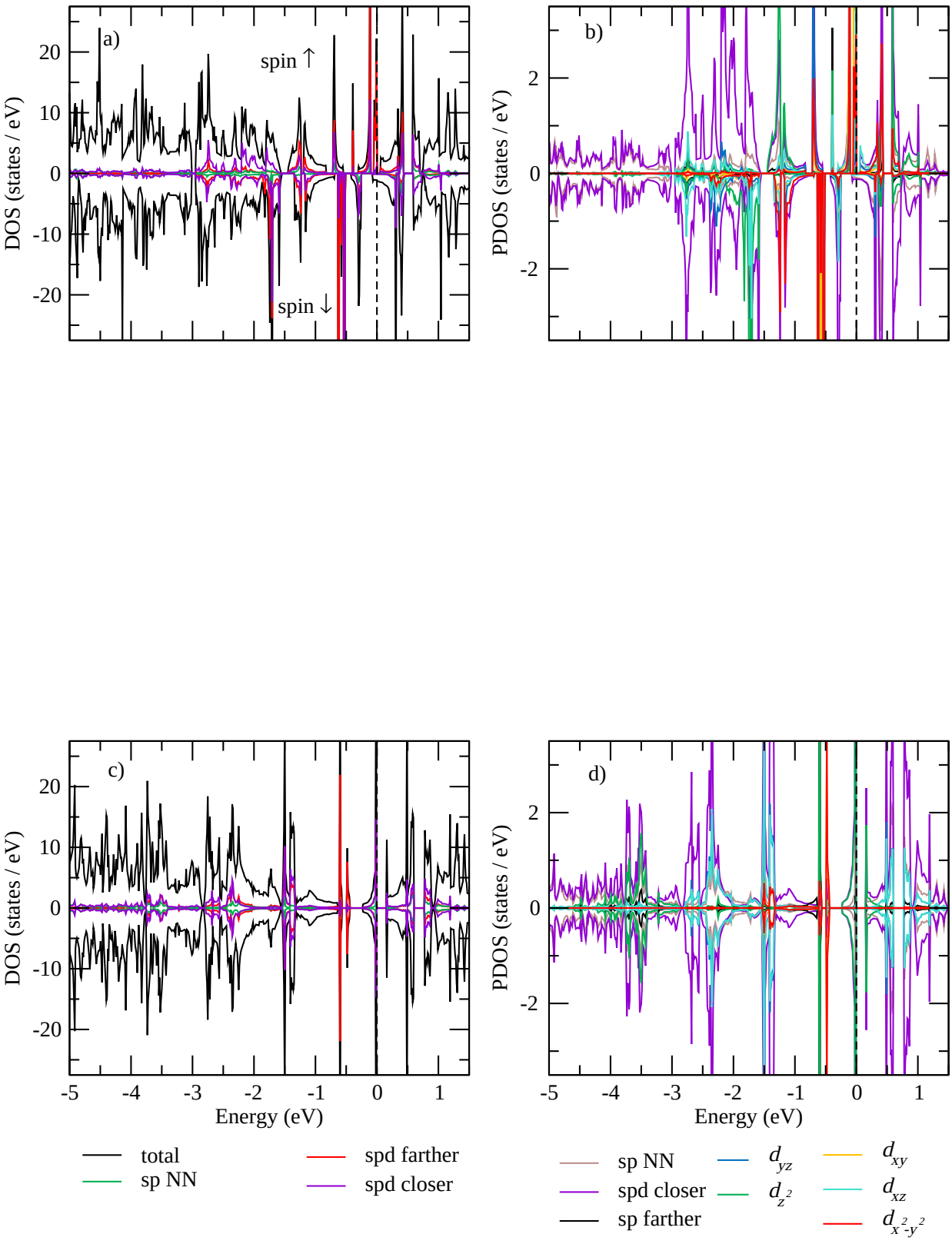


**FIG. A24:** DOS and PDOS plots. NiRh@NSV (a) and (b); PtRh@NSV (c) and (d).

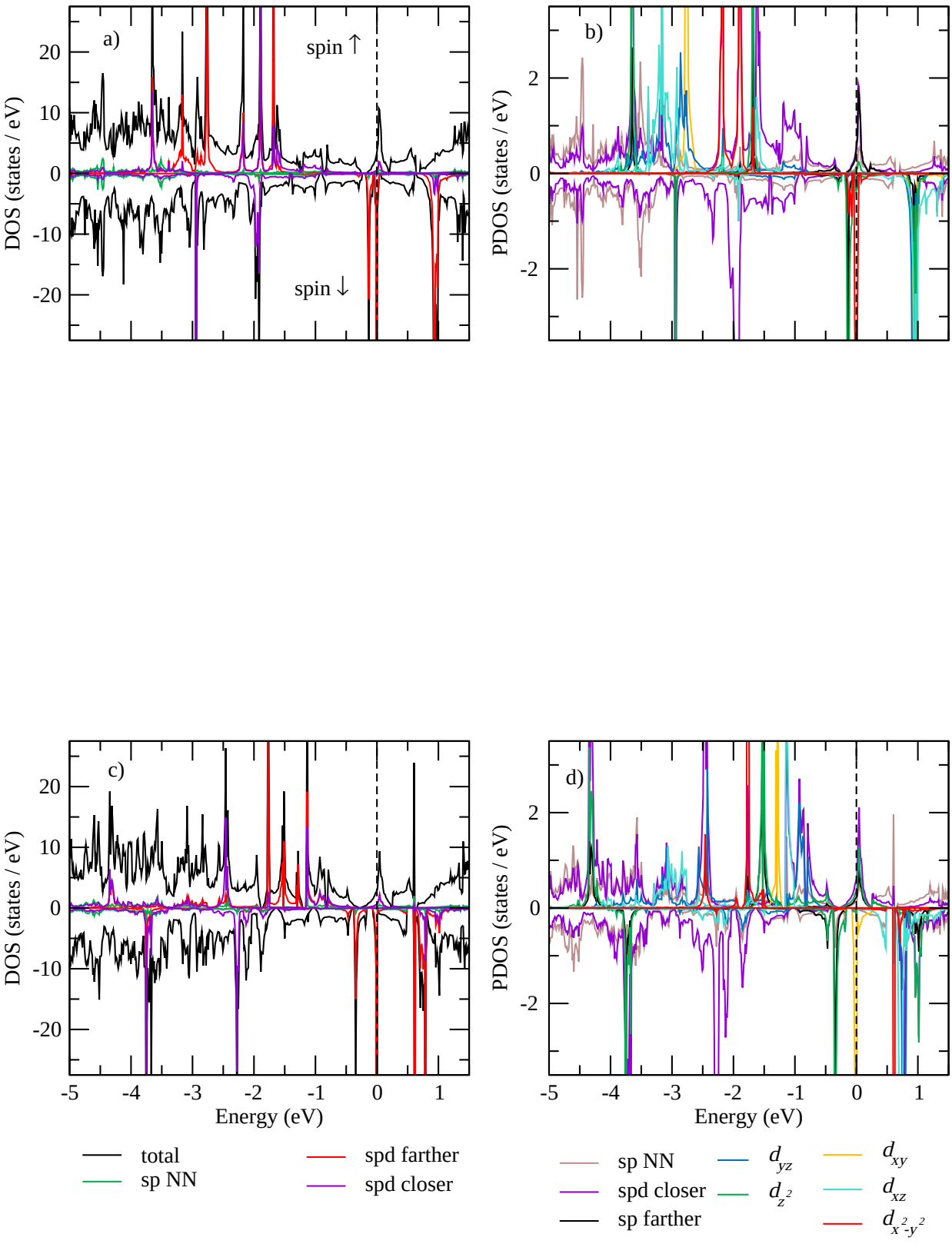


**FIG. A25:** DOS and PDOS plots. FeRh@NDV (a) and (b); OsRh@NDV (c) and (d).

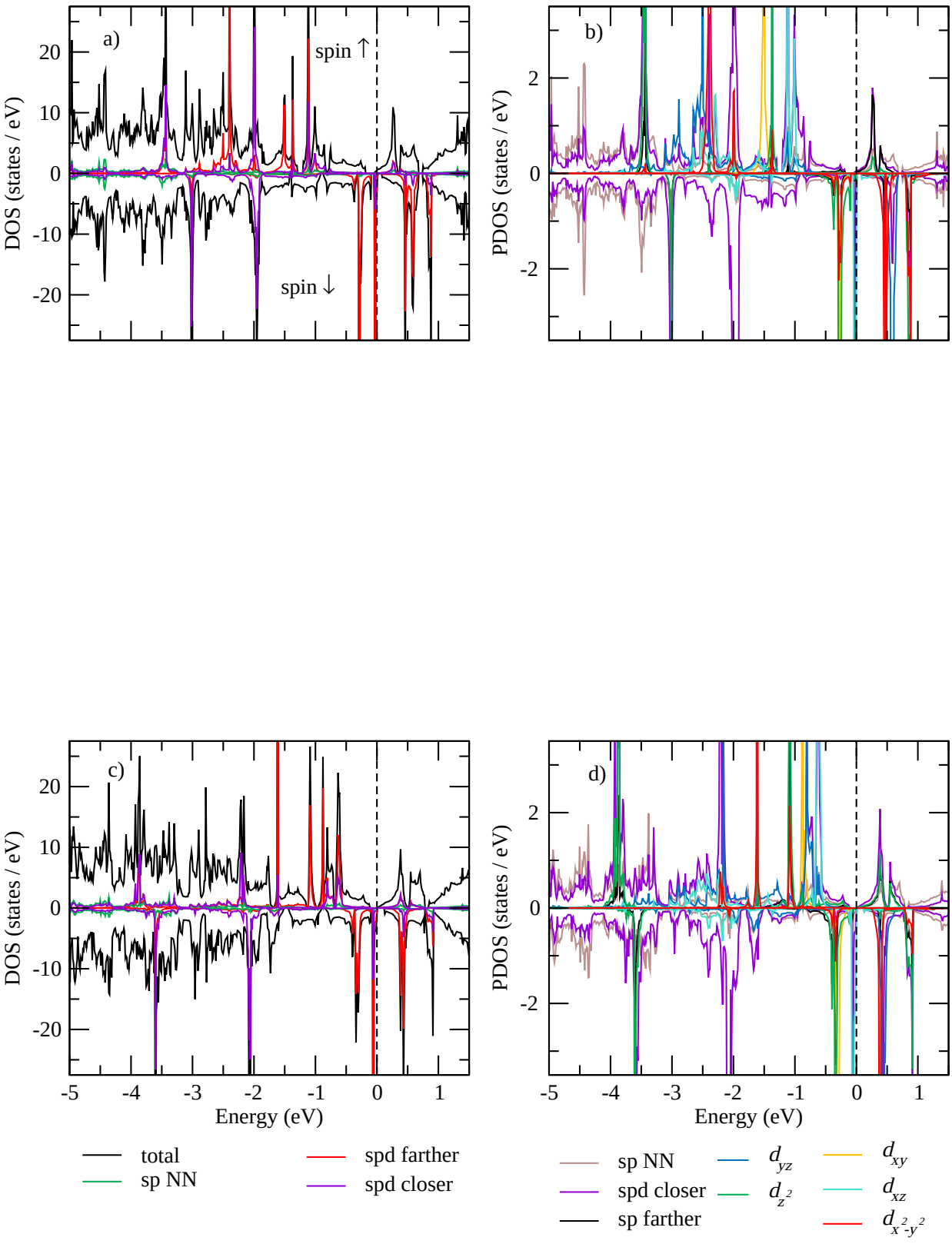


**FIG. A26:** DOS and PDOS plots. CoRh@NDV (a) and (b); IrRh@NDV (c) and (d).

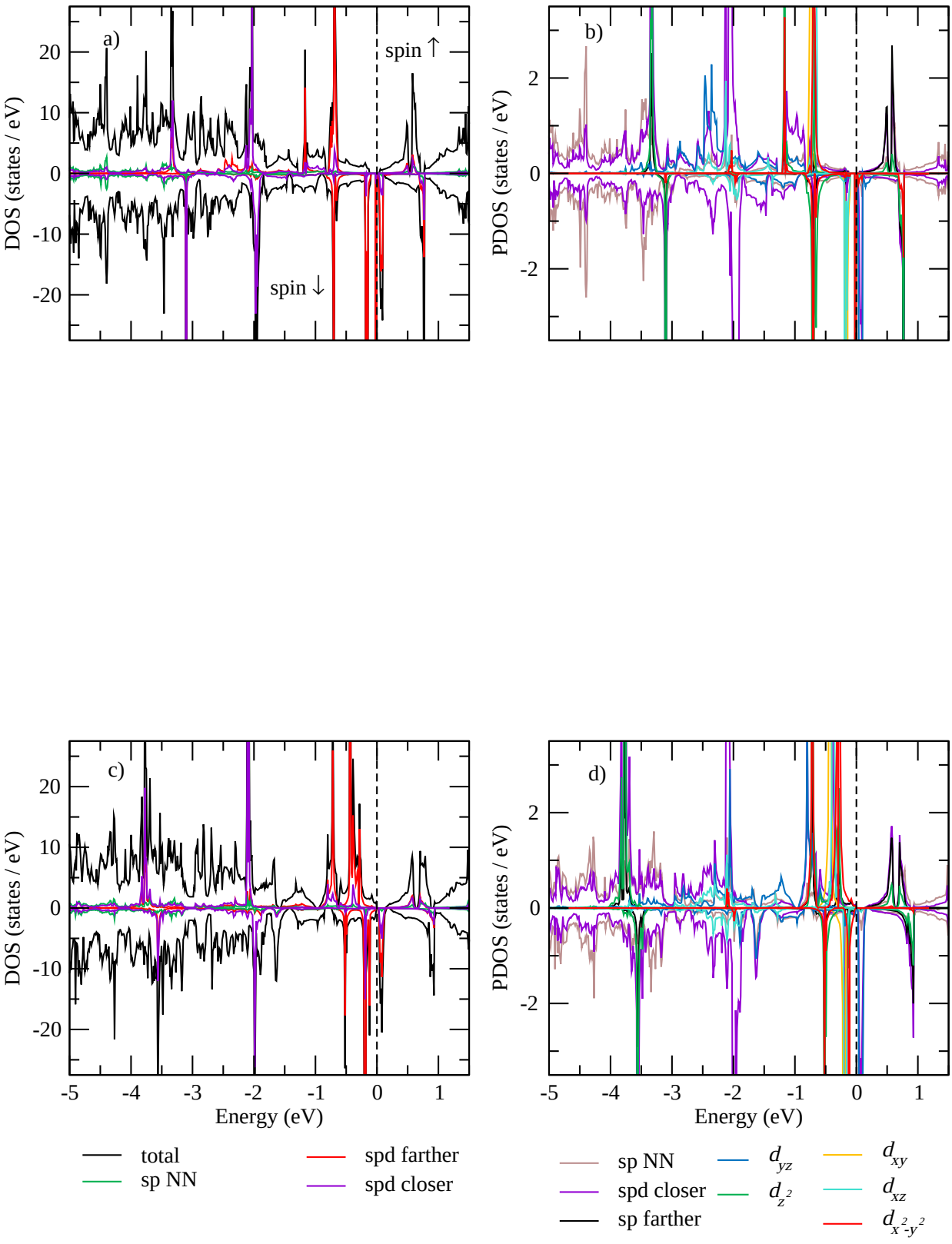


**FIG. A27:** DOS and PDOS plots. NiRh@NDV (a) and (b); PtRh@NDV (c) and (d).

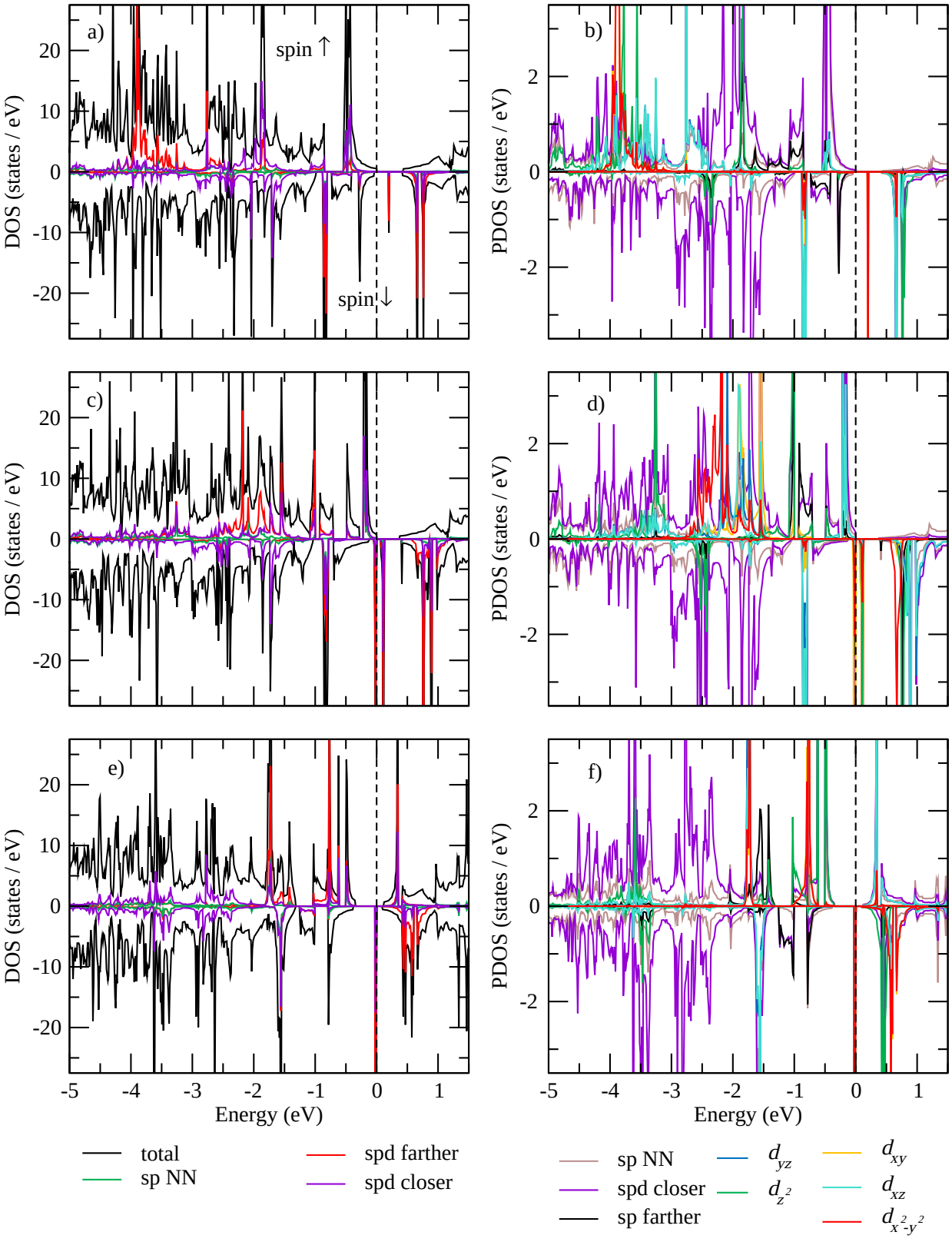


**FIG. A28:** DOS and PDOS plots. FePd@NSV (a) and (b); RuPd@NSV (c) and (d); OsPd@NSV (e) and (f).

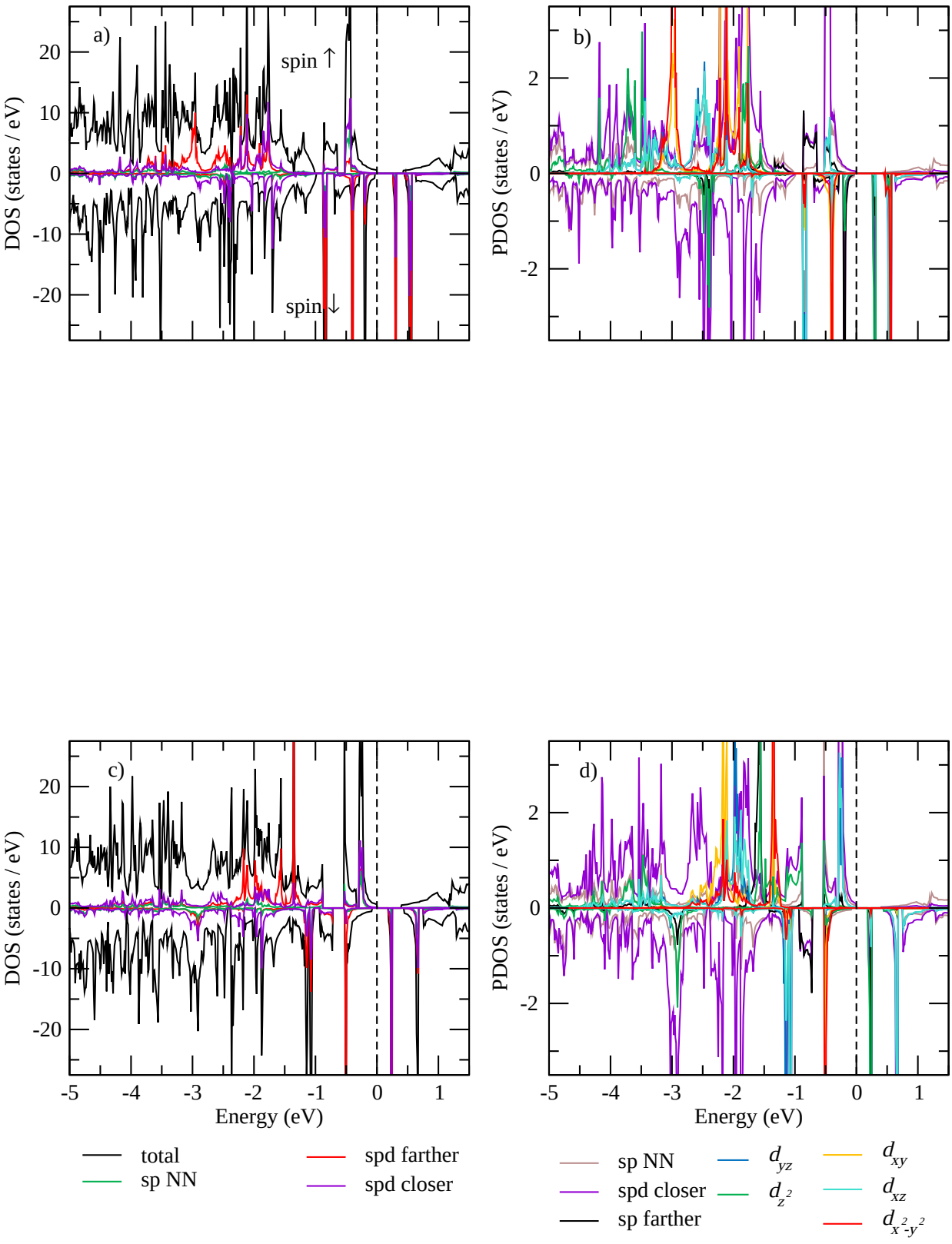


**FIG. A29:** DOS and PDOS plots. CoPd@NSV (a) and (b); IrPd@NSV (c) and (d).

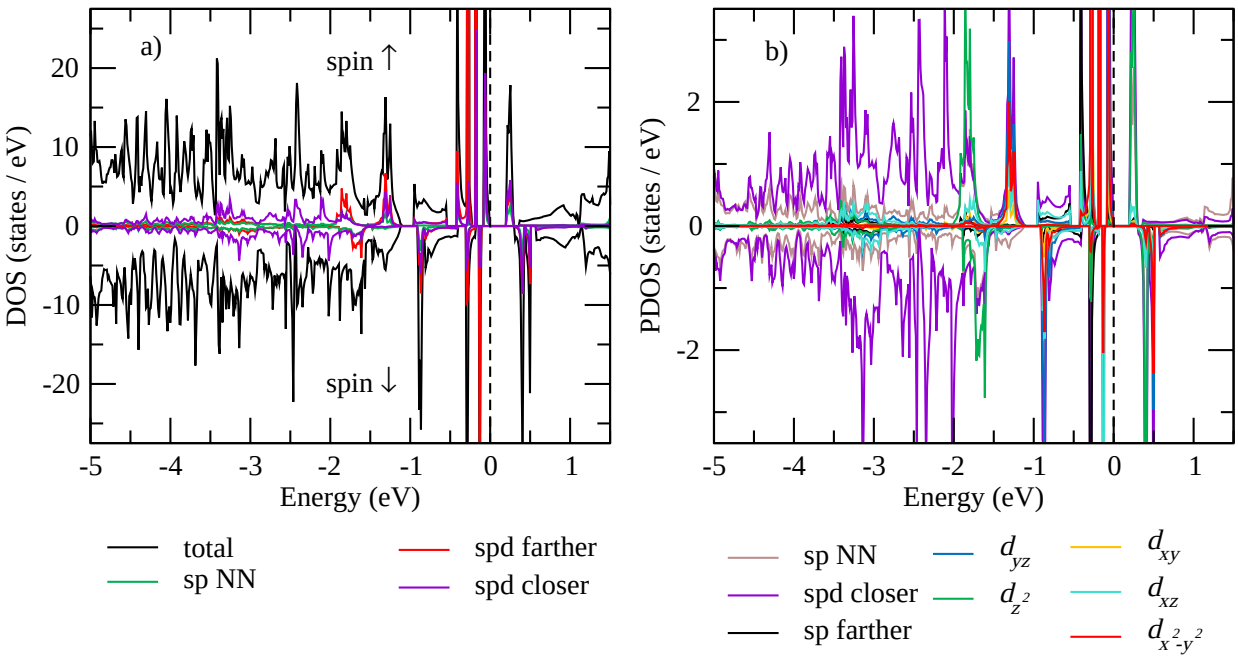


**FIG. A30:** DOS and PDOS plots. PtPd@NSV (a) and (b).

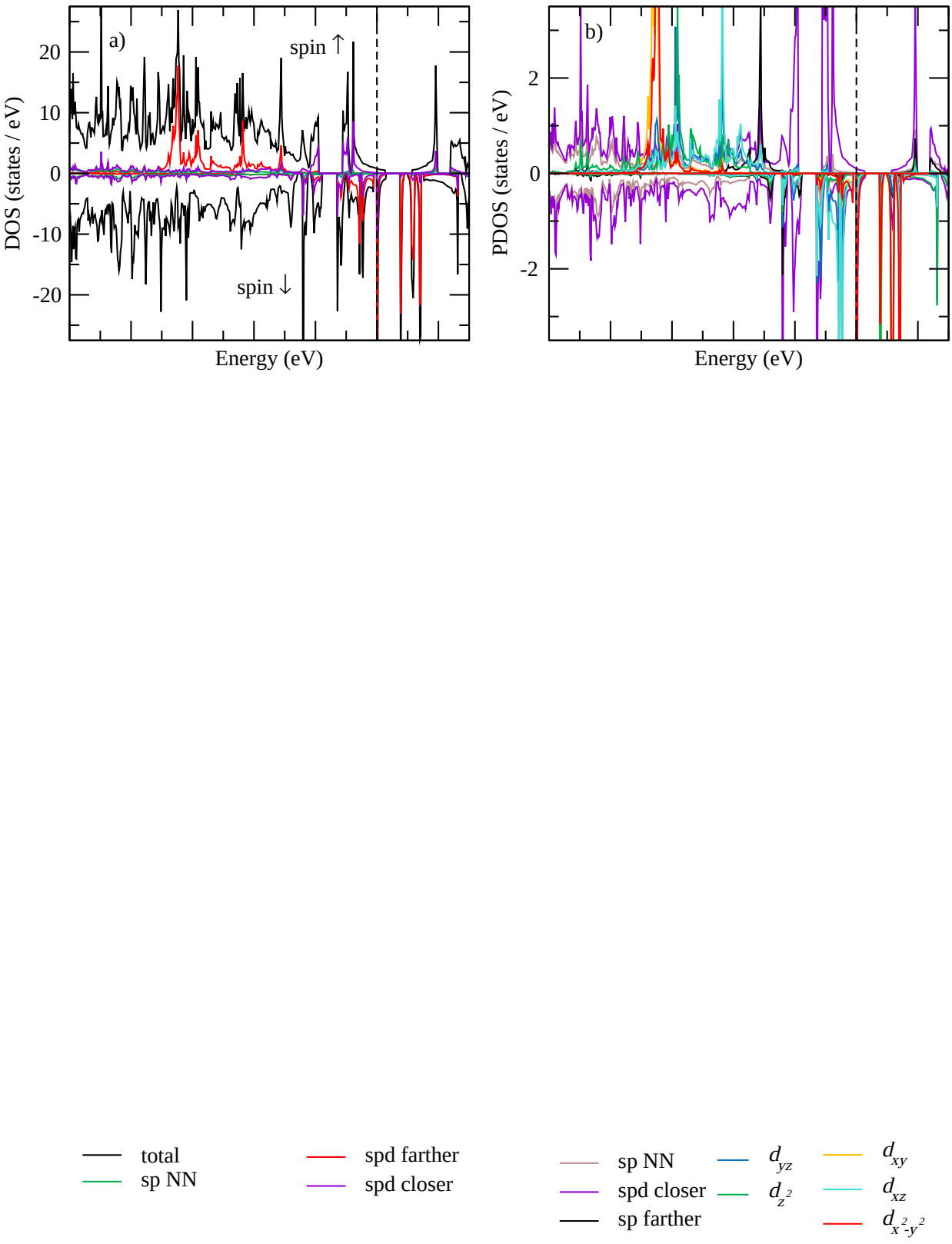


**FIG. A31:** DOS and PDOS plots. FeOs@SV (a) and (b).

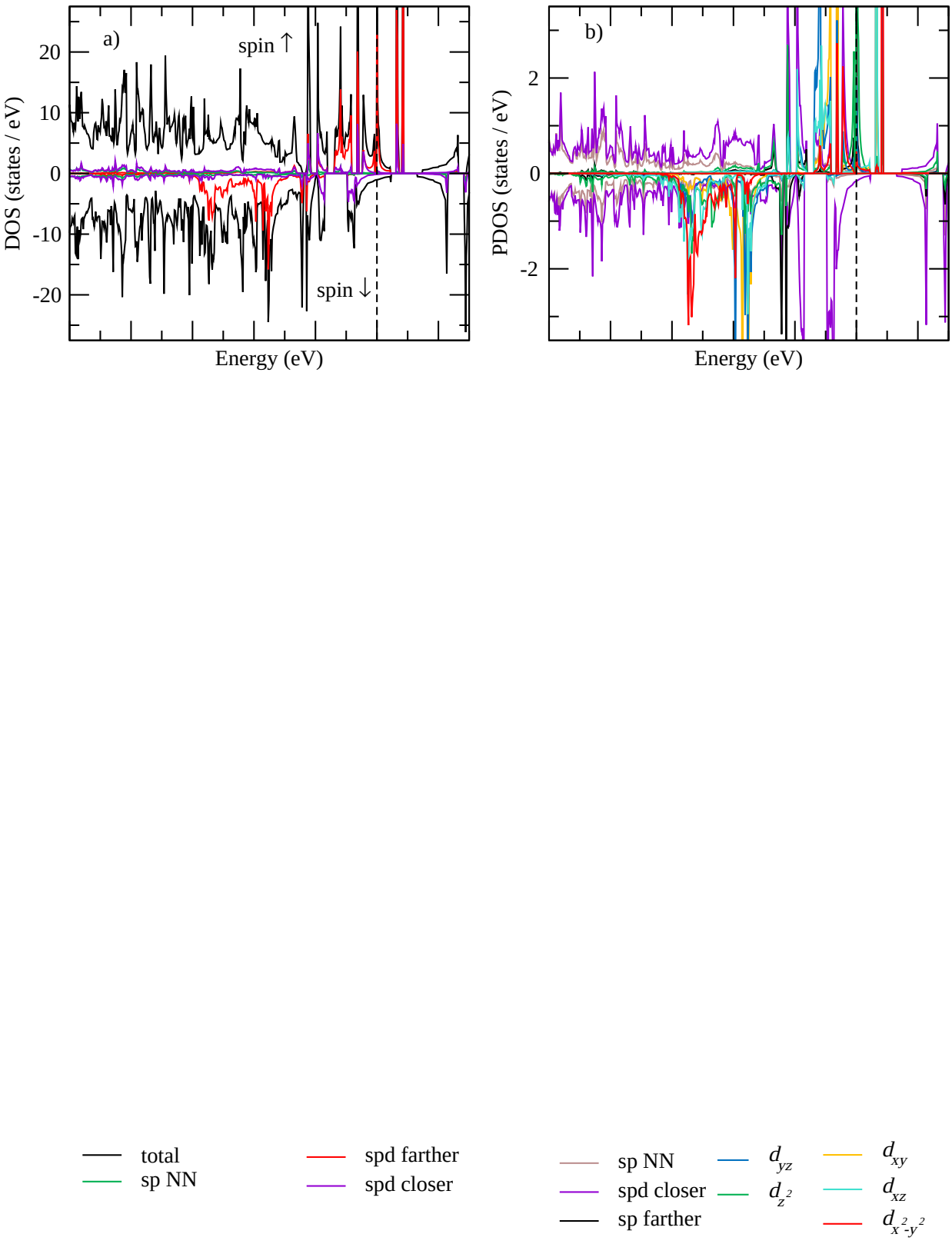


**FIG. A32:** DOS and PDOS plots. CoOs@SV (a) and (b).

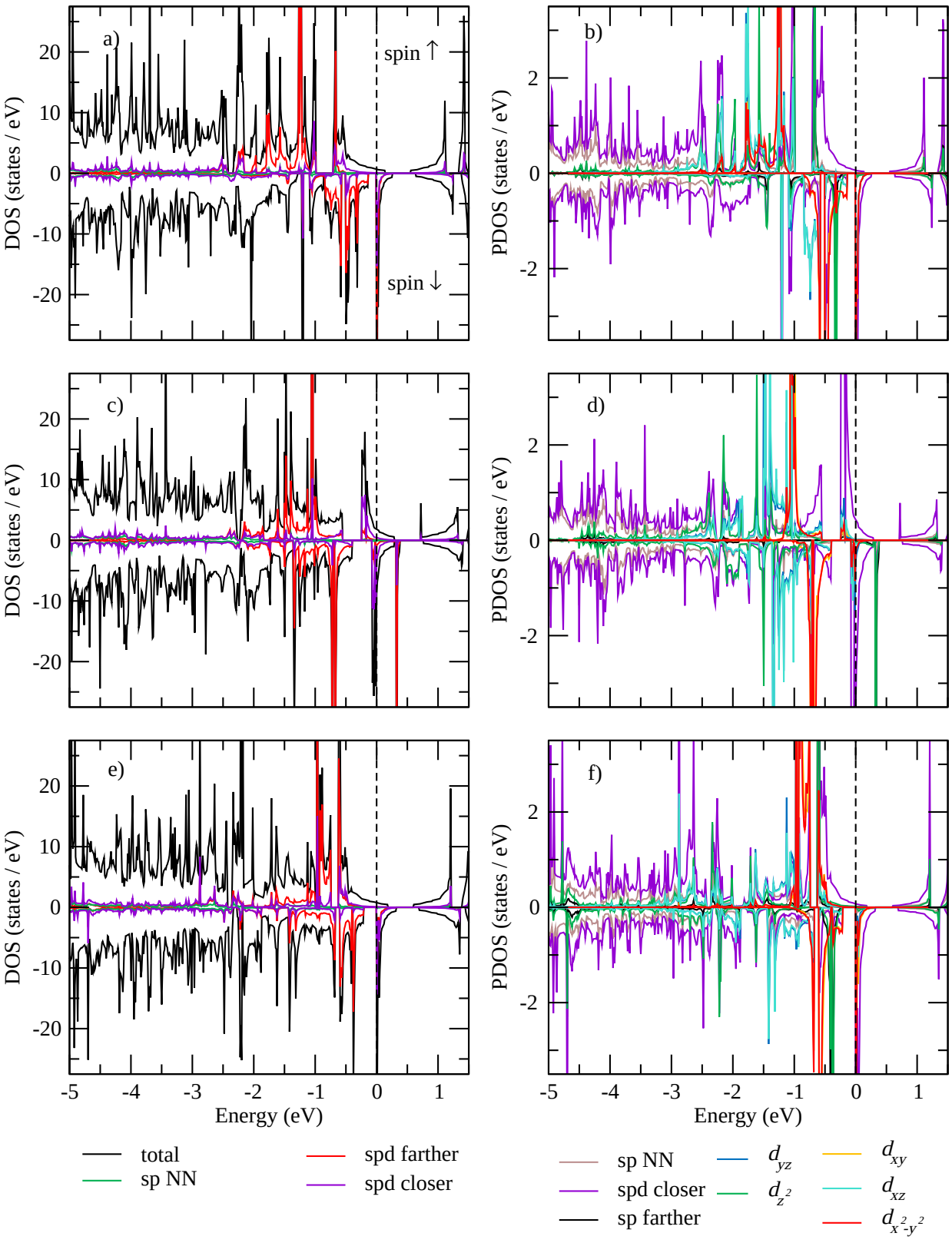


**FIG. A33:** DOS and PDOS plots. NiOs@SV (a) and (b); PdOs@SV (c) and (d); PtOs@SV (e) and (f).

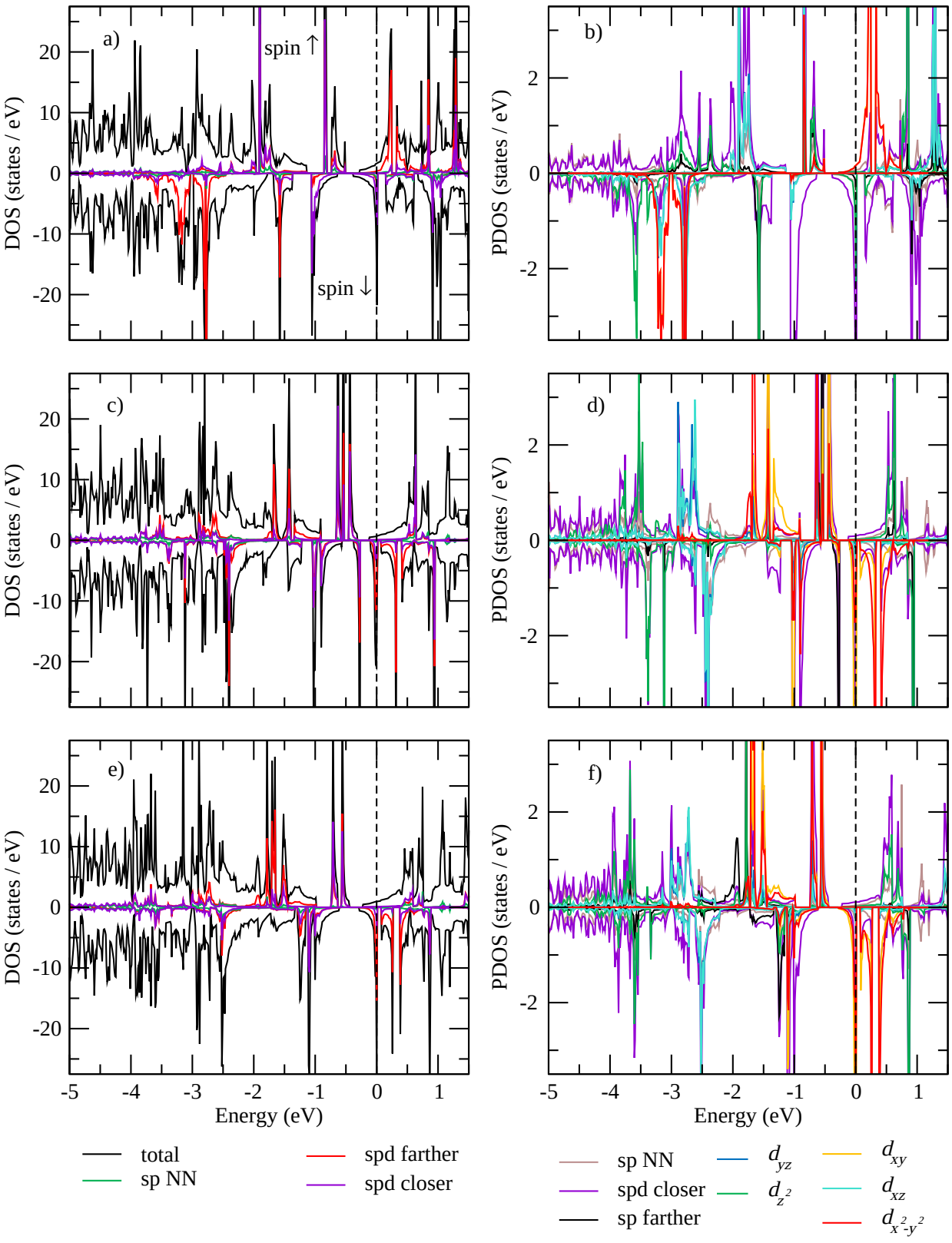


**FIG. A34:** DOS and PDOS plots. FeOs@NSV (a) and (b); RuOs@NSV (c) and (d); OsOs@NSV (e) and (f).

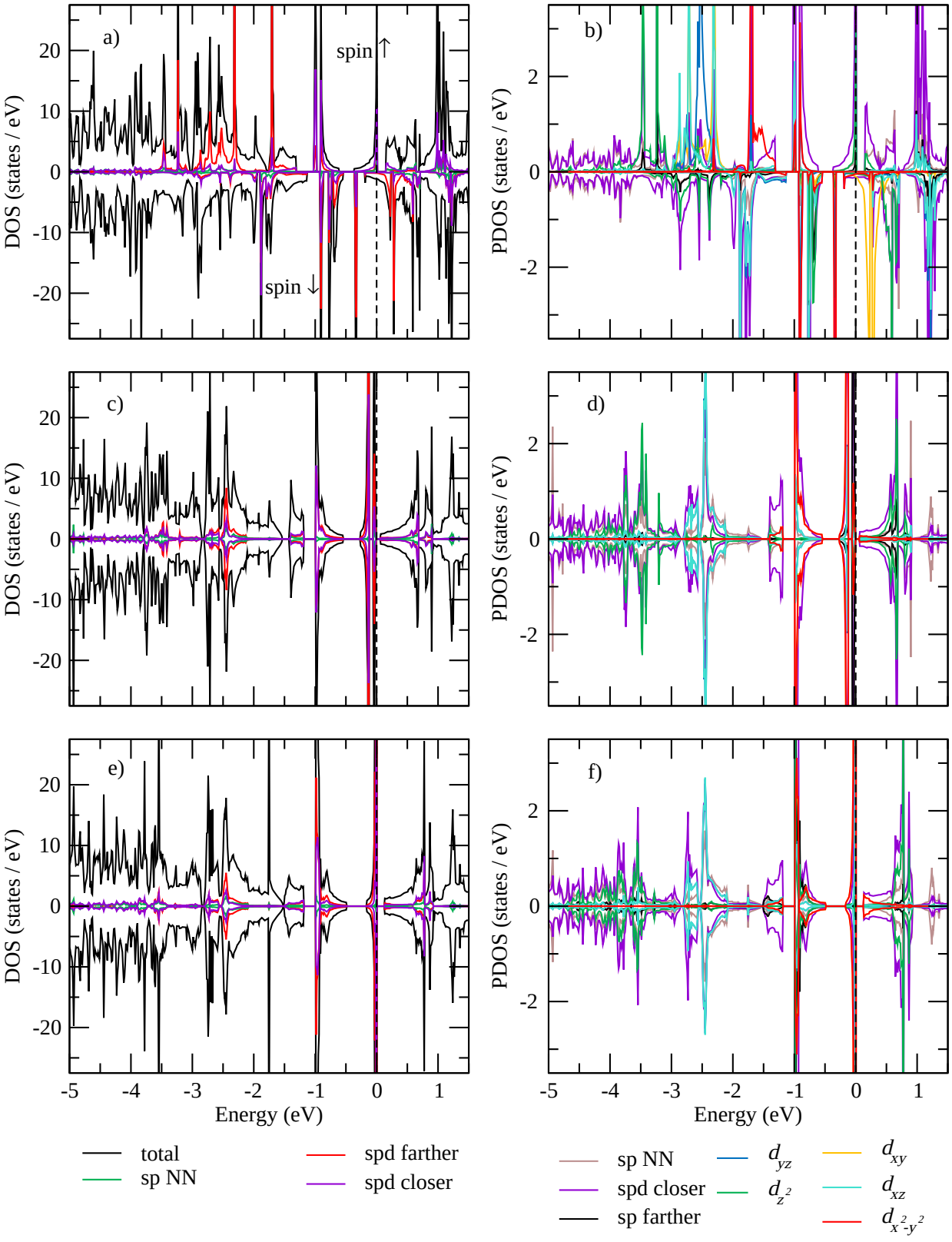


**FIG. A35:** DOS and PDOS plots. CoOs@NSV (a) and (b); RhOs@NSV (c) and (d); IrOs@NSV (e) and (f).

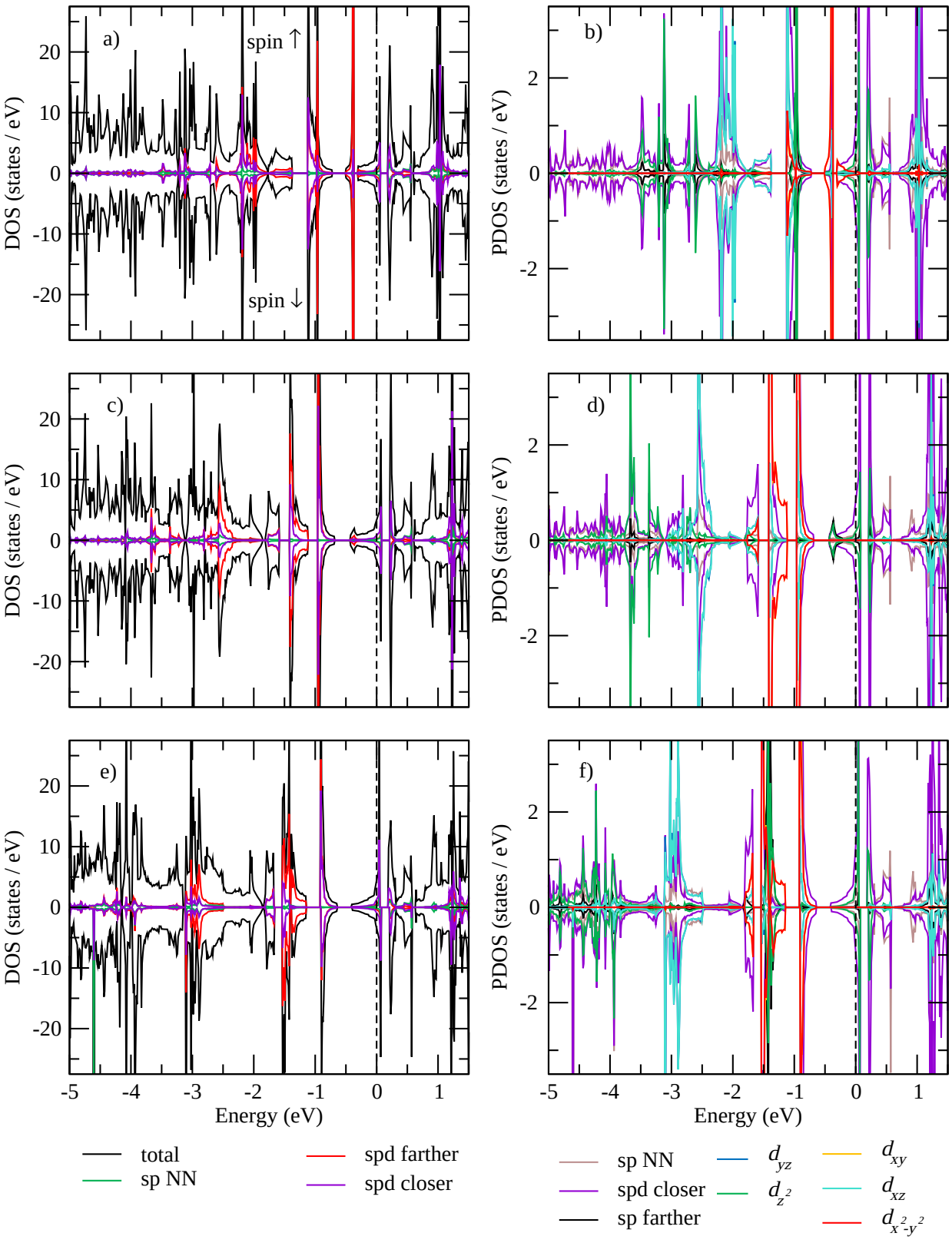


**FIG. A36:** DOS and PDOS plots. NiOs@NSV (a) and (b); PdOs@NSV (c) and (d); PtOs@NSV (e) and (f).

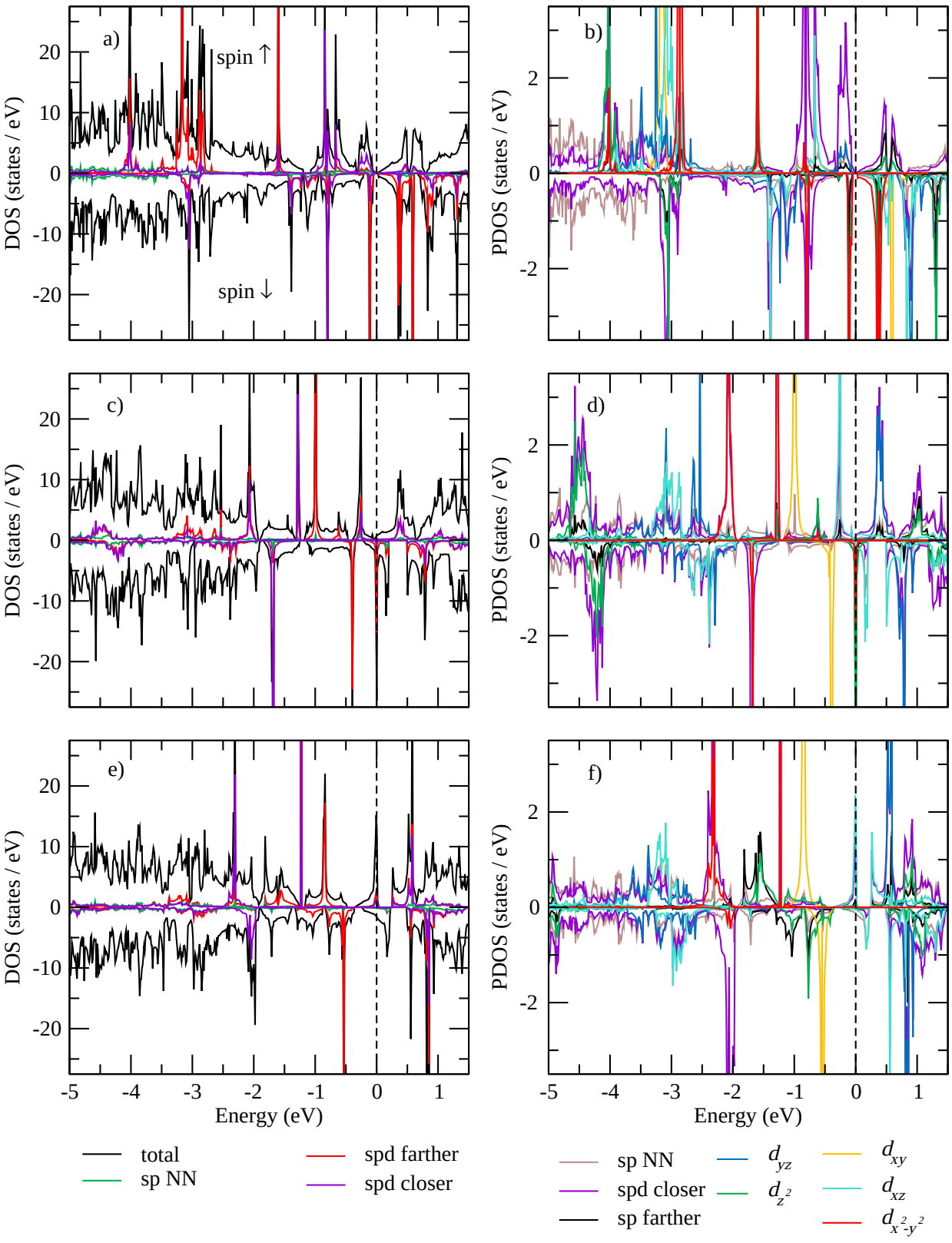


**FIG. A37:** DOS and PDOS plots. FeOs@NDV (a) and (b); RuOs@NDV (c) and (d); OsOs@NDV (e) and (f).

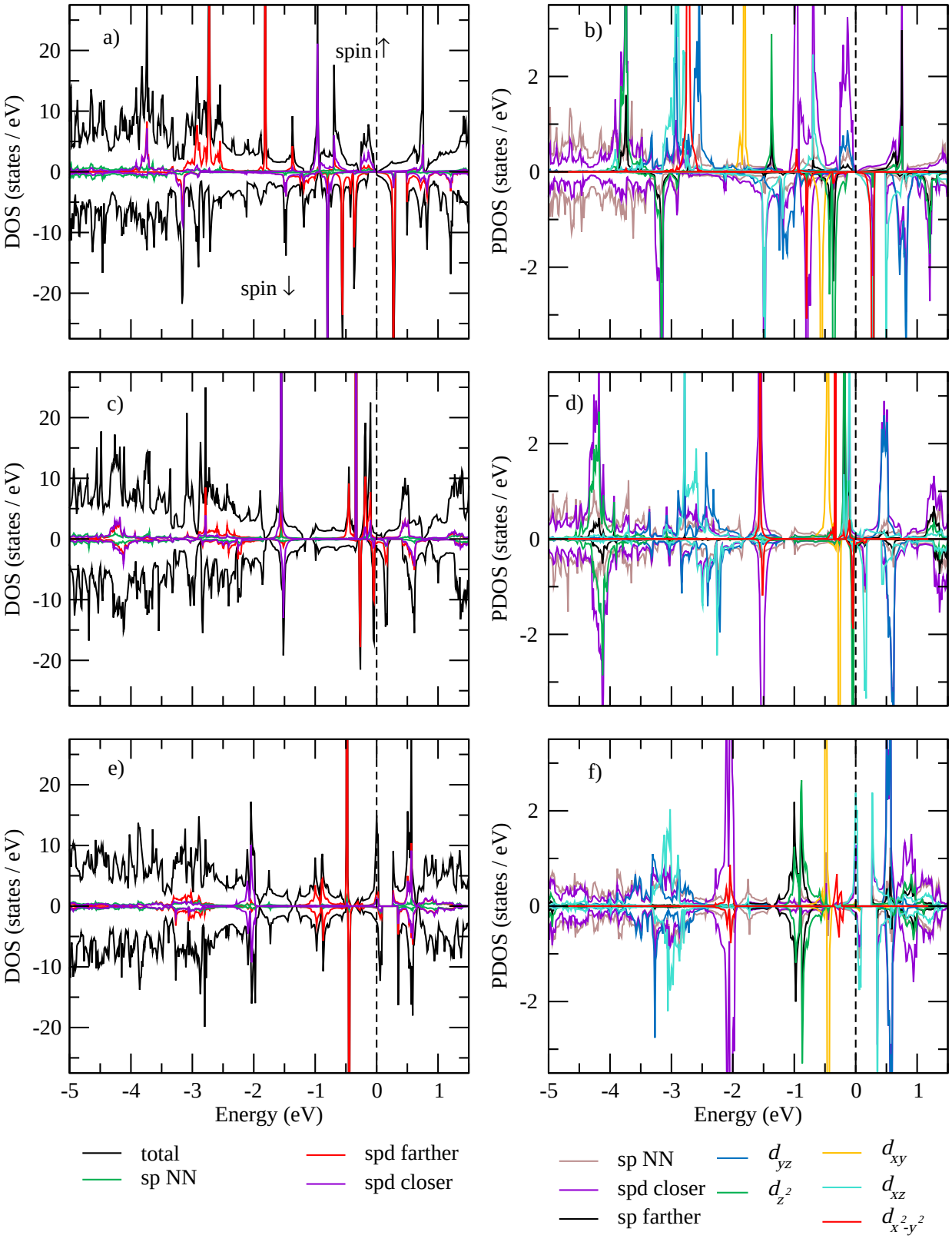


**FIG. A38:** DOS and PDOS plots. CoOs@NDV (a) and (b); RhOs@NDV (c) and (d); IrOs@NDV (e) and (f).

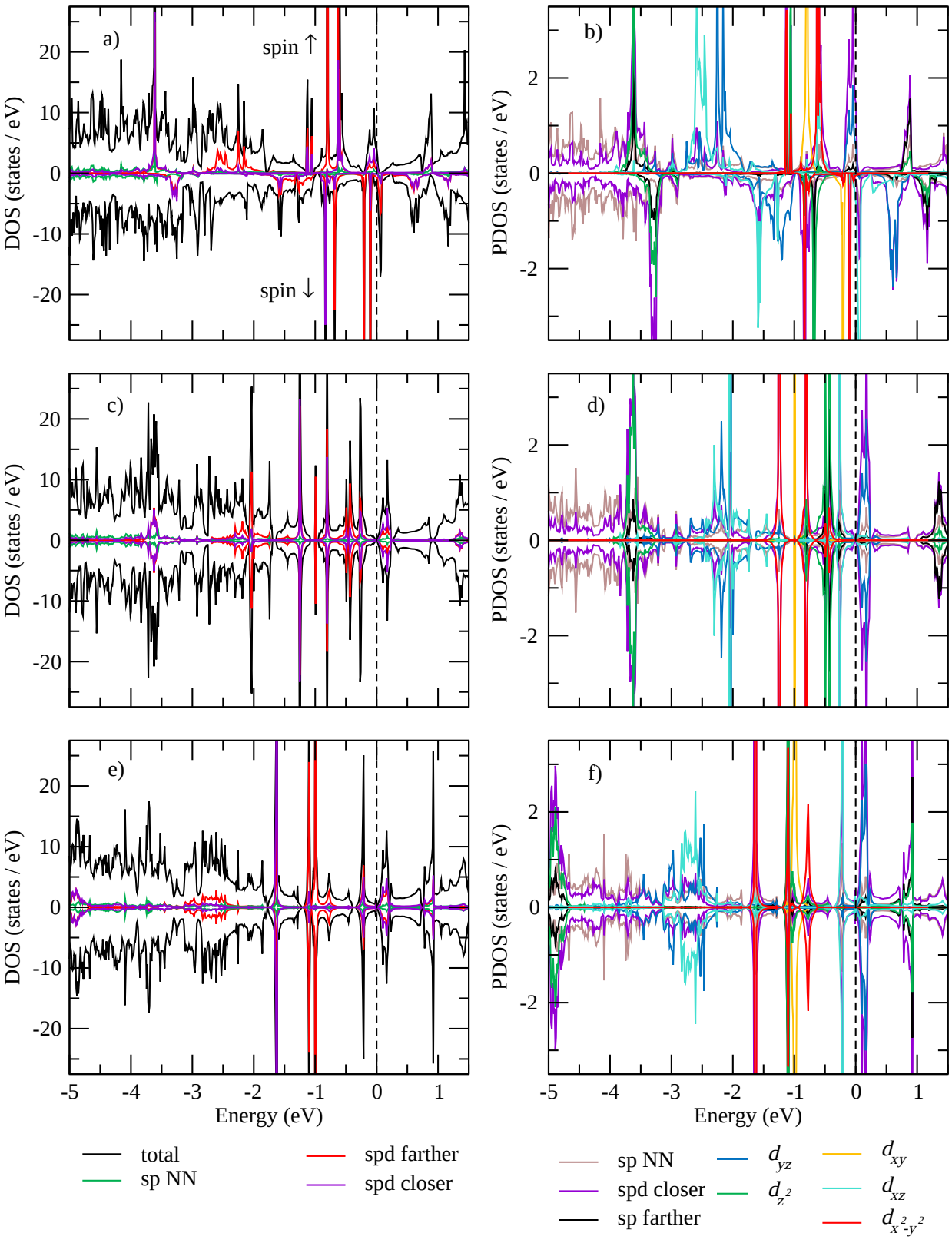


**FIG. A39:** DOS and PDOS plots. NiOs@NDV (a) and (b); PdOs@NDV (c) and (d); PtOs@NDV (e) and (f).

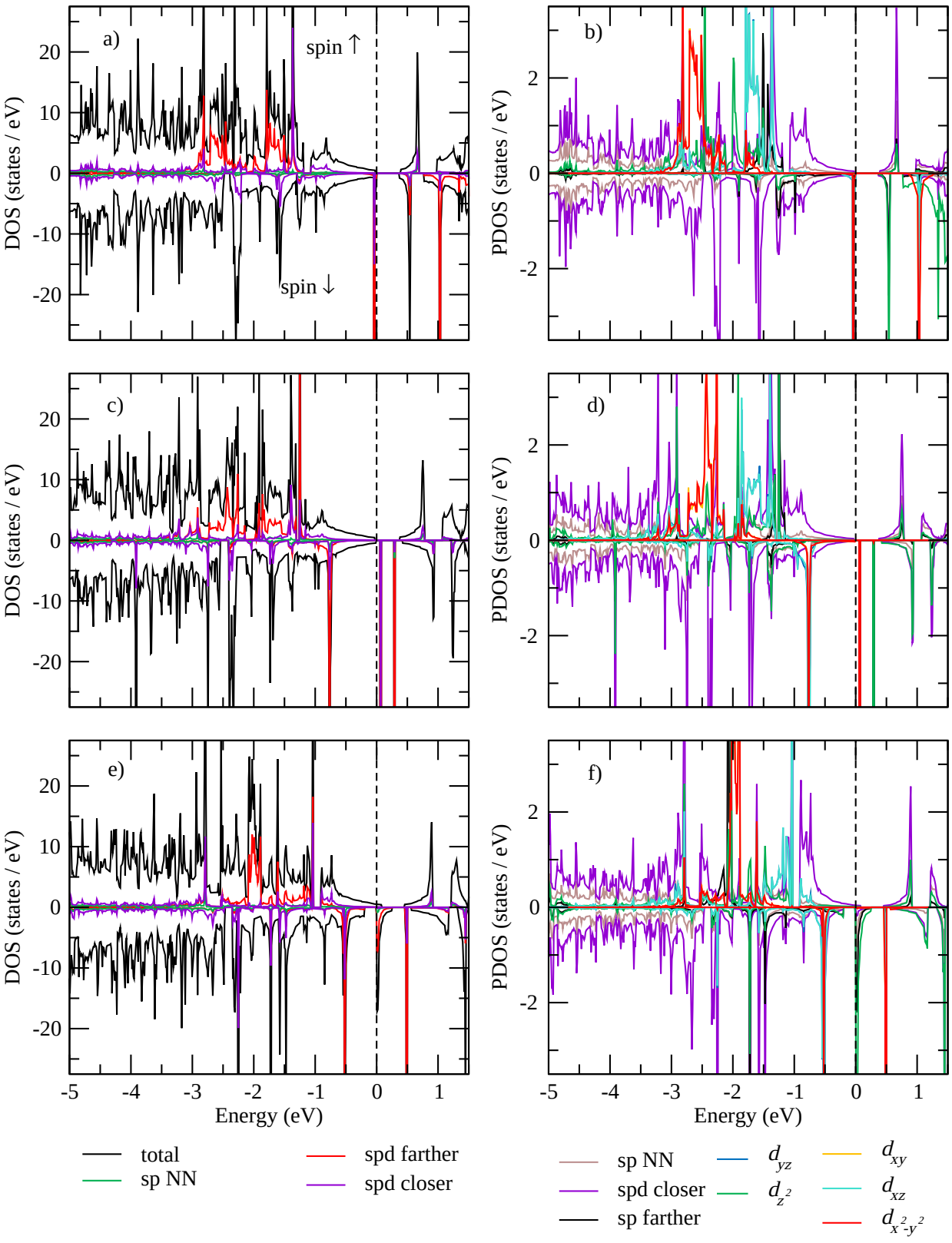


**FIG. A40:** DOS and PDOS plots. FeIr@SV (a) and (b); RuIr@SV (c) and (d); OsIr@SV (e) and (f).

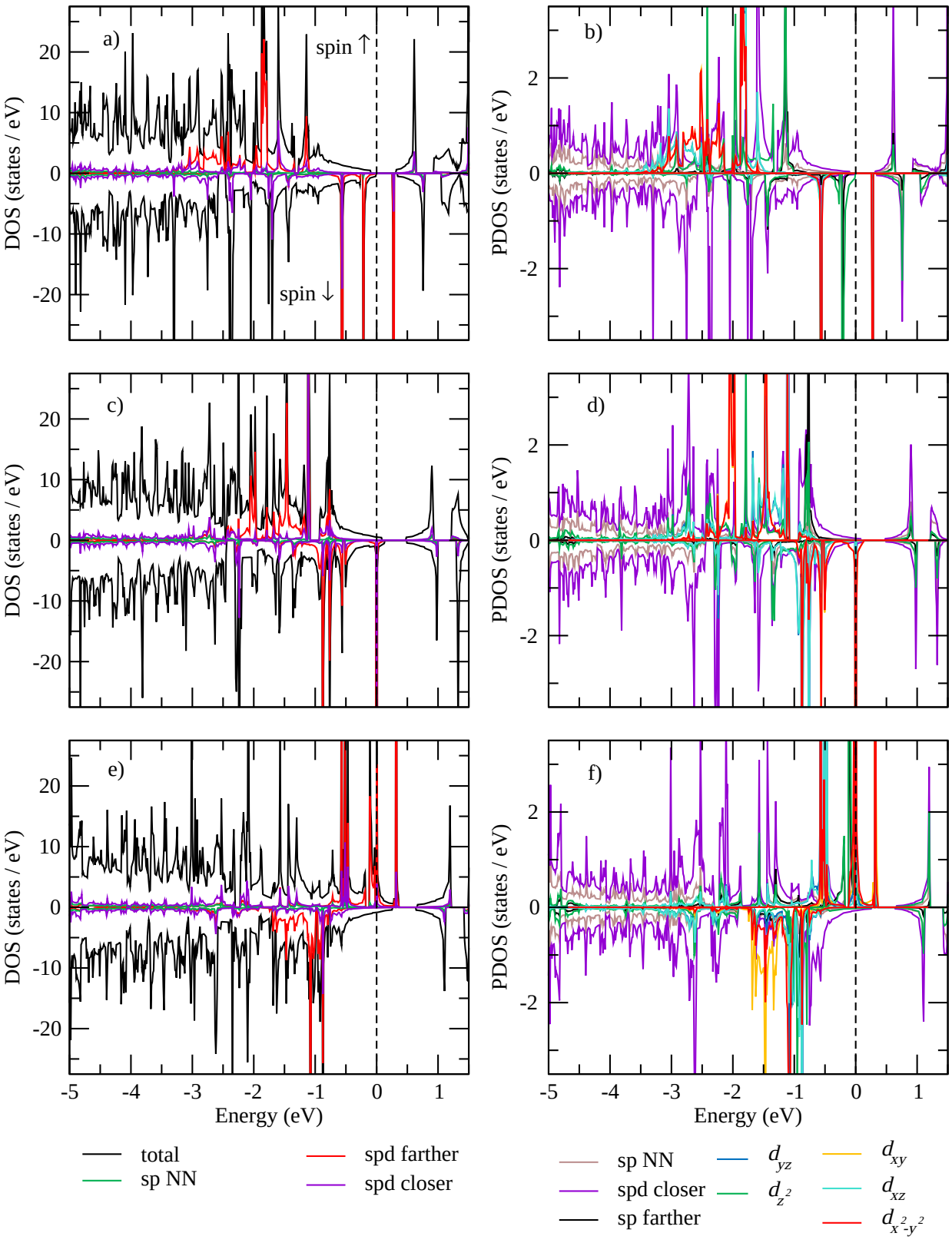


**FIG. A41:** DOS and PDOS plots. CoIr@SV (a) and (b); RhIr@SV (c) and (d); IrIr@SV (e) and (f).

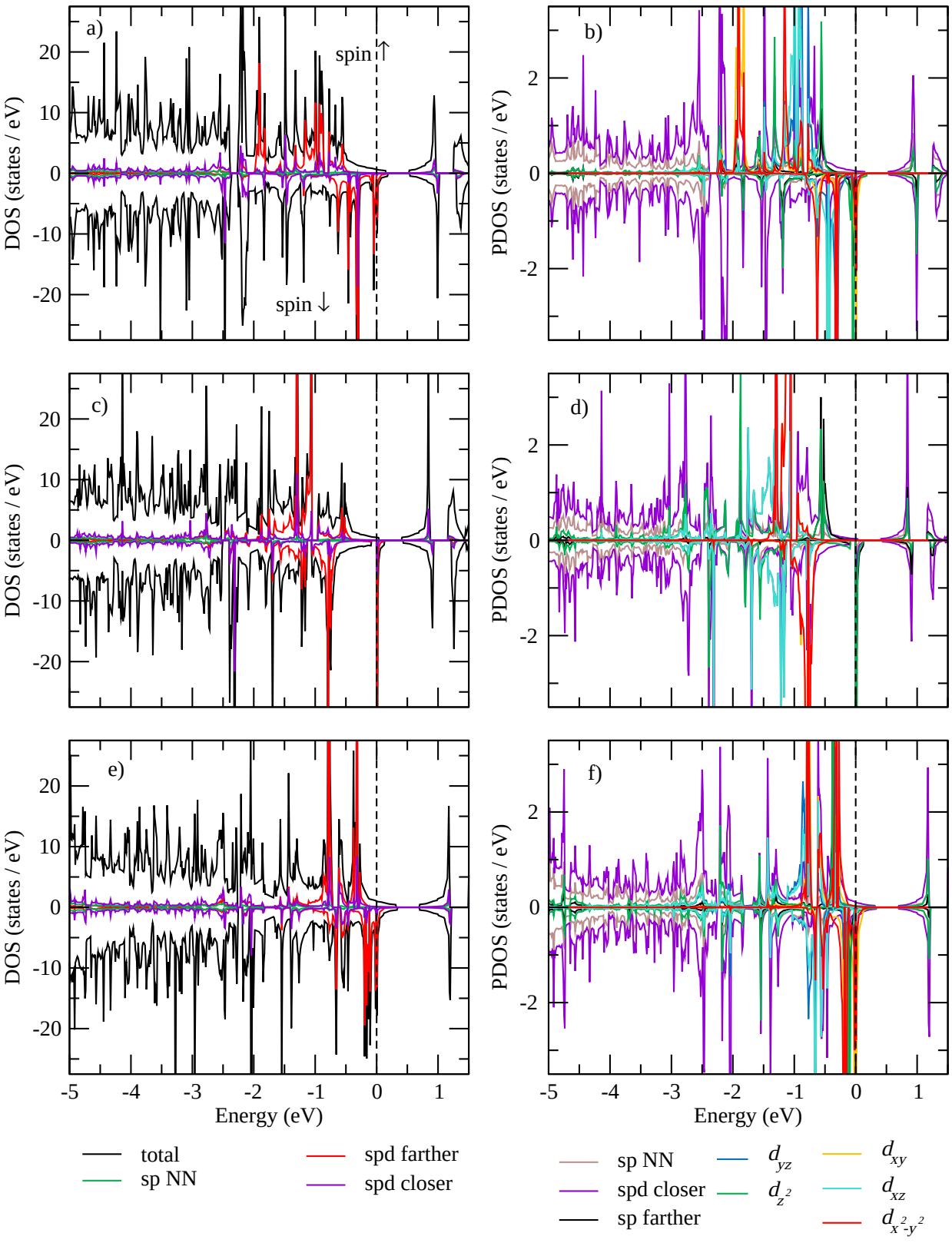


**FIG. A42:** DOS and PDOS plots. NiIr@SV (a) and (b); PdIr@SV (c) and (d); PtIr@SV (e) and (f).

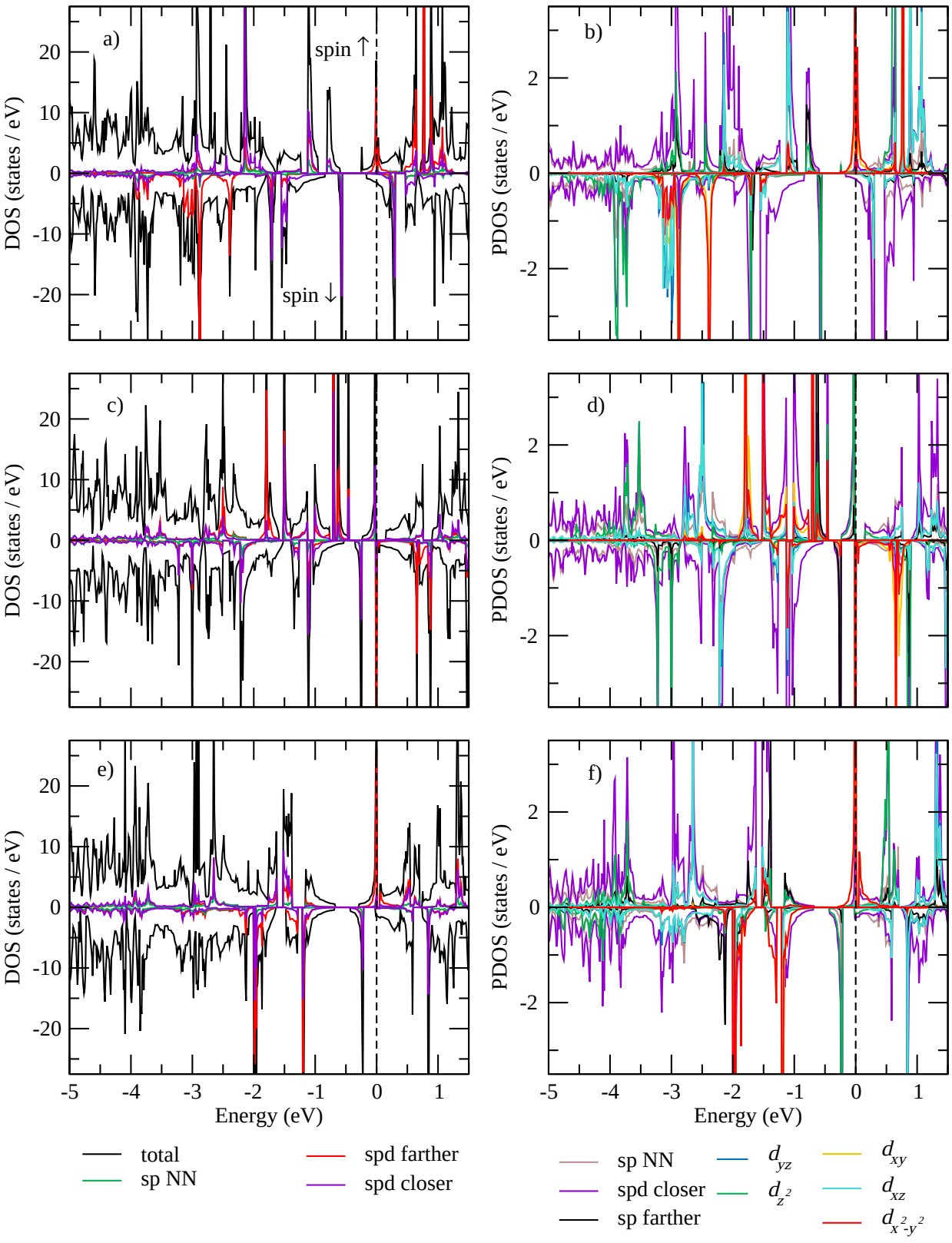


**FIG. A43:** DOS and PDOS plots. FeIr@NSV (a) and (b); RuIr@NSV (c) and (d); OsIr@NSV (e) and (f).

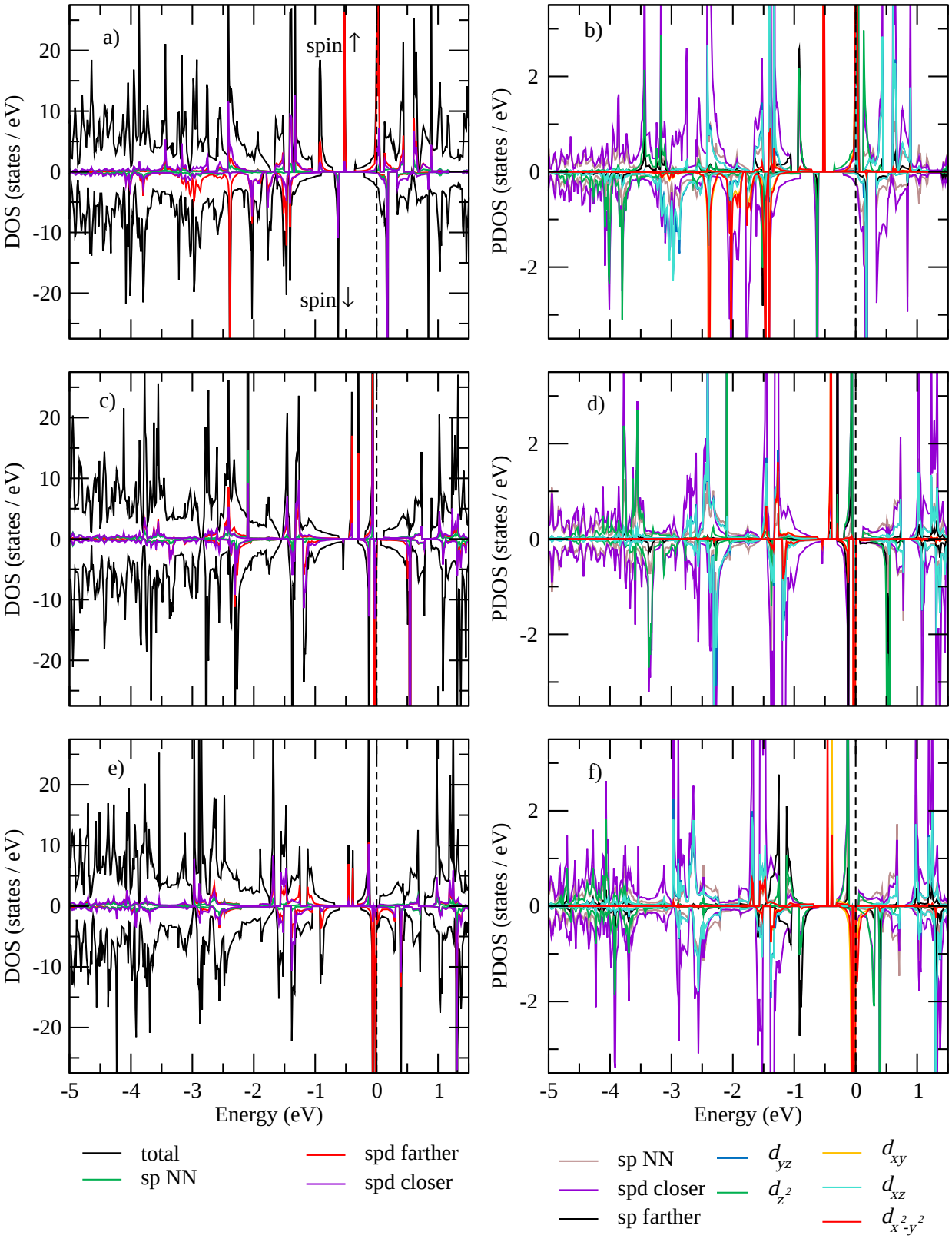


**FIG. A44:** DOS and PDOS plots. CoIr@NSV (a) and (b); RhIr@NSV (c) and (d); IrIr@NSV (e) and (f).

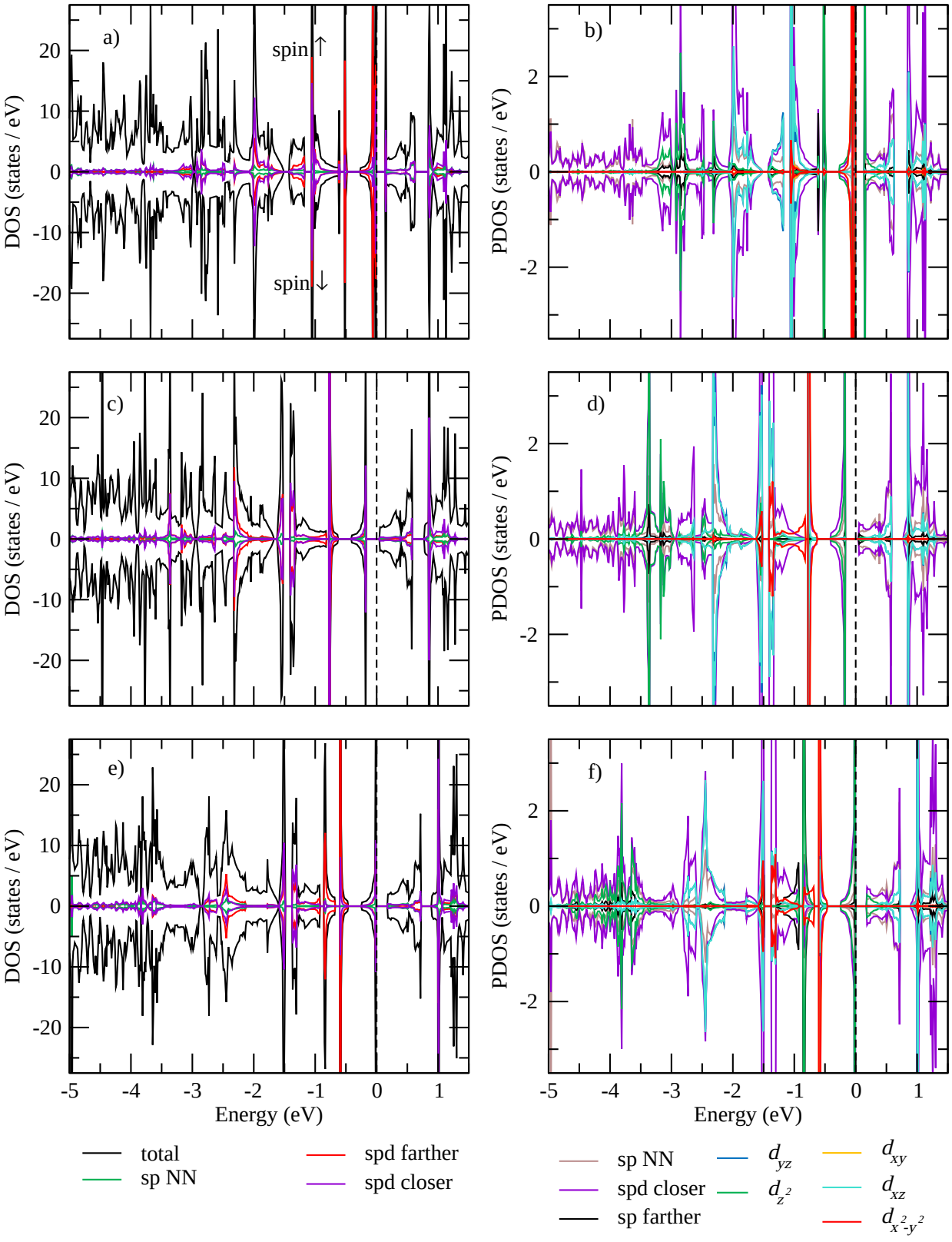


**FIG. A45:** DOS and PDOS plots. NiIr@NSV (a) and (b); PdIr@NSV (c) and (d); PtIr@NSV (e) and (f).

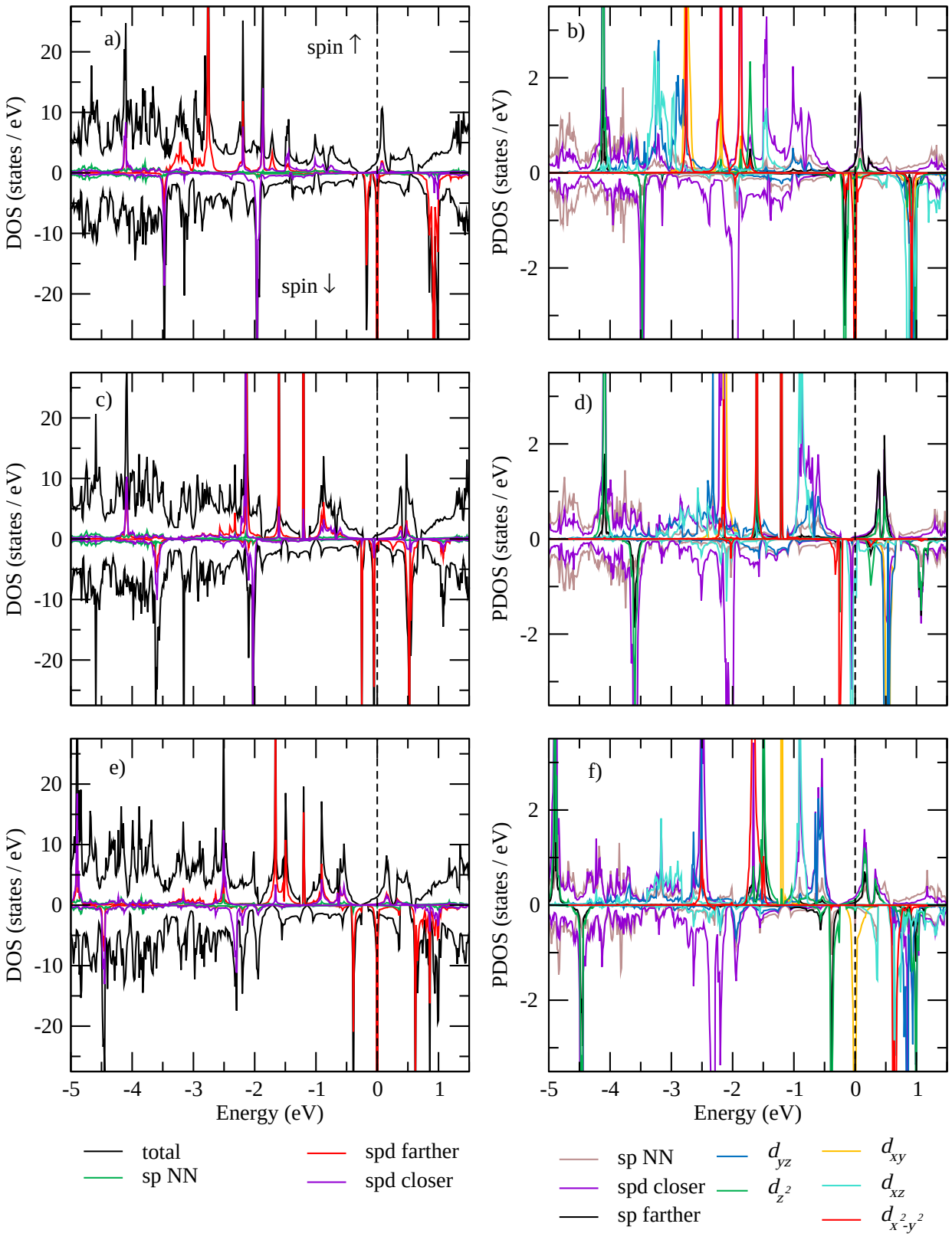


**FIG. A46:** DOS and PDOS plots. FeIr@NDV (a) and (b); RuIr@NDV (c) and (d); OsIr@NDV (e) and (f).

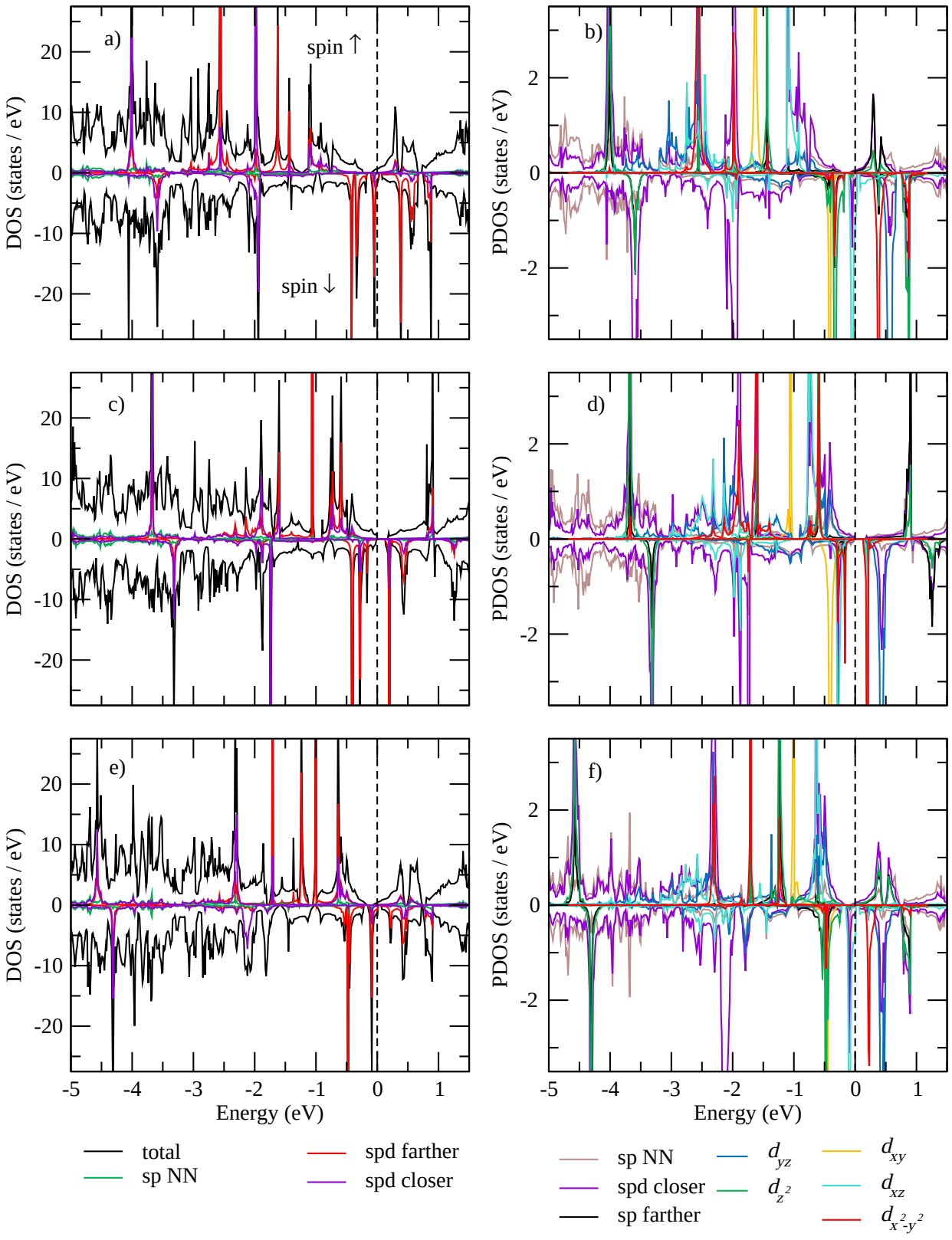


**FIG. A47:** DOS and PDOS plots. CoIr@NDV (a) and (b); RhIr@NDV (c) and (d); IrIr@NDV (e) and (f).

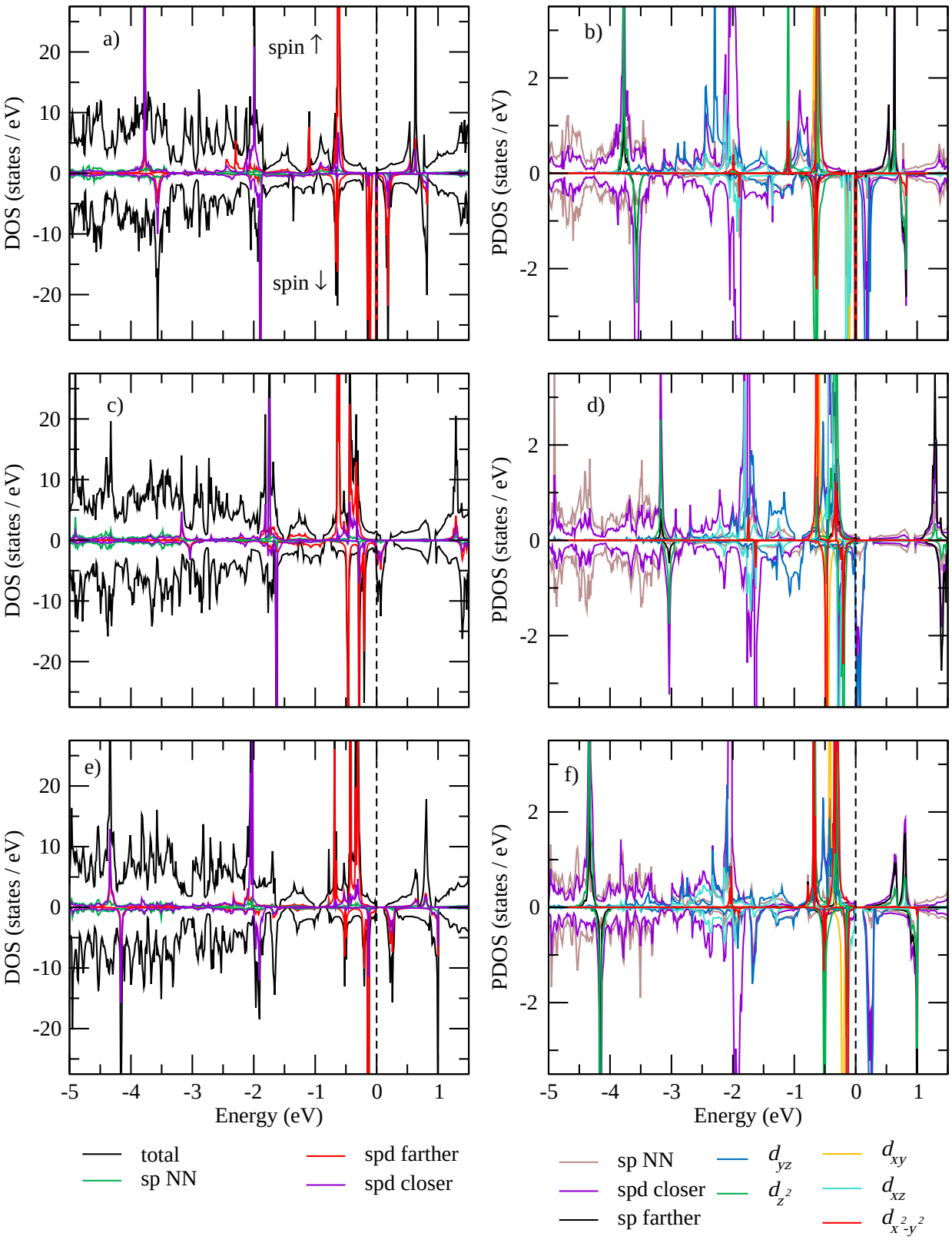


**FIG. A48:** DOS and PDOS plots. NiIr@NDV (a) and (b); PdIr@NDV (c) and (d); PtIr@NDV (e) and (f).

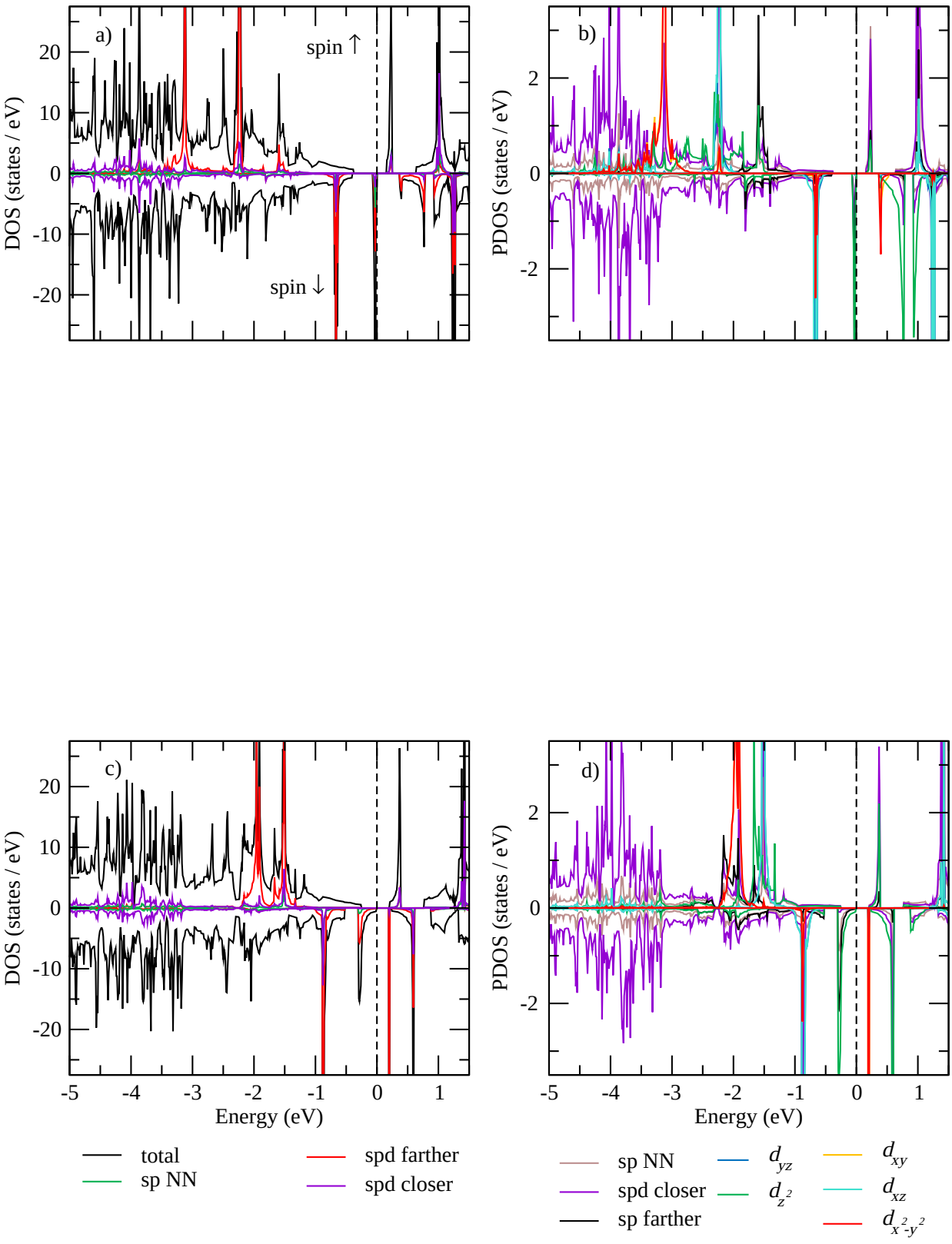


**FIG. A49:** DOS and PDOS plots. FePt@SV (a) and (b); OsPt@SV (c) and (d).

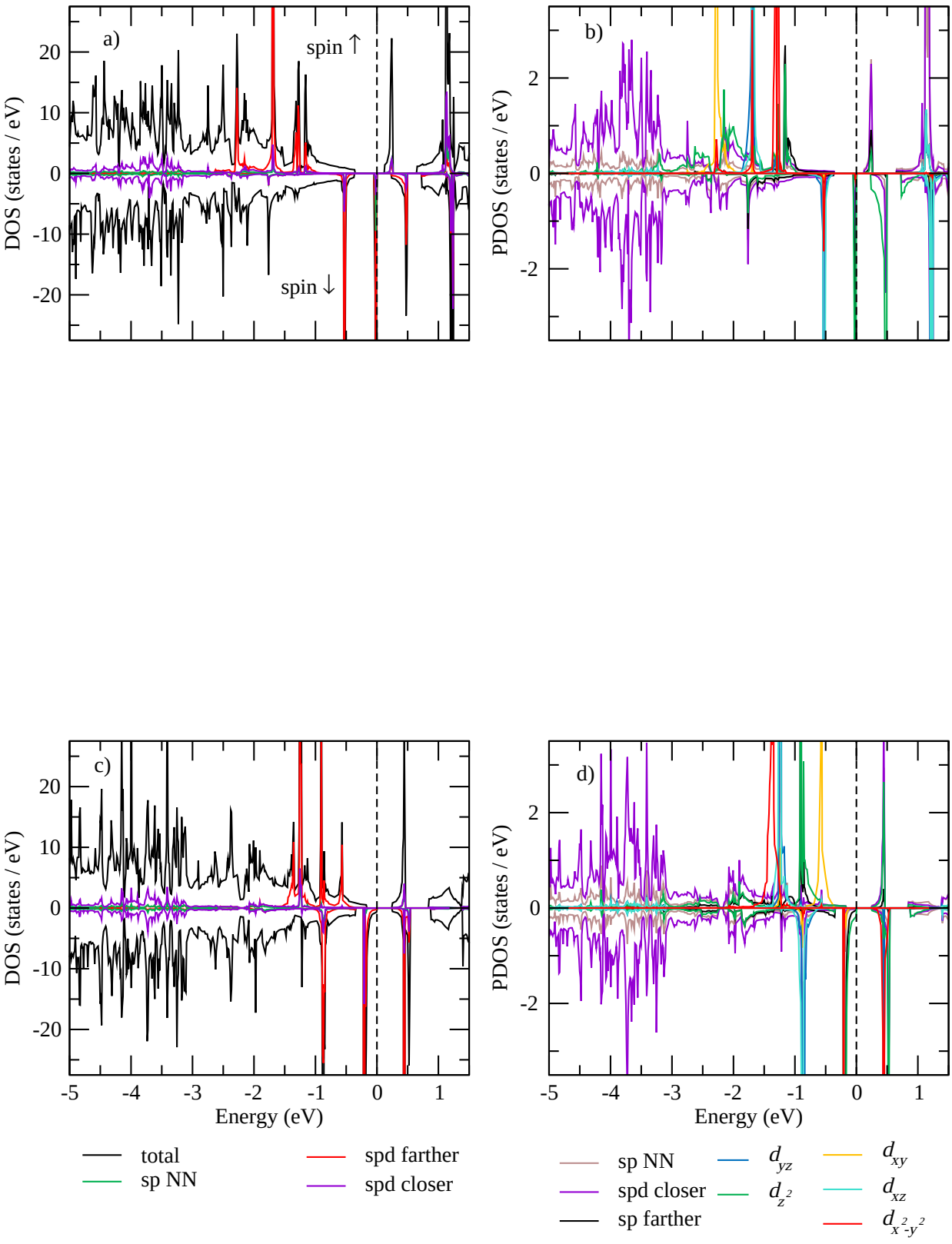


**FIG. A50:** DOS and PDOS plots. CoPt@SV (a) and (b); IrPt@SV (c) and (d).

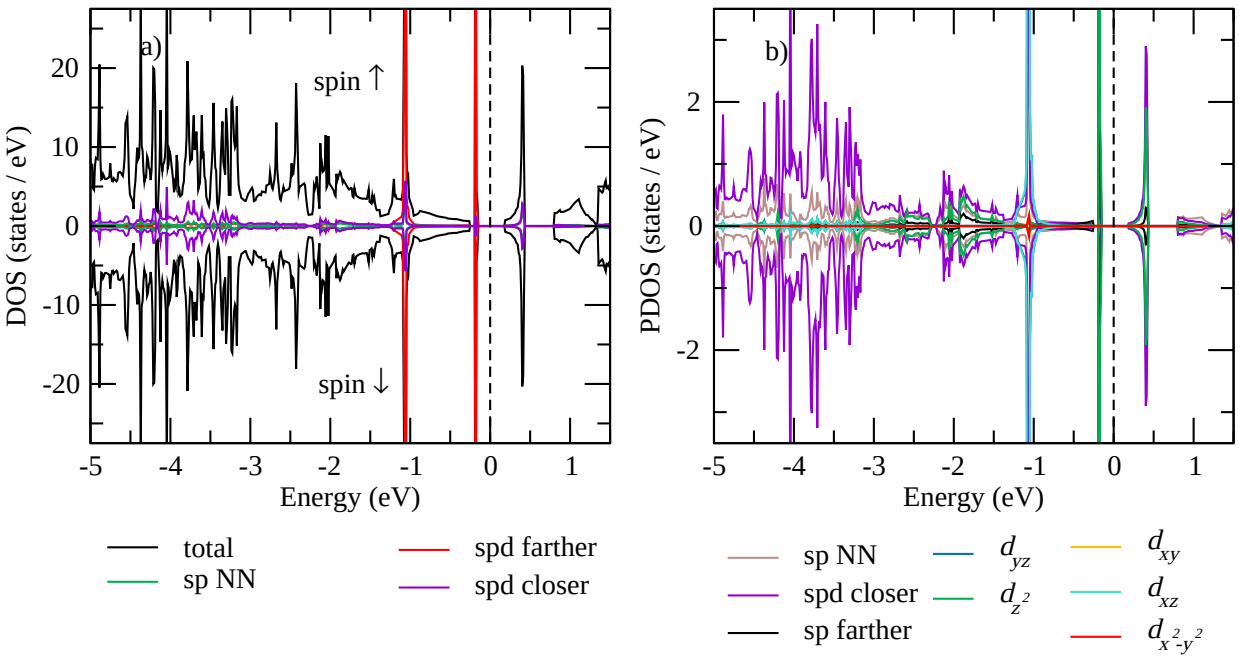


**FIG. A51:** DOS and PDOS plots. PtPt@SV (a) and (b).

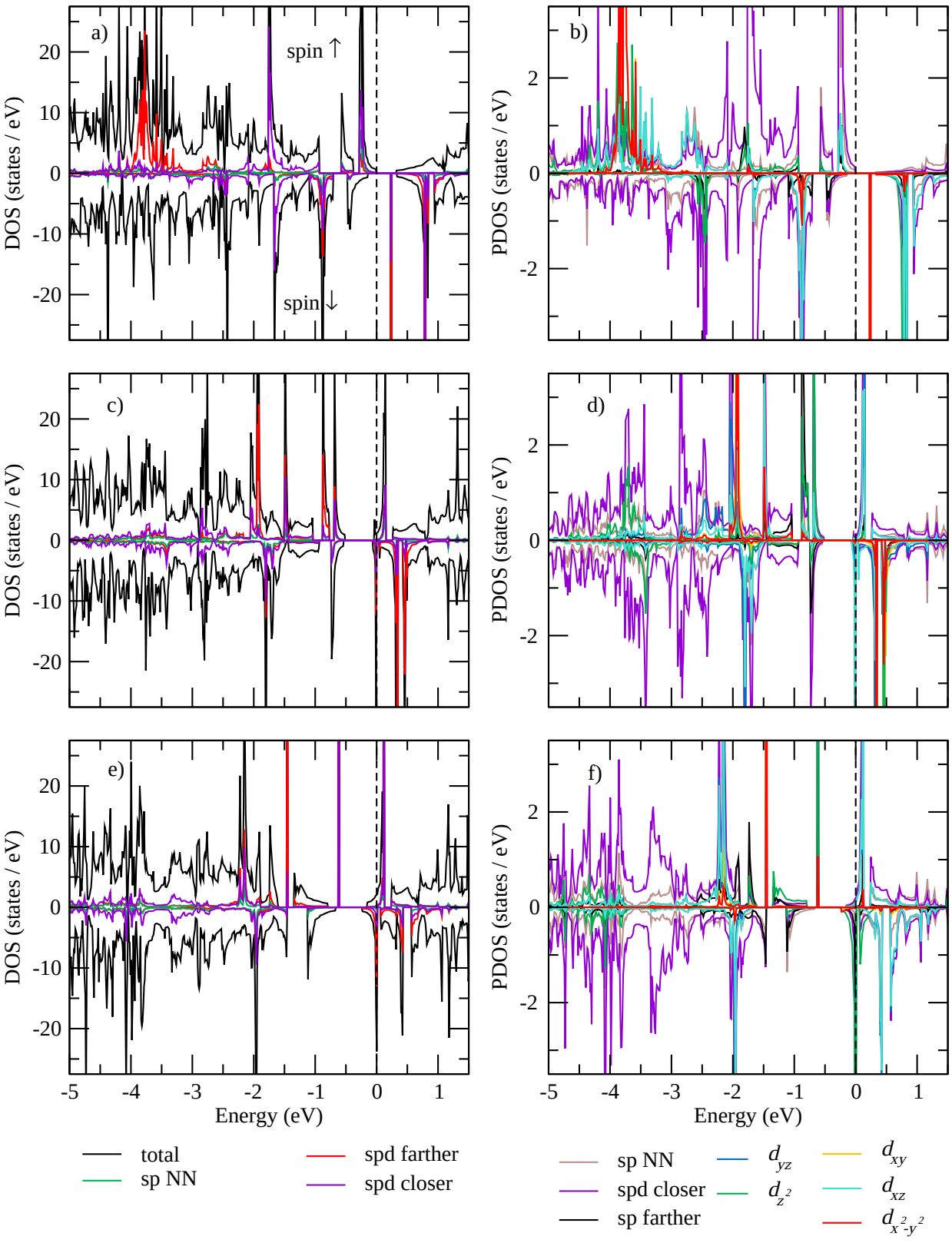


**FIG. A52:** DOS and PDOS plots. FePt@NSV (a) and (b); RuPt@NSV (c) and (d); OsPt@NSV (e) and (f).

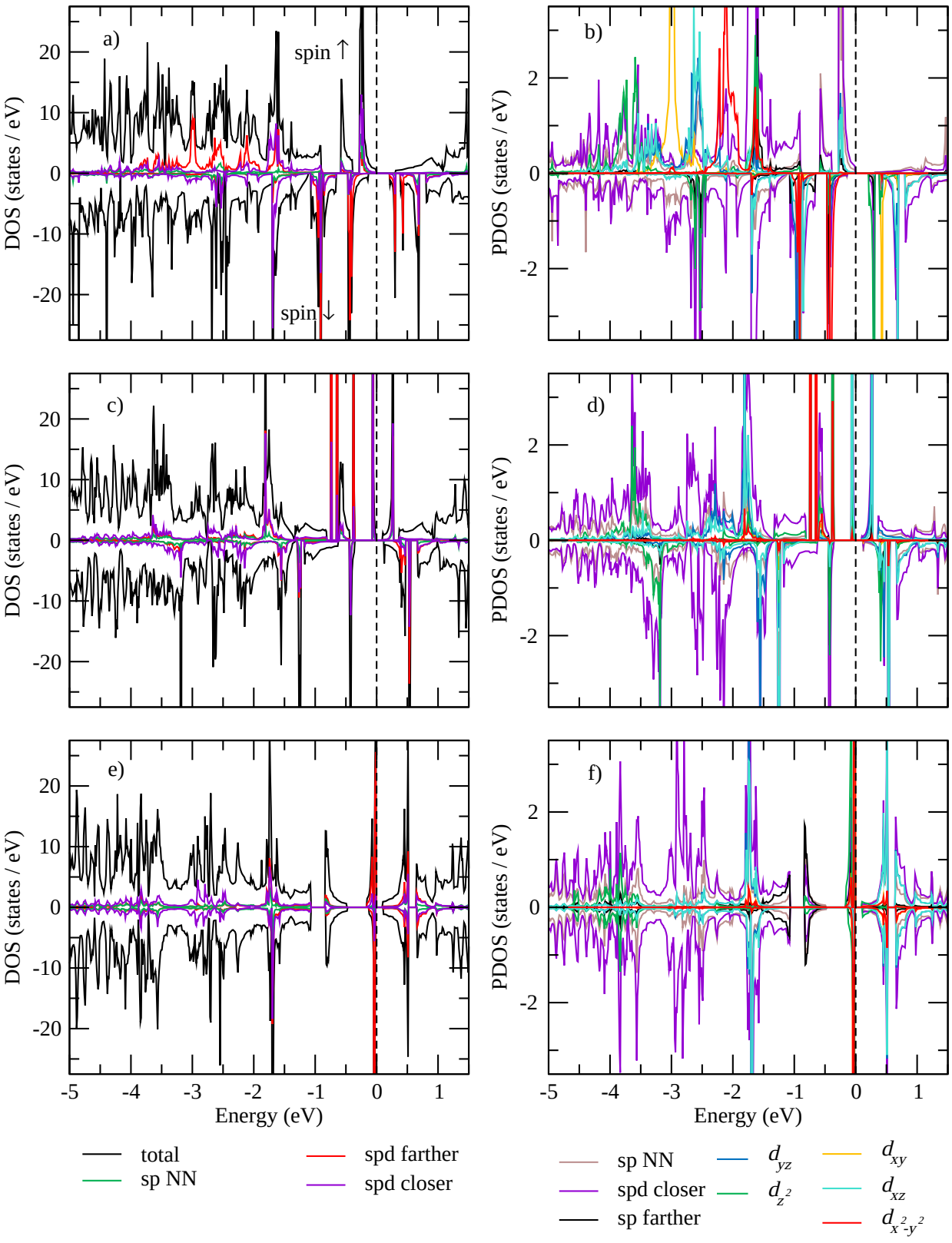


**FIG. A53:** DOS and PDOS plots. CoPt@NSV (a) and (b); RhPt@NSV (c) and (d); IrPt@NSV (e) and (f).

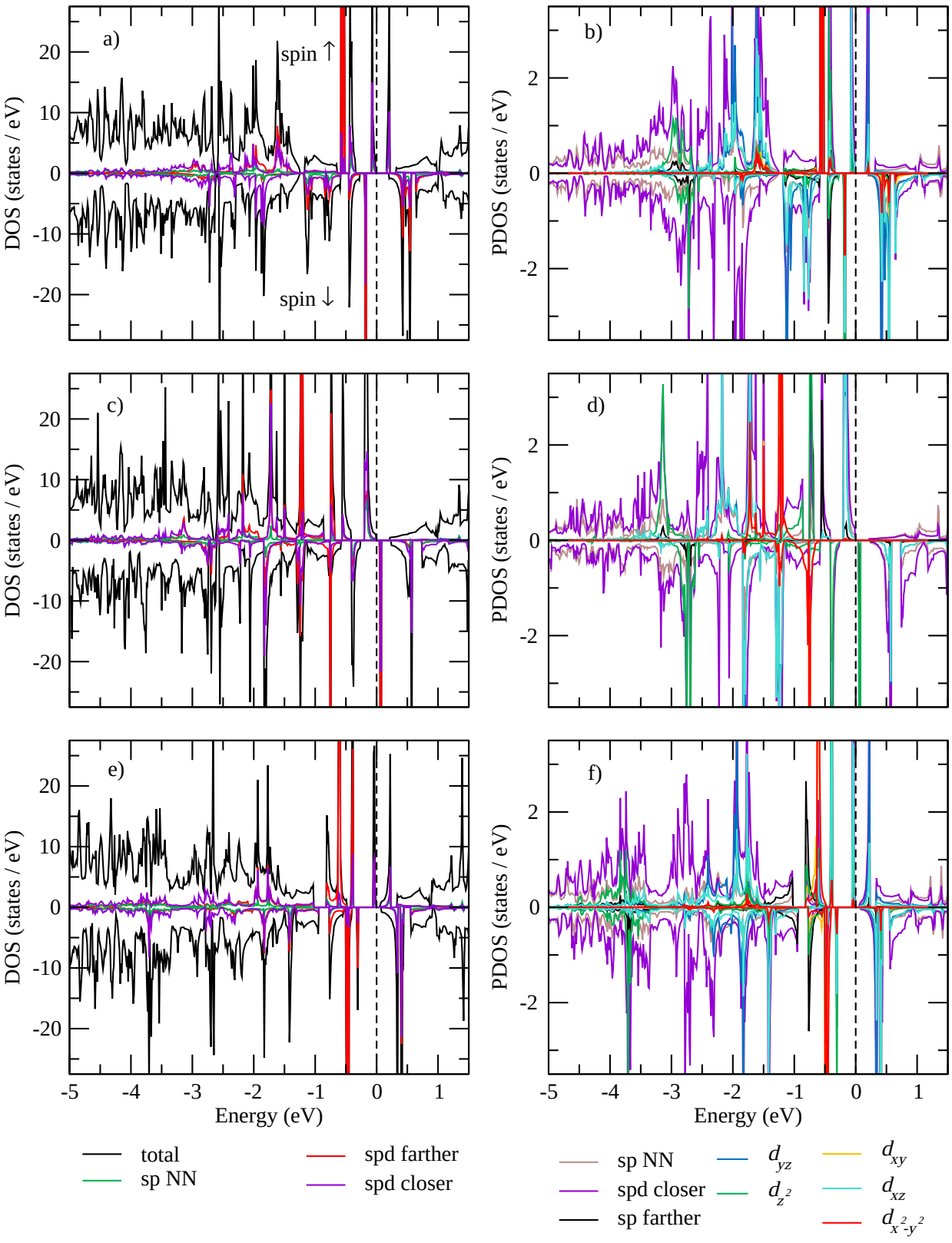


**FIG. A54:** DOS and PDOS plots. NiPt@NSV (a) and (b); PdPt@NSV (c) and (d); PtPt@NSV (e) and (f).

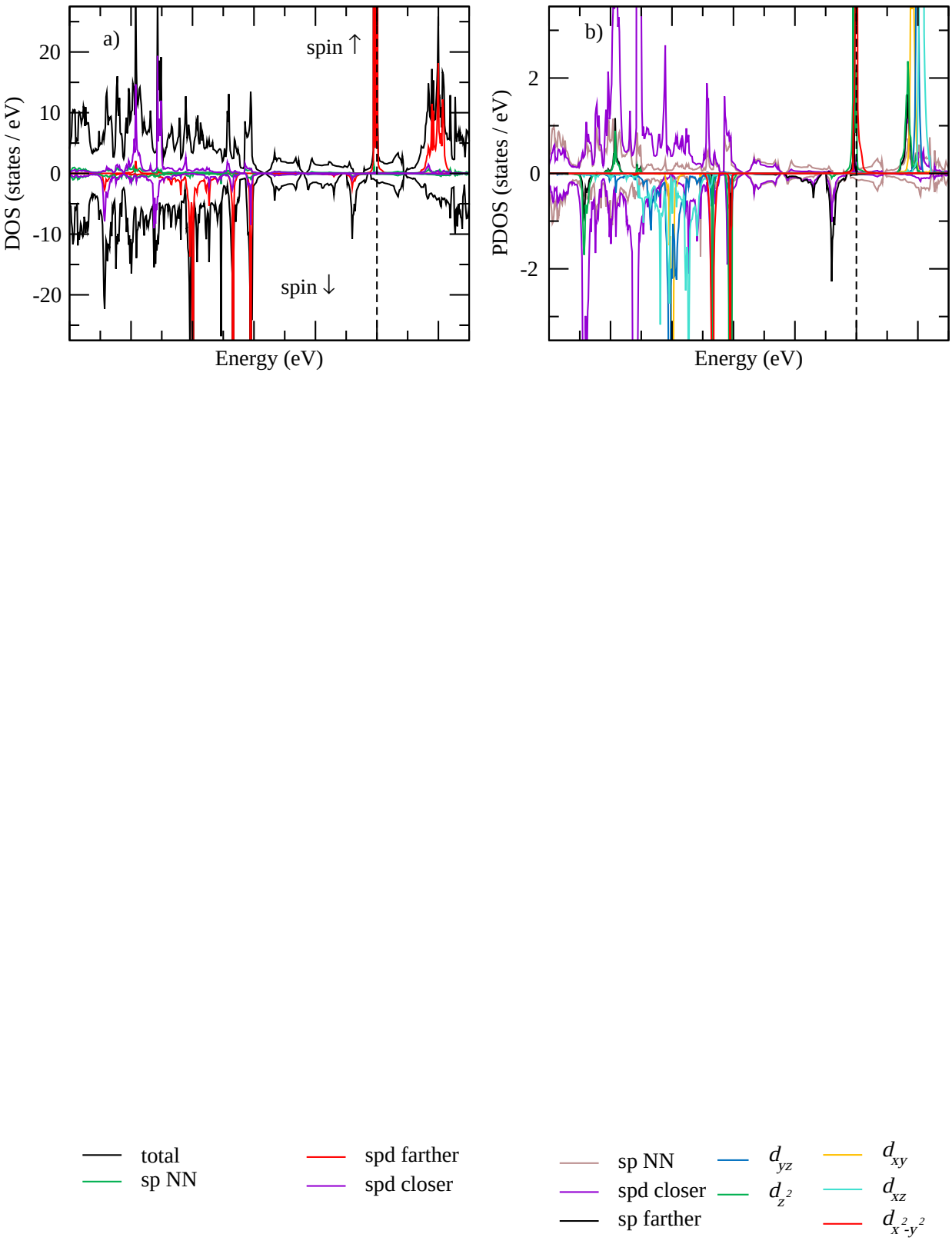


**FIG. A55:** DOS and PDOS plots. FePt@NDV (a) and (b).